Testing of a New Composite Framing System for Vertical Evacuation Structures

Kenneth P. Sullivan

A thesis
submitted in partial fulfillment of the
requirements for the degree of

Master of Science in Civil Engineering

University of Washington

2021

Committee:

Dawn Lehman

Charles W. Roeder

Michael Motley

Program Authorized to Offer Degree:
Civil and Environmental Engineering

University of Washington

Abstract

Testing of a New Composite Framing System for Vertical Evacuation Structures

Kenneth P. Sullivan

Chair of the Supervisory Committee:
Dr. Dawn Lehman
Civil and Environmental Engineering

Communities on the coast of the pacific northwest are vulnerable to earthquakes followed by tsunami. These communities have little to no access to high ground and therefore vertical evaluation structures are needed. Vertical evacuation structures typically take one of two form: a closed structure using shear walls or an open structure using frames. Multipurpose buildings typically utilize shear walls, while single purpose evacuation towers use frame elements. This project investigates a new open frame structure for use in a multipurpose building, where the stories below the inundation depth are sacrificial and detailed with break-away slabs (and break-away walls, although this is beyond the scope of this project). This is the second phase of a two-phase experimental study using the Hinsdale Wave Laboratory at Oregon State University. The first phase studied shear-wall systems (Pyke, 2020). This study investigates a new framing system, using concrete filled steel tube columns and piles. The specimen simulated a single bay by single bay frame. Above the inundation depth, a hat truss provides the stiffness; below that the slabs are detailed with break-away connections. There were three study parameters: (i) wave height, (ii) slab, i.e., no slab, fixed slab and break away slab, and (iii) soil height. Relative to the wall specimen, the CFST frame specimen reduced the forces by 89%. The tests also indicated that the break-away slab can significantly reduce the large fluid pressures within the structure. In contrast, the effects of soil level on the specimen was far smaller, likely due to the relative stiffness of the specimen. However, in a real structure, the stiffness changes resulting from scour and the tsunami could have a more significant impact on the response.

TABLE OF CONTENTS

Page

LIST OF FIGURES

Figure Number Page

LIST OF TABLES

Chapter 1
INTRODUCTION

This thesis represents work conducted between January 2019 and January 2021 during the course of completing a Master of Science in Civil Engineering, at the University of Washington.

1.1 Motivation

Coastal communities in earthquake prone regions face a chance of experiencing the devastating effects of a duel hazard event from a large magnitude earthquake followed shortly by a tsunami. This is especially concerning in low lying coastal areas with no viable means to evacuate to higher ground, such as large sections of the Pacific Northwest in California, Oregon, Washington, and British Columbia. Wood et al. (2015) estimate that 21,500 residents in this region live and sleep more than 15 minutes walk from "safe" ground. This figure does not include tourists and businesses that people may have to evacuate from. At the same time, the NOAA is able to identify and signal a tsunami in approximately five minutes using the Deep-ocean Assessment and Reporting of Tsunami (DART) network. Near shore tsunamis generated from the Cascadia Subduction zone may reach shore in as little as 15-30 minutes (CREW, 2013). A potential solution is to build tsunami vertical evacuation structures in low lying regions with limited evacuation high ground. These structures can take the form of strong but heavy shear wall structures, or more open, frame structures, such as a concrete filled steel tube (CFST) columns. A CFST structure is advantageous, compared to a shear wall structure, because it is lighter and has less area exposed to the wave, due to the possibility of open walls between columns. CFST structures also have columns integral to the piles, with large stiffness and shear capacity. Furthermore, if the floor slabs that are inundated by the waves are able to release some of the upward pressure from the wave surging underneath, the upward force on the the foundation would be greatly diminished. At this time, there is limited research on this possibility of a CFST vertical evacuation structure, or break away slab. This research seeks to investigate the wave structure interaction with a CFST hat truss frame, and the feasibility of a

break away slab in a CFST specimen, when tested in a large wave flume.

1.2 Objectives

The primary objectives of the research presented in this thesis is to:

- Design a flume experiment utilizing the simulation capability of OpenFOAM to predict loads in the wave flume for a frame type specimen.
- Create a preliminary framework for simulating the sequenced loading of an earthquake and tsunami on a tsunami vertical evacuation structure using OpenSees.
- Determine the structural response, including the base shear, axial load in the piles, and pile moments, of the designed specimen when impacted by three types of wave.
- Investigate how changing the soil level around the piles affects the structure response.
- Explore the effects of a first story slab has on the structure response, and if creating a break away connection would provide advantageous effects on the CFST foundations, in the event of wave loading.

1.3 Thesis Organization

This thesis is broken into the following chapters. Chapter 2 provides a literature review on the topic of tsunami design loads for vertical evacuation structures, wave flume testing of frame type specimens, and CFST column to beam connections. Chapter 3 discusses the initial design of the wave flume experiments for a shear wall specimen using OpenFOAM, and the design of a full scale CFST vertical evacuation structure. Chapter 4 details the experiment design for the CFST specimen in the large wave flume. This chapter outlines the design of the specimen, and the arrangement of instruments in the flume. Chapter 4 also details the experimental program and test conditions, as well as the test procedure. Chapter 5 documents the results of the measurements for the experiment conditions. Chapter 6 provides comparisons between instruments and experiment conditions. This chapter also compares the results from this experiment to results from the shear

wall specimen evaluated by Pyke (2020), and an OpenFOAM simulation of the experiment. Finally, Chapter 7 discusses the final conclusions of this experiment and provides a brief summary.

Chapter 2

LITERATURE REVIEW

Vertical evacuation shelters can take multiple forms, and the codified requirements in the United States are relatively new. This chapter examines the existing literature on three key areas. First, current design methods and philosophies for vertical evacuation structures are examined. Second, testing methods and results for piles and frame style specimens are examined in order to provide guidance in this thesis and Chapter 4. Finally, the research that examines the connections between CFST columns and structural braces and beams are examined to guide the design of the wave flume experiment.

2.1 Current Design Methods for Vertical Evacuation Structures

This section examines four peer reviewed papers and ASCE 7-16 for the current design methods used in vertical evacuation structures. These papers collated and summarized findings from multiple sources, such as FEMA P646, and field surveys after the 2011 Greast East Japan Tsunami. Chock (2016) provides a synthesis and additional commentary to ASCE 7-16, so these two sources are discussed together in Section 2.1.4.

2.1.1 Yeh et al. (2005) VES Design Guidelines

Yeh et al. compiled a report of the existing guidelines, criteria and feasibility of tsunami Vertical Evacuation Structures. "Design for tsunami effects requires considerable strength and rigidity," which means designers must take a different approach than typical seismic design (Yeh et al., 2005). Additionally, the tsunami loading patterns are unpredictable and depend on the bathymetry and topography between the tsunami source and the site.

Tsunami run-up behavior is likely one of the largest criteria influencing the loading phenomenon on the structure. Long tsunami waves can run up a steep slope without breaking, appearing as a slow rise and fall on the structure. Alternatively, a bore can form when the tsunami breaks

offshore resulting in turbulent surging up the shore. Tsunami's often occur in series of multiple waves, so a tsunami wave may reach shore before the previous wave has fully receded. The result is a tsunami could form a bore further up the shore, or impact structures by breaking against them. This constructive fluid interaction creates many unpredictable forces and force directions on potential evacuation structures. Finally, structures placed close to the shoreline with a steep slope may experience the tsunami wave breaking directly on the structure similar to the conditions set by a collapsing breaker (Yeh et al., 2005).

Yeh et al. (2005) examines several of the existing force equations and their considerations. Table 2.1 is a reproduction from the report and shows the researcher's comments for each force type. Yeh et al. conclude that while most of the forces exerted by tsunamis are easily and accurately calculated once velocity and flow depth are known, "present [2005], estimations of of the impact force ... are not well established and need to be improved" (2005).

Table 2.1: Reproduction of Table 7: Considerations for tsunami forces (Yeh et al., 2005).

Type of forces	Comments for tsunami considerations
Hydro-static Forces	Not used for the evaluation of a building as a whole, but need to be considered for the strength of each structural wall panel of the building.
Buoyant Forces	Controlled by the inundation depth and the rate of water-level increase.
Hydrodynamic Forces	Controlled by the maximum value of the product of the inundation depth, the square of the flow velocity, and the shape of the structural element.
Surge Forces	Controlled by the flow velocity of the leading tongue of the run-up.
Impact Forces	Controlled by the maximum flow velocity and depth, object mass, and elasticity associated with the impact.
Breaking Wave Forces	May not be relevant to the tsunami forces on onshore buildings: Tsunami waves tend to break offshore and approach the shore as a broken bore.
Scour	Controlled by flow velocity (shear stress), and pore-pressure gradient that can be estimated by the change in inundation depth and its duration.

2.1.2 Heintz and Mahoney (2008) VES Design Guidelines

The paper by Heintz and Mahoney summarizes the findings of the 2008 FEMA P646 report. This report examines past tsunami events, and characterizes similarities and areas designers of vertical evacuation structures should focus on.

Tsunami structural damage typically is a result of:

- Direct forces from water inundation, both hydro-static and hydrodynamic.
- Forces from water borne debris impact.
- "Fire spread by floating debris and combustible liquids".
- Foundation failure from scour.
- Localized wind forces from wave motion (Heintz and Mahoney, 2008).

Considering these failure modes, vertical evacuation structures are a viable method of evacuation when horizontal routes are not possible (Heintz and Mahoney, 2008).

For vertical evacuation structures to be effective, they must be placed in areas, and at distances that the majority of the population can make it to the structure in time. Typical walking speeds range from two miles-per-hour (3.2kmh) to four miles-per-hour (6.4kmh) depending on the population's health, age, and the regions topographical features. If near shore tsunamis are assumed to have a 30 minute warning period, then for a vertical evacuation system to be fully effective, there must be an array of structures spaced every two to three miles (3.2-4.8km). Heintz and Mahoney provide a sample vertical evacuation plan for a fictional community in Figure 2.1 (2008).

Heintz and Mahoney also discuss load conditions caused by tsunamis. Beyond the calculated run-up of the tsunami, the authors recommend applying a factor of 1.3 to the run-up to account for uncertainty in these calculations. Additionally, the evacuation floor should be at least 10 ft (3m) above this factored run-up height on the structure (Heintz and Mahoney, 2008).

Heintz and Mahoney conclude that vertical evacuation structures have the potential to provide essential life-safety capabilities to regions without adequate or realistic evacuation routes out of the tsunami zone 2008. Their observations of structural attributes that behave well are:

- Strong systems with reserve capacity.
- Open systems that allow water to flow through the structure.
- Ductile systems that resist extreme forces without failure.
- Redundant systems that can experience partial failure without progressive collapse.
- Systems with deep foundations to resist scour.
- Breakaway walls to minimize hydrodynamic forces (Heintz and Mahoney, 2008).

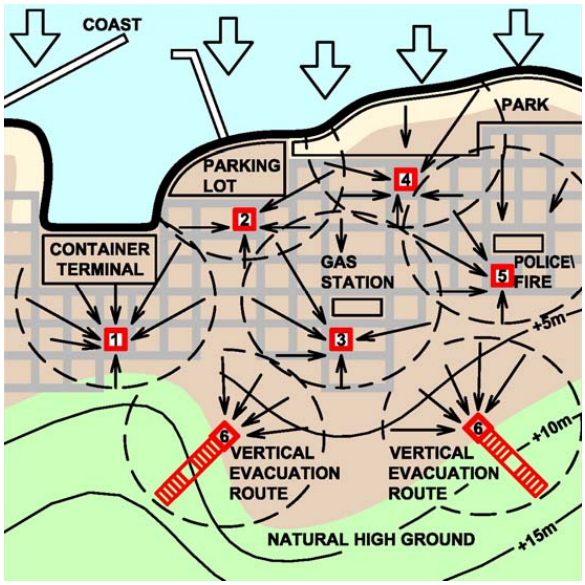

Figure 2.1: Reproduction of Figure 3. Sample layout of vertical evacuation structures in a hypothetical coastal community, considering travel distance, evacuation behavior, and naturally occurring high ground. Arrows show anticipated vertical evacuation routes (Heintz and Mahoney, 2008)

2.1.3 Fraser et al. (2012a) Lessons from 2011 Great East Japan Tsunami

After the 2011 Great East Japan Tsunami, Fraser et al. investigated the response of vertical evacuation structures. The field investigation was conducted seven months after the tsunami. During the tsunami, at least 5,428 people survived by taking refuge in 37 tsunami vertical evacuation buildings (Fraser et al., 2012a).

The designated evacuation structures were reinforced concrete or composite steel with reinforced concrete designed to 1981 building code. Before being designated evacuation structures, additional calculations were preformed to verify the structure had capacity for the anticipated tsunami loads. Structures also had minimum story heights based on the anticipated tsunami run-up (Fraser et al., 2012a).

The field investigation identified that 80% of VES were reinforced concrete, 20% were steel frame, 31% were three story, and 34% were four story or greater. Damage to designated VES was "generally limited to broken glazing, damaged fixtures and fittings, and debris impact to external cladding" (Fraser et al., 2012a). Of the designated structures, reinforced concrete generally performed better, but still experienced overturning, scour causing building collapse, and debris strikes that caused upper story collapse (Fraser et al., 2012a). Table 2.2 shows a summary of the tsunami event, number of people in each VES, and VES construction type.

The vertical evacuation structures in Kesennuma City were close to being over-topped. By some accounts, the refuge floors were within 3.3 ft (1m) of being washed over (Fraser et al., 2012a). Some structures in other parts of the country were over-topped due to inaccurate estimations of the tsunami height, despite the 2011 tsunami arriving at a relatively low tide (Fraser et al., 2012a).

Table 2.2: Reproduction of part of Table 1. Summary of TVEB in locations visited during this research. Field observations were not made at all buildings listed. A full inventory of known building features is provided by Fraser et al. (2012b). Not all buildings were available for observation during field investigations, but data on those buildings has been collected through interviews (Fraser et al., 2012a).

City/Town	Kamaishi City	Ōfunato City	Kesennuma City	Minami-Sanriku Town	Ishinomaki City	Natori City
Max. Tsunami Height[a]	30.4m	32.0m	23.0m	20.5m	25.8m	13.0m
Mean Tsunami Height[a]	14.3m	13.1m	10.5m	12.6m	6.5m	4.4m
First wave arrival time after EQ[a]	28min	25min	n/a	n/a	23min	63min
Fatality rate of area inundated	8%	2%	3%	6%	3%	8%
No. TVEB	3	7	16	4	3	4[b]
No. people saved in TVEB	50	22[c]	2,426	694	500	1,736[d]
Average no. people saved in each TVEB	17	22[c]	152	174	167	579[d]
No. built with TVEB in mind	0	0	2	1	0	0
TVEB Construction	RC, Steel Frame	RC, Steel Frame	RC, Steel Frame	RC	RC, Steel Frame	RC

[a]Tsunami data from field surveys.

[b]Buildings designated as refuges for multiple-hazard evacuation, not specifically as TVEB.

[c]Numbers of people saved are available for only one TVEB in Ōfunato City.

[d]Numbers of people saved at Sendai International Airport are not included.

2.1.4 ASCE 7-16 Tsunami Design Requirements

The tsunami load provisions in chapter six of ASCE 7-16 provide expressions to estimate the loading on a structure subjected to a tsunami. Light wood frame and single story structures have been shown to offer very little resistance to tsunamis (ASCE 7-16). To this end, structures in design category I are not required to meet additional loads beyond the standard seismic provisions. Tsunami load considerations are required for structures in risk categories II and above. The provision emphasizes that the authority having jurisdiction should modify the risk category definitions based on local requirements.

Tsunami historical records do not sufficiently represent the chance of a catastrophic tsunami in a given location. Therefore, ASCE 7-16 created a probabilistic tsunami hazard analysis (Chock, 2016). This hazard analysis uses factors such as locations of subduction zone faults, tsunami wave forms, M_{max} for subduction source regions, among others. This hazard analysis results in an analysis workflow of examining (1) source, (2) propagation, (3) site analysis and design parameters, and (4) design maps.

The performance objectives for tsunamis are similar to earthquakes; however, single story and single family residence structures are not meant to be occupied during a tsunami so they have no additional requirements. The feasibility of this is contingent on early warning systems being in place and the knowledge of a safe and clearly labeled evacuation route. Tsunami vertical evacuation structures must always be designed to meet tsunami risk category IV requirements, and additional importance factor of $I_{tsu} = 1.25$ (ASCE 7-16).

ASCE 7-16 outlines two main methods for calculating inundation depths and flow velocities for a site, the energy grade line method or site-specific probabilistic tsunami hazard analysis. The energy grade line analysis method produces statistically conservative values for inundation depth and flow velocity (Chock, 2016). It is based on estimated run up elevations from the NAVD88 points on the U.S. West Coast[1]. The energy grade line method must be performed for all structures in tsunami risk categories II, III, and IV. The energy grade line method calculates the water level and velocity working from the run-up location down the shore to the site of interest, as shown in Figure 2.2. More involved, site specific, two dimensional analysis is required for tsunami risk category IV structures

[1]These elevations can be found at www.asce7tsunami.online

such as tsunami vertical evacuation shelters. The probabilistic hazard analysis must take into account a more complete set of NOAA bathymetry data and geodata from the ASCE database.

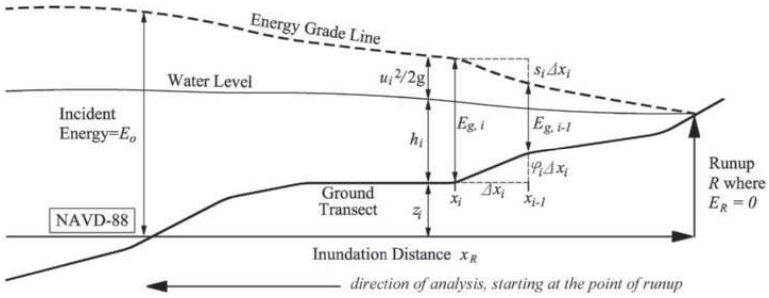

Figure 2.2: Energy Grade Line taken from ASCE 7-16. E_g = Hydraulic head at point i. h = Inundation depth at point i. u = Maximum flow velocity at point i. ϕ = Average ground plope between points i and i-1. Δx = The increment of horizontal distance. x = Horizontal distance inland from NAVD 88 shoreline at point i. s = Friction slope of the energy grade line between points i and i-1. R = Design tsunami runup elevation above NAVD 88 datum. x_R = Design inundation distance inland from NAVD 88 shoreline. z = Ground elevation above NAVD 88 datum at point i.

Once the inundation depth and velocity is known, the loads on the structure are calculated. Chock (2016) outlines the tsunami effects that must be included in the calculations:

- Hydro-static forces, such as
  - Unbalanced lateral forces,
  - Uplift forces, and
  - Residual water on elevated floors.
- Hydrodynamic forces, including
  - Drag forces,
  - Lateral impulse forces,
  - Pressurization by stagnated flow, and

  - Shock pressure effects of entrapped bore impulses.

- Waterborne debris impact related to water velocity

  - Poles, passenger vehicles, medium boulders,
  - Shipping containers and boats if structure is in a hazard zone, and
  - Extraordinary impacts of ships if risk category III or IV are in close proximity.

- Scour effects

  - Local scour and soil pore pressure effects
  - General erosion.

In addition to the strictest load calculations, ASCE 7-16 section 6.14 requires several additional protections against catastrophic failure. The minimum height of the refuge floors is at least 10 ft (3.05m) (or one full story height) above the height calculated from 1.3 times the max inundation depth. The refuge areas must be designed for an occupancy live load of 100 psf (4.8kPa). Under certain circumstances, the lay-down impact of adjacent pole structures must be accounted for in the design of the evacuation structure. Finally, beyond correct labeling on construction documents, designs for tsunami vertical evacuation structures must be independently peer reviewed to emphasize compliance with the requirements in ASCE 7-16.

2.2 Pile and Column Style Structure Experiments in a Wave Flume

This section examines three previous experiments and the instrumentation and test set ups used. Each subsection is broken into (1) objective; (2) test program; (3) test setup; (4) test results; and (5) conclusions. Wienke and Oumeraci (2005) examines wave forces on a slender pile with five (5) different styles of breaking and unbroken wave. Lukkunaprasit et al. (2009) conducted experiments on small scale specimens with varying sizes of openings in the front face of the the specimen. Andersen et al. (2010) conducted experiments with four (4) broken wave heights to determine wave pressures and loads on a slender pile.

2.2.1 Wienke and Oumeraci (2005) Wave Forces on Slender Pile

Objective

Wienke and Oumeraci investigated the impact forces of a breaking wave on a slender pile (2005). The angle of the 2.3 ft (0.7m) diameter pile was adjusted to determine how yaw into or away from the oncoming wave impacted the total force and pressures measured. The measured values were then compared to analytical two dimensional and expanded three dimensional methods.

Test Program

Wienke and Oumeraci (2005) subjected the pile to five types of wave at each angle. The descriptions of the waves are provided in Table 2.3. The yaw angle of the pile varied between 45° into and 45° away from the oncoming wave. The five angles (measured from vertical), tested were $\alpha = -45°$, $\alpha = -25°$, $\alpha = 0°$, $\alpha = 25°$, and $\alpha = 45°$.

Test Setup

The 2.3 ft (0.7m) diameter pile was attached at the bottom and top with a pin type connection. The top connection was attached to a bridge structure that spanned the width of the flume. The water depth varied between 13.1 ft (4m) and 13.9 ft (4.25m) to provide the wave breaking properties needed. The vertical height of the pile was 24.0 ft (7.3m). Strain gauges were placed on the top and bottom connections and along the height of the pile. Pressure transducers, accelerometers, and

Table 2.3: Reproduction of Table 1: Characteristics for the five loading cases (Wienke and Oumeraci, 2005)

Loading case	Description
1	• wave breaking far in front of the cylinder • over curling breaker tongue hits the cylinder far below the wave crest level • breaker tongue has a yaw angle of approximately 45° according to the horizontal plane when hitting the cylinder • broken wave
2	• wave breaking in front of the cylinder • breaker tongue hits cylinder just below wave crest level • breaker tongue is inclined by 25° according to the horizontal plane when hitting the cylinder • strongly breaking wave
3	• wave breaking immediately in front of the cylinder • breaker tongue hits cylinder at wave crest level • breaker tongue moves in horizontal direction when hitting the cylinder • breaking wave
4	• wave breaking at the cylinder • partially breaking wave
5	• no wave breaking in front of and at the cylinder

wave gauges were placed along the height of the pile as shown in Figure 2.3.

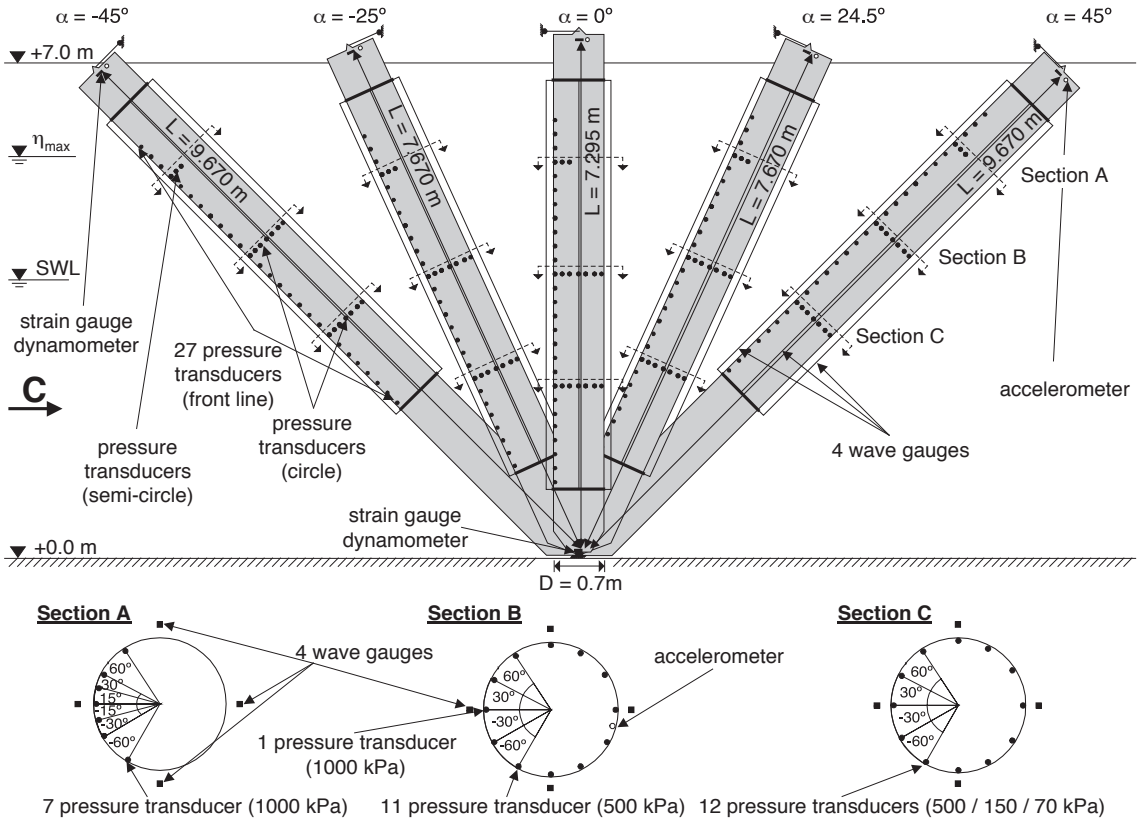

Figure 2.3: Reproduction of Fig. 8. Model set-ups of the test cylinder in the GWK (Wienke and Oumeraci, 2005).

In addition to the wave flume tests, a brief hammer type test was conducted on the pile with a swinging block of concrete. The oscillations were determined for the different water levels used in the wave tests, but not signification differences were recorded. This was done to characterize the types of oscillations in the cylinder under short duration impacts, similar to the crashing wave (Wienke and Oumeraci, 2005).

Test Results

The pressure time histories around the perimeter of the pile are shown in Figure 2.4 and summarized in Table 2.4. The impact period was measured as the time when the wave makes first contact with

the pile until the immersed width is equal to the radius of the pile.

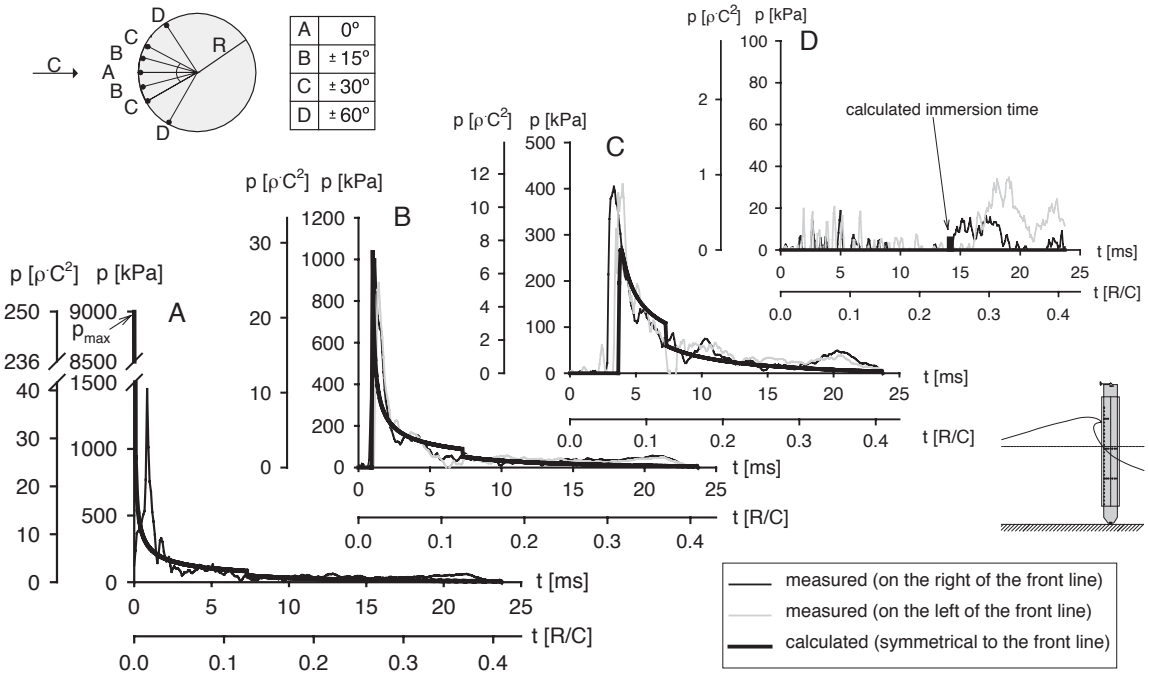

Figure 2.4: Reproduction of Fig. 16. Calculated and measured time histories of the impact pressures induced by a plunging breaker at the front side of the vertical pile (Wienke and Oumeraci, 2005).

Conclusions

Wienke and Oumeraci demonstrated that the measured force is "strongly depend[ent] on the distance between breaking location and the cylinder" (2005). The maximum force occurs when the wave breaks immediately in front of the cylinder. As shown in Figure 2.4, the Calculated pressure values matched the experimental results, within an order of magnitude.

Table 2.4: Reproduction of of Table 2: Maximum pressure at the vertical pile (Wienke and Oumeraci, 2005).

Location	Proposed theory		Groda's theory				Measured on the right				Measured on the left			
	p_{max} $[\rho \cdot C^2]$	t_{pmax} $[R/C]$	p_{max} $[\rho \cdot C^2]$	Δ_p	t_{pmax} $[R/C]$	Δ_t	p_{max} $[\rho \cdot C^2]$	Δ_p	t_{pmax} $[R/C]$	Δ_t	p_{max} $[\rho \cdot C^2]$	Δ_p	t_{pmax} $[R/C]$	Δ_t
A	250	0	250	0%	0	0%	40.3	-84%	0.014					
B	29.4	0.017	6.4	-78%	0.037	+118%	27.8	-5%	0.020	+18%	24.6	-16%	0.024	+41%
C	7.5	0.066	0.8	-89%	0.179	+171%	11.2	+49%	0.057	-14%	11.3	+51%	0.068	+3%
D		0.242*			0.501*	+107%								

* Immersion time.

2.2.2 Lukkunaprasit et al. (2009) Wave Forces Structures with Openings

Objective

In 2009, Lukkunaprasit et al. conducted a series of experiments testing the influence of openings in a structure, on the forces a structure experiences when exposed to a tsunami. The aim of this research is to influence the safe and economical design of structures and vertical evacuations structures in tsunami prone regions.

Test Program

The tests involved placing 1:100 scale models in the flume. Three model configurations were tested with openings in the front and back faces of 0%, 25%, and 50%. The outer dimensions of each model were 5.91 inches (150mm) cubed. Each model was subjected to three sizes of wave. The waves were 1.57 inch (40mm), 2.36 inch (60mm), and 3.15 inch (80mm). The wave height was determined by the maximum water depth at the location of the specimen, when no specimen was in the flume.

Test Setup

The specimens were placed in a gravity fed wave flume with cross section dimensions of 3.3 ft (1m) x 3.3 ft (1m). The specimens were mounted to a multi-axis load cell at the base, and were instrumented with pressure sensors on the front face. Locations of the pressure sensors and openings in the specimens are shown in Figure 2.5. The bathymetry in the flume represented the beach conditions at Kamala, Phuket Thailand.

Test Results

Large splashing was observed up and around the specimens when the wave impacted. The effect of the openings on the structure had minimal influence on the instantaneous pressures recorded, as shown in Table 2.5. The total force, in Table 2.6, significantly decreased when more water could flow through through the specimen.

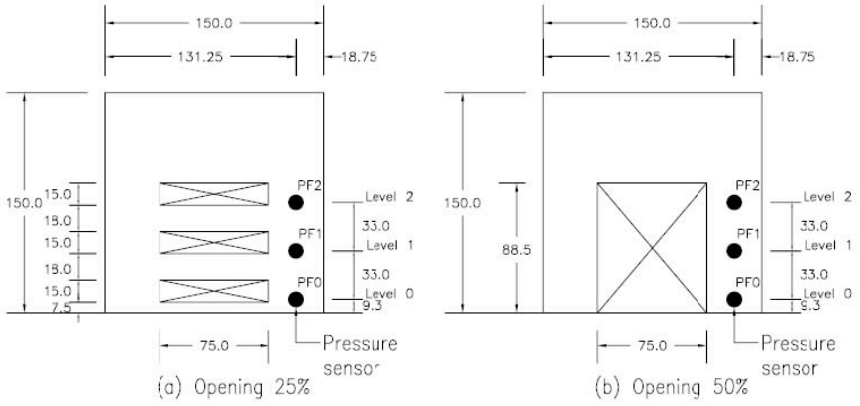

Figure 2.5: Reproduction of Fig. 2. Configurations of the front and back panels of building model with sensor locations (Lukkunaprasit et al., 2009).

Table 2.5: Reproduction of of Table 1. Normalized pressure (Pi/ρ gh) at positions PF0, PF1 and PF2 – square model with different openings. PF0, PF1 and PF2 denote pressure sensor on the front face of model at levels 9.3 mm, 42.3 mm and 75.3 mm above the base, respectively (Lukkunaprasit et al., 2009).

	Nominal Wave height								
	40 mm			60 mm			80 mm		
Opening	PF0	PF1	PF2	PF0	PF1	PF2	PF0	PF1	PF2
0%	2.56	1.23	0.49	3.96	2.08	1.11	4.36	3.10	2.30
25%	2.80	1.04	0.33	4.56	2.04	1.19	4.61	2.71	2.14
50%	2.99	1.16	0.13	4.94	1.93	1.26	4.66	3.07	2.40

Table 2.6: Reproduction of of Table 2. Tsunami Force (N) on square model with different opening configurations. Values in parentheses are percentage of the model without openings (Lukkunaprasit et al., 2009).

	Nominal Wave height		
Opening	40 mm	60 mm	80 mm
0%	6.8 (100%)	18.1 (100%)	37.9 (100%)
25%	5.1 (75%)	15.5 (85%)	31.5 (83%)
50%	4.3 (63%)	11.2 (62%)	26.2 (69%)

Conclusions

The structures with openings allowed water to flow into and through the specimens, thus reducing the total force experienced by the specimen.

2.2.3 Andersen et al. (2010) Wave Runup on Slender Pile

Objective

Andersen et al. conducted wave flume experiments to determine the expected pressures and loads on a slender piles representing the base of wind turbines off the coast of Denmark (2010). The experiments investigated the influence of wave height to water depths (H_{m0}/h) and water depth to pile diameter (h/D) ratios.

Test Program

The test program involved 12 test conditions with two different types of waves. The H_{m0}/h and h/D ratios were varied according to the conditions in Table 2.7. The two wave types tested irregular (broken) waves with two steepnesses for the leading toes. Andersen et al. also ran tests with unbroken waves, but focused on the irregular wave results in this report. The test bathymetry was selected to match the sea floor surrounding the off shore wind turbines of interest.

Table 2.7: Reproduction of of Table 1. Irregular test conditions (Andersen et al., 2010).

	$D = 0.10$m; $h = 0.20$m ($h/D = 2$)	$D = 0.10$m; $h = 0.30$m ($h/D = 3$)	$D = 0.10$m; $h = 0.40$m ($h/D = 4$)
$H_{m0}/h = 0.35$	$H_{m0} = 0.070$m	$H_{m0} = 0.105$m	$H_{m0} = 0.140$m
$H_{m0}/h = 0.40$	$H_{m0} = 0.080$m	$H_{m0} = 0.120$m	$H_{m0} = 0.160$m
$H_{m0}/h = 0.43$	$H_{m0} = 0.086$m	$H_{m0} = 0.129$m	$H_{m0} = 0.172$m
$H_{m0}/h = 0.46$	$H_{m0} = 0.092$m	$H_{m0} = 0.138$m	$H_{m0} = 0.184$m

Test Setup

The pile was placed 56 ft (17m) from the wave maker, with very minimal bathymetry variation between the two. The diameter of pile for all tests was 4 inches (0.1m) and the height was 3.64 ft (1.11m). Wave gauges were placed around the front of the pile, as shown in Figure 2.6. Additional

wave gauges were located near the wave maker, and on the side of the flume near the specimen. The pile was fixed at the bottom and top to the flume and a cross bar.

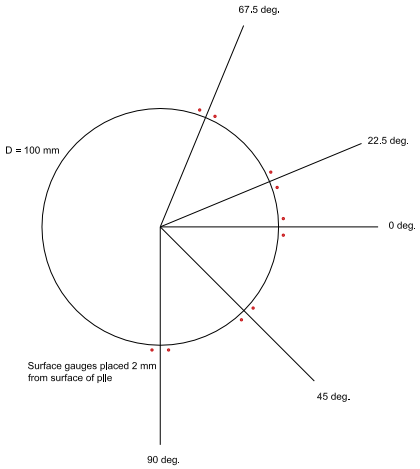

(a) Partial Reproduction of Fig. 5. Run-up model.

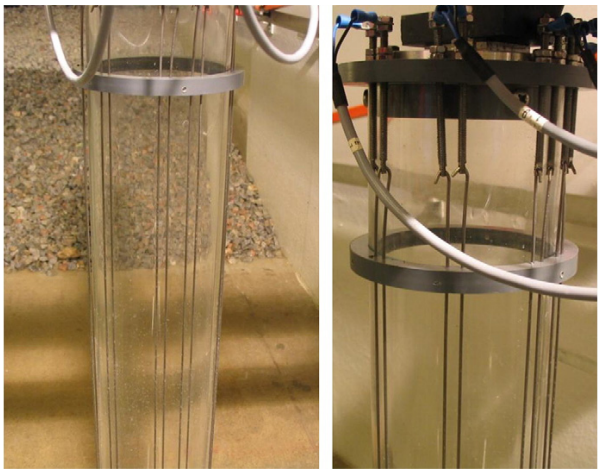

(b) Reproduction of Fig. 4. Pictures of the run-up model.

Figure 2.6: Reproductions of specimen and wire wave gauge locations (Andersen et al., 2010).

Test Results

Results for wave run-up matched well with an equation developed previously ($R_{u,2\%} = \eta_{max,2\%} + m \cdot \frac{u_{2\%}^2}{2g}$), demonstrated in Figure 2.7. Deeper water generally resulted in higher run-up, but there was no clear correlation between wave height and run-up. Despite this correlation, visual observations of the run-up suggest the measured run-up values were low.

Conclusions

Andersen et al. concluded that "the run-up results showed that the empirical run-up factor is highest for waves with low steepness" (2010). Further investigation is needed to more accurately measure the run-up, and then develop a new factor for the corrected measurements. Andersen et al. recommends the use of a high speed camera to record the run-up height (2010).

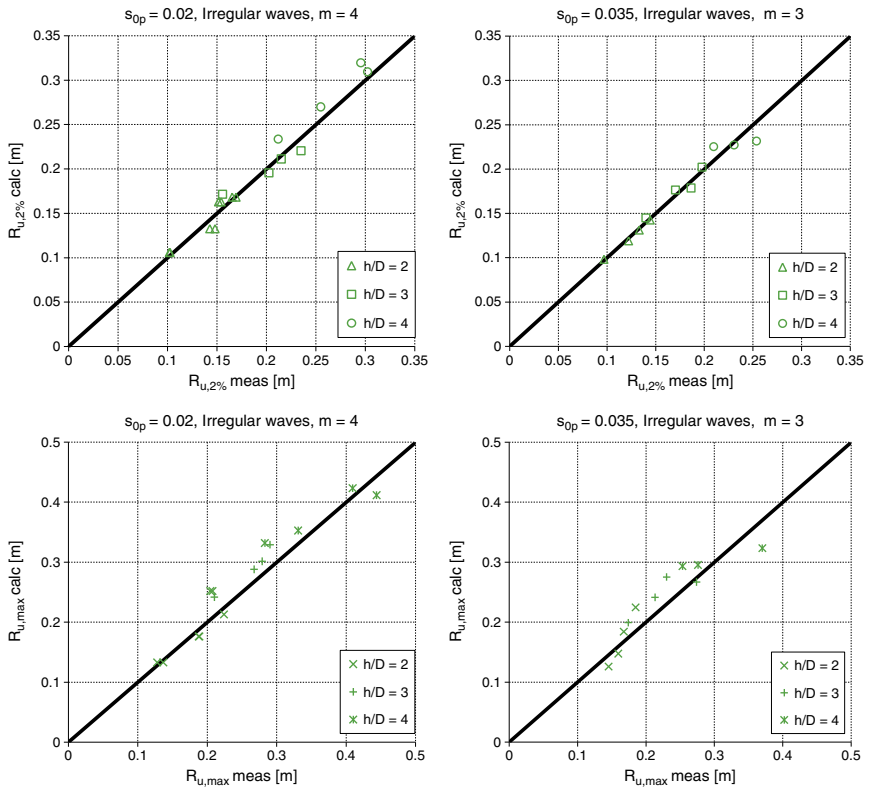

Figure 2.7: Reproduction of Fig. 7. Evaluation of Eq. for 2% and maximum run-up heights using $m = 4$ for $s_{0p} = 0.02$ and $m = 3$ for $s_{0p} = 0.035$. Stream function theory is used with $H = H_{2\%}$ for $R_{u,2\%}$, $H = H_{max}$ for $R_{u,max}$ and $T = T_p$ for both cases (Andersen et al., 2010).

2.3 CFST to Braces and Beams Connections

This section presents six papers on CFSTs and CFST column to brace and beam connections. Each subsection is broken into (1) objective; (2) test program; (3) test setup; (4) test results; and (5) conclusions.

2.3.1 Roeder et al. (1999) CFST Composite Action

Objective

Roeder et al. conducted a series of tests to determine the bond stress transfer between the steel tube and concrete core of a concrete filled tube (1999). The tests specifically examine the stresses associated with braced frame and moment frame seismic connections. SAP90 and ANSYS models were used to determine areas of high stress on prototype structures. Stress demand was highest in connections that did not penetrate into the concrete fill. Additionally, braced frame systems experienced higher stress demand in the regions identified in Figure 2.8, due to the transfer of the vertical component in the brace into the column (Roeder et al., 1999).

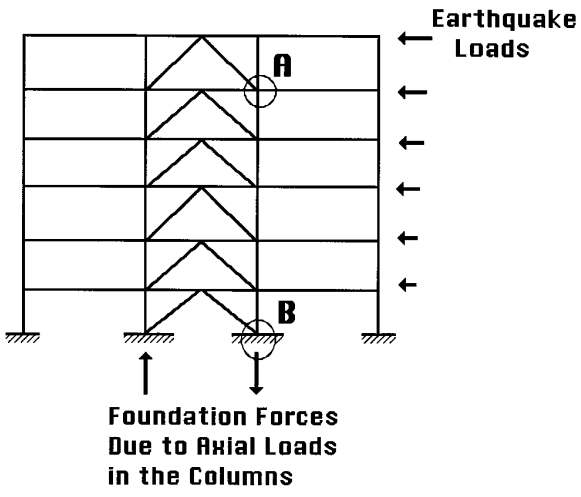

Figure 2.8: Reproduction of Fig. 2. Critical Locations in CFT Braced Frame System (Roeder et al., 1999).

Test Program

The experimental program involved adjusting (a) the diameter of the concrete core; (b) the wall thickness of the steel tube; and (c) the shrinkage of the concrete core. The steel tube diameters varied between 250 mm and 650 mm, and d/t ratios ranged between 20 and 110.

Test Setup

Strain gauges were placed on the steel tube in the arrangement in Figure 2.9. The slip between the concrete was measured with a potentiometer, while the Baldwin hydraulic testing machine applied a vertical load on the specimen. The concrete had approximately 50 mm gap at the bottom of the specimen to accommodate the slip.

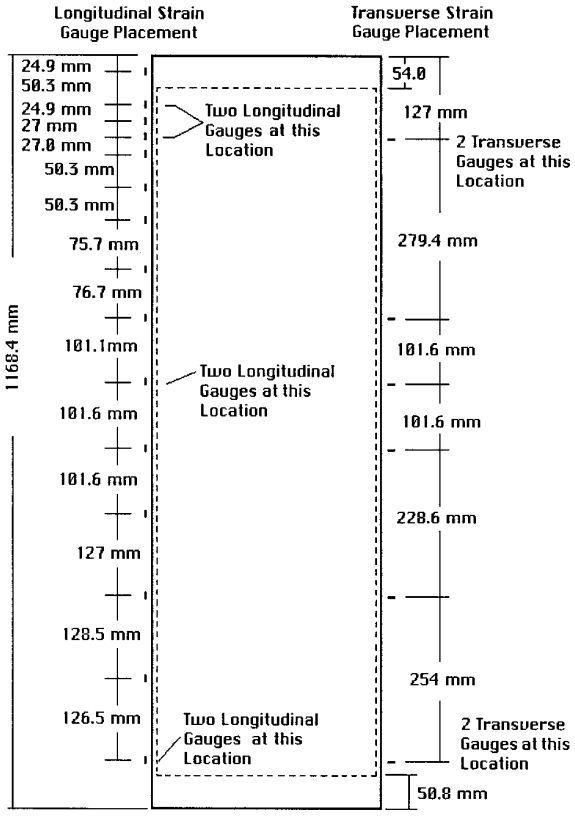

Figure 2.9: Reproduction of Fig. 7. Typical Strain Gauge Spacing (Roeder et al., 1999).

Test Results

Specimens with less shrinkage achieved a higher ultimate load capacity. Once ultimate load was reached, the concrete moved with rigid body characteristics, with some friction on the tube walls. Specimens with small bond stress capacity had negligible tangential strains. Tests with eccentric loading maintained an average bond stress of 123% and 252% of the comparable tests. Linear regression from Figure 2.10 suggests that d/t ratio of greater than 80 cannot reliably produce enough bond strength.

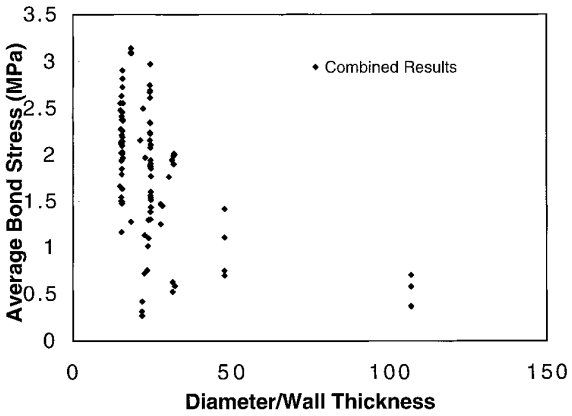

Figure 2.10: Reproduction of Fig. 11. Bond Stress for CFT as Function of d/t Ratio (Roeder et al., 1999).

Conclusions

After slip, bond stress is uniform over slipped region. Previous tests reviewed suggest the strength of concrete does not significantly relate to bond stress capacity. Bond stress capacity is reduced by large d/t ratios. Large diameter tubes can have large shrinkage, essentially eliminating any bond stress capacity. At ultimate load, bond stress is distributed evenly around tube. Other papers suggest having deformations on the inside of tube benefits bond strength. Roeder et al. (1999) determined that large d/t tubes are not stiff enough for this to make a difference.

2.3.2 Schneider et al. (2004) CFST Column to Beam Connection

Objective

Schneider et al. preformed experiments on two types of CFST column to beam connections (2004). The hysteretic behaviour of each was compared to identify the seismic performance of the connections. Additionally, constructability concerns were addressed for each.

Test Program

The two connections tested in the program are generally identified by (a) the beam being welded directly to the steel tube of the column; and (b) the beam extending continuously through the steel and concrete column. Figure 2.11 shows the two connections.

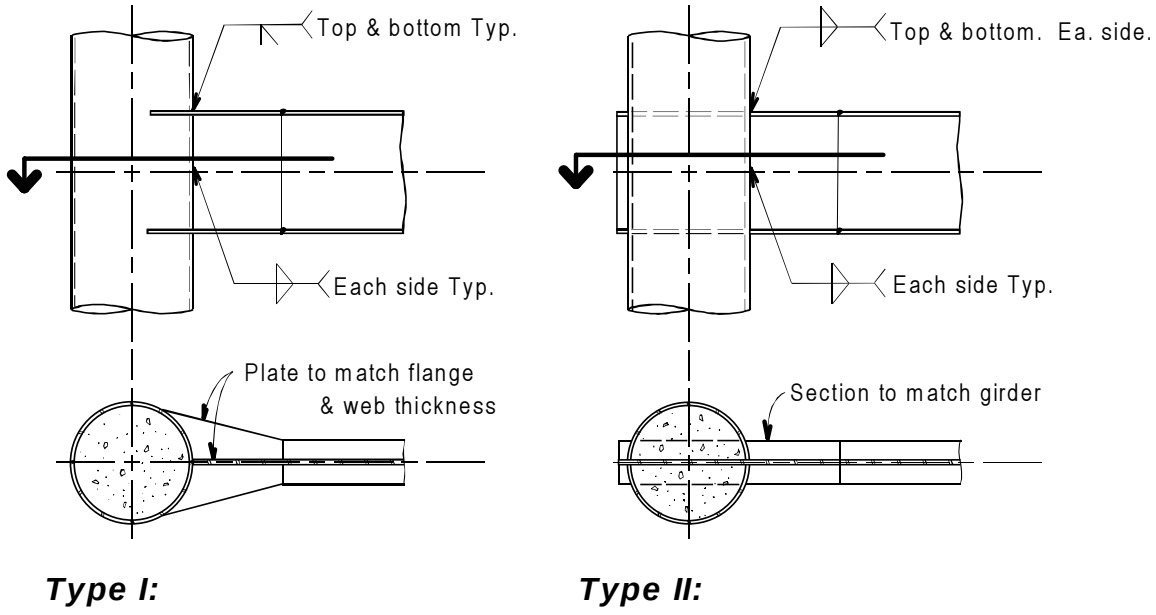

Figure 2.11: Reproduction of portion of Figure 1. Inelastic Moment-rotation Behaviour of Tested CFT Joints (Schneider et al., 2004).

Test Setup

The type I connection consists of a wide flange beam with a plate extended onto each flange and the web to fit curved perimeter of CFST column. The plates are welded to the column and the beam. The type II connections consist of a wide flange that extends through the column. A rectangular section was cut out of both sides of the steel tube to accommodate the beam. The spaces inside the web were then filled in with plate steel, to provide a sealed cavity for the concrete. Both CFST columns were 14 inch (0.36m) outer diameter with 1/4 inch (6.35) wall thickness. The beam used was a W14x38 section.

Test Results

The type II connection exhibited stable inelastic behavior, with rotations twice the type I connection. No concrete crushing observed in the type II connection. The type I connection experienced local distortions in the steel pipe, and tearing at the tips of the flange towards the web. The difference in rotation and moment capacity is illustrated in Figure 2.12.

Conclusions

The results from the specimens demonstrate that CFST connections that allow the beam to fully pass through the column vastly outperform connections that only engage the skin of the CFST column. The connection options examined highlight the option of having the connections fabricated in the shop, so field welds are only necessary to splice the connection to the beams. One difficulty with the beams that pass through the column, is the method of compaction in the lower levels of the column. Schneider et al. (2004) recommends using a self-consolidating-concrete mix to alleviate some of these concerns. Additionally, the ACI 3-18 methods of calculating design capacity provided more strength in the connection than the methods laid out in the AISC/LFRD provisions (Schneider et al., 2004). Finally, "Joint equilibrium requires a distribution of load between the steel tube and the concrete core. Joint equilibrium is highly dependent on the geometry of the CFST column and the wide-flange girder and must be considered in design" (Schneider et al., 2004).

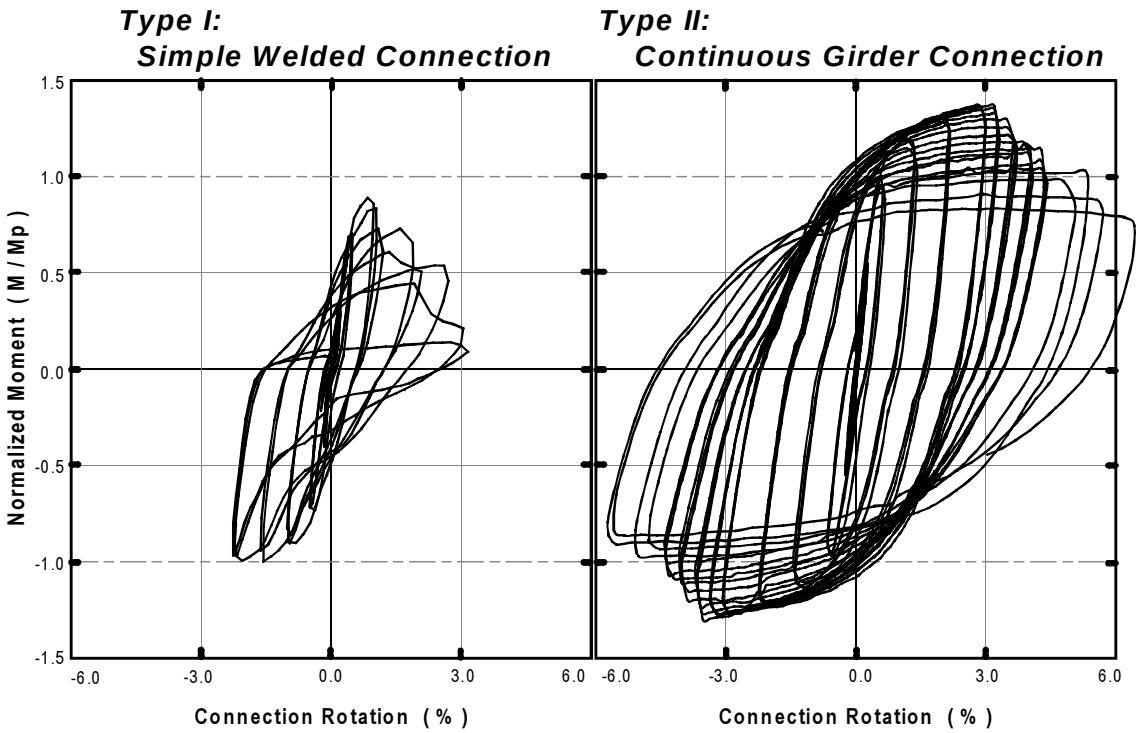

Figure 2.12: Reproduction of portion of Figure 1. Inelastic Moment-rotation Behaviour of Tested CFT Joints (Schneider et al., 2004).

2.3.3 Sheet et al. (2013) CFST Column to Beam Connection

Objective

Sheet et al. conducted a series of tests to examine the feasibility of through ties to connect beams to square and round concrete filled steel tubes (2013). Specifically, the team tested the possibility of bolted connections to avoid field welding, and a stiffening method to move the yielding zone away from the column face (Sheet et al., 2013).

Test Program

The interior joint of a portal frame was tested, with square and round CFSTs. Two types of connection were tested for each column type. The first involved bolts passing through the columns to tension the beams to the column. The second connection utilized a through beam that extended through the column. An outline of the beam was cut through the column in the shape of the beam instead of an entire rectangle being cut out, as in Schneider et al. (2004) tests. The four connections are shown in Figure 2.13 and Figure 2.14.

Test Setup

Each specimen was placed in a hydraulic actuator frame and subjected to cyclic loading of the beams in addition to axial load in the column, as shown in Figure 2.15. Vertical displacements of the beam were measured with the laser sensors in Figure 2.15. Strain gauges were instrumented on the through rods and bolts and the continuous beam in the column. The panel zone shear deformation was recorded with LVDTs across the zone.

Test Results

Results from the test are summarized in Table 2.8. The deformation mode in all four specimens was beam hinging just past the connection stiffening elements. The failure observed was buckling then fracture of the flanges and web (Sheet et al., 2013). Specimen 3, the square CFST with the through beam, experienced the largest plastic rotations and energy dissipation. The rotation and displacement envelope curves are shown in Figure 2.16.

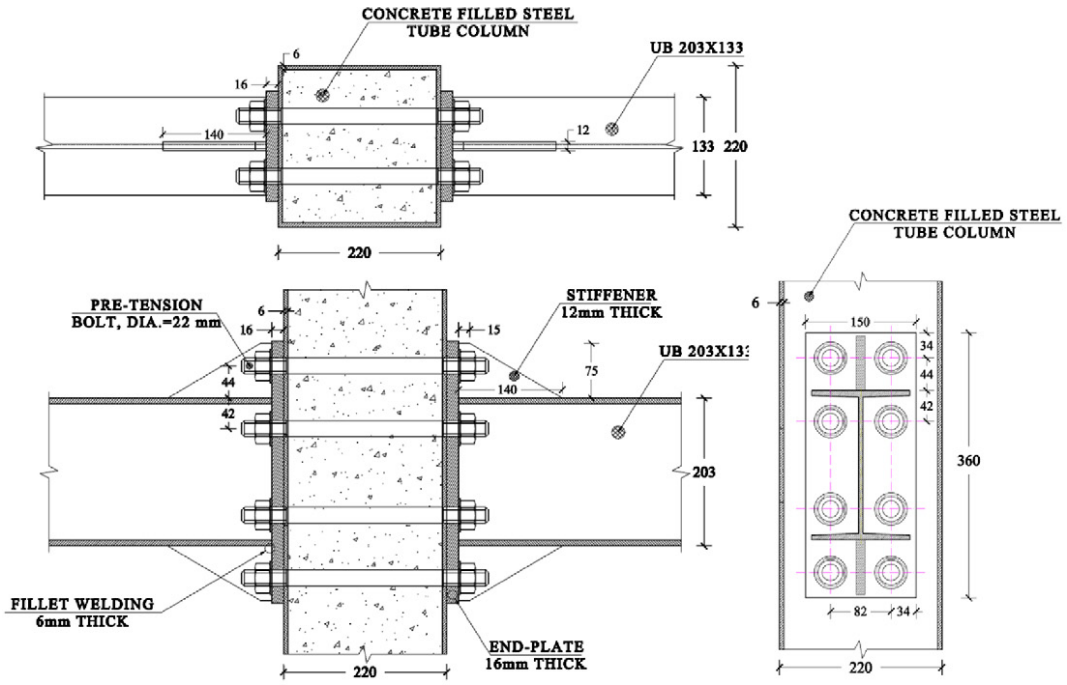

(a) Flat End-plate connection (Specimen No.1)

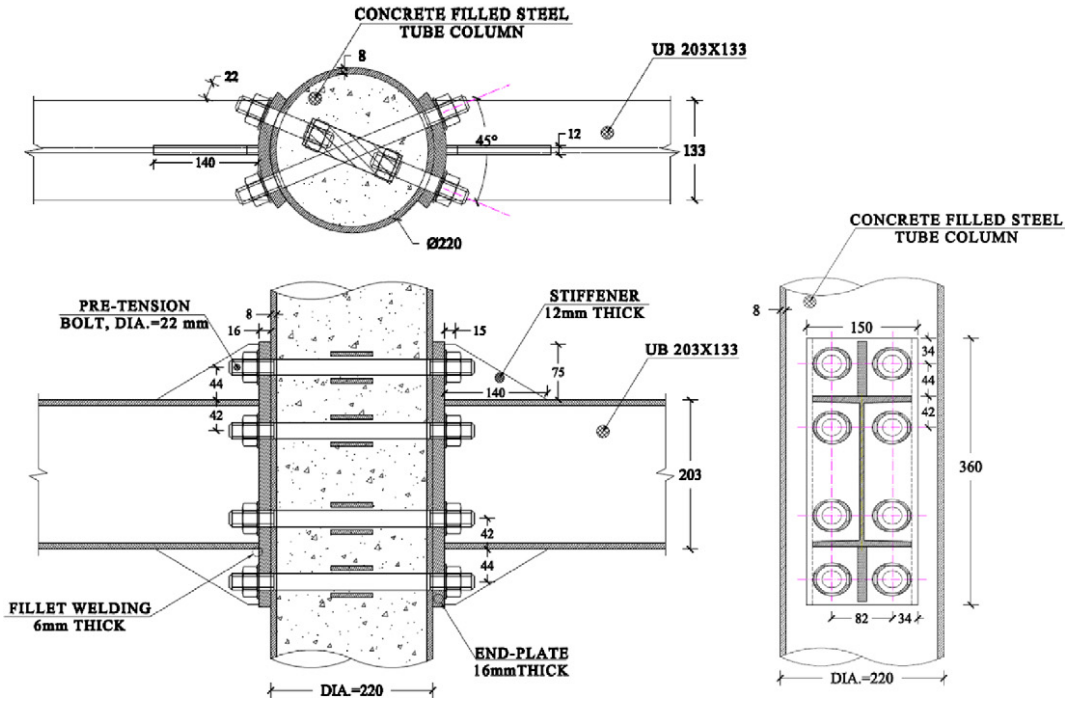

(b) Curved End-plate connection (Specimen No.2)

Figure 2.13: Reproduction of Fig. 2. Details of end-plate type connections (Sheet et al., 2013).

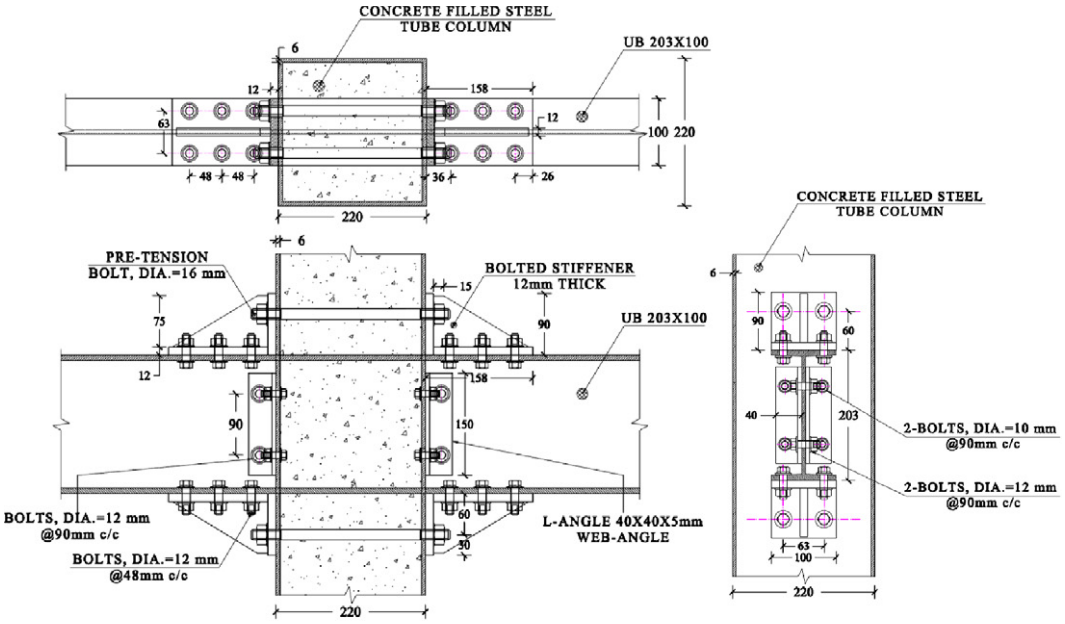

(a) Square CFT column with through beam connection (Specimen No.3)

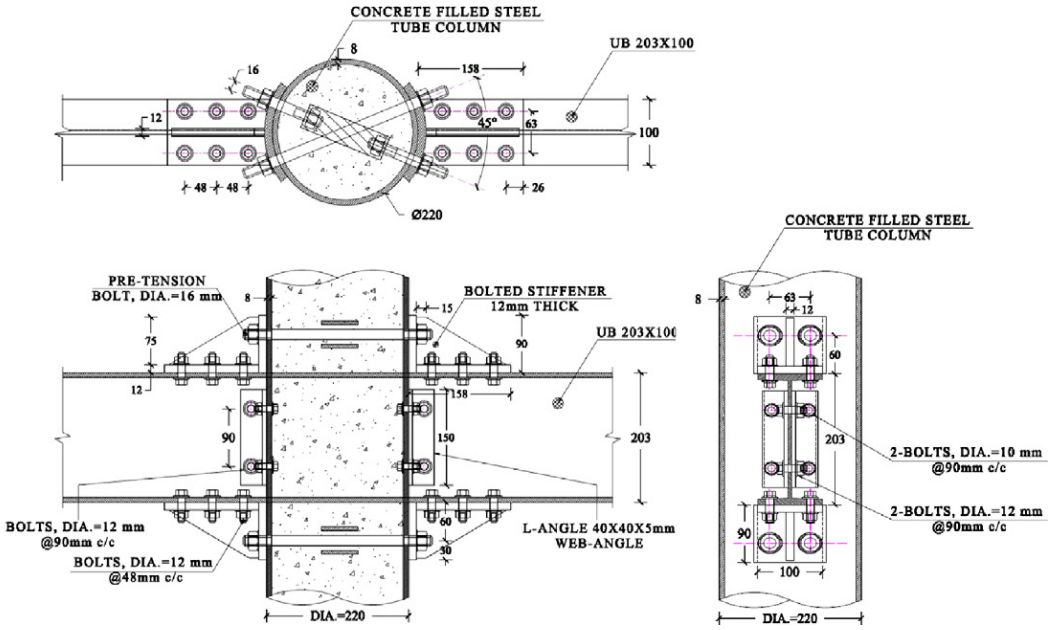

(b) Circular CFT column with through beam connection (Specimen No.4)

Figure 2.14: Reproductions of Fig. 4. Details of through beam type connections (Sheet et al., 2013).

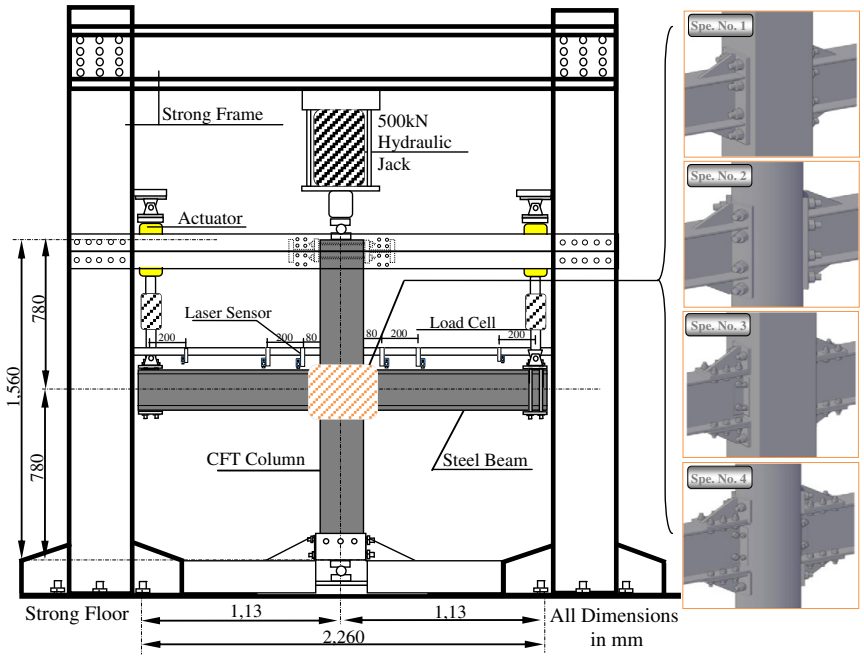

Figure 2.15: Reproduction of Fig. 6. Test set-up (Sheet et al., 2013).

Table 2.8: Reproduction of Table 4. Summary of the test results (Sheet et al., 2013).

Unit Description	Plastic Moment $M_p(kN.m)$	Max. test flexural moment (kN.m)		The ratio of M_{test}/M_p		Max shear V_c (kN)		ult. rotation angle θ_u	Inelastic deformation mode
		$+M_{test}$	$-M_{test}$	$+$	$-$	$+V_c$	$-V_c$		
Specimen No. 1	95.50	126.10	118.96	1.32	1.25	172.98	179.13	0.054	Beam hinging
Specimen No. 2	95.5	127.68	131.29	1.34	1.37	175.77	181.57	0.054	Beam hinging
Specimen No. 3	75.26	144.28	115.79	1.52	1.54	158.02	161.18	0.177	Beam hinging
Specimen No. 4	75.26	115.09	108.40	1.53	1.44	162.03	157.72	0.0591	Beam hinging

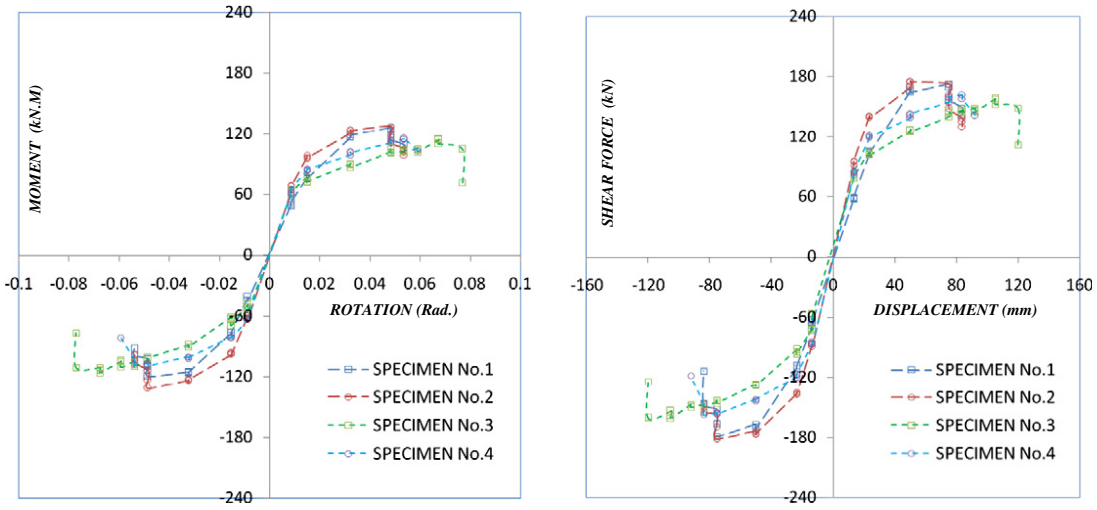

(a) Moment-beam rotation enbelope (b) Column shear force-displacement envelope

Figure 2.16: Reproduction of Fig. 12. Envelope curves for beams and columns of all the tested specimens (Sheet et al., 2013).

Conclusions

Both connection types successfully experienced drift ratios greater than 5% and produced plastic hinges away from the CFST surface (Sheet et al., 2013). Energy for all four specimens was dissipated trough the beam yielding, because the panel zone was strong in comparison. The through rods in the type I specimens transferred the load through the concrete and limited damage in the column tube. The square and round CFST columns performed similarly.

2.3.4 Hassan et al. (2013) CFST Column to Brace Connection

Objective

Hassan et al. conducted a series of tests to determine the characteristics and failure modes of different gusset plate connections to CFST columns (2013). The tests cyclically were broken into two series, one loaded the gusset plates parallel to the column and the other loaded the connection perpendicular to the column.

Test Program

Hassan et al. tested 12 specimens total, with different plate to column connection details. The plan view of the connections are shown in Figure 2.17. Detail type 4 was considered the most basic, so it was tested with concrete fill and without concrete fill. All other specimens were filled with concrete. Each connection type was tested in two principal directions, perpendicular to the column, and parallel to the column. The test matrix is provided in Table 2.9.

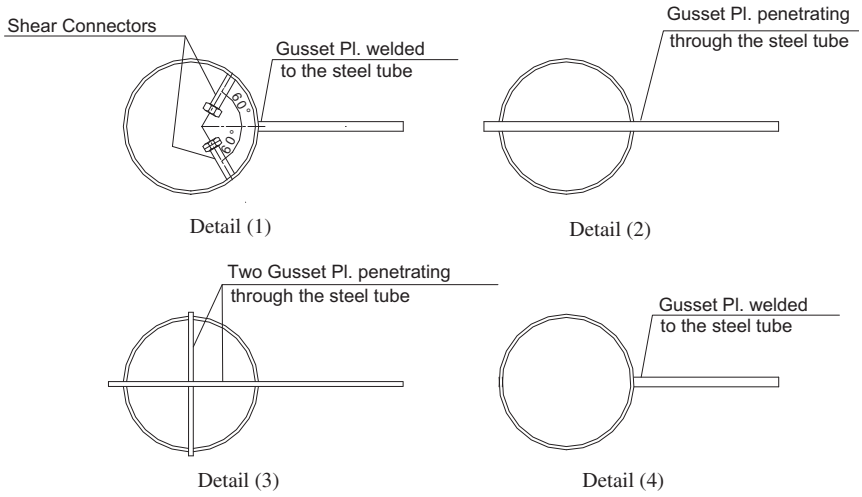

Figure 2.17: Reproduction of Fig. 1a. Configuration of different studied connection details (Hassan et al., 2013).

Test Setup

Ten of the CFST columns are pipes with a 114.3mm outer diameter and a wall thickness of 3mm. Two specimens were tested with an outer diameter of 168.3mm and wall thickness of 5mm. Each specimen was instrumented with strain gauges on the outside of the CFST to record the axial and hoop strain. Deflections in the CFST column were recorded with LVDTs along the column and gusset plate. The loading apparatus and LVDT locations are shown in Figure 2.18. The loading procedure cyclically loaded the specimen between zero and the target load. The target load increased by five kN increments each cycle.

Table 2.9: Partial reproduction of of Table 1. Test unit summary of properties (Hassan et al., 2013).

Test group	Detail number	Test unit	D (mm)	t (mm)	concrete infill	Loading direction
A	1	SP-H1	168.3	5	Filled	Perpendicular
	2	SP-H2	168.3	5		(horizontal)
B	1	H-1	114.3	3	Filled	Perpendicular
	2	H-2				(horizontal)
	3	H-3				
	4	H-4				
	4	H-5			None	
C	1	V-1	114.3	3	Filled	Parallel
	2	V-2				(vertical)
	3	V-3				
	4	V-4				
	4	V-5			None	

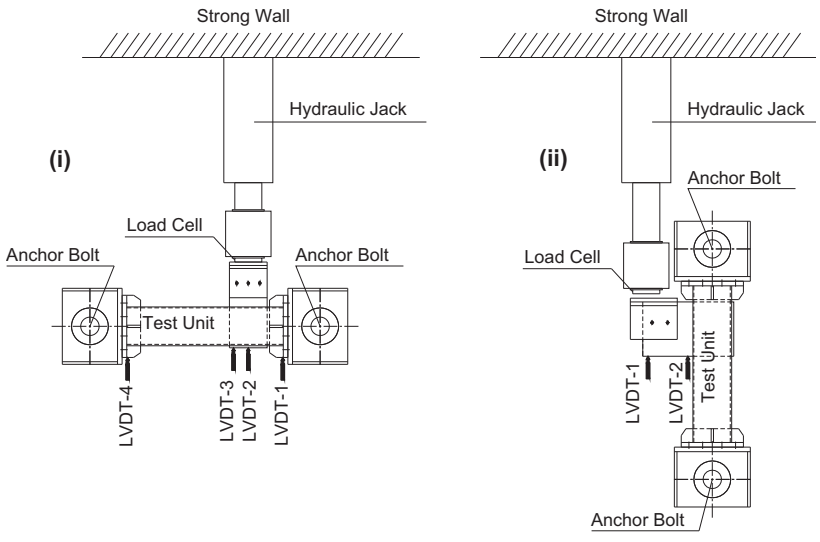

Figure 2.18: Reproduction of Fig. 1d. Test setup for loaded specimens: (i) perpendicular direction and (ii) parallel direction (Hassan et al., 2013).

Test Results

Specimens with the gusset plate only welded to the CFST column retained the lowest stiffness and experienced deformation of the steel tube underneath the gusset plate. Specimens with an embedded gusset plate retained a much higher stiffness, and typically failed with tearing of the steel tube. The two specimens without concrete infill experienced large plastic deformations, and a sudden loss in stiffness.

Conclusions

Concrete filled tubes retained significantly larger capacity, 55% and 74% when loaded parallel and perpendicular to the column respectively, compared to connections without concrete infill (Hassan et al., 2013). In the tests loaded perpendicular to the column, specimens with the gusset plate directly welded to the CFST experienced a larger ultimate load, compared to connections with the gusset plate embedded in the concrete. When loaded parallel to the column, specimens with the embedded gusset plate had a larger ultimate strength, than the flush welded specimens. "This indicates that the behavior of connections depends to some extent on the inclination of the brace force" (Hassan et al., 2013). Finally, when loaded perpendicular to the column, the four connection type stiffnesses were fairly similar. However, when loaded parallel to the column, connections with embedded gusset plates experienced larger stiffness values.

2.3.5 Xu et al. (2014) CFST Column to Brace Connection

Objective

Xu et al. conducted experiments to characterize the behavior of CFST column to brace connections in tension. Columns, beams and braces are round concrete filled tubes (2014). "The chord wall deformation, ultimate strength, and observed failure modes of test specimens were reported" (Xu et al., 2014).

Test Program

The test program consisted of four main types of connection: T-, Y-, K-, and KT-connections. Each connection type was tested with two column D/t ratios, $D/t = 60$ and $D/t = 75$. The column

outer diameters were nominally 300mm, and wall thicknesses were 4.18mm and 5.01mm. The brace outer diameters were nominally 133mm and wall thicknesses were 6.08mm.

Test Setup

The braces/beams were welded to the columns in the four connection types. The 28 day concrete strength was 46.9MPa, from 150mm cube samples. The column was mounted horizontally, as shown in Figure 2.19a, or at an angle, as shown in Figure 2.19b, so that the beam/brace was oriented vertically. The actuator pulled the beam/brace vertically, so the beam/brace was in tension, demonstrated in Figure 2.19. The vertical displacement of the column was recorded with displacement transducers.

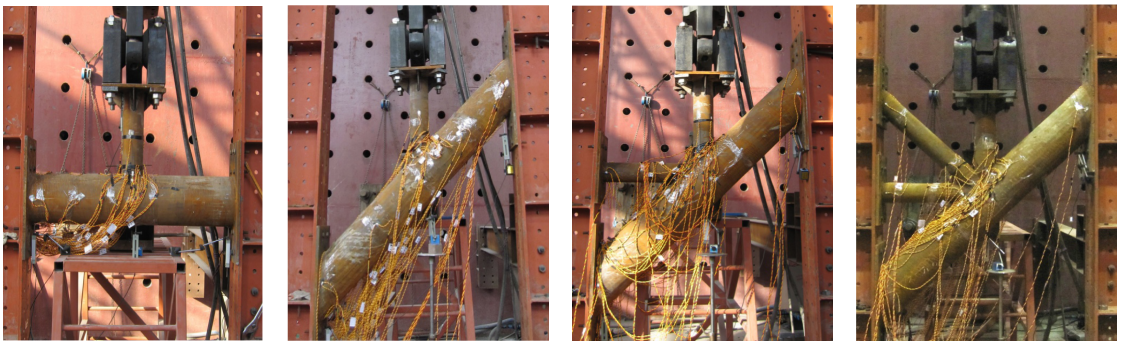

(a) T-connection (b) Y-connection (c) K-connection (d) KT-connection

Figure 2.19: Reproduction of Fig. 1. Test setup (Xu et al., 2014).

Test Results

The T-,Y-,K- connections experienced a brittle punching shear failure of the chord wall at the toe of the weld (Xu et al., 2014). The KT- connections maxed out the capacity of the actuator, and no visible yield lines were present. However, the strain gauge measurements indicated the brace was yielding. As expected, for each connection type, specimens with a lower D/t ratio were stiffer and experienced a higher ultimate load capacity than specimens with a higher D/t ratio. In general,

the T-connections had a lower capacity than the Y-connections. The load to deformation plots for the T- and Y-connection specimens are shown in Figure 2.20.

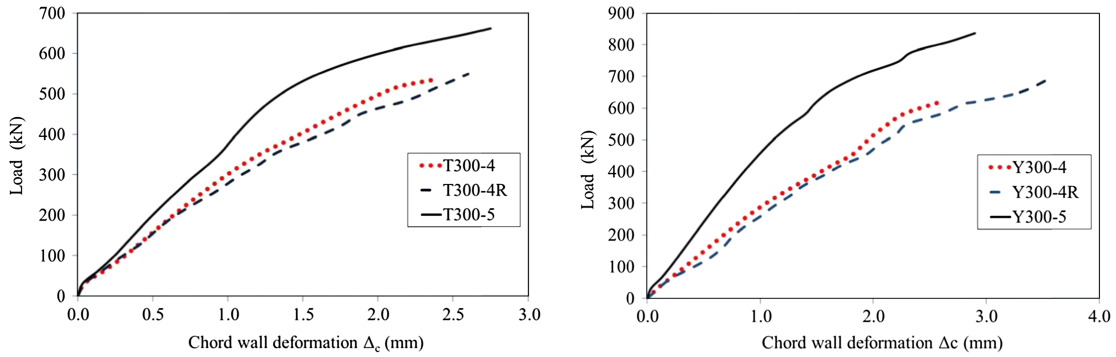

(a) Chord wall deformation versus load curve for T-connections

(b) Chord wall deformation versus load curve for Y-connections

Figure 2.20: Load-deformation curves of CFST column. Reproductions of Fig. 3. and Fig. 4.(Xu et al., 2014).

Conclusions

The test results show that under axial loading of the beams/braces, CFST columns with D/t ratios of 60 and 75 have enhanced load capacity. The concrete serves to preserve the position of the steel tube, thus increasing the axial load, until the limit state of punching shear yielding is reached. Further calculations show that the AISC design requirements adequately calculate the limit state of punch shear yielding for T-, Y-, and K-connections (Xu et al., 2014).

2.3.6 Yang et al. (2019) CFST Column to Brace Truss

Objective

Yang et al. conducted a series of tests on CFST truss tower specimens subjected to cyclic lateral loading (2019). The investigation explored the hysteretic behavior of specimens under the effect of axial loads, concrete filled vs. hollow tubes, and width to thickness ratios. The approximate

scale was 1:8 “to the prototype ribs of typical arch bridges” (Yang et al., 2019). This results in a specimen height of 2m and center to center spacing for the columns of 320mm.

Test Program

The test program consisted of eight specimens with two wall thickness to width ratios for the columns. The cross brace dimensions were the same for all specimens. Two control specimens were not filled with concrete, while all six other specimens were filled with a self consolidating concrete mix with 28 day strength of 55.2MPa. Only the columns were filled with the SCC; the round braces were left unfilled. The axial load applied to the specimens varied for each specimen and is tabulated in Table 2.10.

Table 2.10: Partial reproduction of of Table 1. Information of the specimens (Yang et al., 2019).

No.	Specimen label	β (width-to-thickness ratio)	n (axial compression ratio)
1	Steel-A-0.25	55.6	0.25
2	Steel-B-0.25	28.6	0.25
3	CFST-A-0.05	55.6	0.05
4	CFST-A-0.25	55.6	0.25
5	CFST-A-0.5	55.6	0.5
6	CFST-B-0.05	28.6	0.05
7	CFST-B-0.25	28.6	0.25
8	CFST-B-0.5	28.6	0.5

Test Setup

The specimens were subjected to constant vertical axial load while cyclic horizontal displacements were induced by a horizontal actuator. The vertical actuator was placed on a roller trolley system to ensure the load was always acting vertically on the top of the specimen. The actuator and specimen system is shown in Figure 2.21. No out of plane restraint was provided in the set up; however, out of plane displacement was recorded at the top of the specimen. Additionally, displacement

transducers were placed along the vertical face of one of the columns, in the loading direction. Strain gauge and LVDT placement is identified in Figure 2.22.

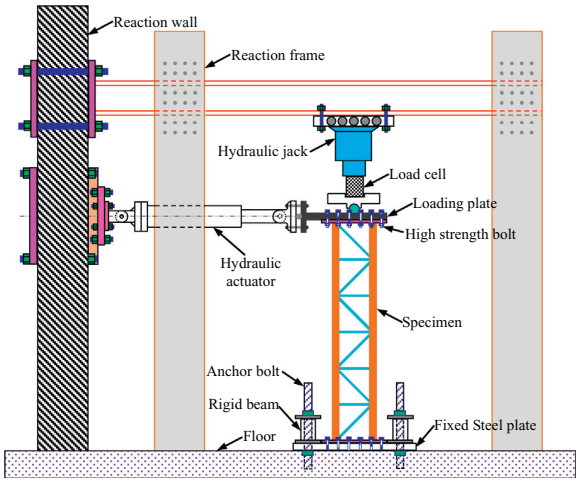

Figure 2.21: Reproduction of Fig. 2. A general view of the test set-up (Yang et al., 2019).

Test Results

Local tube buckling was observed at the bottom of the braces when the lateral force reached approximately 60% to 80% of the bearing capacity. Micro-cracks in the welding in the front K-connections also developed. Specimens with concrete filled tubes delayed the propagation of these failures compared to the hollow specimens. At failure, the concrete core at the base of the bottom connection was found to be crushing. The concrete core helped delay the impacts of local buckling, resulting in better use of the plastic capacity of the steel tube. Most results matched the predictions of an ABAQUS model. Types of failure and locations approximately matched. The ABAQUS predicted hysteretic curves were smaller than the measured values. The force-displacement hysteretic curves for the tested specimens are shown in Figure 2.23.

Conclusions

Yang et al. concluded that CFST latticed specimens possess favorable load versus deformation hysteretic curves, when compared to the specimens without concrete infill. Additionally, "the

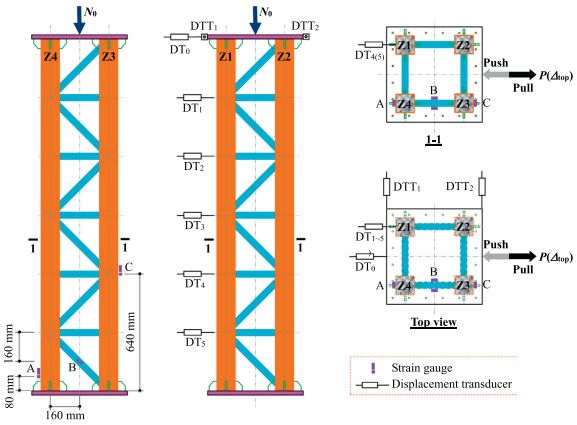

Figure 2.22: Reproduction of Fig. 3. Setting of displacement transducers and strain gauges (Yang et al., 2019).

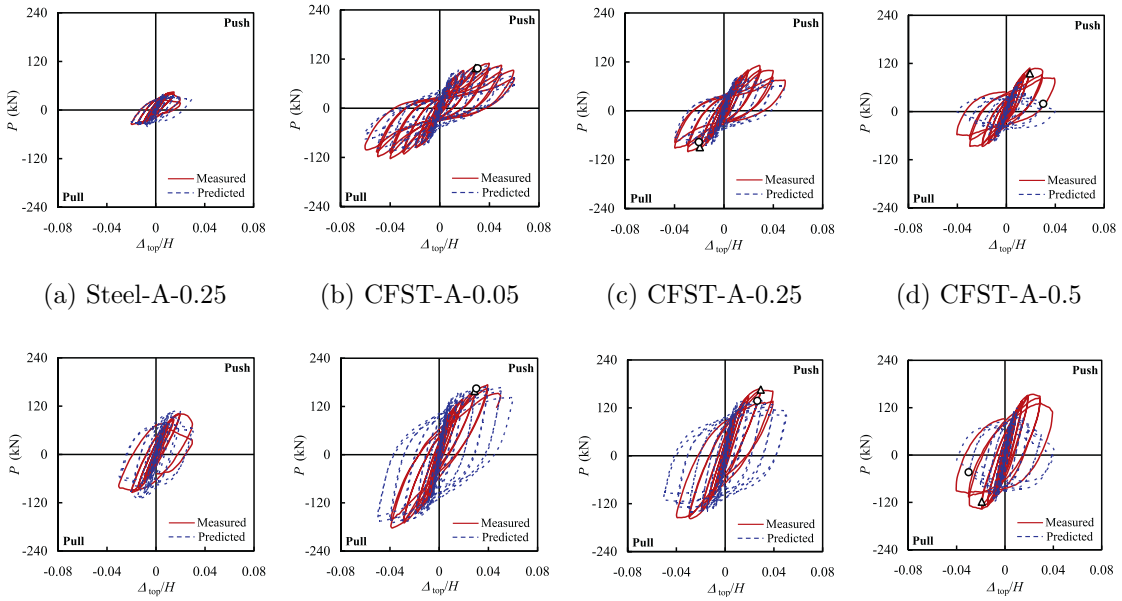

(a) Steel-A-0.25 (b) CFST-A-0.05 (c) CFST-A-0.25 (d) CFST-A-0.5

(e) Steel-B-0.25 (f) CFST-B-0.05 (g) CFST-B-0.25 (h) CFST-B-0.5

Figure 2.23: Reproduction of Fig. 9. Lateral force (P) versus top lateral drift (Δ_{top}/H) hysteretic curve of the specimens (Yang et al., 2019).

lateral displacements along the height of all specimens is similar to ... a frame-bracing" system (Yang et al., 2019). The CFST specimens retained better weld performance at the connections along the height, compared to the hollow tubes, but experienced concrete crushing at the base of the specimen at failure. Finally, within the CFST specimens, specimens with a lower D/t ratio had a higher bearing capacity, initial stiffness, and ductility index (Yang et al., 2019).

Chapter 3

PRELIMINARY DESIGN

This chapter examines

3.1 OpenFOAM based Experiment Design

In support of Pyke (2020) and this thesis, a series of preliminary OpenFOAM models were developed to aid in the design of the physical experiments. These models helped influence and validate design assumptions. This section outlines the study on location and slope of the bathymetry between the wave maker and the specimens, selection of the specimen location, the influence of the OpenFOAM model on instrument location on the specimen, and preliminary force estimates for both the shear wall specimen tested in Pyke (2020) and the CFST specimen.

3.1.1 Rough Parametric Study on Location and Slope

The goal of the parametric study was to understand the relationship of ramp location and steepness on the height of the wave when it impacts the structure. To achieve this, OpenFOAM models were run with many ramp configurations. Ramp steepnesses included rise:run ratios of 2:2, 2:5, 2:10, 2:20, and 2:30. These ramp ratios were tested at several locations along the length of the flume. The top of the ramp was initially placed in 10 meter intervals from the midpoint of the compressible mesh. This point corresponds with the neutral position of the wave maker paddle in the wave flume.

The goal of this exercise was to isolate the configuration in the flume with the largest wave that impacts the specimen. "Largest" was defined as the tallest wave height at the top of the ramp, so the entire front face of the specimen would be engaged. Solitary waves were the primary focus of this series of models because they are repeatable in the physical wave flume. The still water depth was kept constant at 2 meters (6.56ft) to produce the largest stable wave possible. Two meters is the maximum wave depth in the flume due to the capacity of the waver maker actuators.

The results from this initial parametric study are shown in Figure 3.1. The location of the

top of the ramp plays a small role in the wave height. The farther down the flume the ramp is, the lower the height of the wave. According to solitary wave theory, this difference should be minimal or non existent because wave height is not a function distance traveled. The deviation from expectations in the simulation may be from friction, the turbulence model used, and any errors in the meshing. Perhaps more important than ramp location is ramp steepness. At any given point along the flume, the steeper the bathymetry, the taller the free surface elevation, for the same standard wave. This phenomenon can be explained by the momentum of the water particles being reflected upwards rather than slightly redirected and the change in local velocity, where the wave slows down downstream while building up upstream.

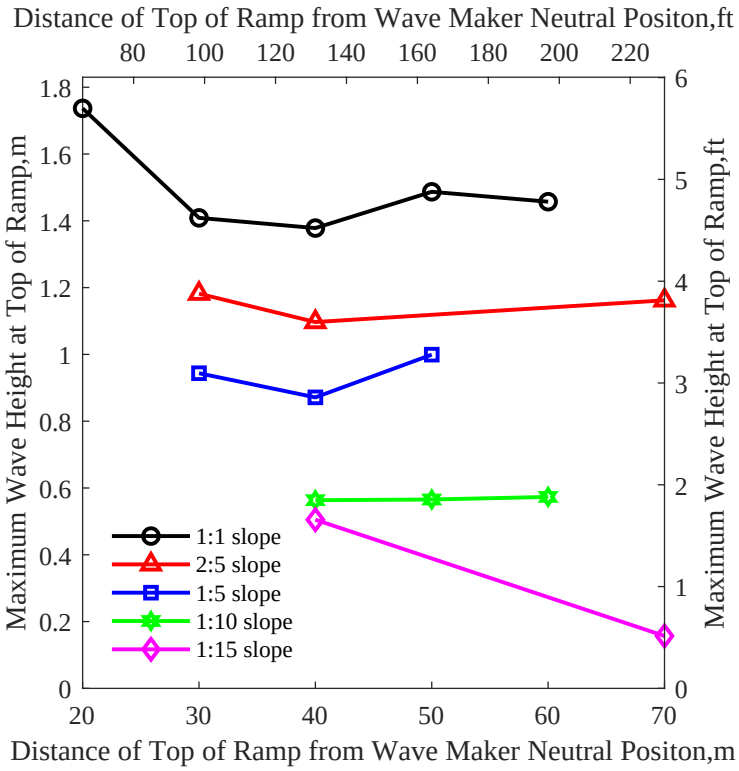

Figure 3.1: Wave height as a function of ramp steepness and location of the ramp in the flume. The distance from the wave maker plays a minor role in the decrease in wave height when compared to the role the slope of the ramp plays.

The structure cannot fit at the very top of the ramp, so wave height was also recorded one meter

(3.28ft) and two meters (6.56ft) horizontally from the top of the ramp. As shown in Figure 3.2, the wave height dramatically decreases the further away from the edge of the beach the structure is placed. This is not surprising because the wave breaks as it travels along the dry bathymetry, releasing energy and collapsing in height until it loses the defined wave shape. Therefore, the structure should be placed as close to the front of the beach as possible.

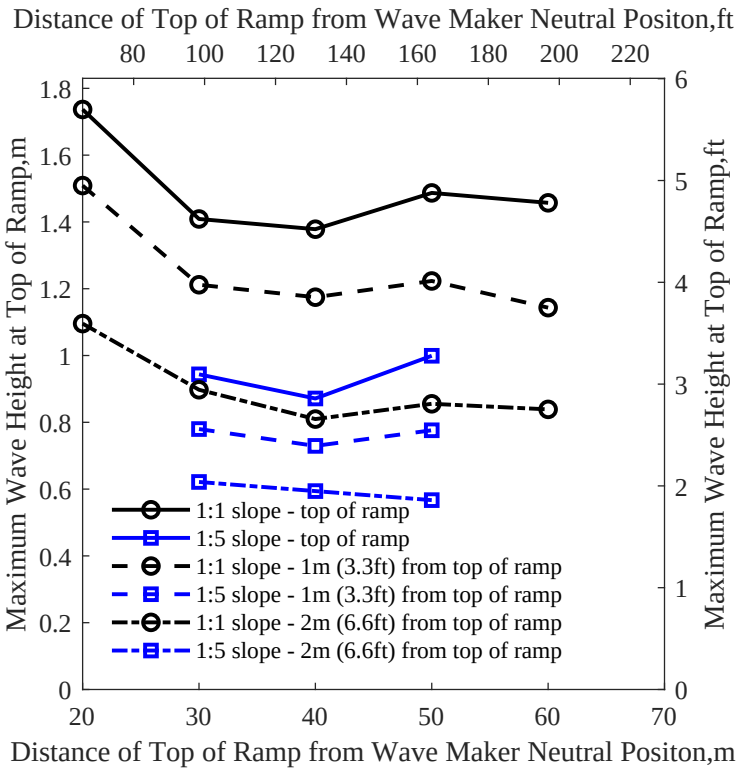

Figure 3.2: Wave height at possible structure locations on beach. As the specimen is moved further back from the top of the ramp, the wave height decreases. Two slope options are shown, the 1:1 slope, and the 1:5 slope. Even as ramp and specimen locations are moved to less desirable positions, wave height can be maximized by maintaining a steep slope.

3.1.2 Possible Locations within the Flume

As discussed in Section 4.1.1, the tie-down locations in the flume provide the constraints for the specimen and ramp locations and slopes. From the models in Section 3.1.1, the ramp and specimen

should be located close to the waver maker, and with a steep slope. With these guidelines, three locations and two ramp steepnesses were modeled. The top of the ramp was placed multiples of 12 feet (3.66m) from the waver maker to accommodate the tie-down points. The hypotenuse of the ramp was restricted to multiples of 12 feet (3.66m) so that the standard bathymetry slabs discussed in Section 4.1.2 could be used. With these constraints, three locations were examined: 72 feet (21.95m), 84 feet (m), and 96 feet (m) from the waver maker. Two ramps were modeled: a ramp composed of 1 panel, with a rise : run of 6.56 : 9.99, and a ramp composed of two panels, with a rise:run of 6.56 : 23.09.

3.1.3 Addition of the Structure

The OpenFOAM model of the specimen was developed concurrently with the actual ramp location and slope. The specimen was modeled as a rigid body within the flume. In reality, the structure will have some slight elastic deformations, however, these will be small, so a rigid body is an acceptable approximation. The dimensions of the concrete shear wall were known, so these values were used in OpenFOAM.

A more detailed discussion of the design and setup of the concrete wall specimen can be found in Pyke (2020). In brief, the specimen is a concrete shear wall scaled to approximately 1/6 of full size to fit within the wave flume. The specimen is 46 inches x 46 inches x 6 feet (1.17m x 1.17m x 1.83m) with five inch (12.7cm) walls and a hollow interior, as shown in Figure 3.3. The OpenFOAM model simplified this to a rigid body with outside dimensions the same as the specimen, and a closed over top. The specimen was created by inserting a non-porous plane for each side and the top. The edges and vertexes intersect to create a closed system with the modeled flume bathymetry. The structure was assumed to be centered in the flume, one meter (3.28ft) from the top of the ramp.

3.1.4 Instrument Location

Another goal of the initial OpenFOAM modeling series was to inform the placement of pressure sensors on the shear wall structure. There are a limited number of pressure sensors at the wave lab, so multiple layouts are needed to characterize the pressure field. Ideally, the entire specimen could be instrumented on all sides; however, this would take too long to be realistic, so an optimized

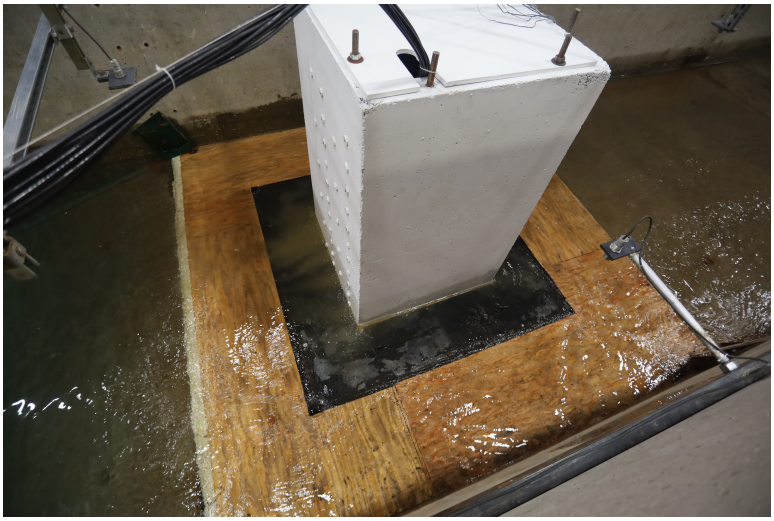

Figure 3.3: Concrete shear wall specimen instrumented in Oregon State University Large Wave Flume.

arrangement was needed. In OpenFOAM probes were placed in a tight grid on the front face of the specimen. Then with data from each of these points, different configurations were used to integrate the pressures to find the total force on the structure. Unsurprisingly, the best configurations involved pressure sensors close to the edges, top, and bottom of the specimen, so that the largest area was covered by sensors. Additionally, the integration method plays a role in how the pressure was interpolated between known points. Primarily a simple three-dimensional trapezoidal integration was used for the integration across the face.

Previously, researchers from the University of Washington expressed the desire to place more pressure sensors along the back face of their structure in the wave flume. This potential was examined in OpenFOAM for the concrete shear wall specimen. As shown in Figure 3.4, the pressure distribution on the back of the specimen is low magnitude and concentrated close to the surface, when compared to the front face. Models showed that the results on the back face were significantly lower magnitude and were determined to be negligible for the purposes of this study.

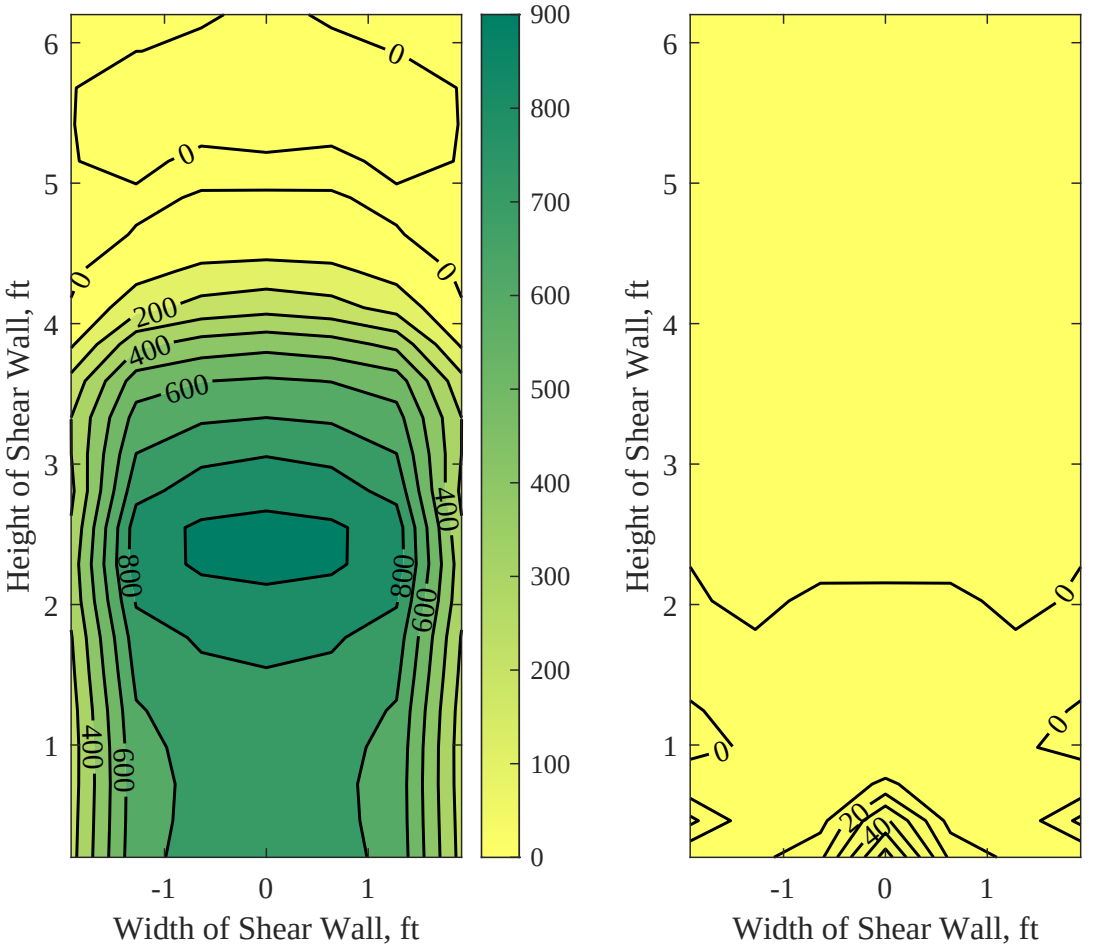

(a) Pressure distribution over off-shore face (b) Pressure distribution over on-shore face

Figure 3.4: Pressure distribution specimen at instant of maximum recorded force. The pressures on the face of the specimen that is hit by the wave are over ten times larger than the pressures on the face protected from the wave.

3.1.5 OpenFOAM Model of CFT Structure

After location, pressures, ramp, and forces were modeled and found for the sear wall specimen, the concrete filled tube specimen was modeled. This rough model was used to determine the order of magnitude for the forces and approximate run up and splash height this specimen would experience. The force, shown in Figure 3.5, was found to be insignificant when compared to the weight of the specimen and anticipated transportation loads. The water fun up along the columns is related to the size of the waves produced, so once the anticipated wave was selected, the height of the specimen and locations of the pressure sensors were designed to ensure the correct wave to structure interaction.

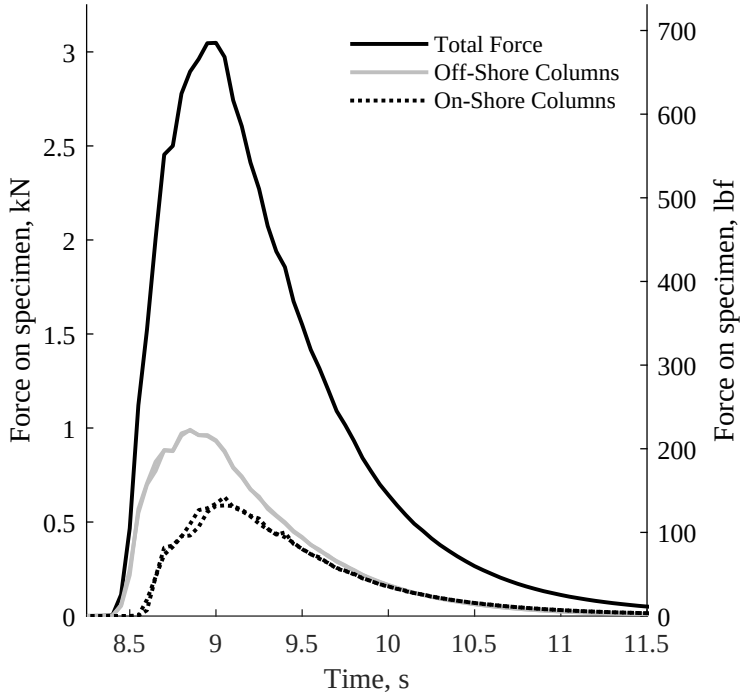

Figure 3.5: Force on the simulated CFT specimen as a function of time. The off-shore columns experience maximum force slightly before and 62% larger than the on-shore columns. Each column experiences forces nearly identical to its symmetric pair.

It is important to note that the model and mesh used in these analyzes was rough and poorly developed. The mistakes with the mesh were found months after construction was completed, but before testing began. This explains the significant difference in force between Figure 3.5 and **??**. Even though the original OpenFOAM model was insufficient for an in-depth parametric study, it provided enough order of magnitude validation to complete design, construction and testing of the specimen.

3.2 Full Scale Preliminary Design

3.2.1 Calculation of Lateral Loads

The design event for a tsunami vertical evacuation structure is two fold. The main purpose of the structure is to provide a safe evacuation zone from the tsunami. However, in the case of near shore tsunami, the structure must be able to maintain sufficient structural capacity during the earthquake event that produces the tsunami. Vertical evacuation shelters located on the pacific northwest coast must be sufficiently designed for a Cascadia Subduction Zone earthquake and the resulting tsunami. This sequenced and inevitable loading means that many of the load reducing features used in conventional structures are not viable, because before a tsunami vertical evacuation structure is exposed to a design level tsunami, it will have been exposed to an earthquake. The preliminary load demand on the vertical evacuation structure was calculated using the ASCE 7-16 provisions without several of the reduction factors normally applied to earthquakes.

The equivalent lateral force method was used to determine the initial design loads on the structure. The design sheet with Microsoft excel formulas is included in Appendix A. The ASCE seismic maps, for Seaside, Oregon, were used determine the site coefficients. An additional step in the equivalent lateral force method is taken in ASCE 7-16 Section 11.4.7 to multiply the S_{DS} and S_{D1} factors by 1.5 for the response spectrum of the Risk Targeted Maximum Considered earthquake. This in effect cancels out the 2/3 reduction from the S_{MS} and S_{M1} factors in ASCE 7-16 Section 11.4.5.

The rough design parameters for the structural response were selected for a structure with the same site layout as the structure selected in Pyke (2020). The plan layout is shown in **??**. The structure's main layout is 150 ft (45.7m) by 60 ft (18.3m). This is equivalent to five bays by two

bays, with a typical bay spacing of 30 ft (9.1m). Additionally, a preliminary slab thickness of 10 inches (0.254m), was selected to provide mass in the lateral load calculation. Once the primary site and structure coefficients and parameters were selected, two variables were examined further. The Response Modification Coefficient, R, for the CFST columns was varied between 1 and 2. The number of frames with braces was varied between two and four. Once the total base shear, tabulated in Table 3.1, and story shear was determined for each scenario, a simple two dimensional model was built in RISA to identify the maximum moment on the piles. Figure 3.6 shows a sample RISA results for a scenario with an R-factor of 1, and three frames with braces (a total of six bays with braces). Table 3.2 tabulates the maximum moment experienced at the base of the piles.

Table 3.1: Base Shear Demand in single column (kips)

		Number of Frames		
		2	3	4
R	1	2700	1800	1400
	2	1400	900	700

Table 3.2: Moment Demand in single column (kips-ft)

		Number of Frames		
		2	3	4
R	1	29000	19300	14500
	2	14500	9600	7200

Having internal braces is not ideal from an architectural perspective, but may be necessary to provide the required lateral load resistance in the structural plan laid out previously in Pyke (2020). The chevron braces allow internal hallways or door frames between bays at the center of each frame, and partition walls where the braces meet the columns. The internal braces in this situation constrain some of the architectural features of the third floor of the tsunami vertical

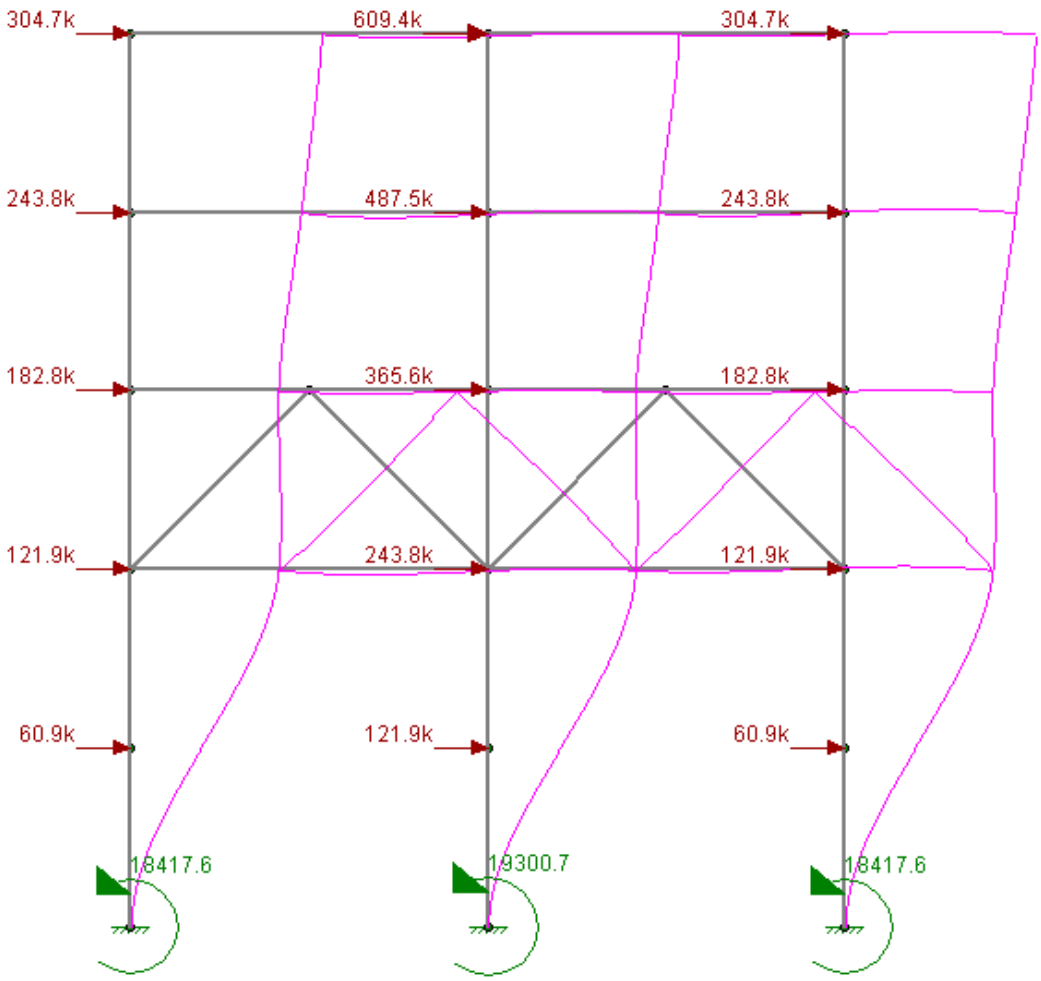

Figure 3.6: Example RISA model for potential structure with three frames and an R-factor or 1.The lateral load inputs were calculated using Appendix A

evacuation structure, but maintain the site footprint.

After the subduction zone earthquake, the structure will likely be subjected to the tsunami. ASCE 7-16 Chapter 6 provides provisions on how to calculate the tsunami force on a structure, based on the off shore bathymetry, and site location. Even though the structure is 150 ft long, perpendicular to the wave flow, the open nature of the first floor means that less than 24 ft of the structure is perpendicular to the wave flow. A conservative assumption of 25% of the structure length is used to account for any damming effects of debris. The total base shear from the tsunami is 3700 kips (16500kN), which is less than the base shear from the maximum considered earthquake, and located lower on the columns, resulting in a smaller moment in each of the columns. As a result, the design load on the structure should be taken from the earthquake loading.

3.2.2 CFST selection

The primary design goal of the tsunami vertical evacuation structure is to maintain safety and stability during and after a large magnitude earthquake, and the subsequent tsunami. In order to achieve this goal, the structure cannot experience extensive damage and yielding during the earthquake, if it compromises the lateral load resisting system to much for the tsunami loads. Ideally the structure will not experience any inelastic deformation during the earthquake, but as shown in Table 3.1 and Table 3.2, when an R-factor of 1 is used, the base shears and column moments are larger. Most structural systems that are designed in earthquake prone regions are able to take advantage of ductile yielding of specific elements, thus reducing the seismic base shear by using a R-factor greater than 1. For this vertical evacuation structure an R-factor of 2 was selected to balance the maximum base shear experienced by the structure and minimize the effect of inelastic yielding after the earthquake event.

Two key assumptions are made at this preliminary stage in the design of the tsunami vertical evacuation structure for an analytical model. The first is that the chevron braces remain elastic during the seismic event. As part of this, the braces are assumed to not buckle in compression. This perfectly elastic yielding in the braces is not entirely realistic due to the size of the member required, but it allows the analytical model to focus on the effects of the CFST columns and piles. Another assumption in the design of the structure for the analytical model is that the slab is a rigid

diaphragm and transfers all the load evenly to the lateral load resisting system.

The distributed plasticity method was used to determine the required pipe elements for the CFST columns. The method described in Stevens (2016) uses the plastic capacity of steel and the cracking capacity of concrete to iterate to the neutral axis by setting the axial load in the column equal to the dead load of the structure. Once the neutral axis is determined the area of steel in tension, and area of steel and concrete in compression is calculated and the resulting axial load is compared to the dead load, and the moment capacity is calculated. The worksheet and formulas are included in **??**. Table 3.3 shows distributed plastic capacity moment for selected CFST column diameters and thicknesses. The column sizes below the horizontal lines meet the AISC diameter over thickness ratio requirements. Three pipe dimensions were selected for further investigation using OpenSees: 1. Pipe with D = 36 inch, thickness = 1.25 inch. 2. Pipe with D = 42 inch, thickness = 0.875 inch. 3. Pipe with D = 48 inch, thickness = 0.875 inch.

3.2.3 OpenSees Simulation Set Up

The preliminary OpenSees simulation is built on the tsunami vertical evacuation structure design developed in Section 3.2.2. The earthquake selected to test the simulation was the series of M9 earthquakes developed by University of Washington M9 project. The earthquakes were adjusted for the structure's site in Seaside, Oregon. The response spectrum for the 30 earthquakes is shown in Figure 3.7.

The circular cross section of the CFST columns and piles are made up of fiber elements. The materials are based on the expected values for typical pipe materials, according the American Petroleum Institute. Furthermore, a basic concrete strength of 6000 psi is used for the concrete interior. The braces of the simulation are elastic material, with a Young's modulus of steel, and an area of 31.2 square inches ($0.02m^2$). The stiff elastic element beams were used in place of a rigid slab in the two dimensional frame simulation of the vertical evacuation structure.Figure 3.8 shows the maximum drift for an OpenSees simulation of the three column sizes selected in Section 3.2.2. This model was run assuming the columns are fixed at the soil level to solid ground.

The simulation is also set up to examine the influence of piles below the CFST columns in the future. The piles are sized at D = 60 in, t = 1.5 in, to allow for construction tolerances when

Table 3.3: Moment Capacity of CFST Column from Distributed Plasticity Method (k-ft). The sections below the horizontal line meet AISC diameter over thickness requirments. Bolded cells meet the moment demand in the from Table 3.2 when four frames are used, and R=2.

Thicknesses (in) \ Diameters (in)	18	24	30	36	42	48	54	60
0.125								
0.25								
0.375	672.8	1232.8						
0.5	830.3	1533.3	2452.5					
0.625	981.6	1822.4	2927.9	4302.5	5949.5			
0.75	1127.4	2101.7	3387.9	4991.7	6917.5	**9168.8**		
0.875	1268.1	2372.2	3834.2	5661.2	**7858.9**	**10431.5**	**13382.9**	
1	1404.0	2634.7	4268.3	6313.5	**8776.8**	**11663.8**	**14978.8**	**18725.8**
1.125	1535.2	2889.7	4691.3	6950.0	**9673.6**	**12868.7**	**16540.4**	**20693.5**
1.25				**7572.0**				
1.5				**8776.6**				

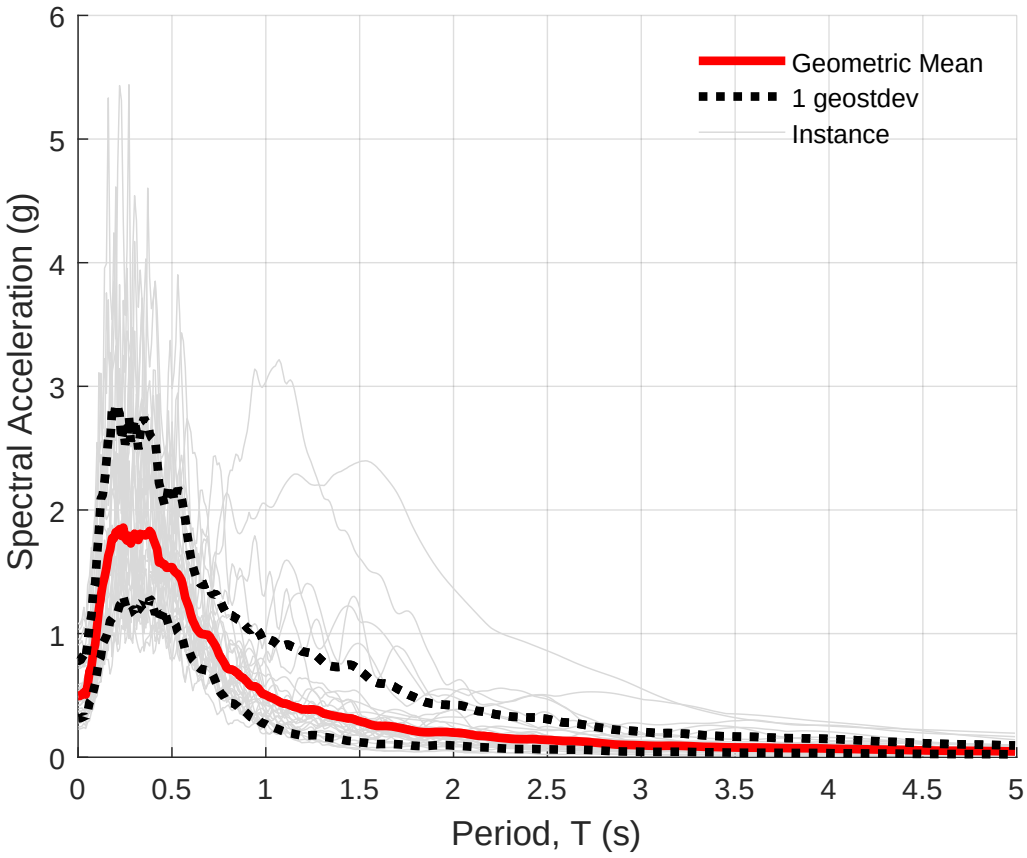

Figure 3.7: Response Spectrum for M9 earthquake in Seaside Oregon, using ground motions developed by UW M9 research group.

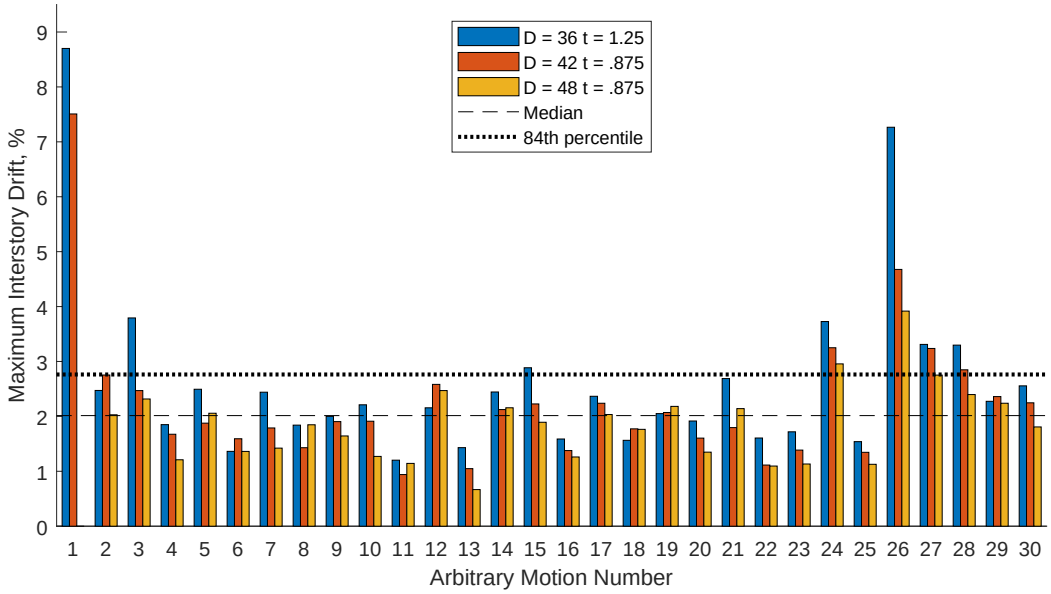

Figure 3.8: The maximum interstory drift in the OpenSees simulations for three column sizes and all 30 M9 earthquakes in the database. The simulation for the D=48in, t=0.875 columns for earthquake 1 failed due to a runtime error.

driving the piles and attaching the columns to the piles. The piles are attached via p-y and t-z springs to elements representing the soil layers below the specimen. No trials have been conducted with the full scale frame with piles.

Chapter 4

EXPERIMENTAL PROGRAM

4.1 Experiment Setup

The physical experiment setup in the large wave flume at the O. H. Hinsdale Wave Research Laboratory can be broken down into five main subsystems. These are the wave flume, the bathymetry, the reaction frame (how the structure is attached to the walls and floor of the wave flume), the structure, and the soil box. Each of these subsystems satisfies and creates constraints for the other subsystems. The result is an integrated design for the specimen, where each component is essential for the successful operation of all of the other components.

4.1.1 Large Wave Flume

The Large Wave Flume in the O. H. Hinsdale Wave Research Laboratory at Oregon State University is the largest in North America. The wave flume is 12 ft (3.7m) wide, and 342 ft (104m) long, with 15 ft (4.6m) tall. The maximum depth for a tsunami type wave is 6.5 ft (2m). The wave maker is a piston-type hydraulic actuator assembly. The wave maker piston's total stroke is 13.1 ft (4m) at 13.1 ft/s (4m/s). This results in a maximum stable wave height of 3.9 ft (1.4m) for tsunami style waves (Hinsdale Wave Lab).

The walls and floors of the wave flume have an array of tie-down locations spaced approximately 12 ft (3.7m) on center. These tie-down locations permit bolted attachment of instruments, structures, and clips for concrete slabs in the flume. The concrete slabs are used to create the desired bathymetry and on shore features.

4.1.2 Bathymetry

The bathymetry in the wave flume primarily consists of (nominally), 12 ft by 12 ft by 6.5 inch (3.66m x 3.66m x 0.165m) concrete slabs placed across the flume. The slabs rest on steel clips at the corners which are bolted to the flume walls at the tie down locations, shown in Figure 4.1.

Sloped geometries are created by hanging one side of the slab lower than the other.

Figure 4.1: Clips bolted to flume wall that concrete slabs rest on

The bathymetry for this experiment was determined with the help of an OpenFOAM computer model. Wave height at the location of the specimen was maximized by running models at a variety of locations along the length of the flume, and with a variety of ramp slopes. The models all used a maximum water depth of 6.5 ft (2m). The analyses showed that a steep ramp would produce a greater wave height at the structure. The final location in the flume was selected with advise from staff at the facility to ensure the wave propagated fully, while maintaining the large wave

requirements of the experiment.

The flume profile for the experiment, as illustrated in Figure 4.2, consists of six sections. The first section is the flat flume floor, 107.6 ft (32.8m) long (measured from the neutral position of the wave maker piston). Next is a flat 12 ft (3.66m) section, 6.5 inches (0.165m) off the floor, made up of one of the concrete slabs placed flat on the flume floor. This slab serves to hold the toe of the ramp in place. The next section comprises one concrete slab sloped from the flume floor to the specimen base elevation, with an angle of 30.5°. At the top of the ramp, a wood framing and plywood horizontal deck was built to surround the specimen, shown in Figure 4.3. This wood deck is the length of one bay, 12 ft (3.7m), and at a surface height of 6.59 ft (2.01m) above the flume floor. The wood deck over sizes the soil box slightly, so no force developed on the deck is transferred to the load cells. The fifth section is 72 ft (7.3m) long and made up of six horizontal concrete slabs, at the same surface elevation as the wood deck, and the top of the ramp. The final concrete slab section is 120 ft (37m) long with a slope of 4.76°.

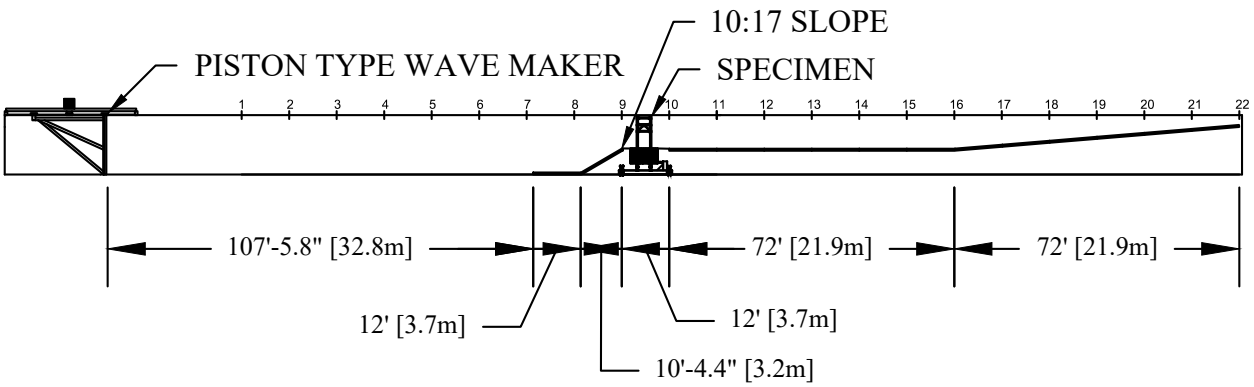

Figure 4.2: Large Wave Flume Bathymetry. The Specimen was placed between bays nine (9) and ten (10), 129 ft 10.2 in (39.6m) from the neutral position of the wave maker paddle. Wave flows from left to right in flume.

4.1.3 Reaction Frame

A reaction frame supports the structure and attaches it to the flume floor at the tie down locations, as shown in Figure 4.4. The base reaction frame is a pair of modified W12x106 steel members with

(a) Deck framing under construction

(b) Completed deck

Figure 4.3: Custom Deck in Bathymetry

two stiffened cross pieces that tie the base beams to the flume floor. The base beam has an upright section complete joint penetration (CJP) welded to the base portion and stiffened with a triangular one inch (2.54cm) plate. The upright portion of the base reaction frame constrain any base shear developed by the wave on the structure, therefore a stiff connection to the flume floor was desired. Additionally, each base beam is stiffened with nine stiffeners in the web of the beam. Each cross beam is stiffened by eight 1/2 inch (1.27cm) stiffeners. These stiffeners are located where threaded rods tie the structure to the flume floor. Details and design on the base reaction frame can be found in Pyke (2020).

The reaction frame also consists of the two side beams, shown in Figure 4.5, that hang on the walls of the wave flume. The primary purpose of these side beams is to attach load cells to the flume walls at locations other than the tie-down points (which are spaced at 12 ft (3.66m) on center). These beams are modified channels that are part of the standard equipment for the Large Wave Flume.

Figure 4.4: Reaction frame in base of flume

Figure 4.5: Beam attached to side of flume that provides anchorage spots in the middle of the bay

4.1.4 Specimen

The specimen is composed of a frame with concrete filled steel tube columns and a hat truss providing lateral stiffness, the soil box conditions, and the bathymetry. Details on the cft structure are discussed in Section 4.2.

4.1.5 Soil Box

The soil box is used to investigate the structure-soil interaction propagated from wave loading. The soil box is formed from the bottom slab that the specimen is cast into, and four half-inch (1.27cm) steel walls that are anchored into the sides of the slab. The steel walls also have a half-inch (1.27cm) steel threaded rod that ties the box together in each cardinal direction. Further details on the soil box design can be found in Pyke (2020).

The soil placed in the box is a 1/4 inch (6.35mm) aggregate. The soil was placed in four lifts of approximately 10 inches (24cm) each, and compacted after each lift using a steel plate compactor hand tool.

4.2 Structure

4.2.1 Scaled Design

The specimen tested in the OSU Large Wave Flume was scaled to fit within the wave flume, and fit on the same reaction frame as the concrete shear wall specimen designed by Pyke (2020). The specimen scale is 1:9 when compared to a structure with 30 ft (9.1m) bay spacing and 36 inch (91.4cm) diameter columns. Additionally, to fit within the width of the flume, the specimen is one bay wide by one bay deep.

Expected loads and forces guided the selection of members. Initially, OpenFOAM analyses provided anticipated loads on the columns. Analysis showed that the small surface area exposed to the water coupled with the hydrodynamic shape of the round columns resulted in relatively low forces being transferred from the wave to the entire specimen. Transportation and installation of the specimen are expected to produce loads larger than the one kip (4.45kN) base shear developed by the wave. Statics and symmetry were used to determine the maximum forces experienced by the specimen in a variety of loading patterns. These internal forces guided the selection of

steel members so that the specimen would remain elastic, and not permanently deform during construction, transportation, installation in the flume, and testing.

The scaled structure is 44 inches (1.12m) by 44 inches (1.12m) in plan, and is 12 ft (3.66m) tall, as illustrated in the elevation drawings in Figure 4.6. Each column is a 3-1/2 schedule 40 pipe, placed 40 inches (1.02m) on center, filled with concrete. This is the same column spacing as the concrete shear wall specimen tested previously (Pyke, 2020). The beams are HSS2x2x0.120 members with slots cut at the ends for the gusset plates. The braces are HSS1.5x1.5x0.25 tubes, also with slots in the ends for the connections to the beams and columns. Such stocky braces were selected because vertical evacuation structures must remain elastic under sequential loading from a design earthquake and design tsunami . In place of a concrete slab on the upper floors, a 1/8 inch (3.175mm) plate is attached to the beams. The large gap between the ground level and the bottom of the hat truss represents where a breakaway slab can be placed. The specimen was designed to be tall enough that a wave will pass through the structure without interacting with the truss. The upper stories are spaced 20 inches (50.8cm) floor to floor to fit the scale of the entire specimen. In the second phase of testing, as described in Table 4.7, plywood and hardy-board panels will be installed at the appropriate location below the hat truss to simulate a fixed in place floor and a break away slab. To create an upward force on the specimen, a back wall was also installed. The back wall serves to direct the wave upward underneath the slab, rather than allowing the wave to flow through the back of the specimen.

The bottoms of the column are embedded in a six and one half inch (16.51cm) concrete slab that serves several purposes. The concrete slab fixes the bottoms of the columns, as if the foundation extended much deeper into the soil layer below the structure. The concrete slab also provides the bottom of the soil box, and connects the side walls of the soil box to the structure. The specimen and soil box are attached to the reaction frames by struts with load cells that attach to anchor points drilled in the steel box walls, and embedded in the concrete slab. As such, the concrete slab transfers any load exerted onto the specimen above the water level down to the load cells. Details on the concrete slab design can be found in Pyke (2020).

Once the specimen is secured by the struts, reaction frame, and flume, it is in a fixed and stable location. The coordinates of the columns in the flume are shown in Table 4.1.

For one portion of the experiment a horizontal panel is installed approximately halfway between

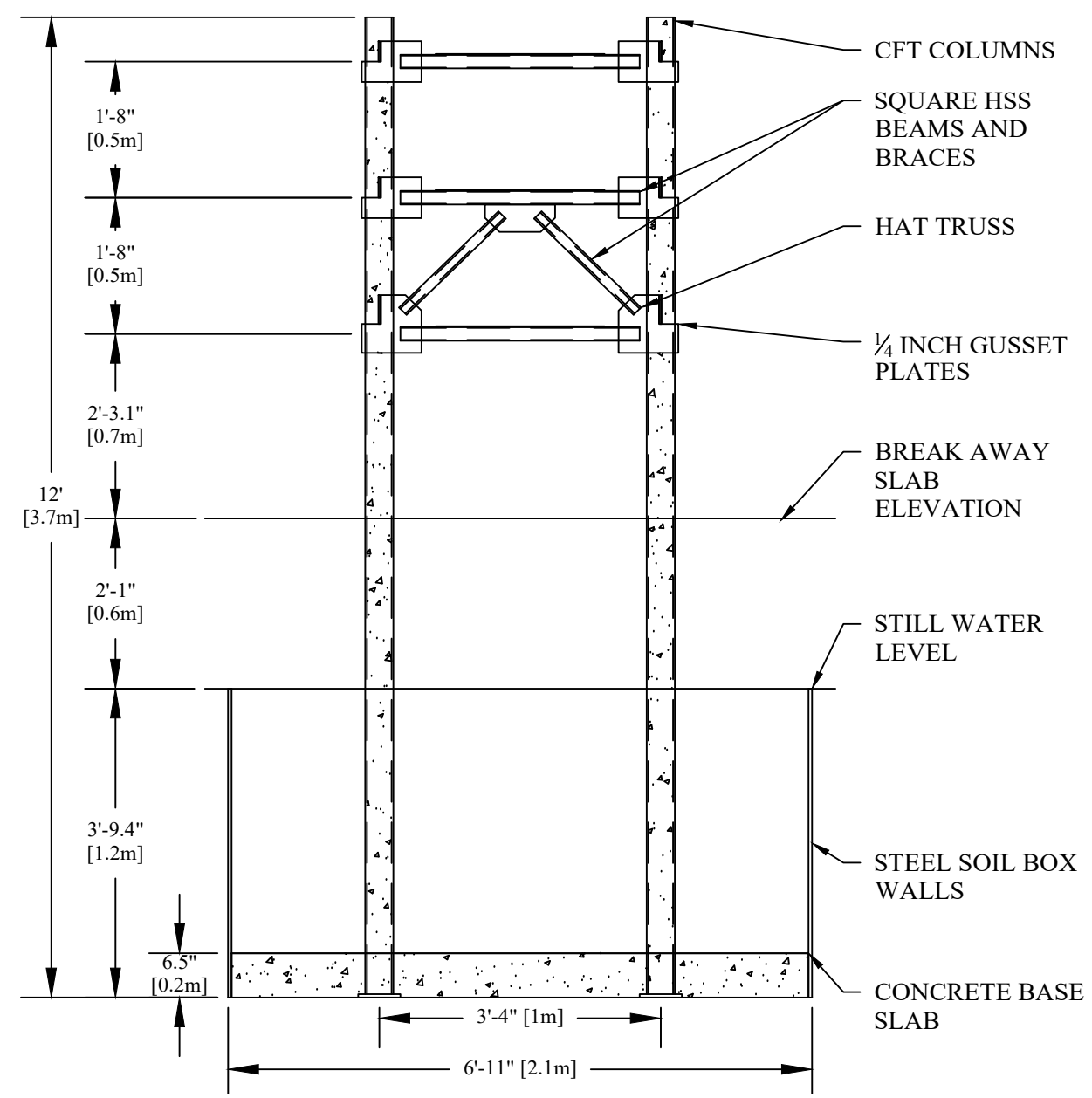

Figure 4.6: Specimen Elevation. Wave flows in flume from left to right.

Table 4.1: Vertical column locations with respect to flume coordinates. The wave flume surveys all locations in metric in the coordinate system described in "README: Guide to the Project Folder" by Maddux (2018)

Column Name	x, m	y, m
A1	40.84	-0.52
A2	41.85	-0.54
B1	40.86	0.50
B2	41.87	0.48

the ground level and the hat truss. This panel serves to simulate a break away slab or floor unit in a vertical evacuation structure.

4.3 Instrumentation

4.3.1 Load Cells

Eight load cells measure the force transferred from the specimen into the reaction frame and flume wall and floor. When a wave hits the structure, the pressure is transferred through the structure to the bottom slab. The force is then transferred through struts with the uni-axial load cells into the reaction frame and flume walls. The wave transfers a variety of eccentric forces into the structure, so it is important for the load cells to be arranged in such a way to capture the full six-degrees of loading. Locations of the load cells with respect to the specimen are illustrated in Figure 4.7. The locations of the load cells in flume coordinates, and other details are specified in Table 4.2.

Pancake Load Cells

The pancake load cells are Interface 2440EZD-10K units with 10,000 pound (44.48kN) capacity. They are connected directly underneath the structure at the columns. The load cells are connected to the struts, as shown in Figure 4.8b. The two dimensional swivels at both end of the load cell struts allow for small rotations and keep the load cell engaged axially. To span the distance between the bottom of the specimen and the top of the reaction frame, the load cells were built up with an

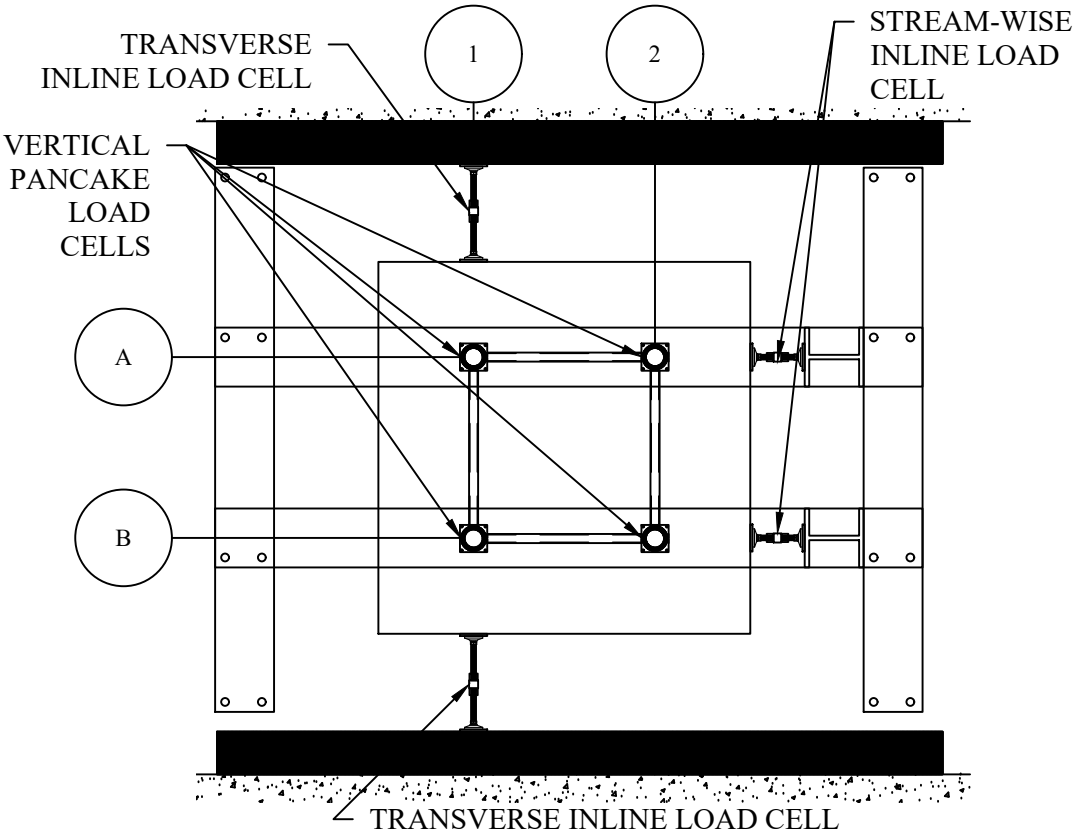

Figure 4.7: Load cell locations with respect to specimen. Load cell nomenclature includes the direction the load cell is experiencing force in, and the column or column line the load cell is attached to.

Table 4.2: Load Cell Details

Instrument Name	Instrument Description	Load Cell Rating, kip	Closest column
B A1	Vertical Pancake Load Cell	10 (44.48kN)	A1
B A2	Vertical Pancake Load Cell	10 (44.48kN)	A2
B B1	Vertical Pancake Load Cell	10 (44.48kN)	B1
B B2	Vertical Pancake Load Cell	10 (44.48kN)	B2
S A2	Stream-wise Inline Load Cell	2 (8.90kN)	A2
S B2	Stream-wise Inline Load Cell	2 (8.90kN)	B2
T A1	Transverse Inline Load Cell	2 (8.90kN)	A1
T B1	Transverse Inline Load Cell	2 (8.90kN)	B1

assemblage comprising half inch (1.27cm) steel plates, five inch (127mm) HSS tube, and one inch (2.54cm) threaded rod, as shown in Figure 4.8a. The HSS tube was used to span the majority of the vertical height becuase they have a larger $^{kl}/_{r}$ than the steel rod required to fit in the swivel leveling mount. Half inch (12.7mm) steel plates were fabricated to fit the bolt spacing required by the Interface load cells and the threaded rod size for the swivels. These plates were welded to both sides of the HSS, and bolted to the respective fixture. The leveling swivels are welded to a 6 inch (152mm) square by Half inch (12.7mm) steel plate that bolts to the bottom of the specimen and top flange of the reaction frame.

These load cell are positioned to monitor the vertical force of the wave on the structure and any overturning moment experienced by the structure. The bottom load cells also measures the overturning moment out of plane with the wave flow, however this is minimal because the flume acts uniformly across its width until it is disturbed in an asymmetric manner.

Inline Load Cells

The inline load cells are Delta Metrics Inc. 99-2638-002K and Delta Metrics Inc. 99-2638-010K units. These load cells have a working capacity of 2,000 pounds (8.90kN) and 10,000 pounds (44.48kN), respectively. The 2,000 pound (8.90kN) load cells are attached horizontally between the

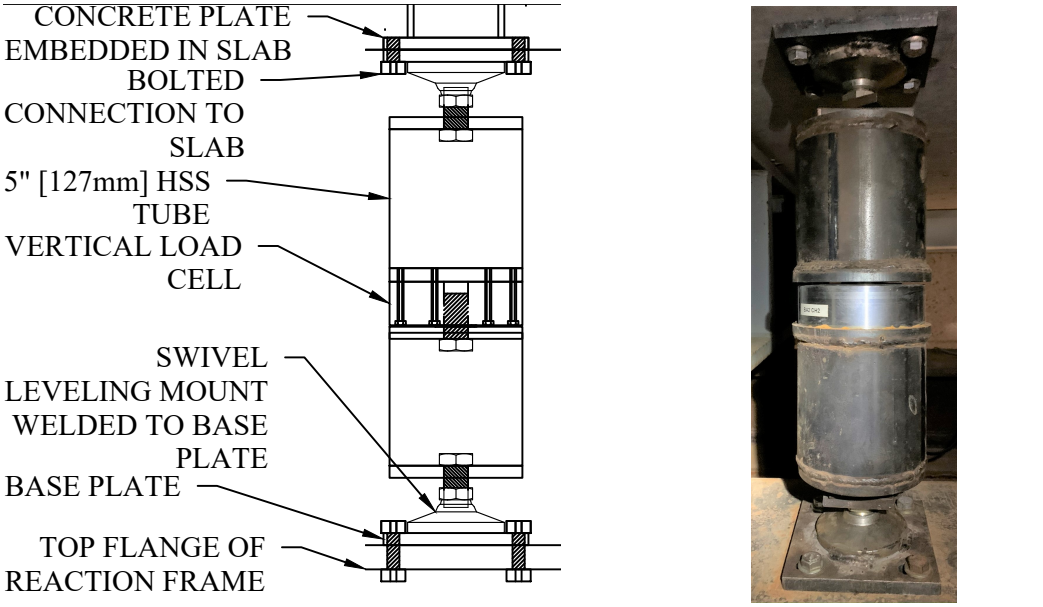

(a) Vertical Load Cell Drawing

(b) Vertical Load Cell Assembly

Figure 4.8: Vertical load cell assembly elevation

east and west sides of the specimen and the wave flume wall. The 10,000 pound (44.48kN) load cells are attached horizontally between the north side of the specimen and the upright portions of the reaction frame. Both load cells use the same configuration of attachment. The load cells are threaded into a rod that spans from the specimen to the end connection points on the reaction frame, shown in Figure 4.9. The steel rod is attached to swivels by a one inch (2.54cm) threaded rod, similar to the pancake load cell struts, to keep the inline load cells loaded axially, and prevent shear and moment transfer through the instrument. The horizontal inline load cells are only attached to the swivels by the threaded rod, because the loads are significantly smaller, and the unbraced lengths are not as large as the bottom load cells.

Two load cells, SA and SB ('S' for streamwise, 'A/B' for the column line), are attached to the back of the structure and the upright portion of the reaction frame. These load cells are placed 'crossshore' in the Hinsdale wave laboratory nomenclature. These load cells record the base shear of the structure and the torsion measurement about the vertical axis. Torsion is minimal, because

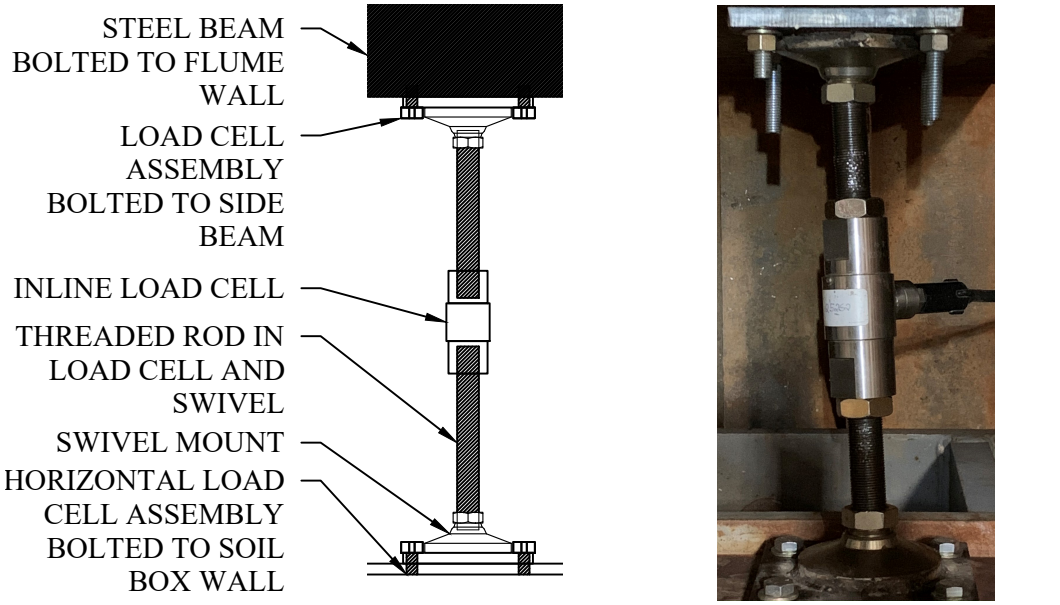

(a) Horizontal Load Cell Drawing

(b) Horizontal Load Cell Assembly

Figure 4.9: Inline load cells used for horizontal force measurements

the specimen is theoretically placed symmetrically in the flume, but in reality there are small eccentricities that can be found in the difference in the load cell measurements between SA and SB.

Two load cells, T1 and T2 ('T' for transverse, '1/2' for the column line), are attached to the sides of the specimen, and the horizontal beams attached to the flume walls. These load cells are placed 'alongshore' in the Hinsdale wave laboratory nomenclature. These two load cells record any shifting or out of plane force in the structure, and can be used to parse out torsion developed in the specimen. These forces are not expected, due to the symmetry of the flume.

Instrumented Tension Member

A threaded rod with eye-nut and clevises, arranged as shown in Figure 4.10, was used to pre-compress the streamwise (crossshore) load cells on the north side of the specimen. Pre-compressing the load cells removed any slop in the swivel connections, thus minimizing the chance of the specimen shifting under the wave load without registering on the load cells. Furthermore, the tension member

helps to ensure the load is more evenly shared between the two load cells. Finally, the tension member serves as a secondary safety measure by restricting movement of the specimen to the South when placed in the wave flume. The threaded rod is instrumented with two strain gauges. The strain gauges were used during the initial tightening to calibrate the preload levels in all the load cells. Additionally, the strain level in this rod is used in calculating the base shear imparted by the wave onto the structure.

4.3.2 Pressure Sensors

Twelve Pressure Sensors are used to record the hydrodynamic and hydrostatic pressures on the specimen. The instruments are PDCR 830 pressure sensors, arranged vertically along the columns. Access ducts were left in the columns during construction to allow for the pressure sensors. The pressure sensors pass through the center line of each column and are arranged as shown in Figure 4.11. The locations of each pressure sensor, given in flume coordinates, is provided in Table 4.3. The pressure sensor values are integrated over the front surface of the columns to approximate the force transferred from the wave into the structure.

4.3.3 Strain Gauges

Each column in the structure is instrumented with six strain gauges, resulting in 24 strain gauges total. The strain gauges are Tokyo Instruments YFLA gauges. The strain gauges are positioned at three heights along the columns, shown in Figure 4.11: (1) the bottom of the soil box, (2) just below the water level (the top of the soil box), and (3) just below the hat truss. Each vertical location, on each column, has a strain gauge on the front and on the back of the column, so the shear force, bending moment, and axial load in that cross section can be calculated. The naming of each strain gauge is provided in Table 4.4. This arrangement of strain gauges allows the moment experienced by the the cross section, at each location, to be calculated. The difference in moments at each location is then used to calculated the shear experienced by each portion of the column. This shear value is in turn used to calculate approximately how much of the base shear force is transferred from the column into the soil, and the approximate force transferred from the wave into the structure.

Figure 4.10: Threaded rod connects the back of the specimen to the reaction frame. The threads on the rod and nuts allow the streamwise load cells to be compressed to a specified preload. At the mid point of the rod, the threads are ground down, so a strain gauge can be applied.

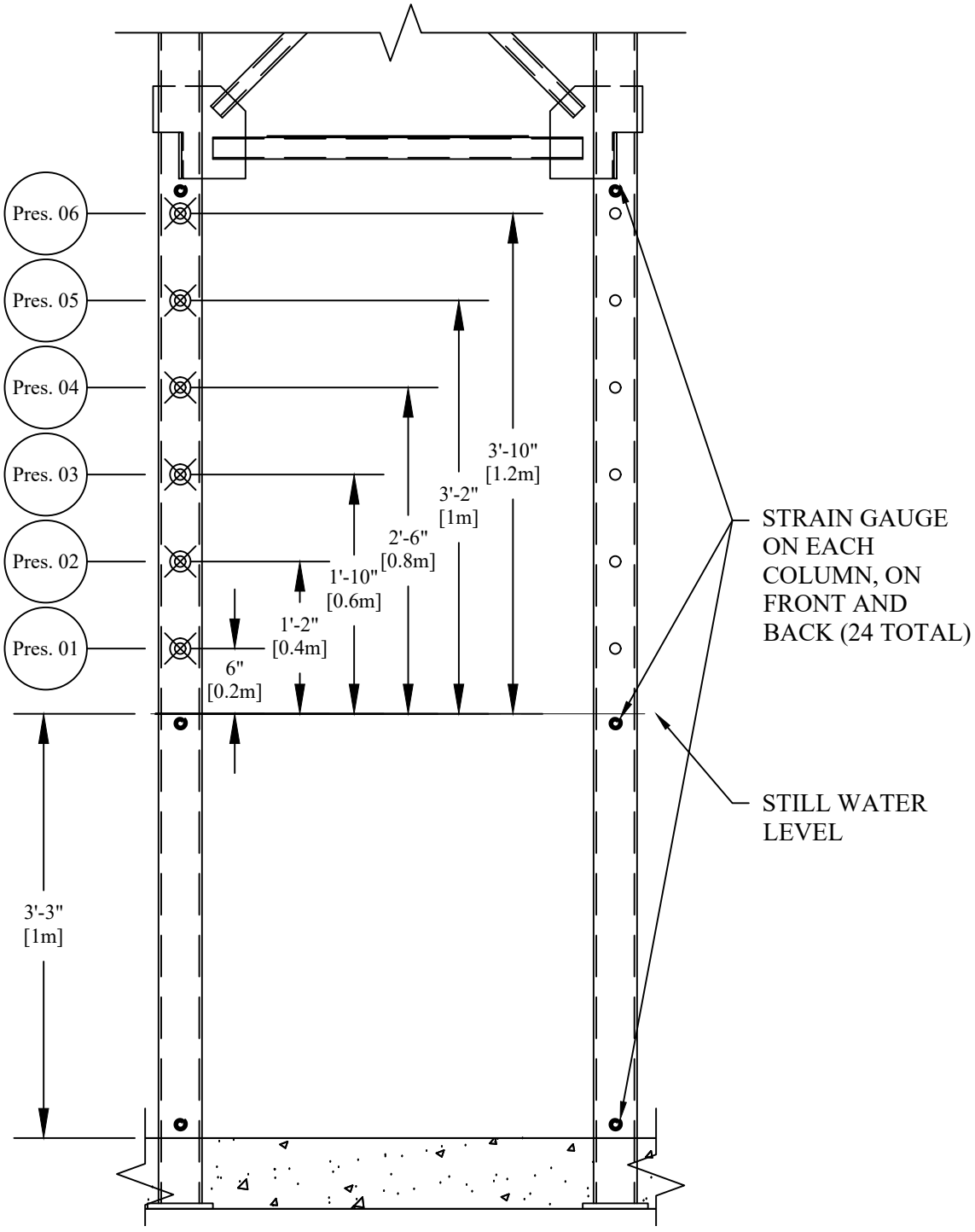

Figure 4.11: Pressure sensor and strain gauge layout. Pressure sensor elevations taken above still water depth. Strain gauges are on front and back of each column. Wave flows into page.

Table 4.3: Pressure Sensor Locations

Pressure Sensor Identification	Column Num.	Elevation Num.	x, m	y, m	x, m
Pres01	A1	01	40.805	0.503	2.192
Pres02	A1	02	40.803	0.497	2.392
Pres03	A1	03	40.808	0.497	2.601
Pres04	A1	04	40.813	0.500	2.796
Pres05	A1	05	40.809	0.497	3.004
Pres06	A1	06	40.812	0.494	3.207
Pres07	A2	02	41.822	0.476	2.388
Pres08	B1	02	40.787	-0.516	2.391
Pres09	B1	05	40.787	-0.516	2.997
Pres11	B2	01	41.796	-0.536	2.182
Pres12	B2	02	41.799	-0.535	2.385
Pres13	B2	03	41.795	-0.533	2.581

Table 4.4: Strain Gauge Locations

Strain Gauge Identification	Gauge Number
E A1 U F	01
E A1 U B	02
E A1 M F	03
E A1 M B	04
E A1 L F	05
E A1 L B	06
E A2 U F	07
E A2 U B	08
E A2 M F	09
E A2 M B	10
E A2 L F	11
E A2 L B	12
E B1 U F	13
E B1 U B	14
E B1 M F	15
E B1 M B	16
E B1 L F	17
E B1 L B	18
E B2 U F	19
E B2 U B	20
E B2 M F	21
E B2 M B	22
E B2 L F	23
E B2 L B	24

It is a multi-step process to apply, protect, and waterproof the strain gauges. The general steps are:

1. Grind the mill scale off the specimen at the locations to be gauged,
2. Clean the specimen with acid, base, and clean cloths,
3. Apply the strain gauge with cellophane tape and proper adhesive,
4. Allow the glue adequate time to adhere,
5. Apply a generous layer of M-Coat B from Micro Measurements on strain gauge and up wire at least two inches (5cm) (Figure 4.12a),
6. Allow adequate time for M-Coat B to cure, approximately 24 hours depending on temperature,
7. Melt M-Coat W and brush over strain gauge, M-Coat B, and approximately one inch (2.5cm) up wire (Figure 4.12b),
8. Cut and stretch thick layer of Mastic Tape over the strain gauge application region, and
9. Apply polyurethane sealant over entire length of strain gauge wire attached to structure (Figure 4.12c).

4.3.4 Wave Measurements

Wave gauges and acoustic doppler velocimeters are arranged in the flume to capture the wave propagation and interaction with the bathymetry and specimen. The instrument name, type and location are given in Table 4.5. In addition to wave gauges and velocity measurements, the position of the wave maker paddle is recorded to validate consistency between tests.

(a) M-Coat B

(b) M-Coat W

(c) Completed and protected strain gauge

Figure 4.12: Strain Gauge Application Process

Table 4.5: Wave Measurement Details

Instrument Name	Instrument type	x, m	y, m	z, m
wg1	Wire Wave Gauge	13.957	-1.389	-
wg2	Wire Wave Gauge	17.620	-1.391	-
wg3	Wire Wave Gauge	21.284	-1.389	-
wg4	Wire Wave Gauge	24.934	-1.383	-
wg5	Wire Wave Gauge	28.588	-1.380	-
wg6	Wire Wave Gauge	32.237	-1.376	-
wmwg	Wire Wave Gauge	-	0.000	-
uswg1	Ultrasonic Wave Gauge	36.044	-1.373	3.632
uswg2	Ultrasonic Wave Gauge	39.650	0.002	3.717
uswg3	Ultrasonic Wave Gauge	41.432	-1.336	3.642
uswg4	Ultrasonic Wave Gauge	43.388	0.022	3.631
adv1	Acoustic Doppler Velocimeters	28.579	-1.451	0.916
adv2	Acoustic Doppler Velocimeters	32.220	-1.454	0.932
adv3	Acoustic Doppler Velocimeters	36.078	-1.460	0.926
adv4	Acoustic Doppler Velocimeters	36.576	-1.420	2.461
wmdisp	Wave Maker Displacement	-	0.000	-

Wave Gauges

Two types of wave gauges were installed in the flume to measure the free surface elevation of the wave. Seven Wire resistance wave gauges were placed along the length of the flume and one is permanently attached to the front face of the wave maker. Four ultra sonic wave gauges (USWG) were placed in the flume, approximately five feet (1.52m) above the free surface. One was placed at the bottom of the ramp in bay eight and three were placed around the structure, as shown in Figure 4.13. This arrangement is consistent with the concrete shear wall specimen. On some tests the front and side USWGs got splashed. When this occurred, the sensor was wiped dry before running the next test.

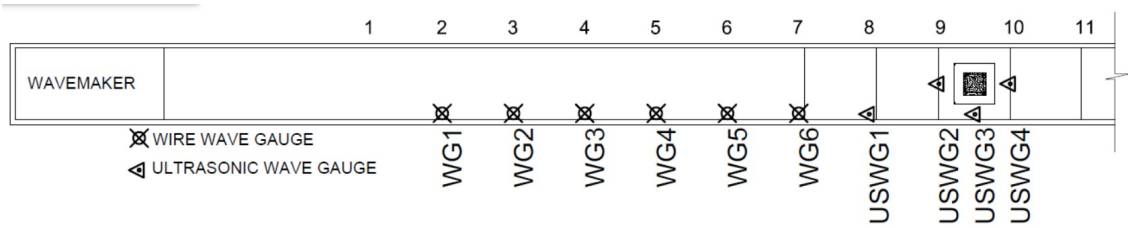

Figure 4.13: Wave gauge locations

Acoustic Doppler Velocimeters

Acoustic doppler velocimeters (ADV) record the velocity vectors in the water in the form of vectrinos. Three ADVs are placed along the flume approximately 3 ft (0.9m) above the flume floor. One was placed at the top of the ramp. This instrument, adv4, only records vectrinos when submerged in water, so there is a moment of noise as it is inundated. The sensor then records information as the wave surges above and past it. The ADVs are placed in the flume in the positions shown in Figure 4.14.

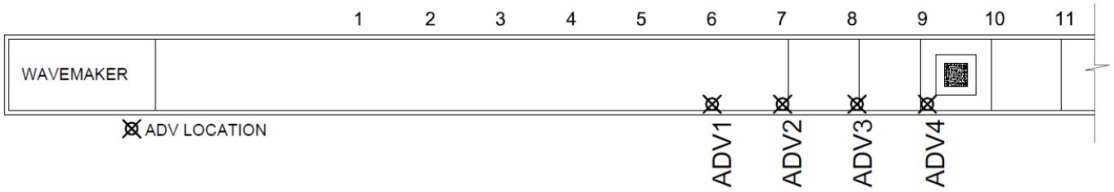

Figure 4.14: ADV Locations

4.4 Test Conditions

4.4.1 Wave Generation

The waves in the Large Wave Flume are generated by the displacement controlled wave maker piston. The displacement time history is calculated using solitary wave theory. While this theory is not perfect in representing a tsunami, it produces a close approximation that is commonly used in structural engineering and hazard modeling simulations (Winter, 2019). Four sizes of wave are generated by adjusting the time history of the wave maker and the water depth of the flume. These are discussed in Table 4.6. The wave maker displacement time histories for each wave are shown in Figure 4.15.

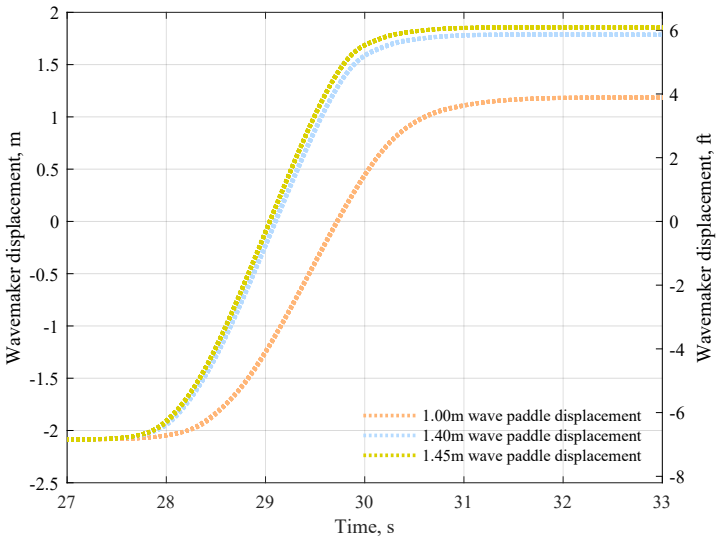

Figure 4.15: Wave Maker Displacement Time Histories

Table 4.6: Wave Descriptions

Type	Flume Depth	Wave ID	Description
Unbroken	6.56 ft (2m)	`Uw1_00`	Short unbroken wave used for calibrating future models.
		`Uw1_40`	Tall unbroken wave. This surging wave is the largest stable solitary wave the wave maker can produce.
Broken	6.56 ft (2m)	`Bw1_45`	Large slipping wave. Created by inputting a slightly different displacement time history into the wave maker. This wave is an unstable solitary wave, that consistently started breaking between bays three and four.

4.4.2 Test Cases

The test is broken into several subsections that comprise two main categories: tests without a floor slab below the maximum inundation height, and tests with a floor slab in place. The breakdown of each test case is provided in Table 4.7. Because the Large Wave Flume uses the physical medium of water, multiple trials are taken for each test case. The staff at the wave lab have found that between five and ten trials are needed for the coefficient of variation to stabilise to a constant value. More trials are required for breaking waves than for unbroken waves. Additionally, tsunami style waves must be run with at least fifteen minutes wait between each trial (Maddux, 2018). This is to allow the water to settle to the level that the wave instruments cannot distinguish the residual sloshing from the waves from the normal surging of the flume.

Table 4.7: Test Conditions

Break Away Slab	Soil Box Depth	Flume Depth	Wave ID	Test Condition ID	# trials
No Slab	Soil Box Full	6.56 ft (2m)	Uw1_00	CFST_NS_F_100	5
			Uw1_40	CFST_NS_F_140	5
			Bw1_45	CFST_NS_F_145	13
	Soil Box Half Full	6.56 ft (2m)	Uw1_00	CFST_NS_H_100	5
			Uw1_40	CFST_NS_H_140	5
			Bw1_45	CFST_NS_H_145	10
	Soil Box Empty	6.56 ft (2m)	Uw1_00	CFST_NS_E_100	5
			Uw1_40	CFST_NS_E_140	5
			Bw1_45	CFST_NS_E_145	10
Fixed Slab	Soil Box Empty	6.56 ft (2m)	Uw1_00	CFST_FS_E_100	3
			Uw1_40	CFST_FS_E_140	5
			Bw1_45	CFST_FS_E_145	2
Break Away Slab	Soil Box Empty	6.56 ft (2m)	Uw1_00	CFST_BA_E_100	0
			Uw1_40	CFST_BA_E_140	5
			Bw1_45	CFST_BA_E_145	0

4.5 Specimen Construction

The specimen was constructed at the University of Washington Structures Research Laboratory in Seattle, Washington. Construction took place from July to October 2019. Graduate and undergraduate students worked on the specimen with the help of the technician, Vince Chaijaroen, and a professional welder. Critical bolt holes and slots were machined by the steel supplier.

Slots for the gusset plates in the columns, braces, and beams were cut using pilot holes and a hand grinder. Holes for the pressure sensors were drilled using a magnetic drill, then filled with a temporary pvc pipe to prevent these holes filling with concrete. After fabrication and fit up, all connections were welded with 3/16 fillet welds. Next the specimen was placed right way up in the concrete slab form work. Reinforcing bars for the slab were placed then placed and tied in the form work, as shown in Figure 4.16b. Additionally, two twelve inch (30cm) straight bars were welded near the base of each column, in the mid depth of the base slab, to provide additional load transfer between the column and the slab. The slab was poured with 3/4 inch aggregate concrete with a 28 day compressive strength of 5000 pounds per square inch. The specimen post cast is shown in Figure 4.16c. This same concrete did not fit within the internal gusset plates in the columns, so grout was later used to complete the concrete filled steel tubes. The finished specimen is shown in Figure 4.16d.

After the concrete had cured, the specimen was loaded onto a flat bed trailer and shipped to Corvallis, Oregon. Once there, the specimen was unloaded and instrumented with strain gauges before being installed in the flume. Details on the installation process are included in Appendix C.1. After the Specimen was installed in the wave flume, a wood deck was built around the specimen, shown in Figure 4.3. The wood deck was built the measured dimensions of the specimen and flume. The pressure sensors were placed in the instrument holes of the specimen columns using small rectangular 1”x5” (25mm x 127mm) sheets of metal with the correct thread size for the pressure gauges. The metal sheets were held in place by black electrical tape wrapped all the way around the column. The back side of the column was open for the instrument wiring.

(a) Specimen welded and turned upright

(b) Specimen prepared for base concrete base slab cast

(c) Specimen after base slab is cast

(d) Built Specimen, ready for shipping

(e) Specimen ready to be rotated upright after transportation

(f) Specimen in wave flume, ready for final placement

Figure 4.16: Construction Process

4.6 Test Procedures

Once the specimen was properly placed in the flume, according to the procedure detailed in Appendix C.1, all instruments were deployed to the locations and by the methods specified in section Section 4.3 and Section 4.5. After the instruments were in place and working properly, the approximate stiffness for the system was determined using the procedure outlined in Appendix C.3. This stiffness test is also an opportunity to ensure all instruments are operating properly and the specimen is seated on the struts in the flume.

Testing in the flume is conducted under the guidance and procedures of the O.H.Hinsdale staff:

1. Fill the flume to approximately seven feet (2.25m).

2. Allow the water to settle overnight. This step is required to ensure the bulk of the unbonded chlorine has evaporated, thus stabilizing the waters resistance to current.

3. Lower the water level to the depth specified in Table 4.7.

4. (a) On the first day of testing, a series of waves were run, ramping up in size until the full wave specified in Table 4.7 was reached.

   (b) Subsequently, only the specified waves need to be run.

5. Run a set of five to ten waves.

   - Fifteen minutes resting period occurs between the end of one wave and the beginning of the next.
   - Periodically, the raw data should be checked to ensure all instruments are operating correctly.
   - After each wave, during the fifteen minute waiting period, the ultrasonic wave gauges must be dried off with a soft cloth.

6. After a set of ten waves is complete, the wave height, water depth, and experiment name in the daq must be adjusted and reset for the next set of waves.

7. Pressure sensors are removed from the flume.

8. The ‘break-away slab’ is installed in a fixed position.

9. Steps 1-6 are repeated with the soil box empty.

10. The ‘break-away slab’ is installed with the break-away initial conditions.

11. Steps 1-6 are repeated with the soil box empty.

    - The ‘break-away slab’ must be replaced after each wave.

12. Redeploy the pressure sensors. The ‘break-away’ slab tests do not need to be run for the filled soil box.

13. Once all waves are run for a particular soil box condition, the wave flume should be drained approximately three feet (1m). The wave gauge calibration should be run by wave lab staff while this is happening.

14. Soil is added to the specified level from Table 4.7 in two lifts and compacted.

15. Steps 1-6 and 13-14 are repeated for all waves and soil box depths specified in Table 4.7.

Once all the waves are run according to Table 4.7, the structure is removed from the flume according to Appendix C.2.

Raw data is configured into a usable format after the wave gauges are calibrated. This means a more in depth check on results is possible each time the water level is lowered to produce a new wave, and when the soil level is changed.

Chapter 5

EXPERIMENTAL RESULTS

This chapter presents results from the flume tests conducted at Oregon State University in August 2020. The data are presented in two sections. The first section presents data from the wave maker, wave gauges, and ADVs prior to the wave impacting the specimen. This data is evaluated from the perspective of repeatability of the waves. As indicated in Table XX, three different wave heights were used in the experimental program; the first section presents data for each wave height and each trial (number of trials for each wave height are presented in the table). From examining the time history data for all the wave trials, the creation and propagation along the flume of each wave is highly repeatable. The second section of the chapter examines investigates the demand on and the response of the specimen using the instrumentation placed on the specimen as described in Section 4.3. Pressure distributions and histories were determined from the pressure gauges. Reactions were measured in three ways. Load cells were placed to measure the base shear, torsion, and overturning moment of the specimen (Figure 4.7). In addition, strain gauges placed on the piles were used to calculate the base shear and overturning moment. This chapter provides the data for each trial, where a trial is a wave height, soil condition and inclusion or absence of the slab/wall. Comparison between these trials is provided in Chapter 6 Evaluation of Experimental Study Parameters. Table 5.1 shows the experiment conditions conducted and number of trials.

5.1 Measurements of Wave Characteristics

The measuring of the structural response of the impact of the wave on the specimen is dependent on a repeatable and consistent wave being generated and moving down the flume. This section examines the repeatability of the waves and the instruments measuring the waves as the wave moves down the flume. Once the measurements for the waves are shown to be repeatable, the structural response from the wave impact is shown in the next section.

Table 5.1: Test Conditions

Break Away Slab	Soil Box Depth	Test Condition ID	# trials
CFST columns only	Soil Box Full	CFST_NS_F_100	5
		CFST_NS_F_140	5
		CFST_NS_F_145	13
	Soil Box Half Full	CFST_NS_H_100	5
		CFST_NS_H_140	5
		CFST_NS_H_145	10
	Soil Box Empty	CFST_NS_E_100	5
		CFST_NS_E_140	5
		CFST_NS_E_145	10
Fixed Slab and back wall	Soil Box Empty	CFST_FS_E_100	3
		CFST_FS_E_140	5
		CFST_FS_E_145	2
Break Away Slab and fixed back wall	Soil Box Empty	CFST_BA_E_140	5

5.1.1 Wave Maker displacements

The wave maker displaces the water in the flume to create the wave. The wave maker control system creates the specified wave by adjusting the displacement and velocity time histories of the wave maker paddle. While the wave maker control system is calibrated to move the wave maker in the same way on every experiment trial, a comparison is valuable assurance. Figure 5.1 shows the wave maker displacements for the 18 1.00m waves, 25 1.40m waves, and 35 1.45m waves. The wave maker displacement is nearly identical for each type of wave, giving confidence that the input conditions for each experiment are controlled. Each line in Figure 5.1 is actually made up of at least 18 trials, with high repeatability. The wave maker displacements are identical to those given by Pyke (2020), giving credence and validity to the comparison of the shear wall and CFST specimens in Chapter 6. The wave maker displacements in Figure 5.1 are also comparable to the displacements reported in Gills (2018) and Winter (2019).

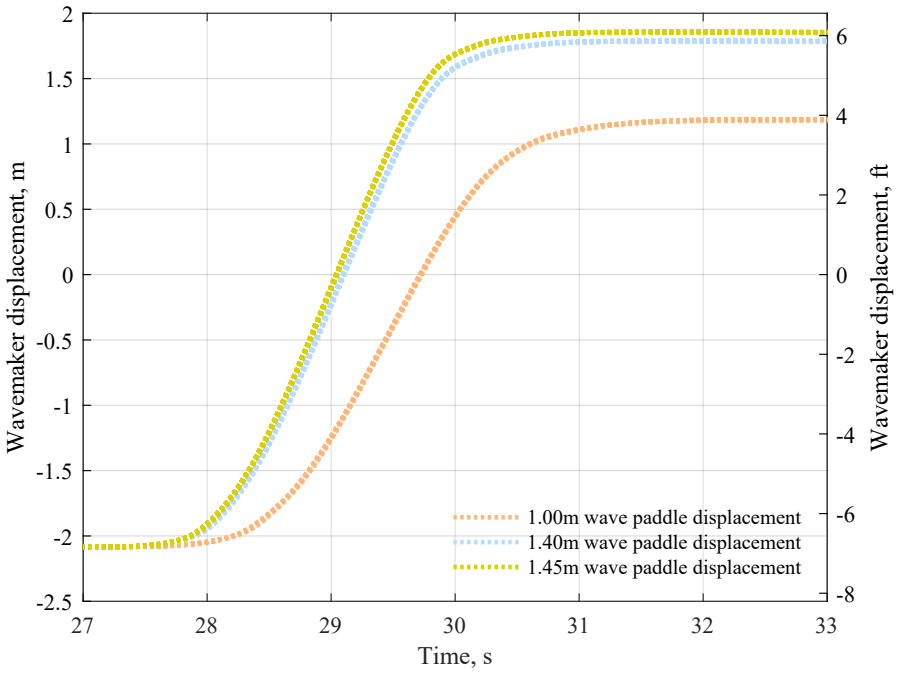

Figure 5.1: Wave maker displacement time history for CFST specimen. The time history is highly repeatable, each line on this plot comprises at least 18 trials.

5.1.2 Wave Height

The wave gauges recorded the wave height at twelve-foot (3.66m) intervals, corresponding to the bay numbering shown in Figure 4.13. In addition to the plan of the flume and the locations of the wire (WWG) and ultrasonic (USWG), the figure also presents the measured time histories for each trial. The 1.00m and 1.40m waves maintained strong repeatability with coefficients of variation at the maximum height in the wire wave gauges of 2.0% and 2.4% respectively. The coefficients of variation in the ultrasonic wave gauges were measurably larger, at 24% and 41% for the 1.00m wave and 1.40m wave, respectively. Figure 5.4 and Figure 4 show the time histories for each wave at each of the instrument points. Splashing on the sensor faces and the inherent precision of the instrument are responsible for the larger coefficients of variation recorded in the ultrasonic wave gauges. When water splashes and forms a meniscus on the emitter face, the instrument is unable to emit and record the sound waves properly. As discussed in **??**, the 1.00m and 1.40m waves meet the requirements for a stable solitary wave because their wave height to water depth ratio is less than 0.7.

The wave gauge time histories for the 1.45m wave are shown in Figure 5. The coefficient of variation in the wire wave gauges for this wave is 3.6%. This variation is larger than for the 1.00m and 1.40m waves, due to the turbulent nature of the bore. By its very nature, this wave is considered unstable (with a wave height to water depth ratio of 0.725) and has the propensity to break between bays three and four in the wave flume. The turbulent bore results in a larger coefficient of variation after the wave begins breaking. Again, the ultrasonic wave gauges are less precise than the wire wave gauges due to the splashing interference on the sensor face. The COV of the ultrasonic wave gauges is 56%.

5.1.3 Wave Particle Velocities

As discussed in Section 4.3.4, the acoustic Doppler velocimeters were used to record the fluid particle velocity at four points along the flume, shown in Figure 4.14 (reproduced here in Figure 5.5. Figure 5.6a, Figure 5.6b and Figure 5.7 show the velocity time histories in the x-direction, along the flume, for the four sensors for the three wave types. ADV 1 has the lowest variation from the mean for the 1.00m wave, as shown in Table 5.2, likely because the flume bathymetry is very

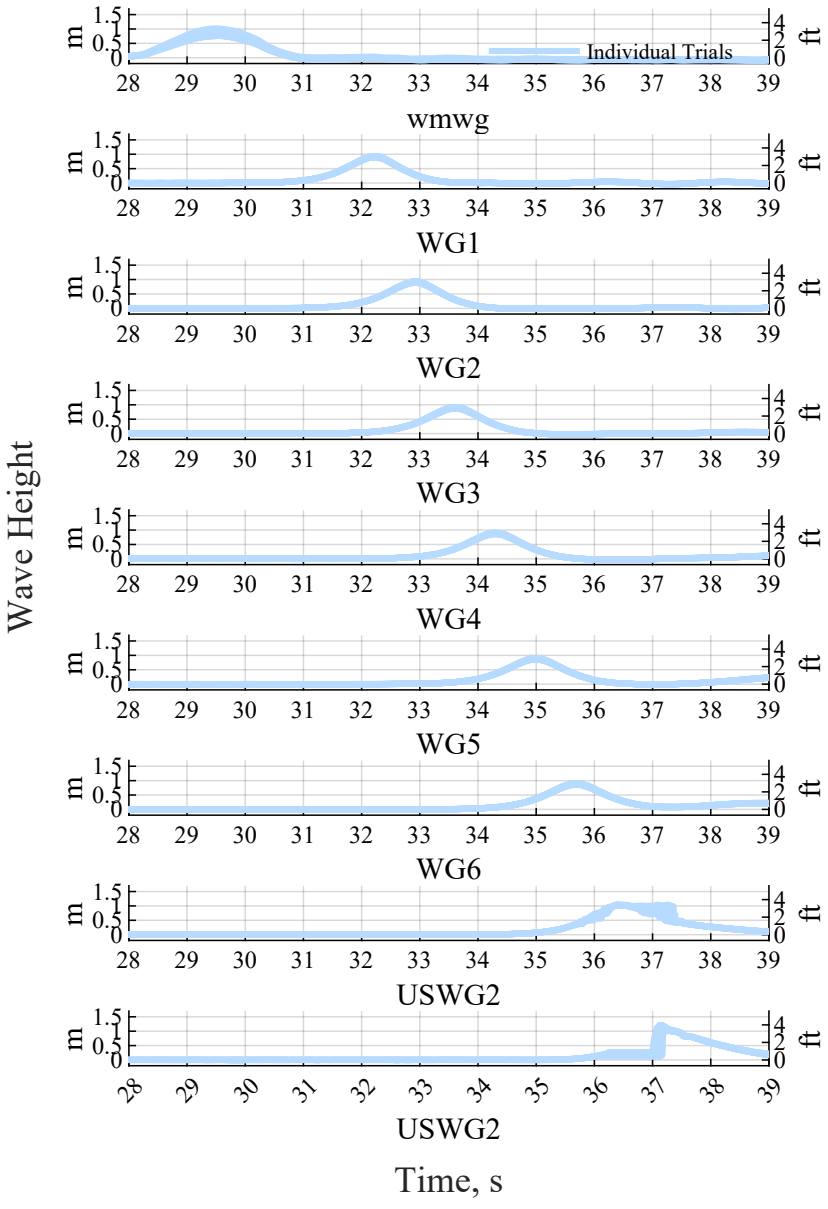

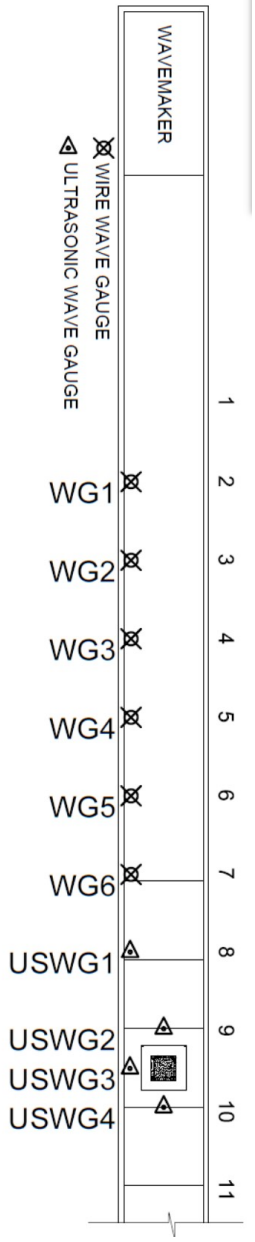

(a) wave gauge Locations

Figure 5.2: Wave gauge time histories for 18 individual trials of the 1.00m wave.

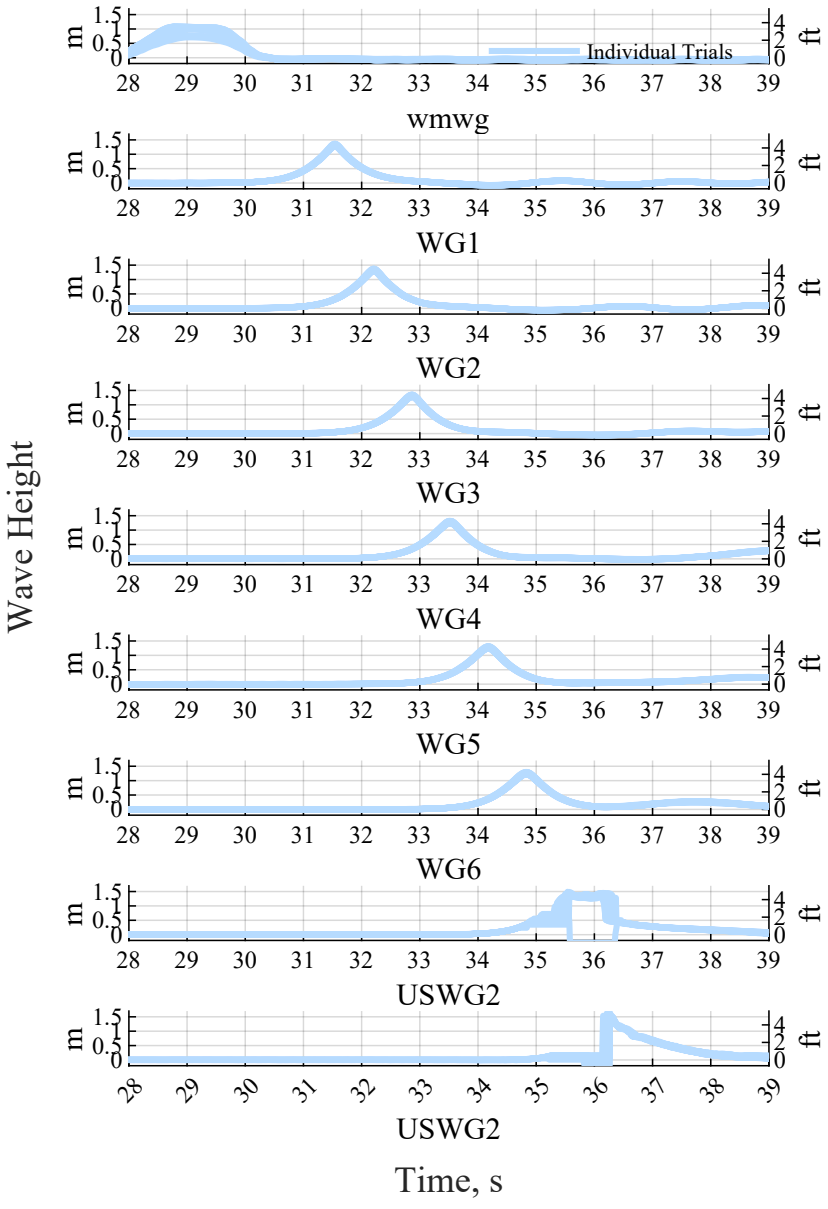

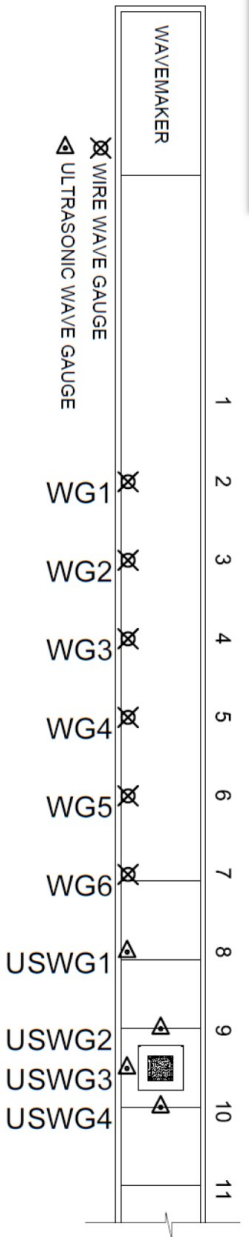

(a) wave gauge Locations

Figure 5.3: Wave gauge time histories for 25 individual trials of the 1.40m wave.

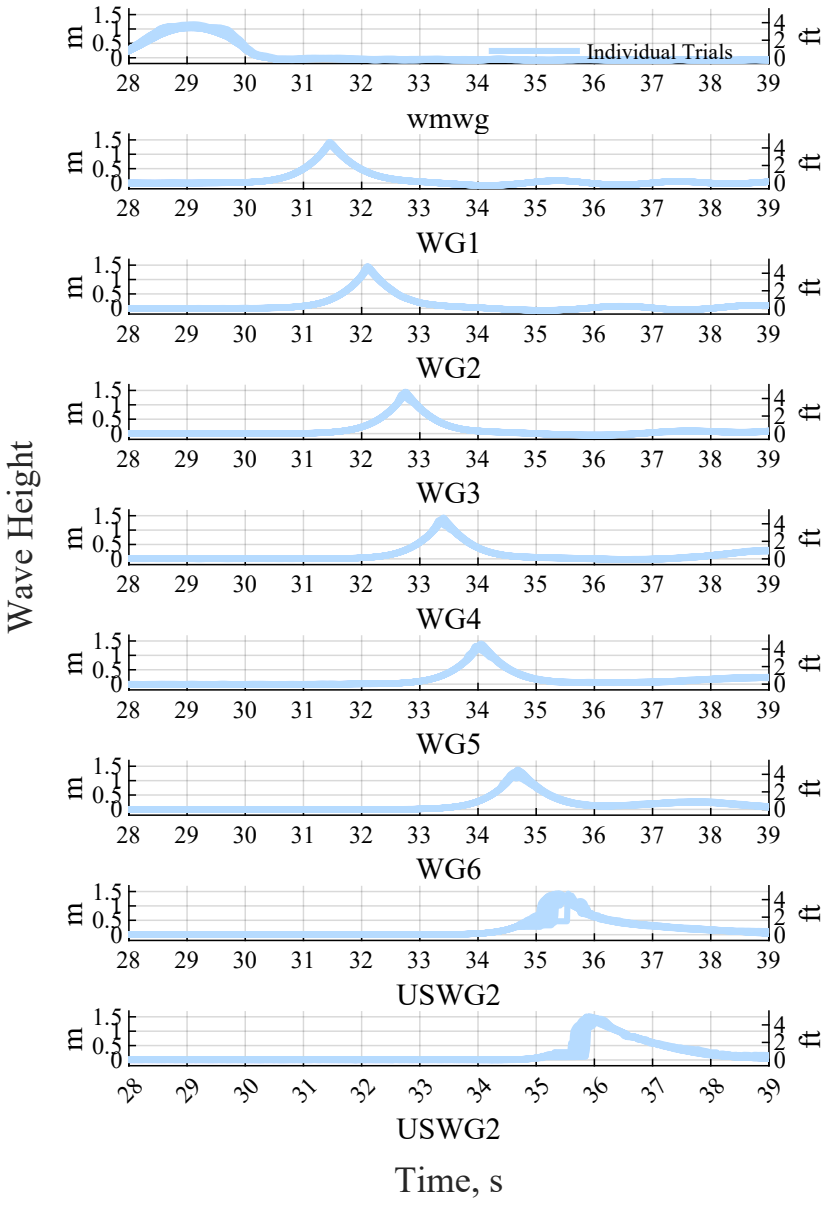

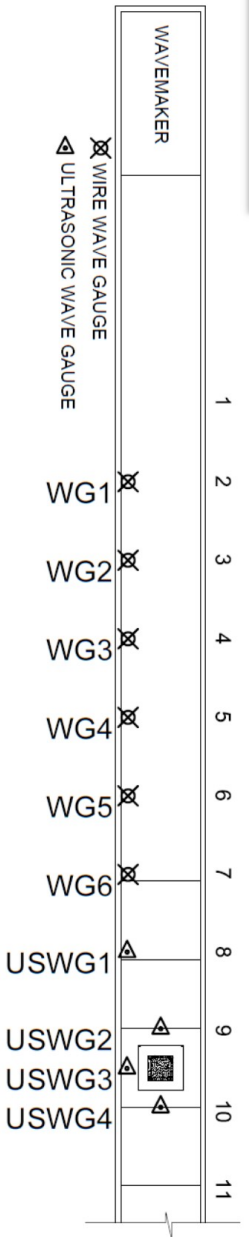

(a) wave gauge Locations

Figure 5.4: Wave gauge time histories for 35 individual trials of the 1.45m wave.

consistent at this point. ADV 2 is located near a 6.5 inch (165mm) step up to the toe slab. This slight disruption to the bathymetry produces more variability in the recorded velocity. ADV 3 is located at the base of the ramp. This results in a large disruption to the direction of flow, producing turbulence that results in even larger variation in the recorded velocity. ADV 4 is located at the top of the ramp, out of the water. As the wave surges up the ramp and impacts the structure, ADV 4 becomes submerged. The fluid particle velocity for this instrument is quite noisy, because the transition from air to water is chaotic. The coefficients of variation for each instrument and wave type are given in Table 5.2.

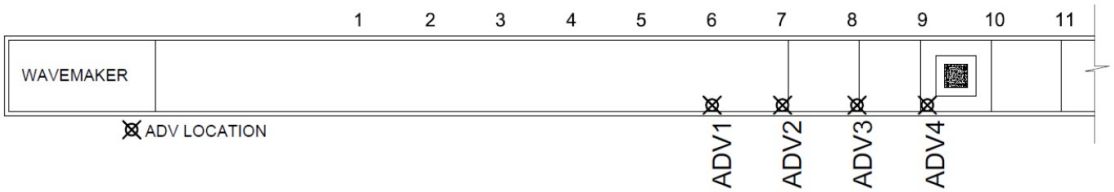

Figure 5.5: ADV Locations

Table 5.2: Coefficient of Variation and maximum at maximum absolute x-direction velocity. Values are the mean of the trials for each wave type.

	ADV 1		ADV 2		ADV 3		ADV 4	
Wave Height	instant. Max, m/s	COV %	instant. Max, m/s	COV %	instant. Max, m/s	COV %	instant. Max, m/s	COV %
1.00m	-4.04	22.8	-3.77	25.7	-4.01	25.1	-3.84	23.5
1.40m	-2.98	93.5	-4.59	17.2	-4.30	25.0	-4.49	17.6
1.45m	-4.70	53.4	-4.80	21.0	-4.76	22.3	-4.70	20.8

In summary, by examining the wave maker displacement, wave gauges, and ADVs, up until impact with the structure, the trials tested in this experiment are repeatable for each type of

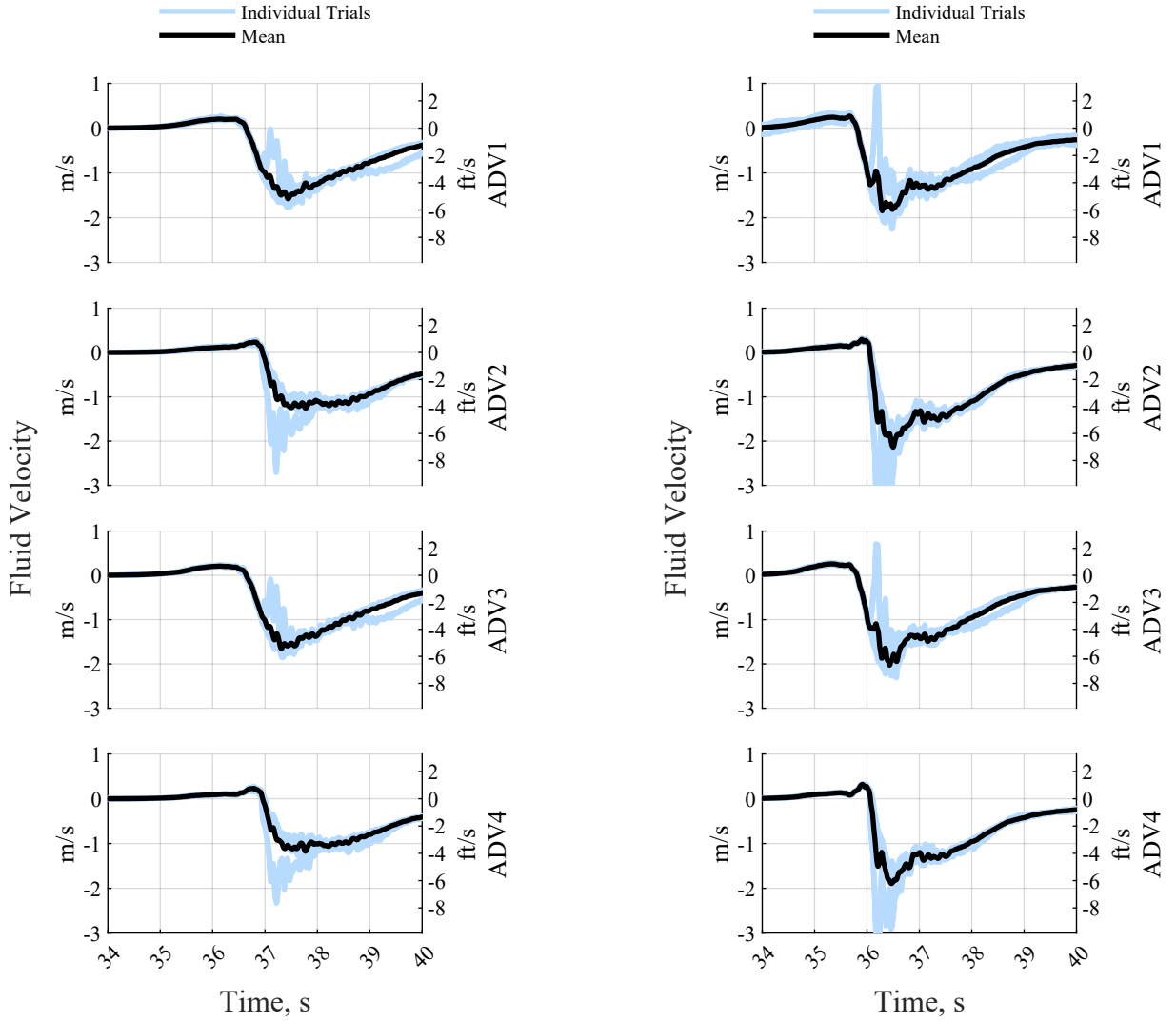

(a) ADV time history results for 1.00m wave. Plots show 18 trials.

(b) ADV time history results for 1.40m wave. Plots show 25 trials.

Figure 5.6: ADV time history results for 1.00m wave and 1.45m wave.

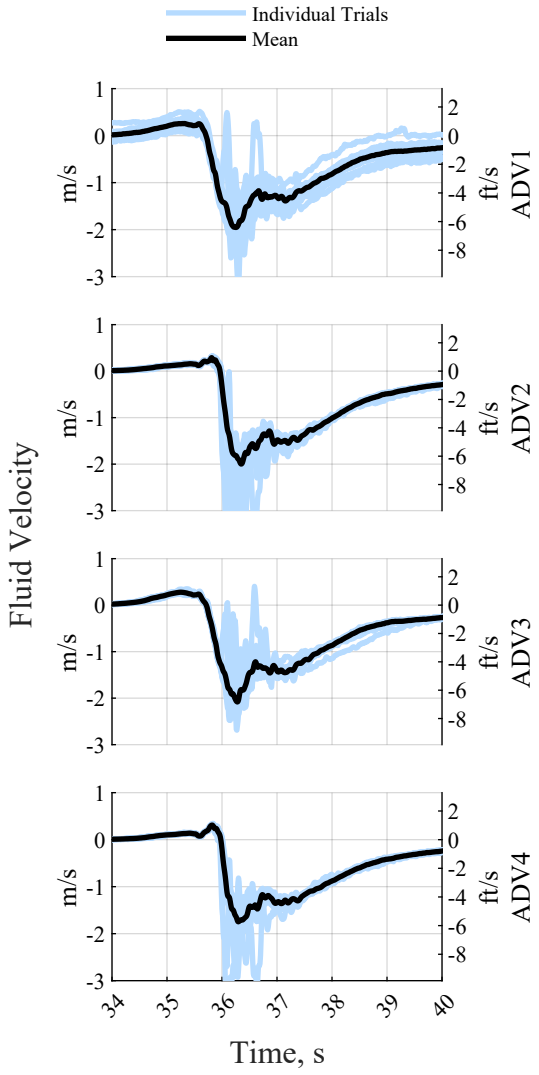

Figure 5.7: ADV time history results for 1.45m wave. Plots show 35 trials.

wave. The 1.00m and 1.40m waves were the most repeatable due to the stable solitary nature of their generation. The 1.45m wave was less consistent, so more trials were run for each experiment condition.

5.2 Processing of Raw Results

5.2.1 Utilizing strain in the Piles

Twenty-four strain gauges are instrumented on the specimen, located in the positions detailed in Figure Figure 4.11. While each gauge only produces strain data in in/in for a single point, the relative position of each strain gauge can be used to calculate the moment at several points, and the total shear within the column, using elastic material properties, and Bernoulli beam theory. Figure 5.8 shows the strain measured in each gauge for CFST_NS_E_140 trial 3 as a representative example. The figure is organized to show the column inundated by the wave first on the left, the column further from the bathymetry edge on the right. The bottom plots are the strain gauges located near the concrete slab, the plots in the middle are the strain gauges near the still water level, and the top plots show the strain gauges located immediately underneath the hat truss. Note the time phasing as the load is transferred through the hat truss, and the wave inundates the back columns of the specimen.

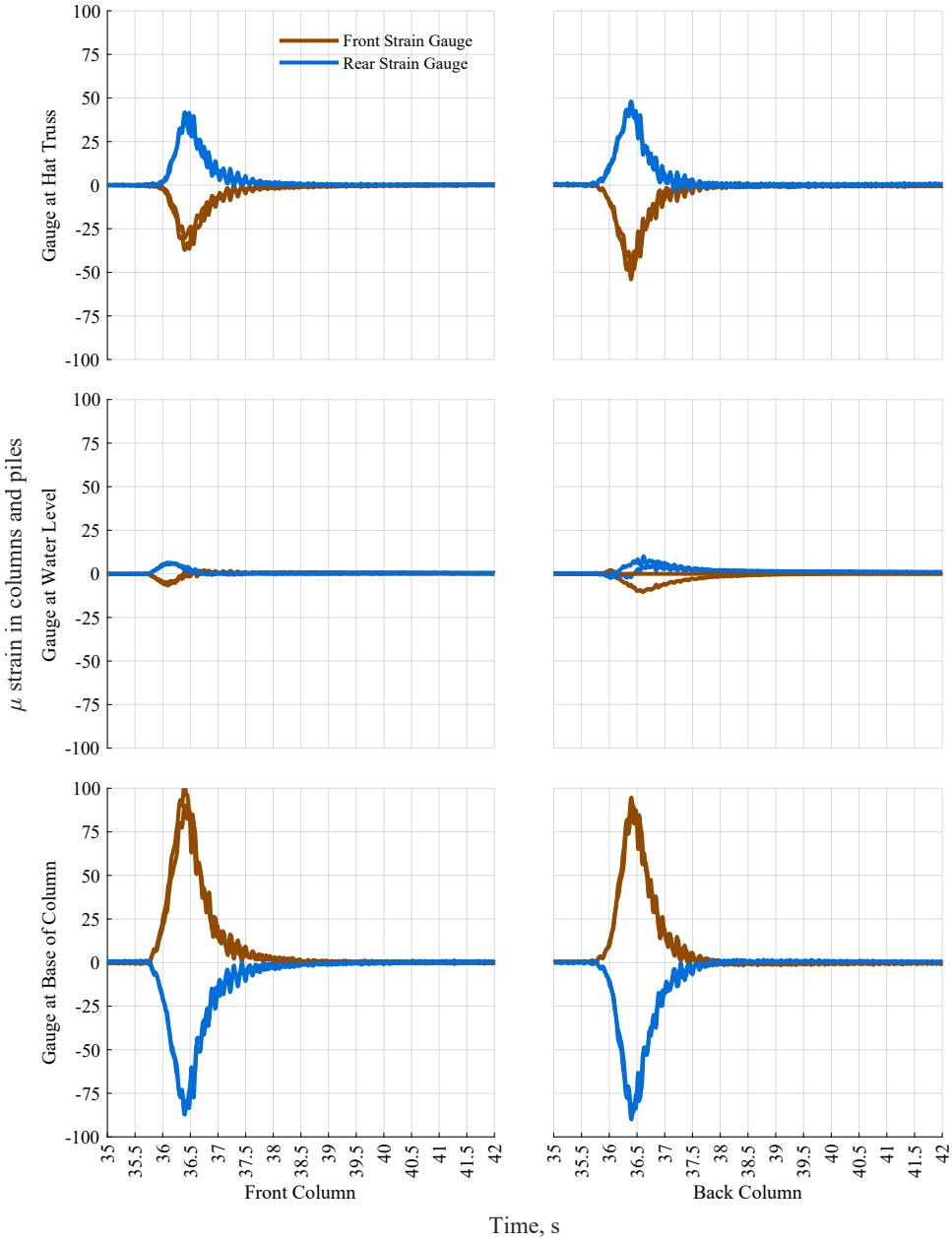

Figure 5.8: Strain in strain gauges along columns and piles for CFST_NS_E_140 trial 3. The top gauges are located immediately underneath the hat truss. The middle gauges are located at the still water level, which is approximately the point of inflection. The bottom gauges are located at the fixed base of the piles.

The moment at each elevation in each column is calculated for each instant in time using a custom made MATLAB function. First the neutral axis and curvature of the cross section at a given point in time and location along the column was calculated from the strains at opposite extreme fibers of the cross section using Equation 5.1 and Equation 5.2.

$$c = \frac{D * \epsilon_1}{\epsilon_1 - \epsilon_2} \tag{5.1}$$

$$\Phi = \frac{\epsilon_1}{c} \tag{5.2}$$

Where

- D is the diameter of the pile,
- ϵ_1 is the strain on the front of the cross section,
- ϵ_2 is the strain on the back of the cross section,
- c is the distance from the top of the cross section to the neutral axis, and
- Φ is the curvature in the cross section.

Next, the cross section was discretized into 100 equal thickness fibers to allow numerical calculation of the areas and forces. The area of steel and area of concrete for each layer was calculated using trigonometry and distilled to the MATLAB loop below.

```
for ii = 1:numLayers % Loop through each layer
    layerdepth = ii * layerthick; % Get depth of current layer
    if layerdepth < thick || layerdepth > Diam - thick
    % Check if current layer comprises only steel
        concwidth = 0;
    else
        concwidth = 2 * sqrt(ri^2 - abs(Diam/2 - layerdepth)^2);
        % Calculate chord width associated with concrete based on interior radius
```

```
        % of steel tube
    end
    steelwidth = 2*sqrt(ro^2 - abs(Diam/2 - layerdepth)^2) - concwidth;
    % Calculate chord width associated with steel based on outer radius of tube,
    % subtract concrete to achive width of steel in given layer
    areas(ii,1) = concwidth*layerthick;
    % multiply the chord length and layer thickness to get area
    areas(ii,2) = steelwidth*layerthick;
end
```

The strain in each layer of the cross section was then calculated using the curvature. The strain in each layer was then multiplied by the material area and associated modulus of elasticity, as shown in Equation 5.3. Finally, the moment at a given location along the column was calculated by multiplying the force in each layer by the depth to that point in the cross section using MATLAB Equation 5.4.

$$layerforce = strains * E_{steel} * areas(:,2)' + strains * E_c * areas(:,1)'; \tag{5.3}$$

$$Moment = sum(layerforce. * [layerthick : layerthick : Diam]); \%pound - inch \tag{5.4}$$

The complete function can be found in Appendix D. The moment time histories for raw strains in Figure 5.8 are calculated and shown in Figure 5.9. The calculated moments are for experiment condition CFST_NS_E_140 trial 3 as a representative example. The figure is organized to show the column inundated by the wave first on the left, the column further from the bathymetry edge on the right. The bottom plots are the cross sections located near the concrete slab, the plots in the middle are the cross sections near the still water level, and the top plots show the cross sections located immediately underneath the hat truss.

The shear transferred through the specimen is calculated from then difference in moment in each column. This is then divided by the distance between each cross section to calculate the shear in each column. Figure 5.10 shows the shear carried below the still water depth in each column for experiment condition CFST_NS_E_140 trial 3. All four columns are shown on the same axis to

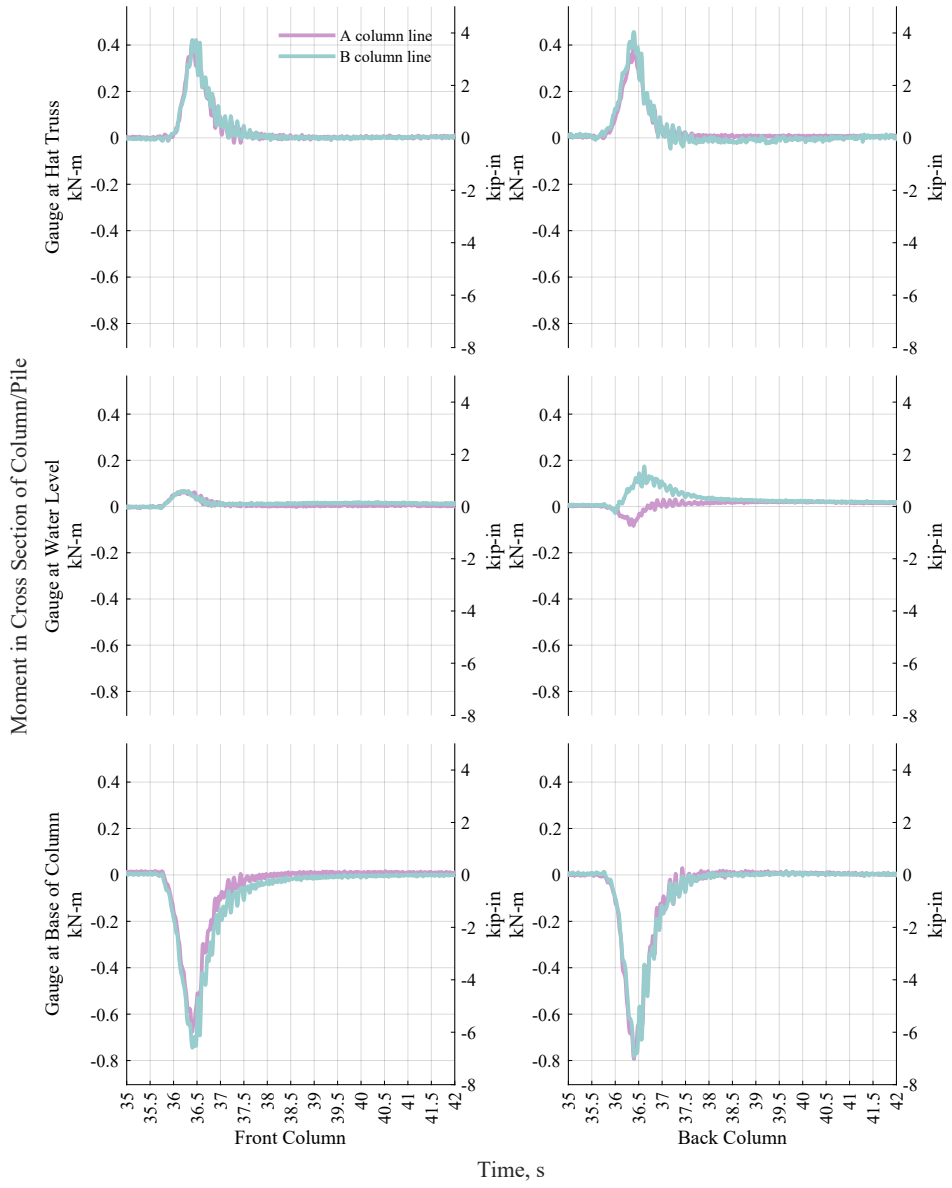

Figure 5.9: Moment calculated in each cross section along the columns and piles for CFST_NS_E_140 trial 3

show the time difference and magnitude interactions of the front and back columns. The sum of all four columns is also shown in the solid black line type.

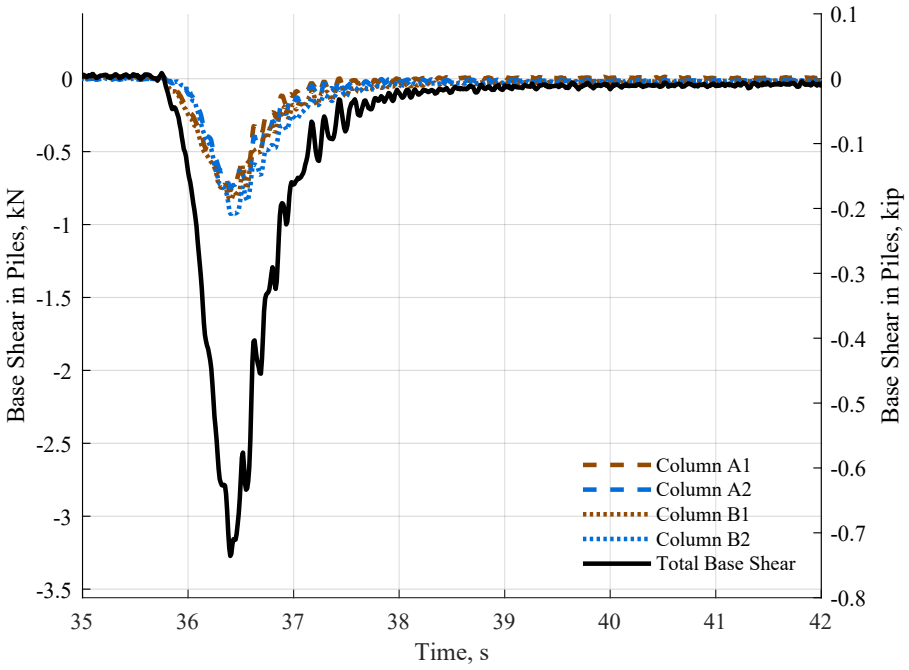

Figure 5.10: Total base shear in the piles for CFST_NS_E_140 trial 3. The shear transferred in each column is similar meaning the frame transfers load through all columns.

5.2.2 Calculating and Filtering Base Shear from Load Cells

The specimen reactions were measured with a series of eight load cells arranged to measure shear, moment and axial forces. The configuration and location of the load cells are shown in Figure 4.7. The base shear was measured using load cells SA2 and SB2, and strain gauges on the tension member. The Force resisted by the tension member was determined by calibration from the dry run test. The known input force in the dry run test was used to determine the load read by the load cells SA2 and SB2. The difference between the applied and measured load was correlated to the strain measured in the tension member. A linear regression was conducted to determine the force to strain calibration for the tension member. Figure 5.11, and Figure 5.12 show the force in load cells SA2 and SB2 and strain in the tension member for test CFST_NS_E_140 trial 3 as an example.

During set up, the load cells were adjusted to attract similar magnitude of loads and minimize the effect of torsional stiffness irregularities. In actuality, the specimen did not allow the loads to be aligned perfectly. This results in one load cell attracting slightly more load than the other. The tension member is located between the two load cells, to minimize any off axis components of the force.

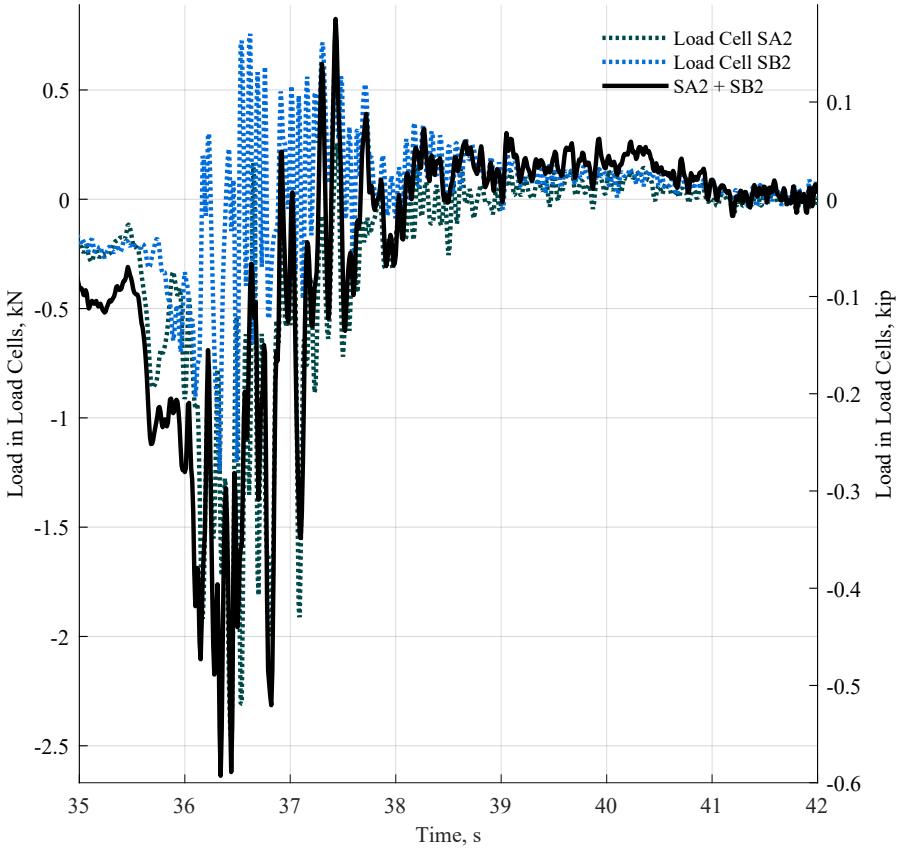

Figure 5.11: Force in crossshore load cell during test CFST_NS_E_140 trial 3. High levels of periodic noise observed in experiments with low base shear. The Lines represent the individual load cells, and the combined load in the load cells.

The tension member was pre-loaded to a tension of approximately 1500 pounds (6.67kN). Any change in that force is a change in the reaction. Figure 5.13 shows the total base shear as calculated from the load cells and tension member.

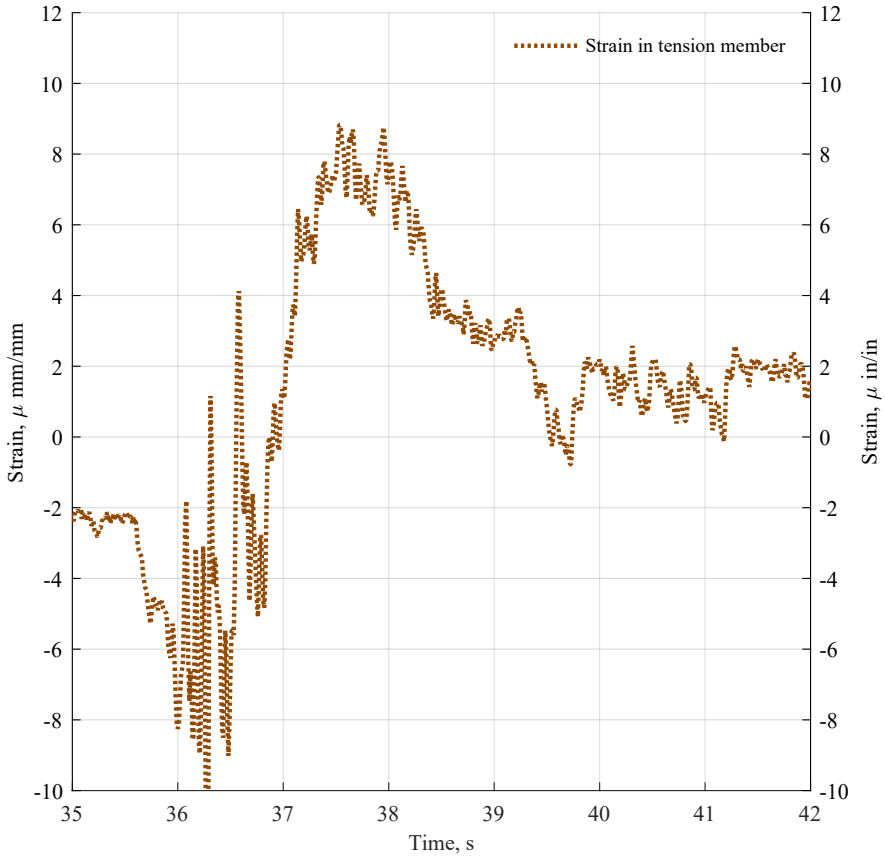

Figure 5.12: Strain recorded in tension member during test CTST_NS_E_140 trial 3. The measurement was zeroed to the beginning of the trial. Negative strain on the y-axis represents less tension in the member. The tension member did not go into compression.

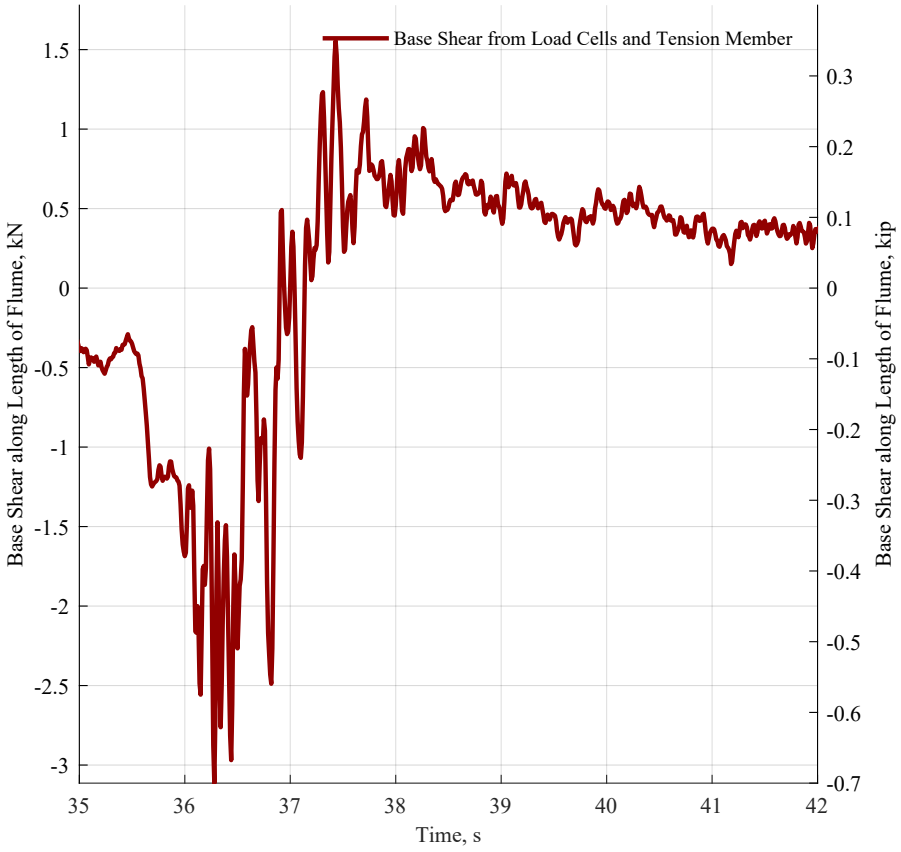

Figure 5.13: Calculated base shear from cross shore load cells and tension member. The strain in the tension member was used to adjust the base shear for load transferred through the experiment configuration.

While Figure 5.13 shows significant high frequency noise it is most prominent in trials with a low total base shear in the specimen. To cut down on the destructive influence of the noise a fast Fourier transform (FFT) was performed on the trials with no slab or back wall. The frequency spectrum is shown in Figure 5.15, and a Gaussian distribution was applied to the frequency to amplify the target frequency. Figure 14 shows the calculated base shear experienced by the specimen during CFST_NS_E_140 trial 3 after the FFT filtering and smoothing has been conducted.

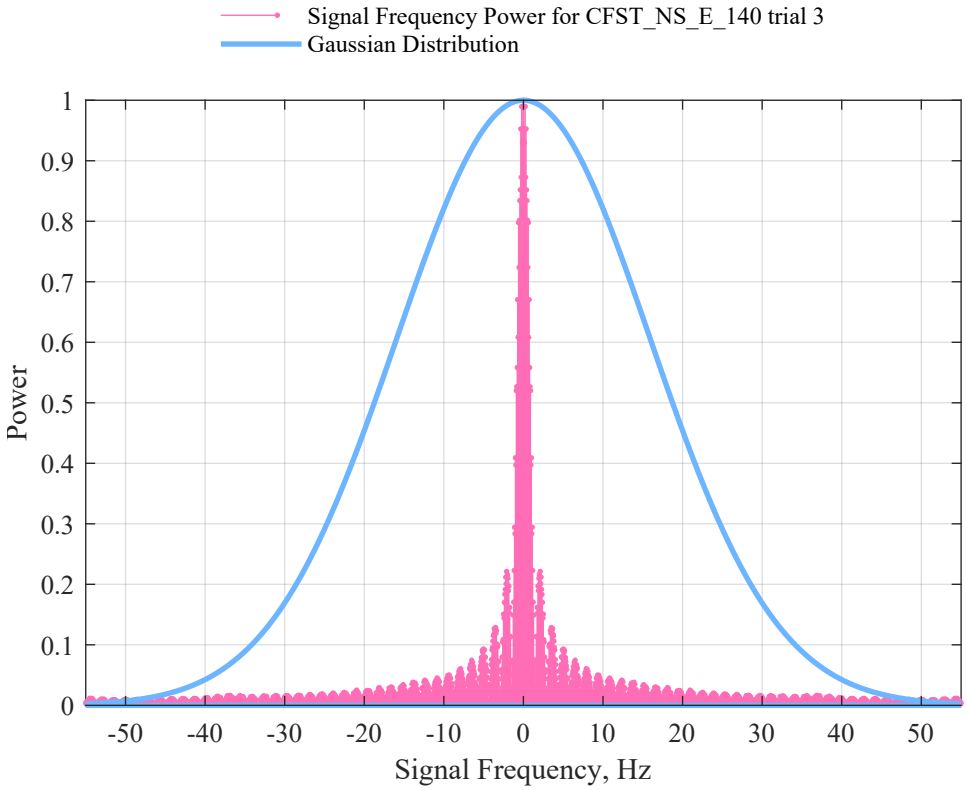

Figure 5.14: Frequency distribution and power of base shear for CTST_NS_E_140 trial 3. The Gaussian distribution is used to filter out and dampen the high frequency noise in the base shear plots.

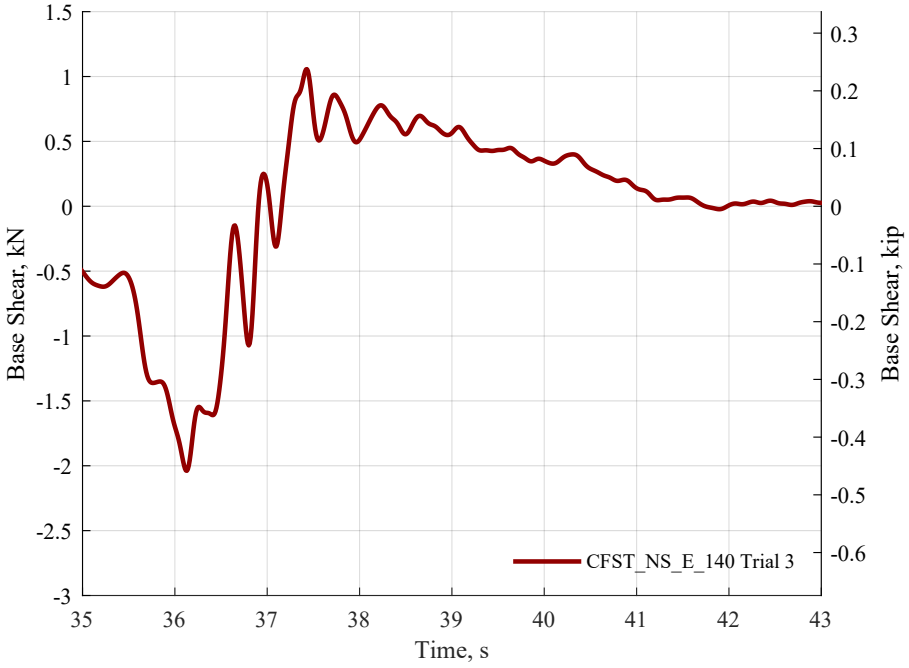

Figure 5.15: Filtered Base shear for CFST_NS_E_140 trial 3.

5.3 Structural Measurements

5.3.1 Step by Step discussion of Structural Response

As the wave impacts the specimen, several events happen in the space of 0.8 seconds. Figure 5.16 and Figure 5.17 show the wave approaching and impacting the specimen. The structural response is shown in Figure 5.18 and Figure 5.19.

At instant A, the vertical load cells are experiencing a negative moment tipping the specimen forward. This is before instant B, when the maximum wave height is reached at the top of the ramp. This suggests that the maximum negative moment is happening before the mass of water is on top of the front load cells. This is still the instant with maximum negative moment, because the hydrostatic load of the water on top of the yellow plate around the specimen is largest on the front of the plate, and negligible on the load cells VA2 and VB2. Once the bulk of the wave passes up the ramp, a larger wave height is observed on the front two load cells, but there is also more mass and hydrostatic pressure on the rear load cells, canceling out a portion of the moment. The maximum

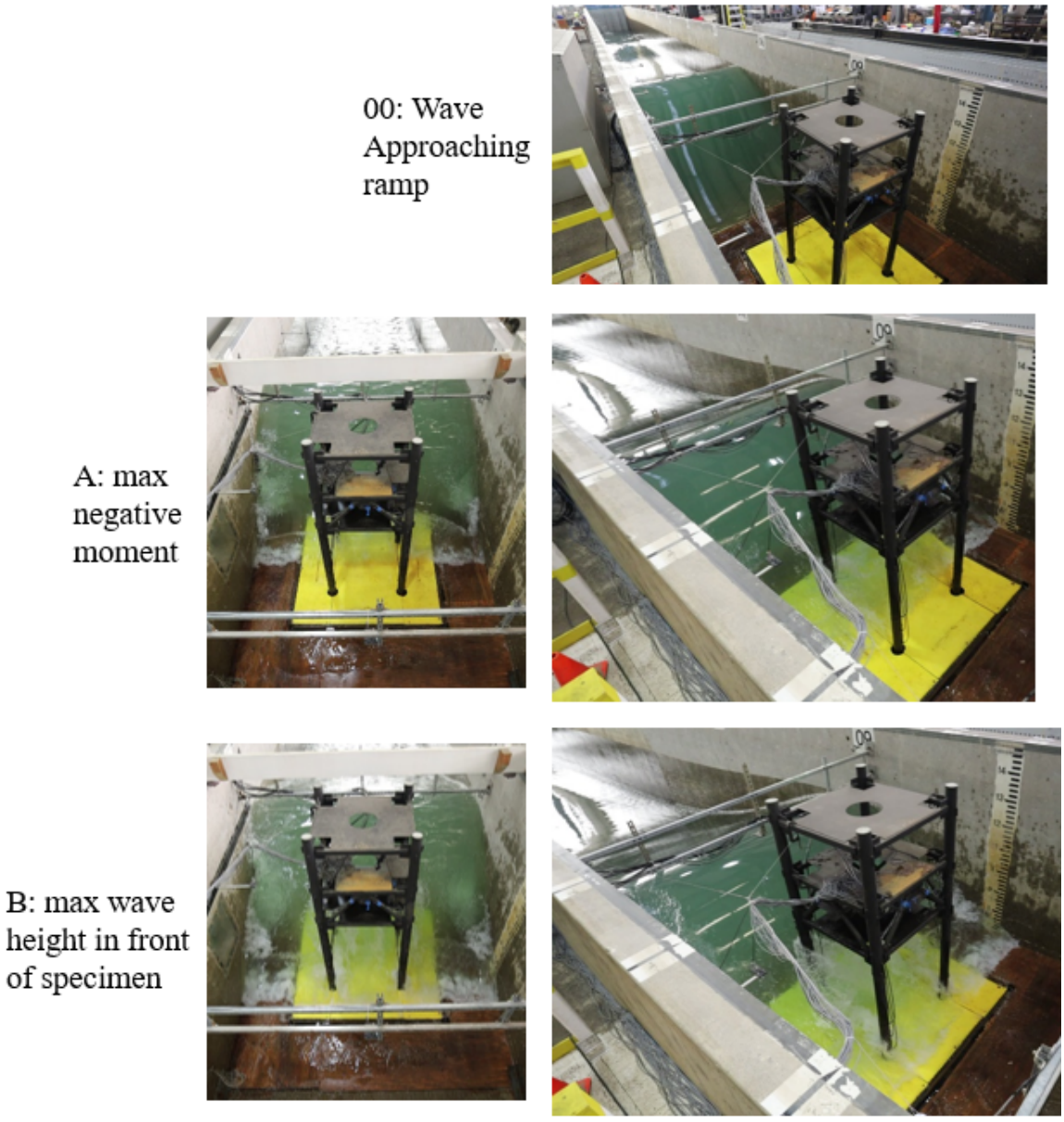

Figure 5.16: Wave approaching and beginning impact with specimen

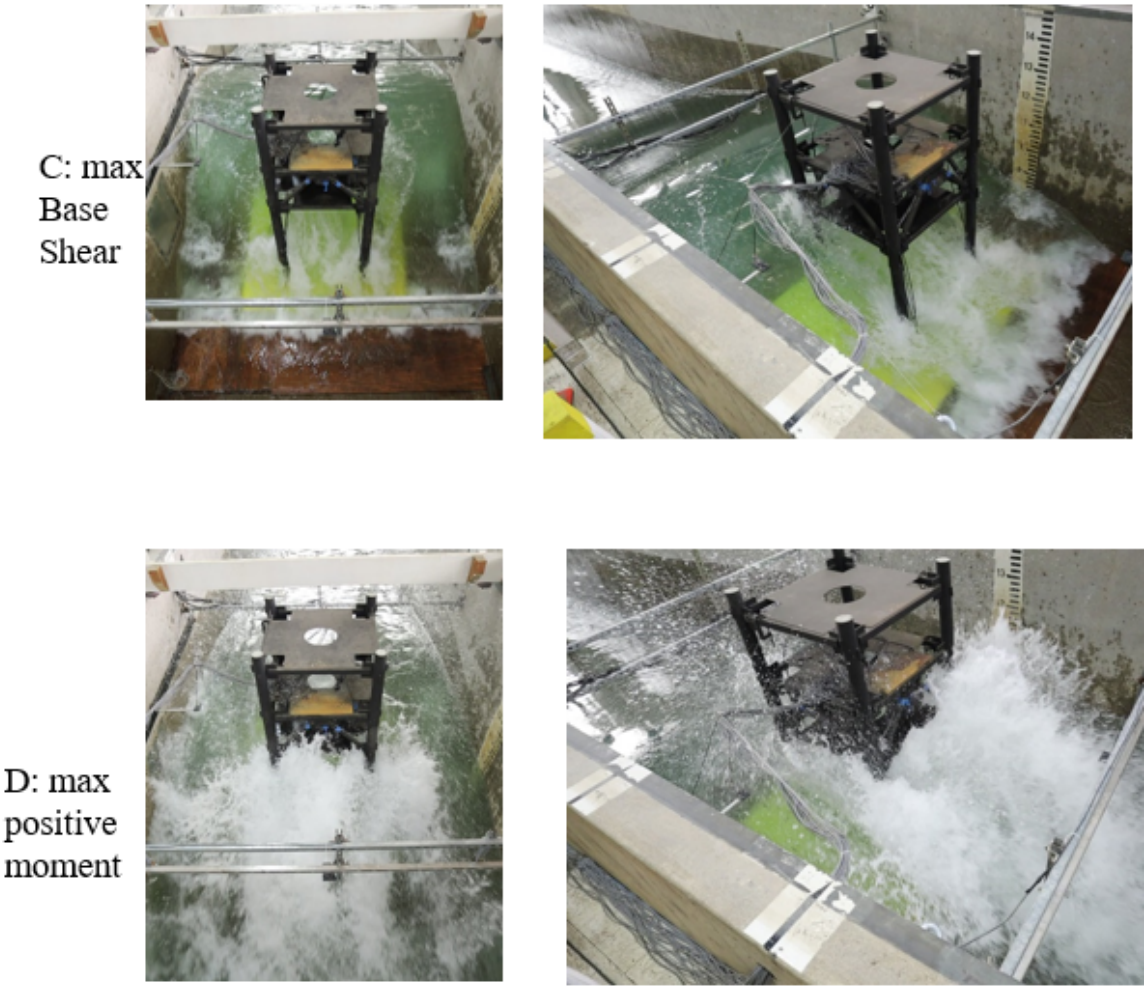

Figure 5.17: Wave impacting specimen

base shear in the piles is observed at instant C, when the wave fully inundates the front columns, and has started impacting the rear columns. This is also when the pressure gauges on the rear columns and half of the pressure gauges on the front columns experience their maximum pressure. Finally, the maximum positive moment in the vertical load cells occurs at instant D, when the bulk of the water has passed through the specimen, and is bearing on load cells VA2 and VB2.

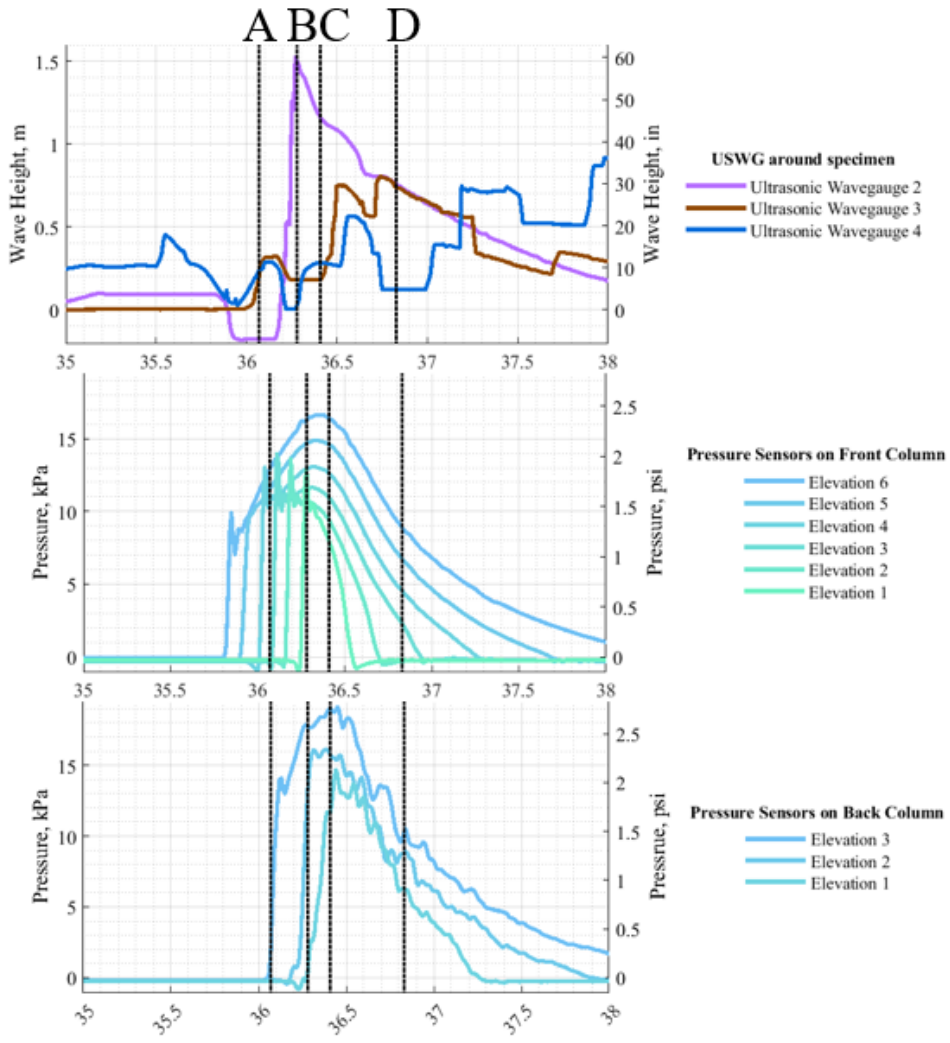

Figure 5.18: Wave height and pressure on Specimen columns.

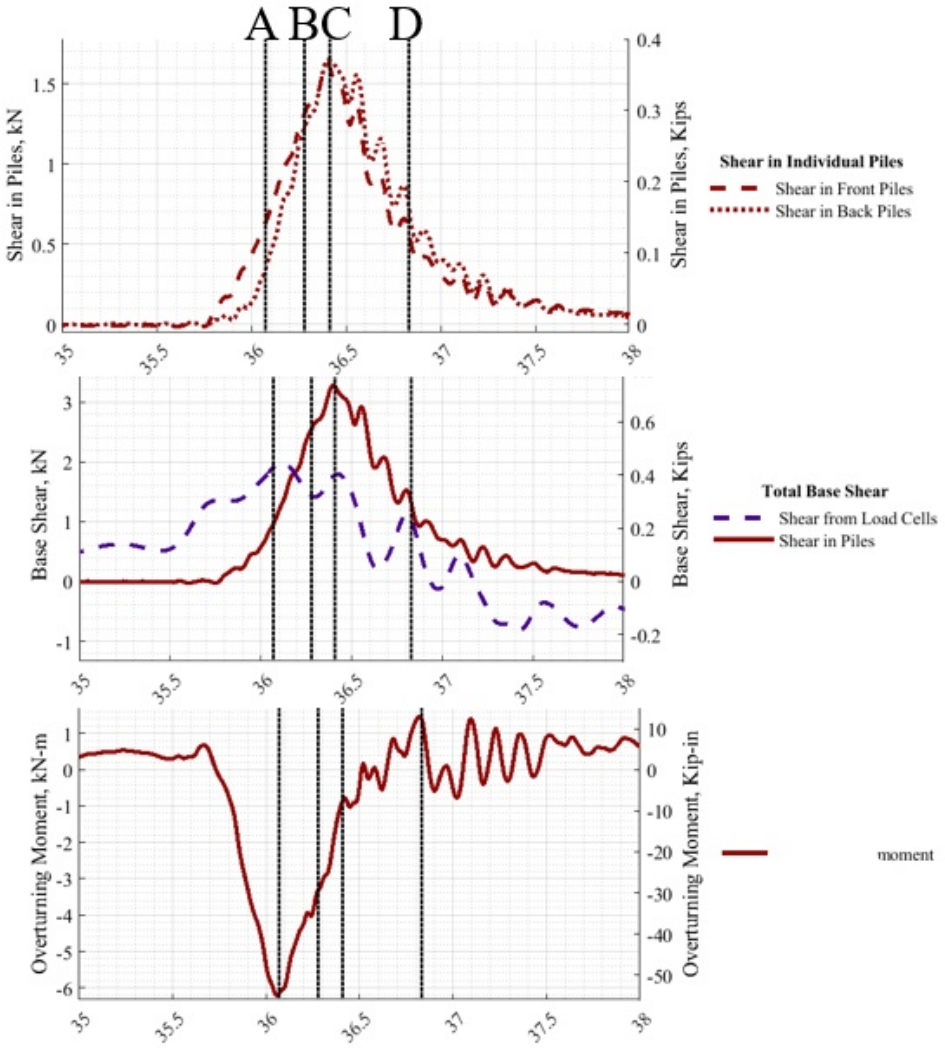

Figure 5.19: Shear in piles and load cells.

5.3.2 Pressure Time Histories

The pressure sensors measure the instantaneous pressure at discrete points along the height of the columns, in Figure 4.11, reproduced in **??** for reference. Figure 5.22 and **??** shows the pressure time histories for the front and back columns for the 1.00m wave. Each trial is plotted individually to show how congruent the repeated trials are. Experiment conditions with the fixed or break away slab could not use the pressure sensors due to concern of damaging the instruments, however, the high consistency between trials across conditions means these results can be applied to all trials. Figure 5.24 and **??** shows the pressure time histories for the front and back columns for the 1.40m wave. This trial shows pressure at the top pressure sensor, meaning there is the potential for some pressure and force to be applied due to splashing above the top pressure sensor. Figure 5.26 and **??** shows the pressure time histories for the front and back columns for the 1.45m wave. This wave breaks further down the flume, so the chaotic, turbulent bore causes more variation in the results for this wave type, when compared to others.

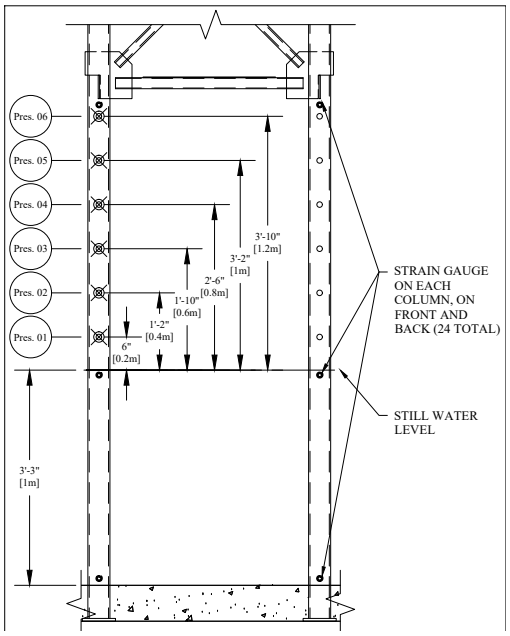

Figure 5.20: Pressure Sensor Locations along column

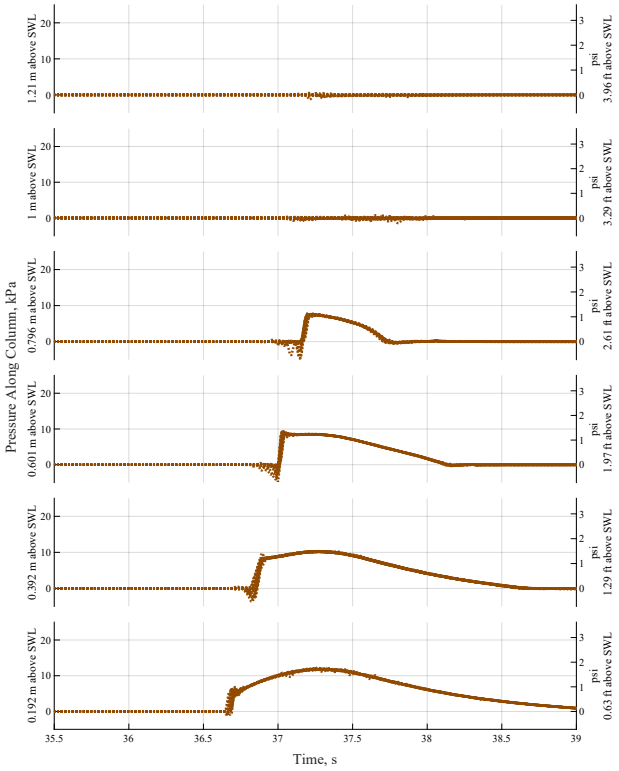

Figure 5.21: Pressures along Front Column for 1.00m wave.

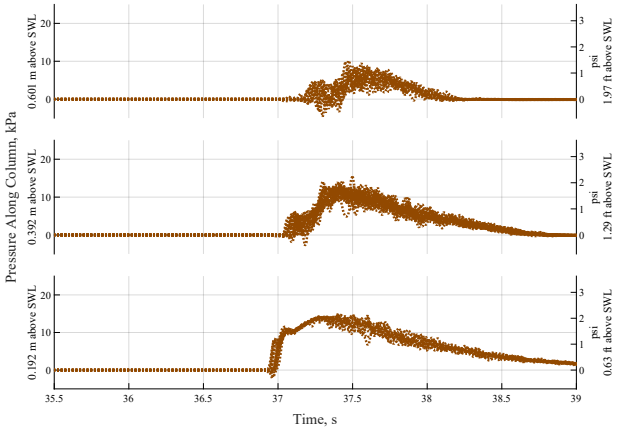

Figure 5.22: Pressures along Back Column for 1.00m wave.

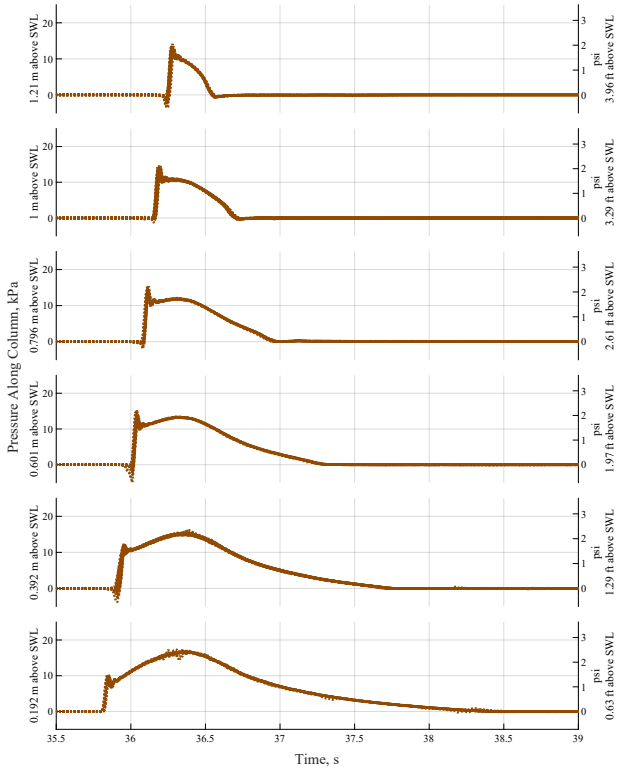

Figure 5.23: Pressures along Front Column for 1.40m wave.

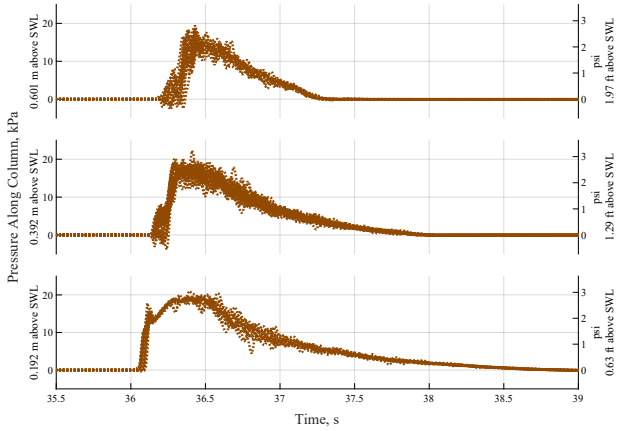

Figure 5.24: Pressures along Back Column for 1.40m wave.

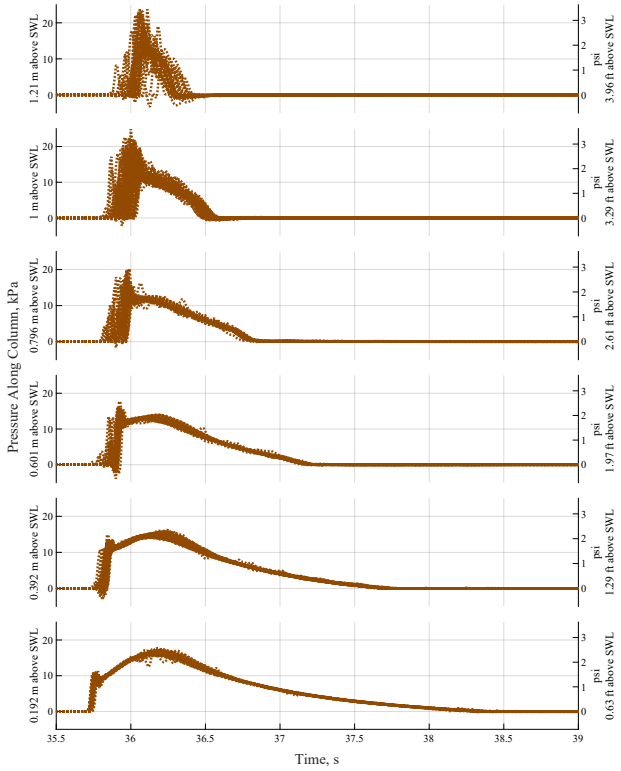

Figure 5.25: Pressures along Front Column for 1.45m wave.

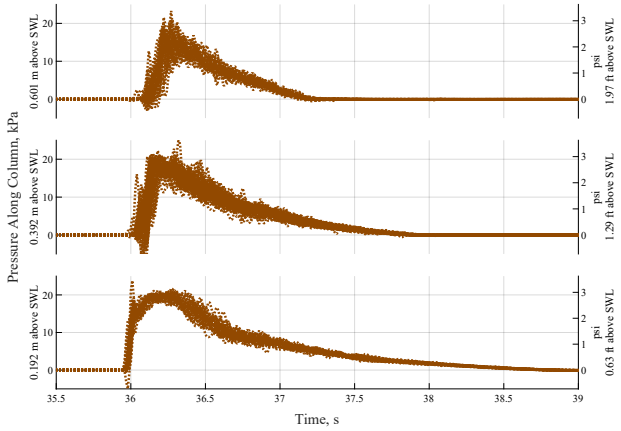

Figure 5.26: Pressures along Back Column for 1.45m wave.

5.3.3 Load Cells and Base Shear

The base shear for each experiment condition is calculated as outlined in **??**. The plots below include trials for all of the soil box conditions on one plot, because the soil condition should not affect the force applied to the specimen from the wave, and thus should not affect the force measured by the load cell and tension member. The impact of soil level on the load cell results are further investigated in Chapter 6. As shown in Figure 5.27, Figure 5.29, and Figure 5.31, this is a reasonable grouping to make. For the 1.00m wave without a back wall or midlevel slab, shown in Figure 5.27, the mean maximum base shear is -0.303kips (-1.35kN]) with a coefficient of variation of 8.5%. When the back wall and mid level slab are installed, the maximum force increases to -2.178 kips (-9.69kN]) with a coefficient of variation of 1.8%, as shown in Figure 5.28. For the 1.40m wave without a back wall or midlevel slab, shown in Figure 5.29, the mean maximum base shear is -0.483kips (-2.15kN]) with a coefficient of variation of 14.6%. When the back wall and mid level slab are installed, the maximum force increases to -3.530kips (-15.7kN]) with a coefficient of variation of 2.6%, as shown in Figure 5.30. For the 1.45m wave without a back wall or midlevel slab, shown in Figure 5.31, the mean maximum base shear is -0.576kips (-2.56kN]) with a coefficient of variation of 9.27%.

The trials with the break away slab and fixed back wall (CFST_BA_E_140) show twice the variation than the 1.40m (unbroken) wave. This is because the tuning of the break away slab is dependent on irregularities of the hardyboard "slab". Figure 5.32 shows the base shear from the break away slab and fixed back wall trials. The coefficient of variation is 5.2%, slightly higher than Figure 5.30, however, the maximum force is only -3.071kips (-13.66 kN), as opposed to -3.536 kip (-15.73kN) for the fixed slab and back wall scenario.

5.3.4 Load Cells and Moment and Torsion

Four additional load cells are located underneath the specimen measuring force in the vertical direction in the flume. These load cells, VA1, VA2, VB1, and VB2, measure the vertical load experienced by the specimen and transferred into the slab underneath the four columns. Taking the moment about the center of gravity of the concrete base slab produces the moment experienced by the specimen set up. Figure 5.33 and Figure 5.34 show the moment from the 1.00m wave without (CFST_NS_E_100) and with (CFST_FS_E_100) the fixed slab and back wall, respectively. As ex-

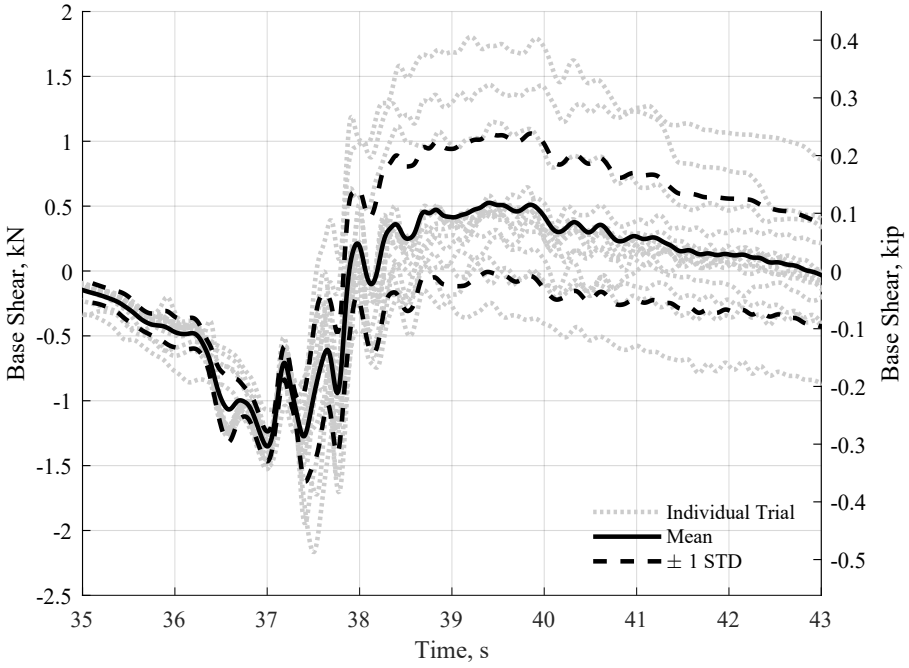

Figure 5.27: Filtered Base shear for 1.00m wave without intermediate floor or back wall. Larger variation occurs after wave impacts the specimen, likely due to the turbulent nature of the fluid structure interaction.

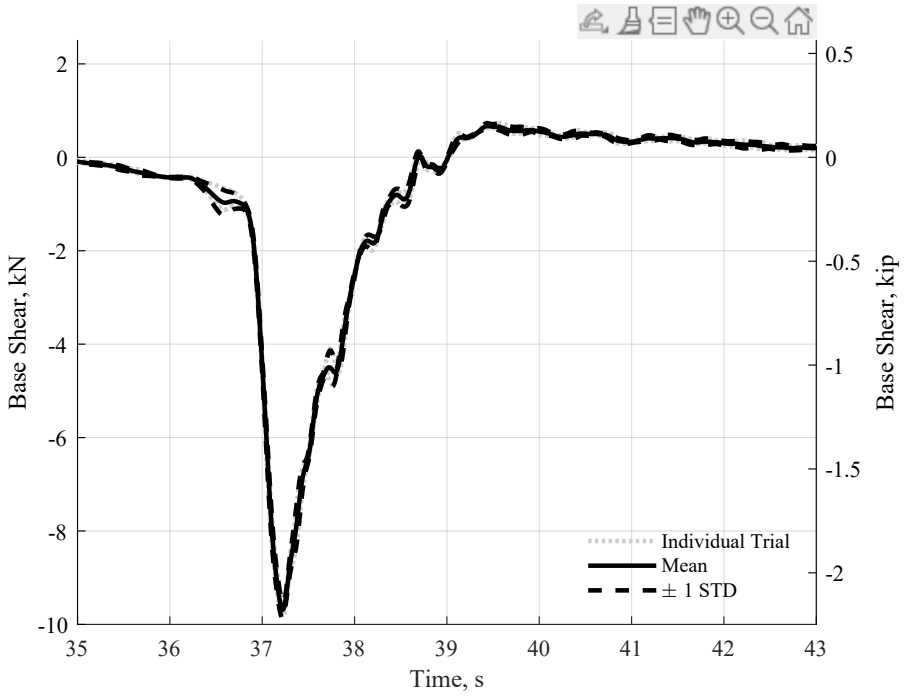

Figure 5.28: Filtered base shear for 1.00m wave with a fixed first story slab and back wall.

pected, the conditions with the fixed slab and back wall produce a larger and different manifestation of the moment in the specimen set up. Similarly, Figure 5.35 and Figure 5.36 show the moment in the specimen set up for the 1.40m wave. The general shape of the reaction are similar between Figure 5.33 and Figure 5.35, and between Figure 5.34 and Figure 5.36, with the expected difference in magnitude, for the larger wave. Figure 5.37 shows the calculated moment in the specimen set up from the 1.45m wave. As shown typically, the coefficient of variation is larger for this wave type, due to the chaotic nature of the turbulent bore, however, more trials were run, to produce more data points from which to take statistical meaning.

In addition to the moment in the specimen set up and base shear, the load cells can be used to calculate the torsion about the vertical axis of the specimen. Theoretically, the torsion should sum to zero, because the wave should be symmetric, the specimen be placed in the exact center of the wave flume, and there are no torsional stiffness irregularities. In reality, there are slight eccentricities related to the placement of the specimen and the exact stiffness of the components

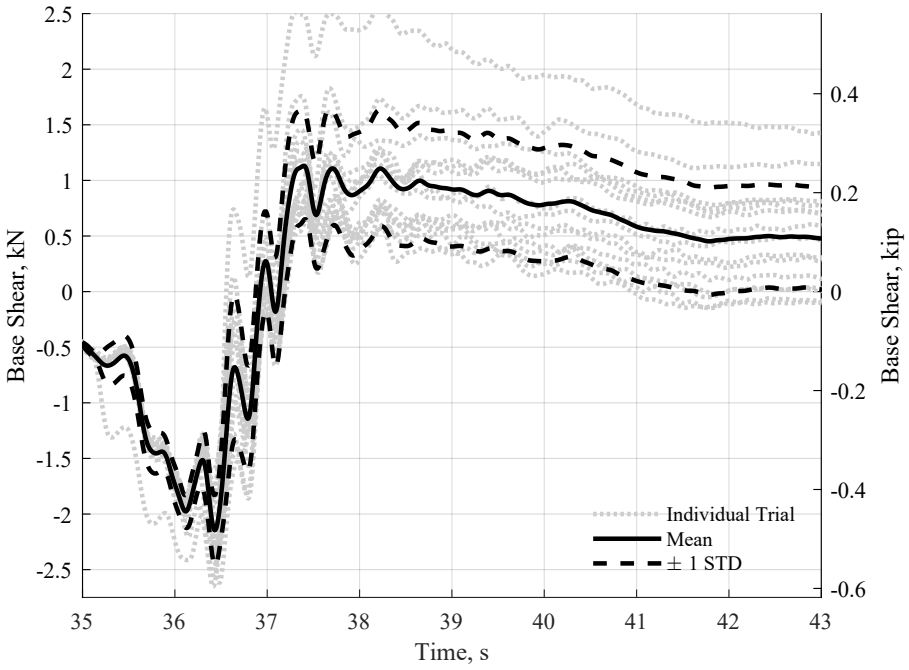

Figure 5.29: Filtered base shear for 1.40m wave without intermediate floor or back wall. The general shape of this impact is similar to Figure 5.27, while the magnitude is slightly larger, corresponding to the larger wave.

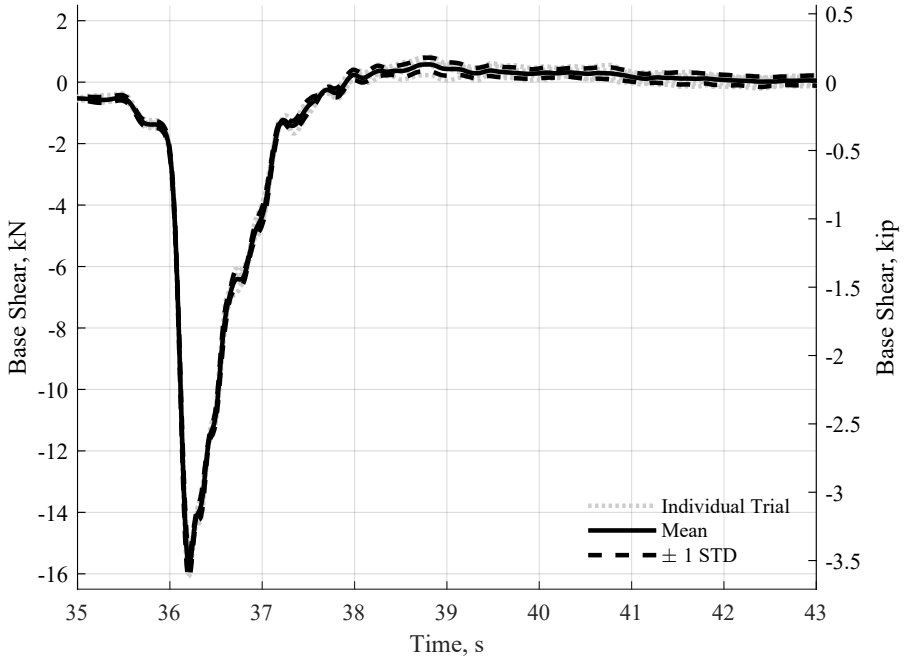

Figure 5.30: Filtered base shear for 1.f0m wave with a fixed first story slab and back wall.

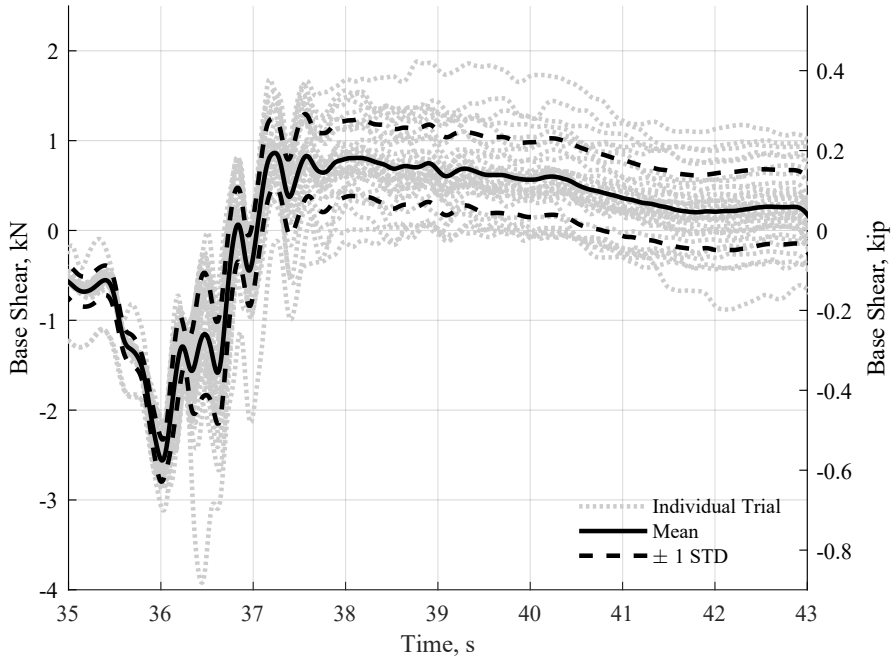

Figure 5.31: Filtered base shear for 1.45m wave without fixed first story slab or back wall.

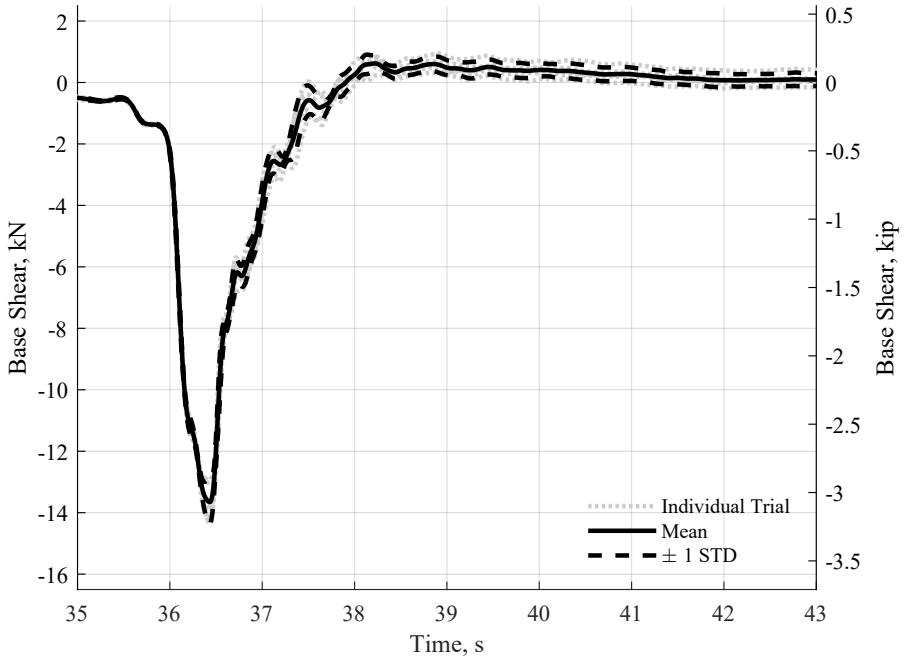

Figure 5.32: Filtered base shear for 1.40m wave with breakaway first story slab and fixed back wall.

connecting the specimen to the reaction frame and reaction frame to the flume floor and walls. The torsion on the specimen is calculated by summing the torsions about the midpoint of the back face of the soil box. This position was chosen because the tension member points directly through this point, thus zeroing any contribution from the tension member. The calculated torsion is the same if taken about any point in the wave flume, however this point was chosen for convenience. Figure 5.38 and Figure 5.39 show the torsion from the 1.00m wave without, and with the fixed slab and back wall. The torsion measured without the fixed slab or back wall is similar to the torsion with the fixed slab and back wall. Figure 5.40 and Figure 5.41 show similar results for the 1.40m wave. Unlike the moment in the specimen set up, the general shape type of reaction, and magnitude are consistent across all wave types, and with or without the fixed slab and back wall. Figure 5.42 demonstrates the torsion reaction from the 1.45m breaking wave. This trial was conducted without a slab or back wall, and again, the shape, and magnitude are most similar to the other trials without the back wall and slab. This is easily explained by the similarities between the specimen geometry and magnitude of the forces transferred from the wave.

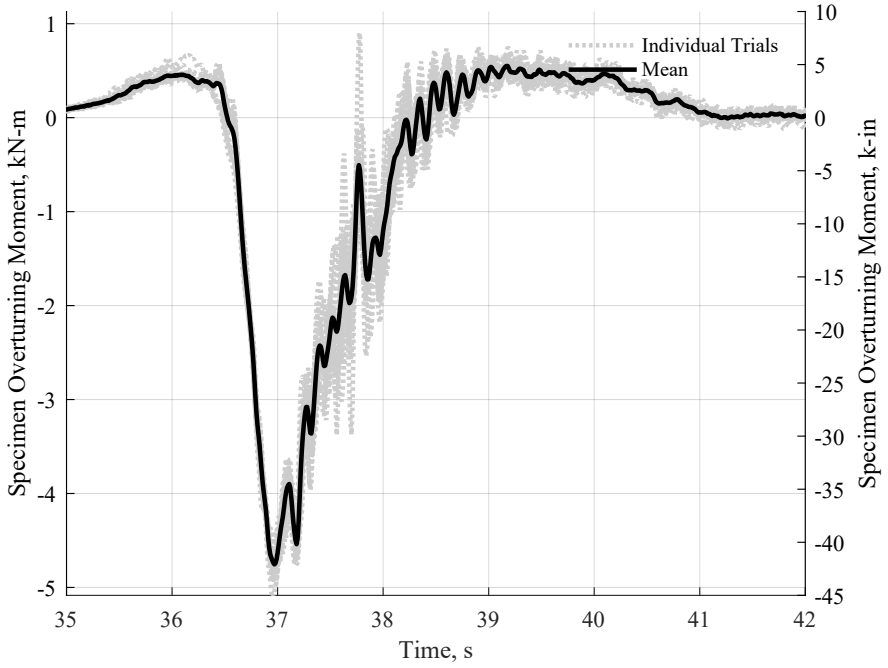

Figure 5.33: Moment in the specimen set up forthe 1.00m wave without intermediate floor or back wall. Larger variation occurs after wave impacts the specimen, likely due to the turbulent nature of the fluid structure interaction.

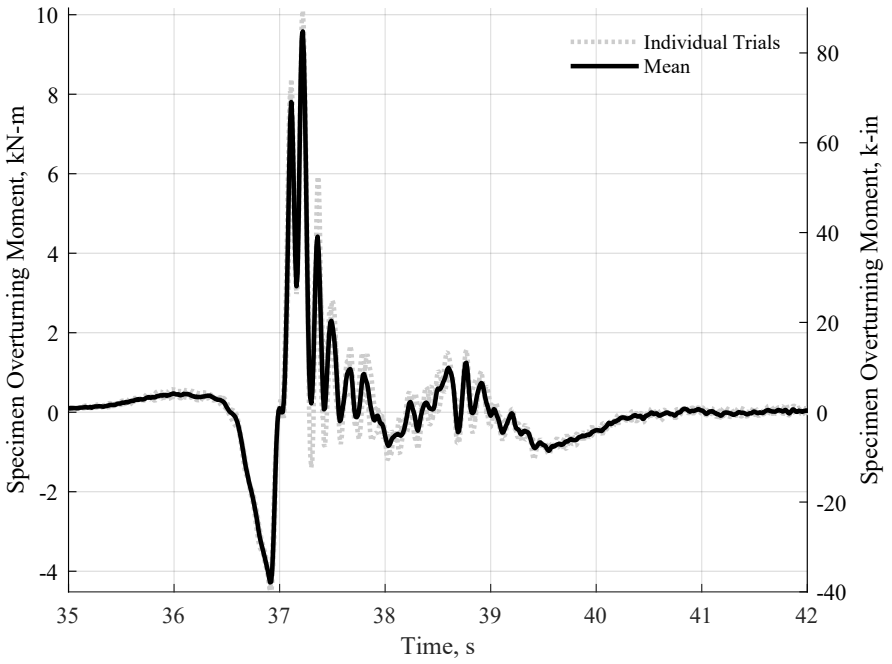

Figure 5.34: Moment in the specimen set up for 1.00m wave, with a fixed first story slab and back wall.

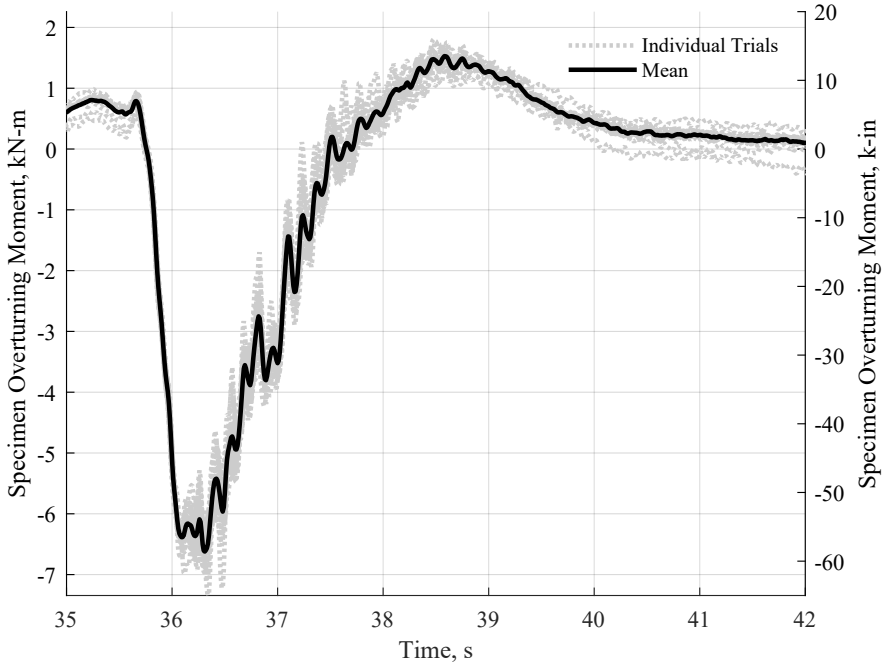

Figure 5.35: : Moment in the specimen set up for 1.40m wave, without first story slab or back wall.

5.3.5 Strain Gauge Measurements

All of the raw strain gauge measurements are plotted in Appendix E. From these plots, it is clear that two gauges broke in the course of changing the experimental conditions. To compensate for this, the broken gauge values were replaced by the strain measured in the corresponding gauge on the opposite column.This section presents the base shears in the piles calculated from the measured strains. Further comparisons between overturning moments and soil level are done in Chapter 6.

Base shear in piles with no soil present

The base shear calculated from the strain in the piles for all trials of a given experiment condition are included below. Similar to the load cells, smaller waves produce results with a smaller coefficient of variation. Figure 5.43 and Figure 5.44 show the base shear in the piles for the 1.00m wave without and with the fixed slab and back wall, respectively. Figure 5.45 and Figure 5.46 represent the data for the 1.40m wave, and Figure 5.47 shows the base shear as calculated from the strain gauges for

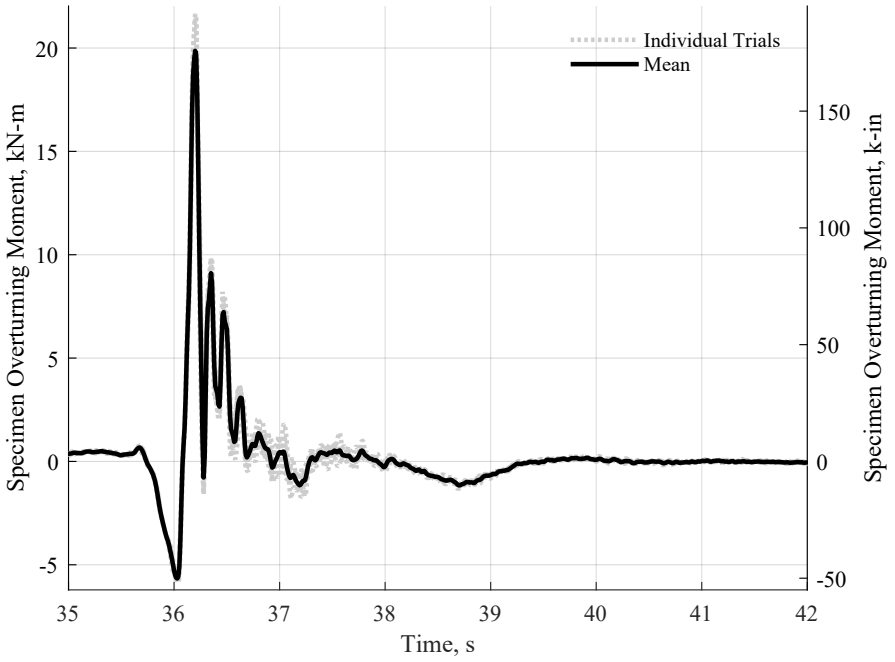

Figure 5.36: Moment in the specimen set up for 1.40m wave with a fixed first story slab and back wall.

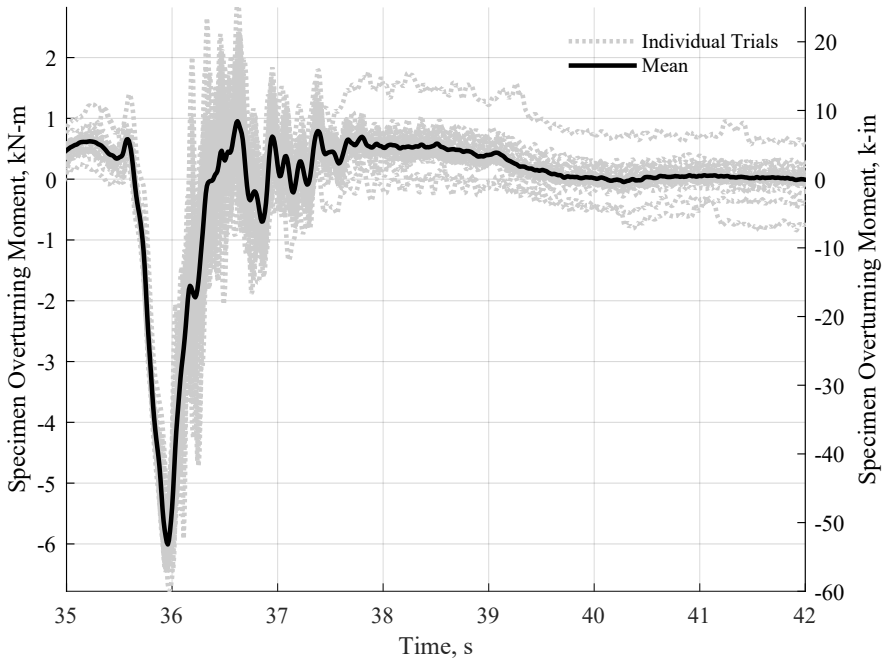

Figure 5.37: Moment in the specimen set up for 1.45m wave without fixed first story slab or back wall.

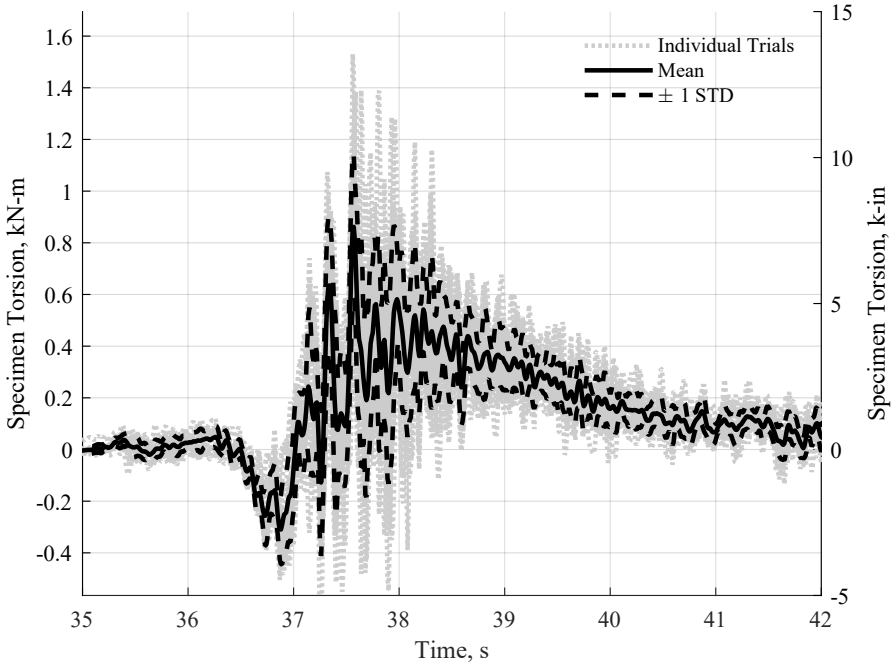

Figure 5.38: Torsion in specimen set up measured by load cells, 1.00m wave, no first story slab or back wall

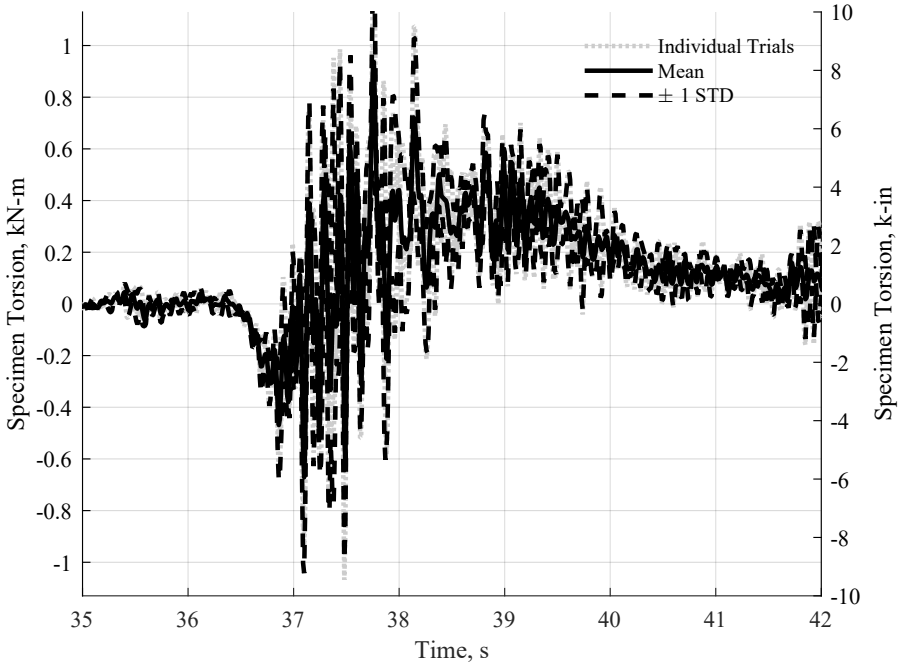

Figure 5.39: Torsion in specimen set up measured by load cells, 1.00m wave, with first story slab and back wall.

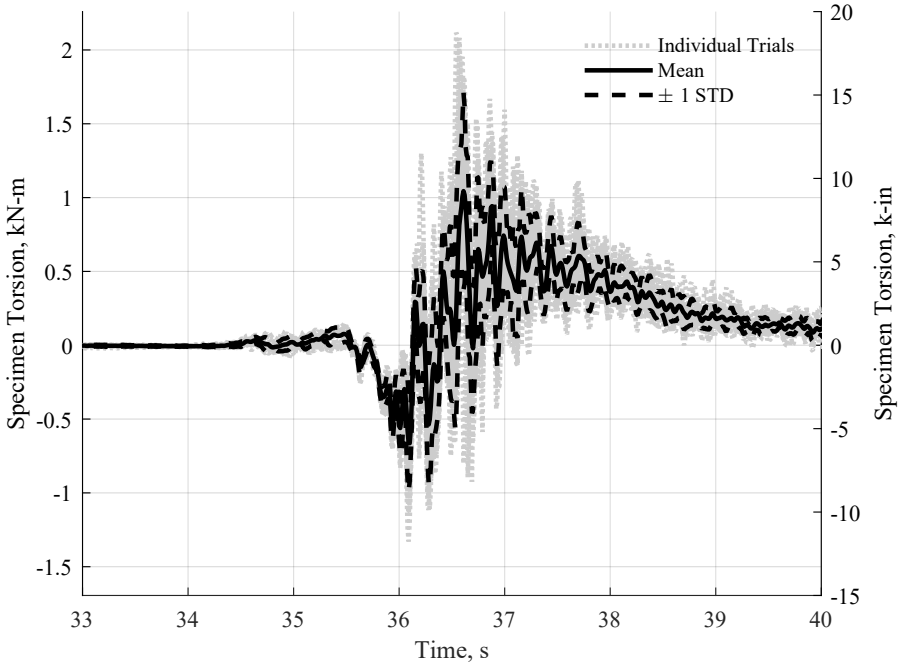

Figure 5.40: Torsion in specimen set up measured by load cells, 1.40m wave, no first story slab or back wall

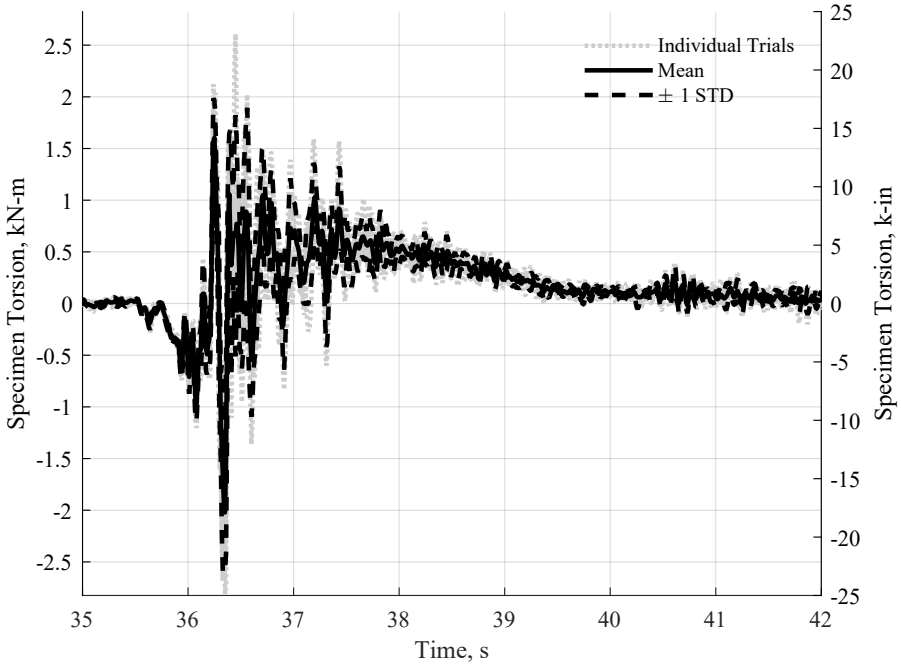

Figure 5.41: Torsion in specimen set up measured by load cells, 1.40m wave, with first story slab and back wall.

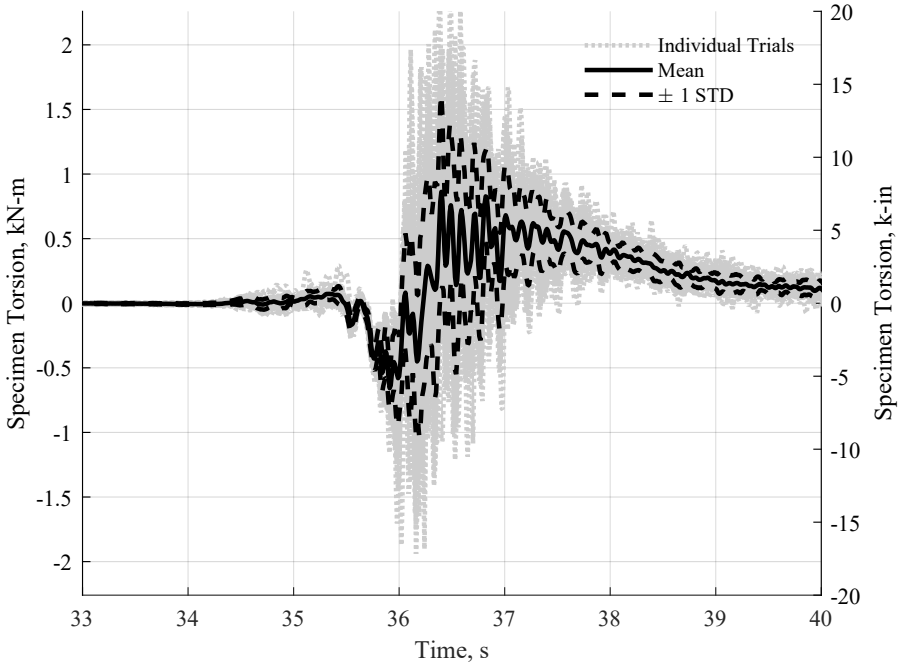

Figure 5.42: Torsion in specimen set up measured by load cells, 1.45m wave, no first story slab or back wall

the 1.45m breaking wave.

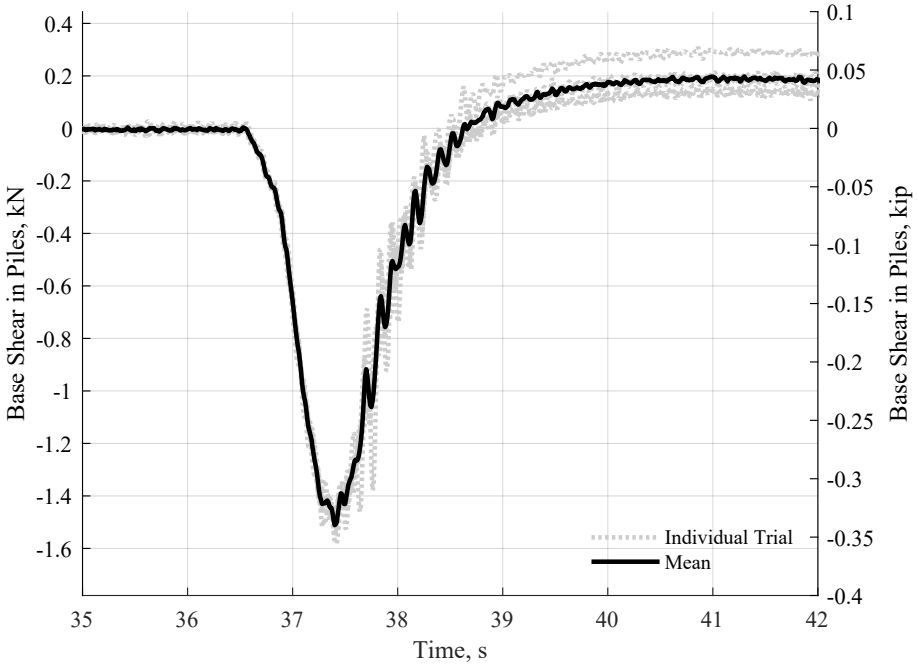

Figure 5.43: Base shear calculated from strain for 1.00m wave without the first floor slab or back wall, and with an empty soil box. CFST_NS_E_100

Shear in piles with soil present

The previous section compared the base shear carried in the piles of the specimen when the soil box was empty. This section examines the shear in the same piles, but in the experiment cases with soil in the soil box. Theoretically, some of the force will be transferred into the soil over the length of the piles, thus reducing the total shear calculated in the piles. Figure 5.48 shows the shear carried in the piles for the 1.00m wave under a half full soil box, and Figure 5.49 shows filled soil box. Figure 5.50 shows the shear carried in the piles for the 1.40m wave under a half full soil box , and Figure 5.51 shows a filled soil box. Figure 5.53 show the shear carried in the piles for the 1.45m breaking wave under a full soil box, and Figure 5.52 shows a half filled soil box. On preliminary examination, the shear carried by the columns when the soil box is half full, and empty are similar in magnitude. The shear in the columns, however, is about 30% lower in the trials with the soil

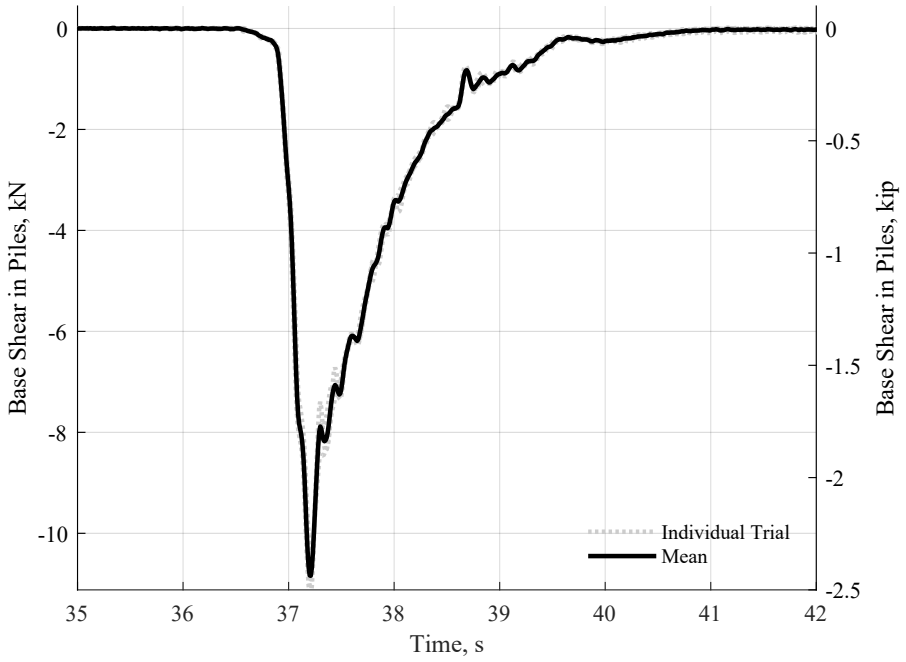

Figure 5.44: Base shear calculated from strain for 1.00m wave with the first floor slab and back wall, and with an empty soil box. CFST_FS_E_100

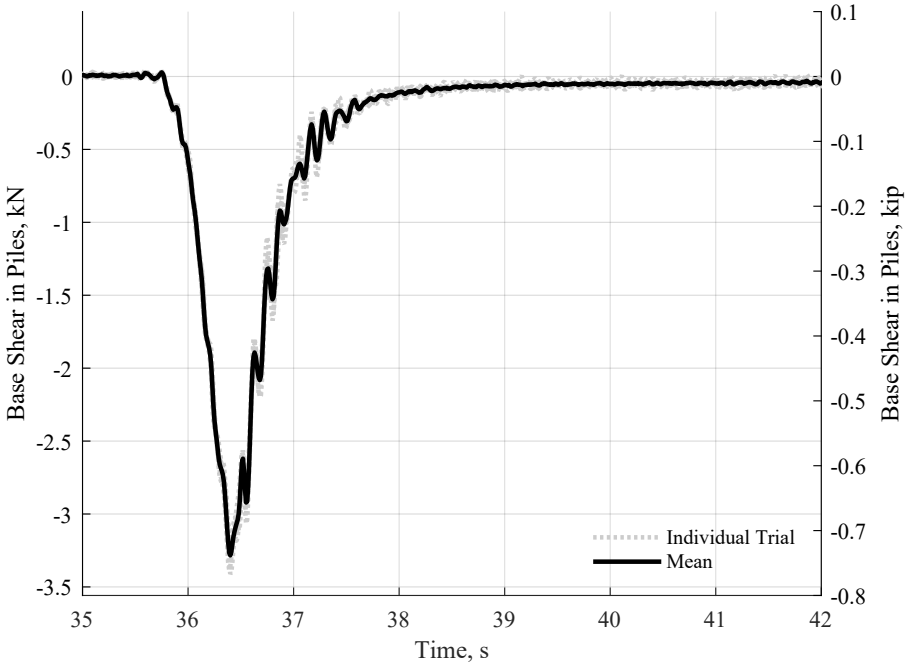

Figure 5.45: Base shear calculated from strain for 1.40m wave without the first floor slab or back wall, and with an empty soil box. CFST_NS_E_140

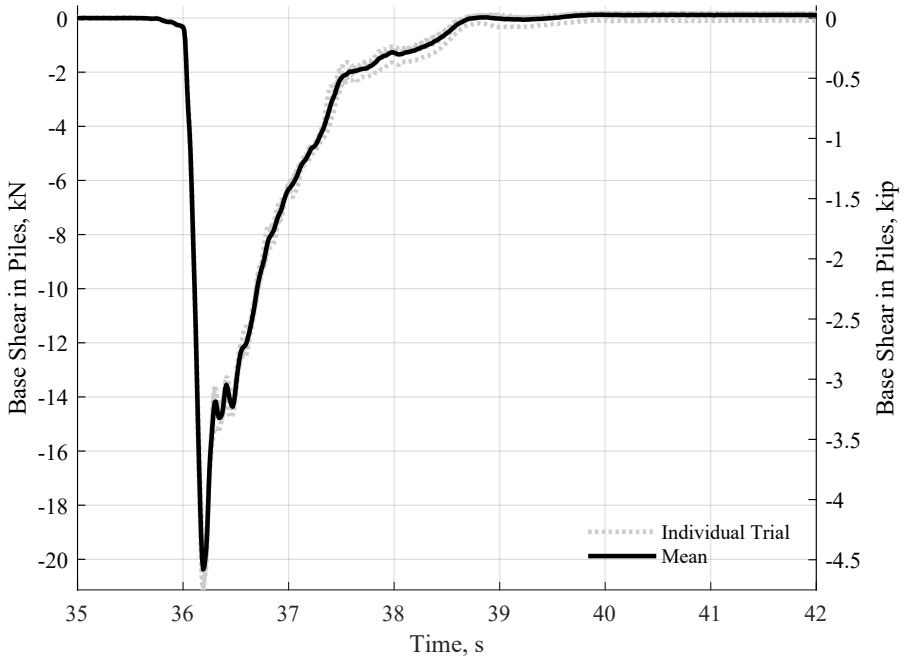

Figure 5.46: Base shear calculated from strain for 1.40m wave with the first floor slab and back wall, and with an empty soil box. CFST_FS_E_140

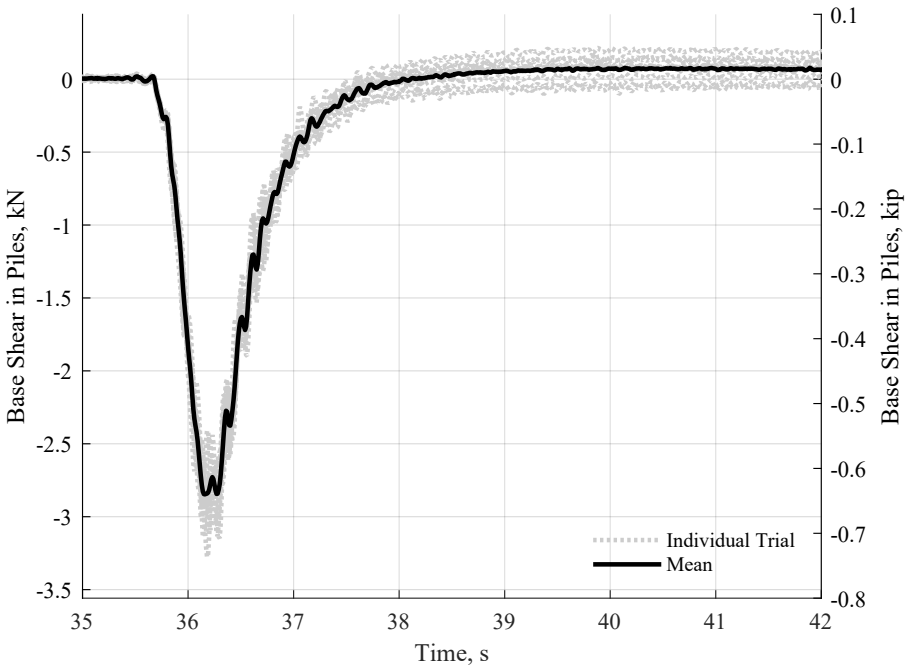

Figure 5.47: Base shear calculated from strain for 1.45m wave without the intermediate slab or back wall, and with an empty soil box. CFST_NS_E_145. The base shear in the columns in this trial is slightly lower than CFST_NS_E_140 in Figure 5.45. This may be because the breaking wave has released some of the moment when the wave starts slipping between bays 3 and 4, rather than only on impact, like the 1.40m wave.

box full, meaning the soil is taking approximately 30% of the base shear from the columns over the depth of the piles. The remaining 70% of the base shear is being transferred into the slab and load cells at the base of the piles.

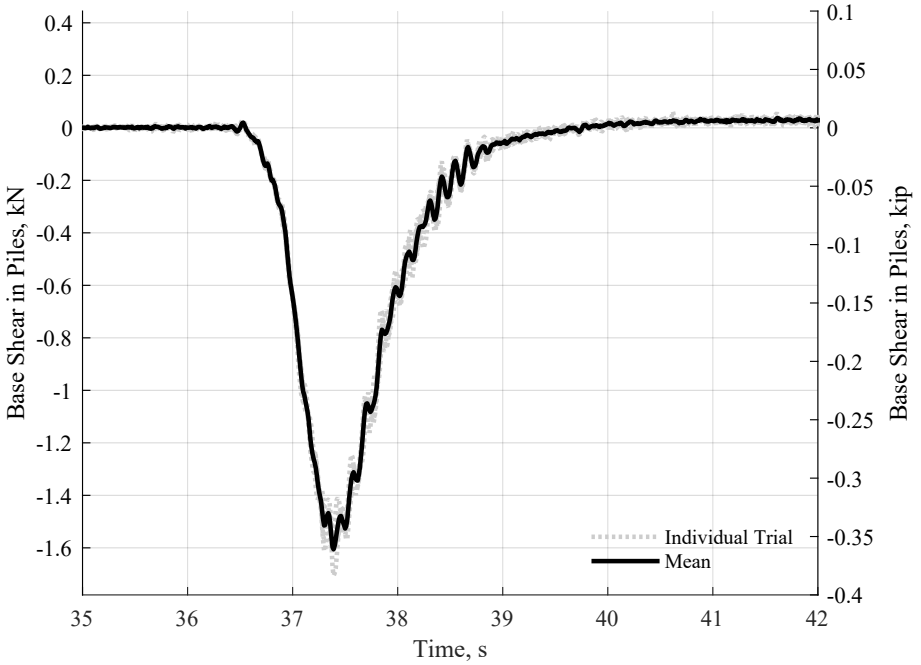

Figure 5.48: Base shear calculated from strain for 1.00m wave without the first floor slab or back wall, and with half filled soil box. CFST_NS_H_100

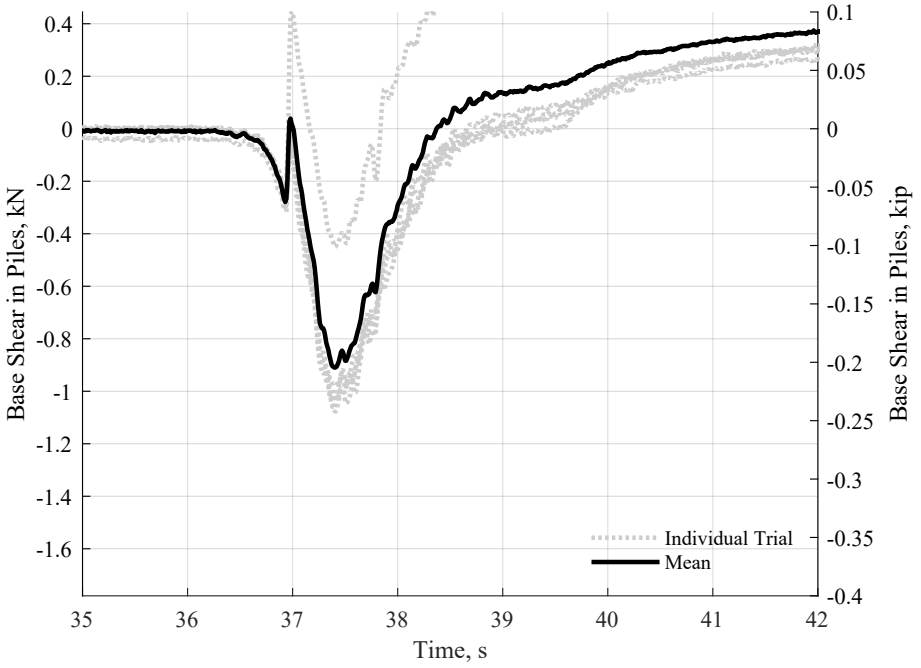

Figure 5.49: Base shear calculated from strain for 1.00m wave without the first floor slab or back wall, and a full soil box. CFST_NS_F_100

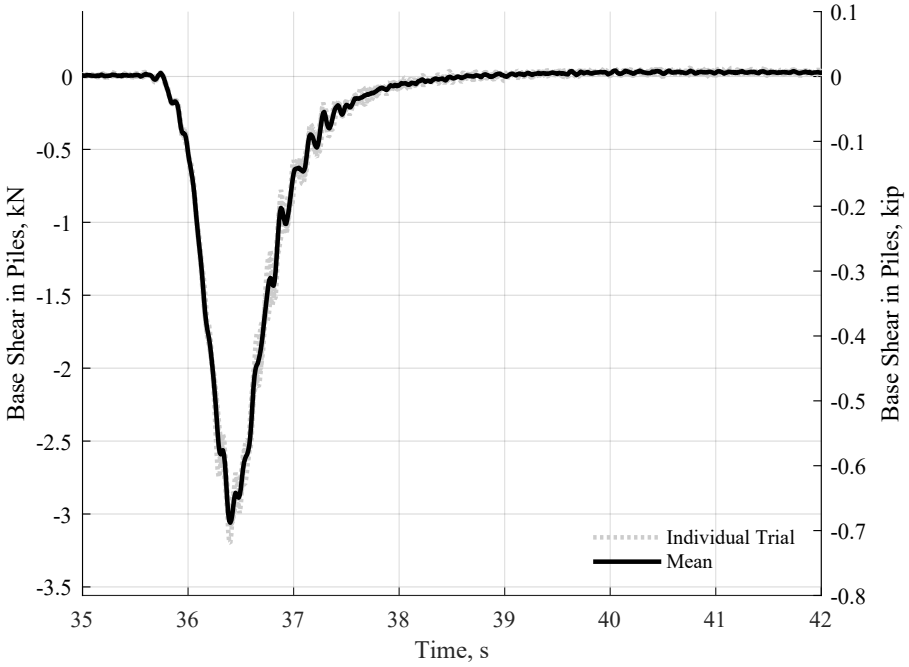

Figure 5.50: Base shear calculated from strain for 1.40m wave without the first floor slab or back wall, and with half filled soil box. CFST_NS_H_140

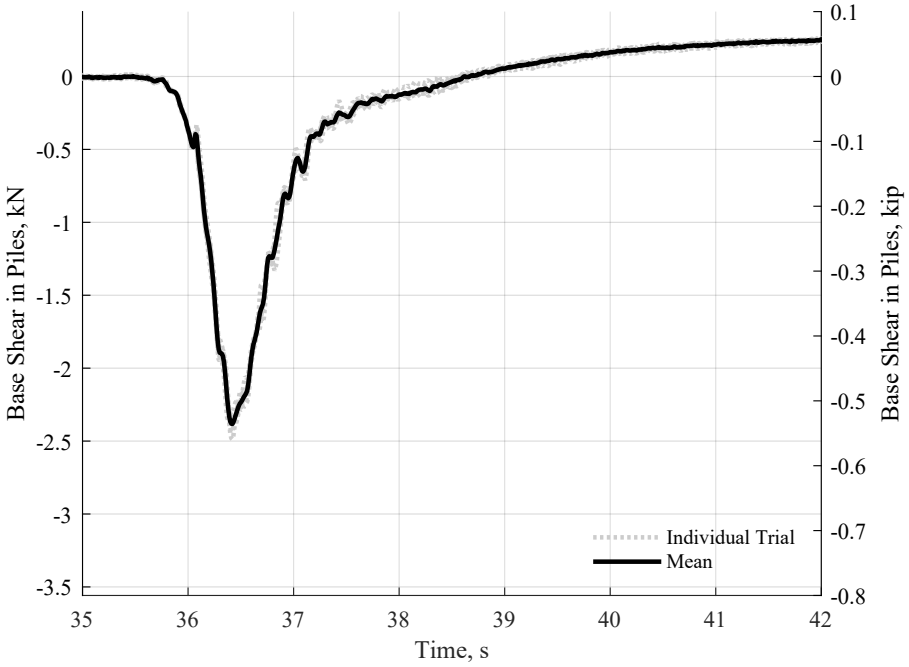

Figure 5.51: Base shear calculated from strain for 1.40m wave without the first floor slab or back wall, and a full soil box. CFST_NS_F_140

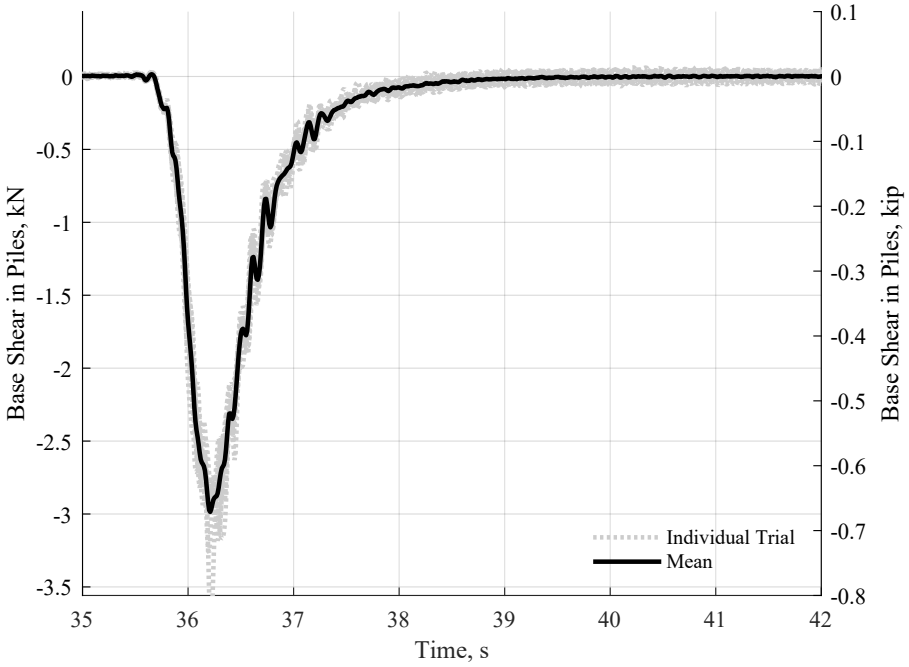

Figure 5.52: Base shear calculated from strain for 1.45m wave without the first floor slab or back wall, and with half filled soil box. CFST_NS_H_145

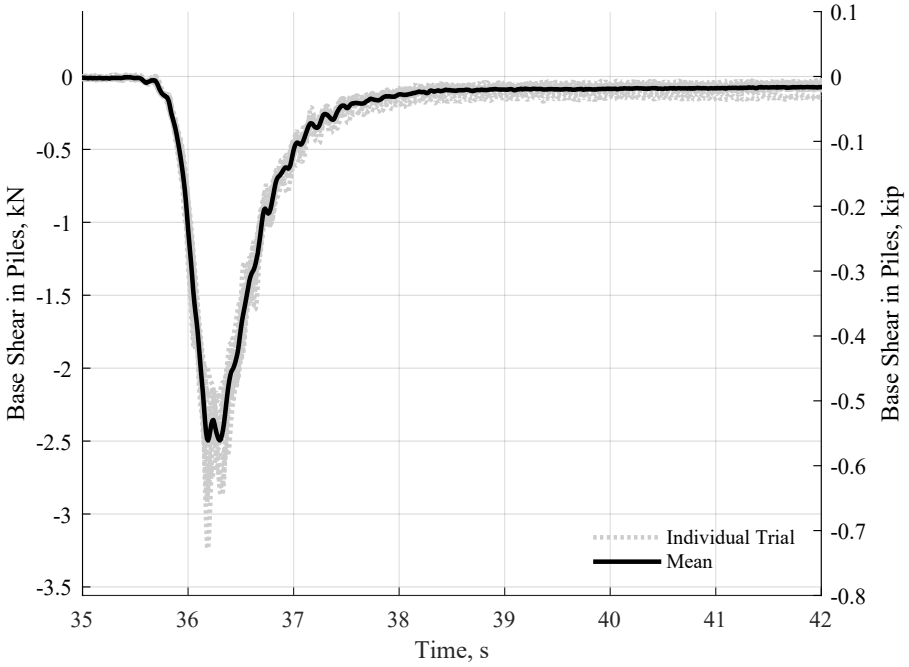

Figure 5.53: Base shear calculated from strain for 1.45m wave without the first floor slab or back wall, and a full soil box. CFST_NS_F_145

Chapter 6

EVALUATION OF EXPERIMENTAL STUDY PARAMETERS

While Chapter 5 presents results for individual experiment conditions, this chapter builds on those results and compares the experiment conditions to understand how the response of the specimen changes. This chapter begins by examining how the results measured in the wave flume compare against a refined version of the OpenFOAM simulations developed in Chapter 3. The peak pressures and mean pressures of the inundation time are compared to understand how the fluid is flowing around the specimen. Next the base shear simulated in OpenFOAM is compared to the measured response for each wave type. The second portion of this chapter evaluates how the different test conditions compare against each other for the CFST specimen. Examinations include the wave types produced by the wave maker, the influence of soil around the piles of the specimen, and the impact a fixed back wall and first floor make on the base shear response of the specimen compared to a specimen where the first floor is able to break away, or a design with a completely open first two stories. Finally, the CFST specimen response is compared to the Shear wall specimen tested in Autumn of 2019.

6.1 Comparison of Measured and Simulated Specimens

The OpenFOAM simulation used to design and compare against the experimental results was developed by Nikki Lewis for her dissertation and is based on the model developed by Gills (2018), and is identical to the model used by Pyke (2020). The main changes in the simulation between the preliminary design stage addressed in Chapter 3 and the model addressed in this chapter are refinement of the mesh around the model and changes to the turbulence model.

The OpenFOAM simulation mesh was refined around the specimen to account for the circular shape in the prismatic model space. To achieve this, the mesh size was linearly scaled between prisms with 1mm sides near the specimen, and 50mm sides in the undisturbed portion of the flume. Figure 6.2 shows an example of the mesh around the columns. This final mesh size was chosen

when the results from the simulation began to converge.

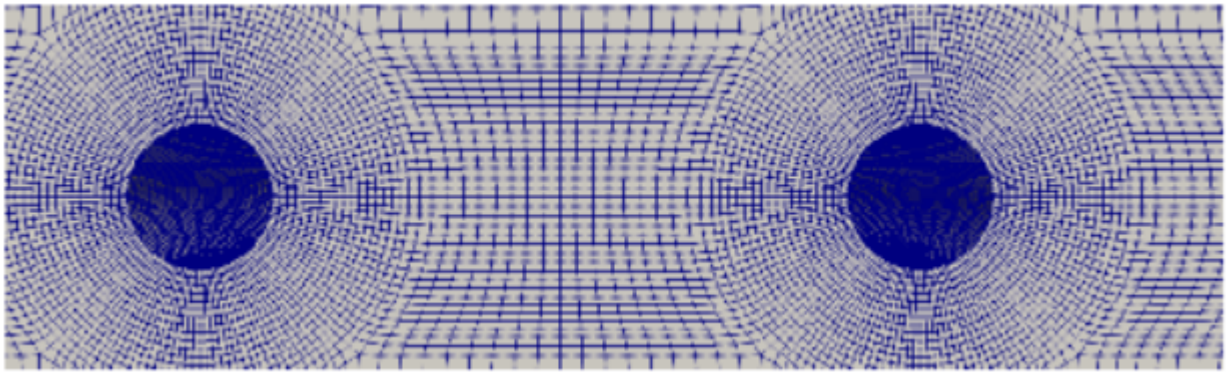

Figure 6.1: OpenFOAM mesh around CFST specimen

The turbulence model for the simulation was also changed from a standard k-epsilon (KE) model to a k-omega-shear-stress-transport (k-omega-sst) model. The primary difference between the two turbulence models is that the KE model characterizes the mean turbulence of a general region of flow using two partial differential equations, while the k-omega-sst uses a different partial differential equation to characterize the turbulent kinetic energy. This equation does a much better job of capturing the turbulent kinetic energy generation near the CFST, resulting in a higher resolution of shear stresses and forces imparted upon objects within the flow. The two turbulence models give nearly the same results for the case of general flow far from boundary conditions however the k-omega-sst does a much better job near the boundaries. Pressures from this analysis were recorded by placing probes that recorded pressures at the same locations as the pressure sensors in the experiment. Forces from the analysis were then found by integrating those pressures using the same integration method described in Chapter 5 for the experiment.

6.1.1 Wave Fluid Measurements

Wave fluid measurements are the wave height, and wave particle velocity results measured from the wave gauges, ultrasonic wave gauges, and Acoustic Doppler Velocimeters (ADVs) Because only the mesh close to the model was changed, to account for the circular columns, the validation of the

flume model presented in Chapter 6 of Pyke (2020) represents a good validation of the accuracy of the OpenFOAM simulation in predicting the wave flume measurements. The same wave maker displacement time history was used for the simulation, the shear wall specimen, and the CFST specimen. This means the simulation saw the same excitation and fluid dynamics as the wave flume. The wave height measured by wave gauges for the 1.40m wave are within 4% between simulation and flume tests. The wave height of the 1.45m breaking wave is slightly less consistent, with a percent difference of 6%. The percent difference for wave particle velocity at the ADV points along the flume are 3% for the 1.40m wave, and 2% for the 1.45m wave.

6.1.2 Pressures along Columns

The pressures along the columns are the main transfer of energy from the wave to the specimen. Therefore it is important that the simulation produces accurate fluid pressures at the interface with the specimen. Figure 1 shows the pressures in the center of the column along the height of the front column for the 1.40m wave impacting the specimen. The blue diamonds are the instantaneous maximum pressures at the designated heights from the OpenFOAM simulation. The brown squares are the instantaneous maximum pressures measured in the wave flume. Because these measurements are instantaneous, there is more variation, and the potential for an individual reading to be larger than realistic. The green stars and purple 'x's are the mean pressures averaged over a period of 0.2s. For both the simulation and the measured results, this corresponds to 20 instrument readings (time step of 0.01s). This period of time is also the length of time that the wave fully inundates the columns as it passes through the specimen. In general, the simulated pressures are slightly higher than what was measured in the flume. A convergence test was performed to show that the computed pressures were not influenced by mesh size. The most likely influence is the flexibility of the column and test setup in the experiment compared to the rigid column assumed by the simulation.

6.1.3 Specimen Base Shear

To determine the validity of the OpenFOAM model of the specimen, base shear calculated from strain in the piles in Section 5.2.1 is compared to the base shear results simulated. Figure 6.3

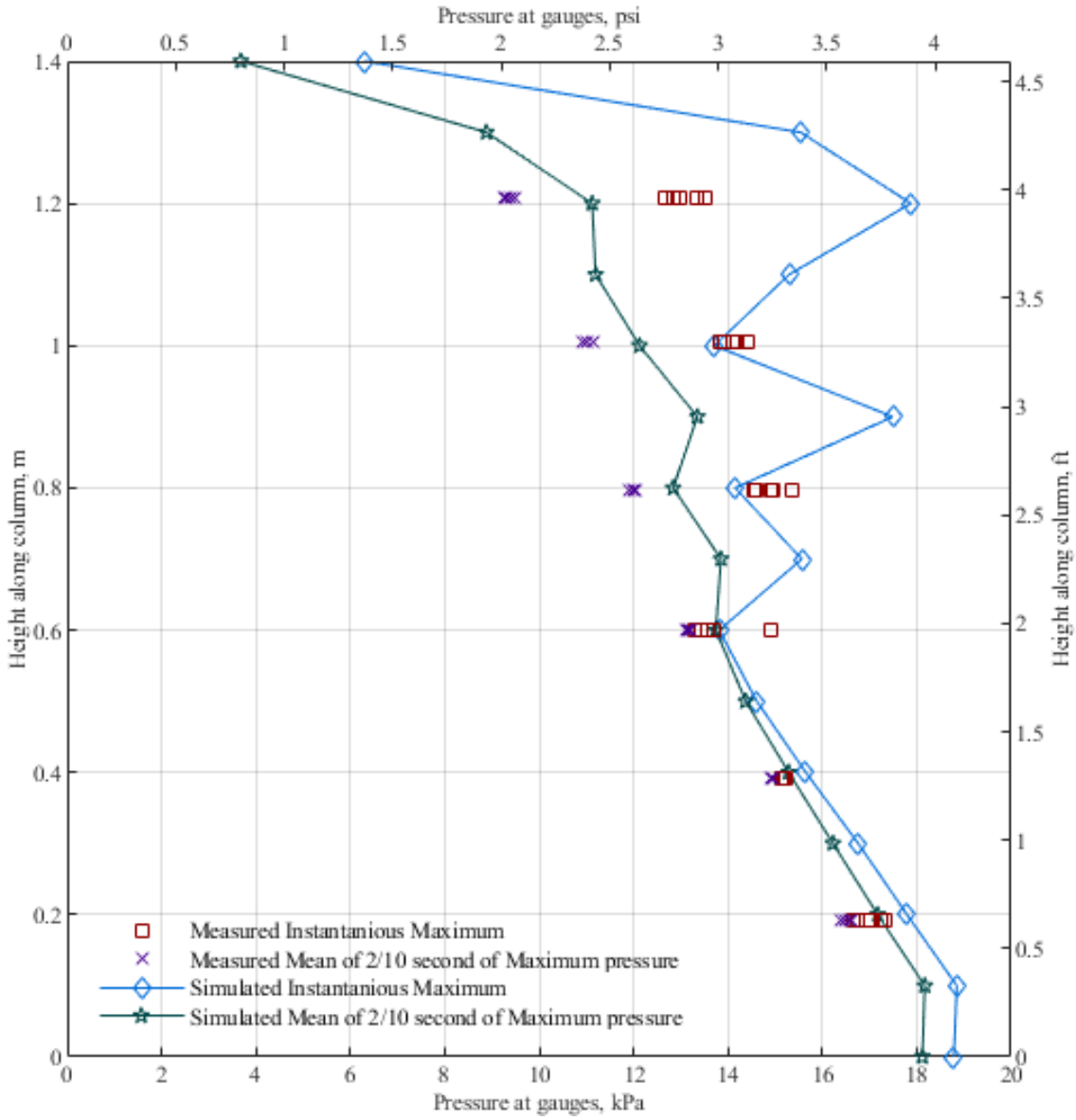

Figure 6.2: Comparison of pressure on columns measured and simulated for the 1.40m wave with soil box empty. Instantaneous and mean pressures of impact are shown for both the flume and experiment and simulated model.

and Figure 6.4 show the base shear time histories for the 1.00m wave and the 1.40m wave. In each, the general shape of the time history is similar, but the maximum simulated base shear is significantly higher than the maximum measured base shear. Additionally, for these two wave heights, the integration of force over time of the waves on the specimens are significantly different between the simulated and measured results. The forces are summarized in Table 6.1. The change in momentum, or impulse, is calculated by integrating the base shear over the time of impact.

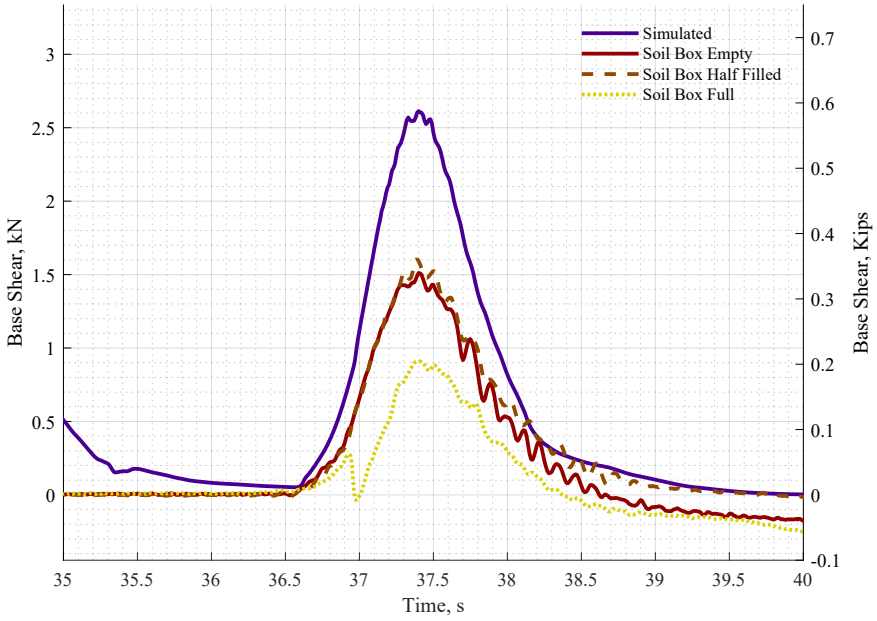

Figure 6.3: Comparison of base shear from 1.00m wave between simulated and measured results.

Figure 6.5 shows that the base shear time histories for the 1.45m wave simulated and experimental waves are similar in shape and magnitude. The percent difference in maximum base shear in 30%, and the percent difference in impulse is 4%, despite the simulated base shear being 1.25 kN (280lbf) larger than the measured base shear. The base shear and integrated force over time are recorded in Table 6.1.

Continuing the discussion of comparing the simulated to experimental waves, Figure 6.6 compares the simulated and measured base shears for a specimen with a fixed back wall and first story slab. The overall shape of the time histories follow a similar trend, and the percent difference in the instantaneous base shears is 43%. The simulated base shear jumps up very quickly to the

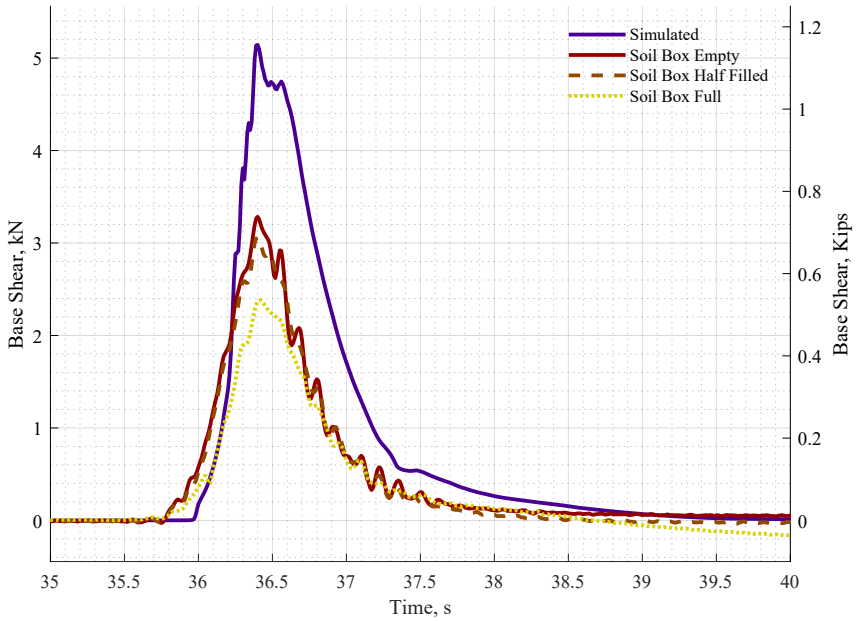

Figure 6.4: Comparison of base shear from 1.40m wave between simulated and measured results.

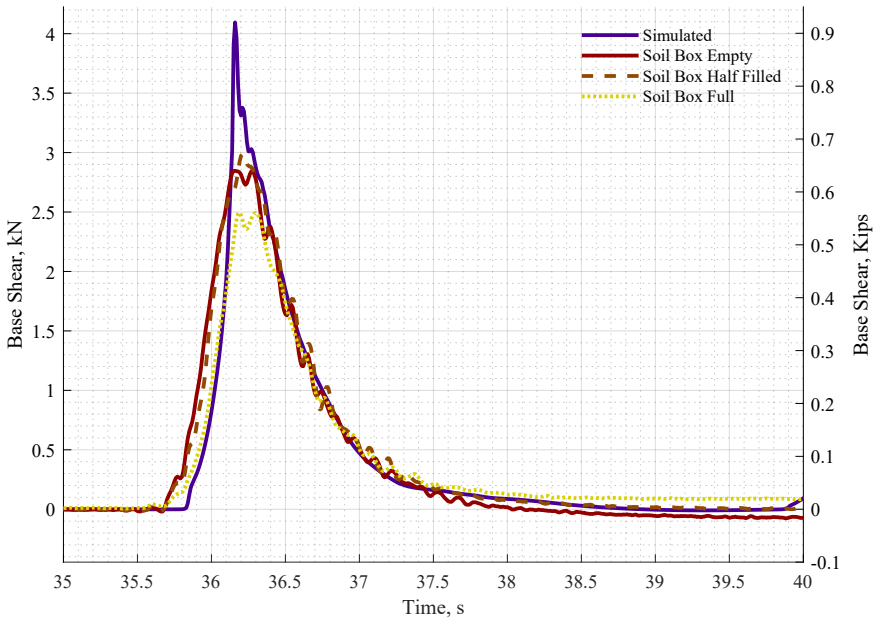

Figure 6.5: Comparison of base shear from 1.45m wave between simulated and measured results.

maximum, then descends again. This occurs over 0.1s and symmetrically increases and decreases with 10 time steps recording this jump, meaning it is less likely to be noise or an anomalous jump in the results. This spike is narrow compared to the entire response, so it has minimal impact on the integrated force over time. The percent difference in this impulse is 15% and is recorded in Table 6.1.

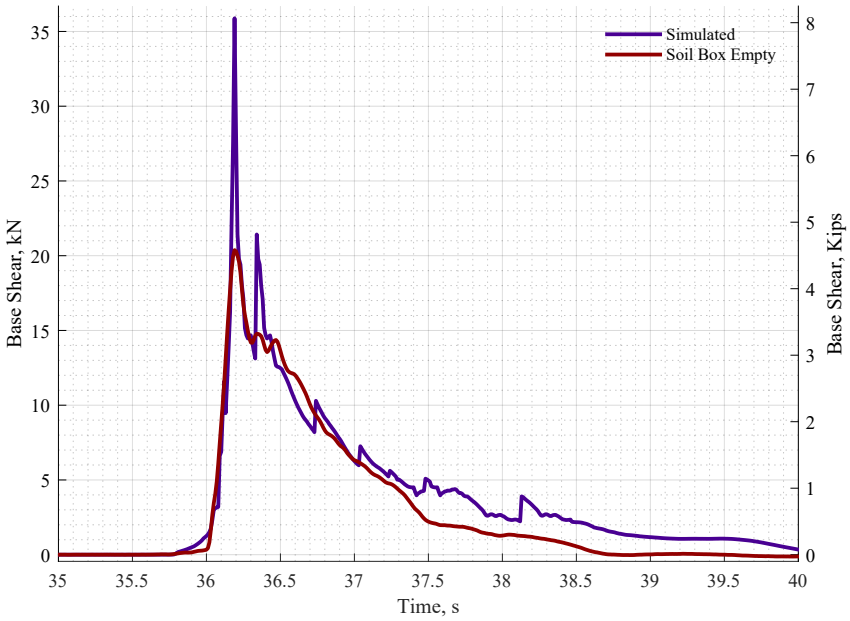

Figure 6.6: Comparison of base shear from 1.40m wave between simulated and measured specimens with back wall and intermediate floor installed.

Based on the maximum base shears and impulses in Table 6.1, the difference in the integration of force over time is greatest at the smaller forces. For the specimens with only CFST columns, the actual difference in base shear is similar, but not identical, across the three wave heights. The difference in maximum base shear between the experiments and simulations vary between 1.1kN and 1.9kN, but do not scale with wave height, or total base shear. The hypothesis is that there is a physical phenomenon that is not being captured by the simulation. The OpenFOAM model treats the CFST columns as a rigid boundary condition that has infinite stiffness. This is obviously not the case in the experiments. Another possibility is flexibility in the specimen setup, below the water level and around the soil box. The simulated specimen does not characterize any of the

Table 6.1: Maximum base shear and integrated force over time for experiment and simulated experiment conditions

	Experiment		Simulation		Ratio: Experiment/Simulation	
	instant max V	impulse	instant max V	impulse	instant max V	Impulse
1.00m wave	1.51 kN (0.34 kip)	1.33 kN-s (0.30 kip-s)	2.61 kN (0.59 kip)	2.38 kN-s (0.54 kip-s)	0.58	0.56
1.40m wave	3.28 kN (0.74 kip)	2.30 kN-s (0.52 kip-s)	5.14 kN (1.16 kip)	3.77 kN-s (0.85 kip-s)	0.64	0.61
1.45m wave	2.85 kN (0.64 kip)	2.11 kN-s (0.48 kip-s)	4.09 kN (0.92 kip)	2.04 kN-s (0.46 kip-s)	0.70	1.04
1.40m w/ back wall	20.37 kN (4.58kip)	14.92 kN-s (3.35 kip-s)	35.88 kN (8.07 kip)	17.64 kN-s (3.96 kip-s)	0.57	0.85

interaction below the flume bathymetry, it is fixed in place. All of the force must pass through two 1 inch threaded rods connected to the cross shore (streamwise) load cells, before the force passes through the flange of a cantilevered W12x106 steel section. Each individual component is stiff and easily handles the force input by the wave. However, when all of these components are combined in series, the total stiffness of the system does not correspond with the stiffness of any one member. For example, when a load of 3 kN (674lbf) is applied to a 1 inch threaded rod, the associated strain experienced by the bar is approximately 38.4 in/in micro strain. Over the 8 inches of 1 inch threaded rod, this comes to 0.0003 inches deformation. The cantilevered W12x106 steel sections may experience a deformation of up to 0.0001 inches, but likely less, due to the stiffeners and angled plate on the cantilevered upright section. These individual components do not produce large deformations, but they do not account for the unknown deformation in the swivel ball and sockets, deformation in the load cell, or slight amounts of shifting not restrained by other load cell assemblies.

In Table 6.1, as the force on the specimen is larger the difference, between the experiment and simulation, in maximum base shear as a proportion of the maximum value decreases. The physical response in the wave flume, made up of small deformations in many components in series, plays a smaller role in the total response in the base shear and the integration of force over time. This means that the simulation produces more realistic results for high force events, which carry more engineering significance. The OpenFOAM base shears may become more accurate if the simulation is able to account for the stiffness of the specimen.

6.2 Comparison of Experiment Measured Results

This section of the chapter examines how changing the experiment conditions impacts the results recorded. First the wave Heights are compared, then the impact of soil in the soil box on the structural response. Third, the presence of a back wall and first floor fixed and break away slab are compared to the specimen with only CFST columns exposed to the wave inundation are examined.

6.2.1 Wave Heights

The wave height generated by the wave maker, 1.00 unbroken, 1.40 unbroken, or 1.45 broken wave, plays a large role in the size and type of response in the specimen. The first difference between

wave types is the time until arrival at the specimen. In a perfect model, the waves should travel with the same speed, due to shallow water wave velocity, when the ratio of wavelength to water depth is greater than 20, being most dependent on water depth, as shown in Equation 6.1.

$$v = \sqrt{g * d} \tag{6.1}$$

Where,

- g is the acceleration due to gravity, and
- d is the depth of the water where the shallow water wave is traveling.

From Equation 6.1, it is inferred that the three waves travel at the same velocity down the wave flume, and impact the specimen at the same time. However, on examination of Figure 6 (and all the other figures in this section), the waves are impacting the specimen at slightly different times. The 1.45m wave arrives first, 0.2 seconds before the 1.40m wave, and the 1.00m wave arrives last, 1.0 second after the 1.40m wave. This difference is attributed to the way the wave maker piston displaces the fluid to produce the wave traveling down the flume. Examining Figure 5.1, the wave maker paddle velocities correspond to the sequence the wave reach the specimen.

Figure 6.7 shows the base shear in the piles of the specimen for the experiment condition with the soil box empty. The 1.40m wave produces the largest base shear of 3.28 kN (740lbf). Interestingly, despite displacing more water in the flume, the 1.45m wave produces a smaller base shear, of 2.85 kN (640lbf). The 1.45m wave is larger and unstable at a water depth of two meters (6.56ft), therefore it begins breaking at bay three and four in the wave flume. The breaking and slipping behavior dissipates some of the energy originally displaced by the wave maker prior to impact with the specimen, located in bay nine of the wave flume. The 1.40m wave is stable at the flume's water depth, so a larger portion of the total energy input by the wave maker is available for transfer into the specimen. The 1.00m wave displaces the least amount of water initially, so it has the smallest impact on the specimen, with a base shear of 1.51 kN (340lbf) in the piles.

The magnitudes of axial force in the vertical load cells and overturning moment follow the same trends as the base shear, shown in Figure 6.8 and Figure 6.9. The 1.40m wave produces the largest 'negative' overturning moment of -6.22 kN-m (-55.08kips-in). The 1.45m wave is next highest with

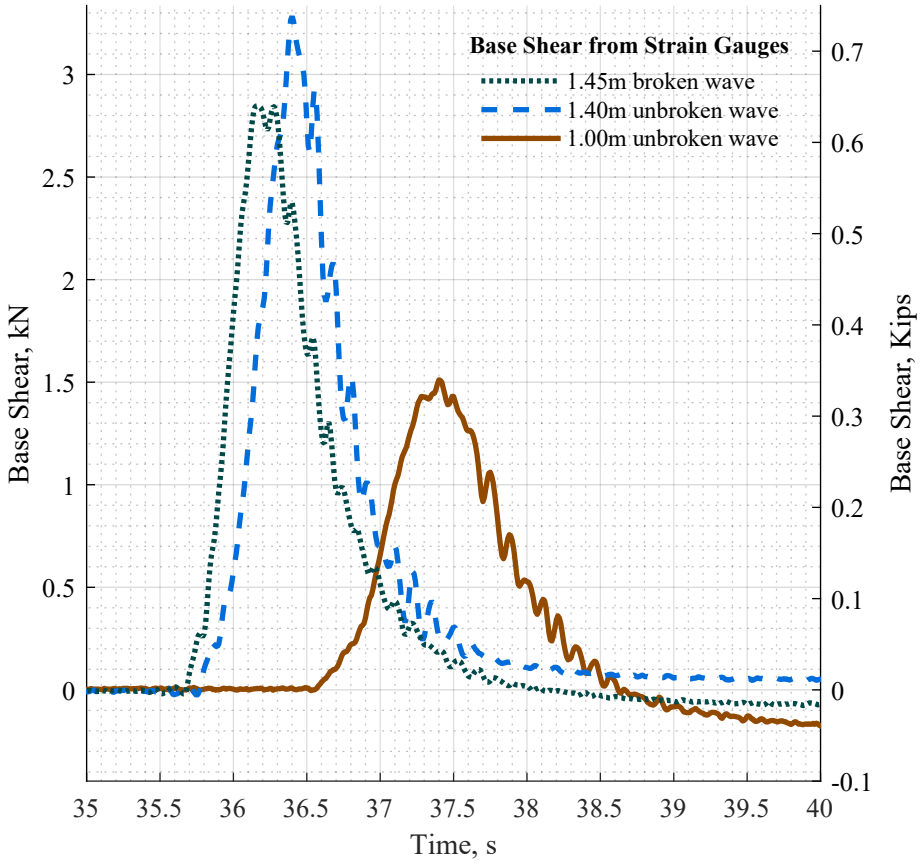

Figure 6.7: Comparison of Base shear between wave types for experiment conditions with the soil box empty.

an overturning moment of -5.89 kN-m (-52.10kips-in), and the 1.00m wave is smallest with an overturning moment of 4.87 kN-m (-43.12 kips-in), as measured by the vertical load cells located directly underneath each column. The negative overturning moment is moment that acts to rotate the specimen forwards, into the approaching wave. Positive overturning moment acts to rotate the specimen in the direction of the wave, towards the back of the flume. The magnitude and sign of the overturning moment is tied to the hydrostatic weight of the wave and dynamic influence underneath the flume bathymetry, as discussed in Section 5.3.1.

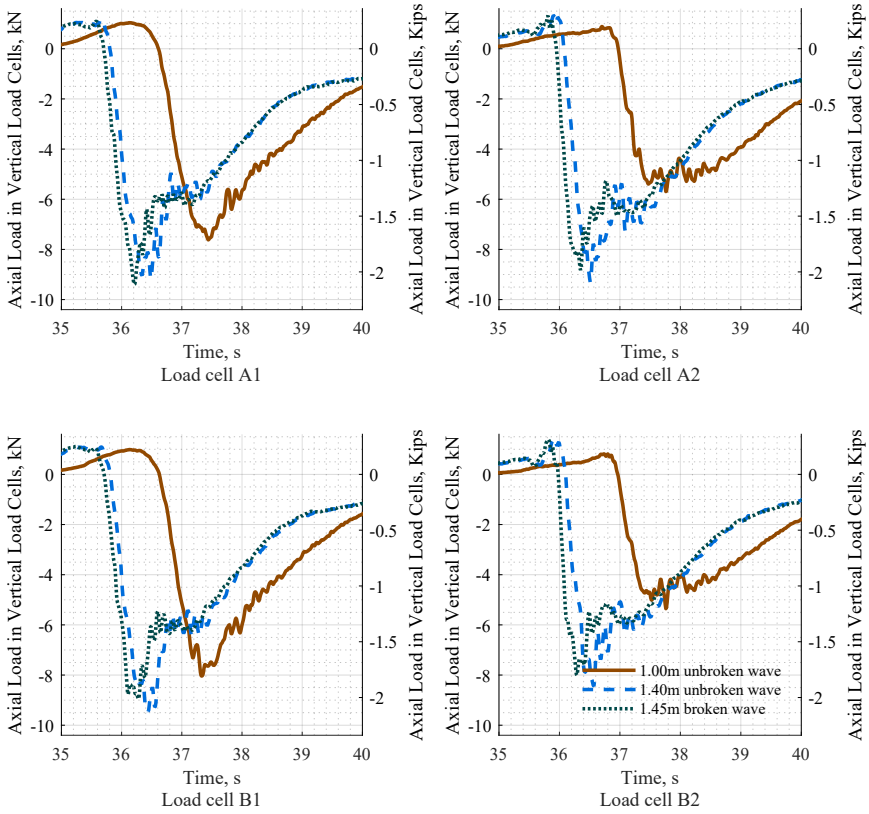

Figure 6.8: Axial Load in the vertical load cells underneath the specimen with an empty soil box.

Once soil is added to the experiment, the fluid, soil, structure influence on the results becomes more complex and chaotic. In the experiment condition with the soil box half filled, shown in Figure 6.10, the 1.45m and 1.40m waves produce similar levels of base shear in the piles of 2.99 kN (0.64kips) and 3.06 kN (0.69kips). The 1.00m wave is still the smallest with base shear in the piles

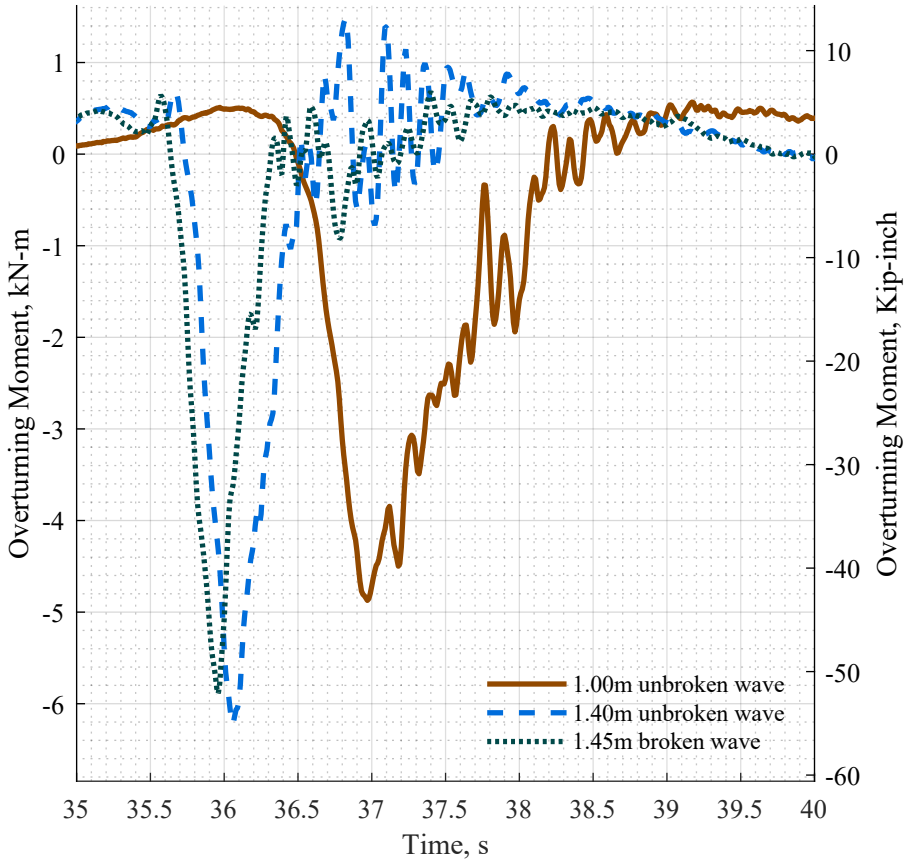

Figure 6.9: Moment in the specimen set up from the vertical load cells with the empty soil box

of 1.61 kN (0.36kips). This change in trend, compared to Figure 6.7 is due to the soil structure influence in the soil box. The axial force in the vertical load cells and the overturning moment in Figure 6.11 and Figure 6.12 follow the same trend as in Figure 6.8 and Figure 6.9, because the wave is the same and these load cells are not influence by the soil in soil box. Furthermore, the axial loads measured by the vertical load cells are dominated by the weight of the water acting on the soil box around the specimen, not the overturning moment in the slender piles and columns.

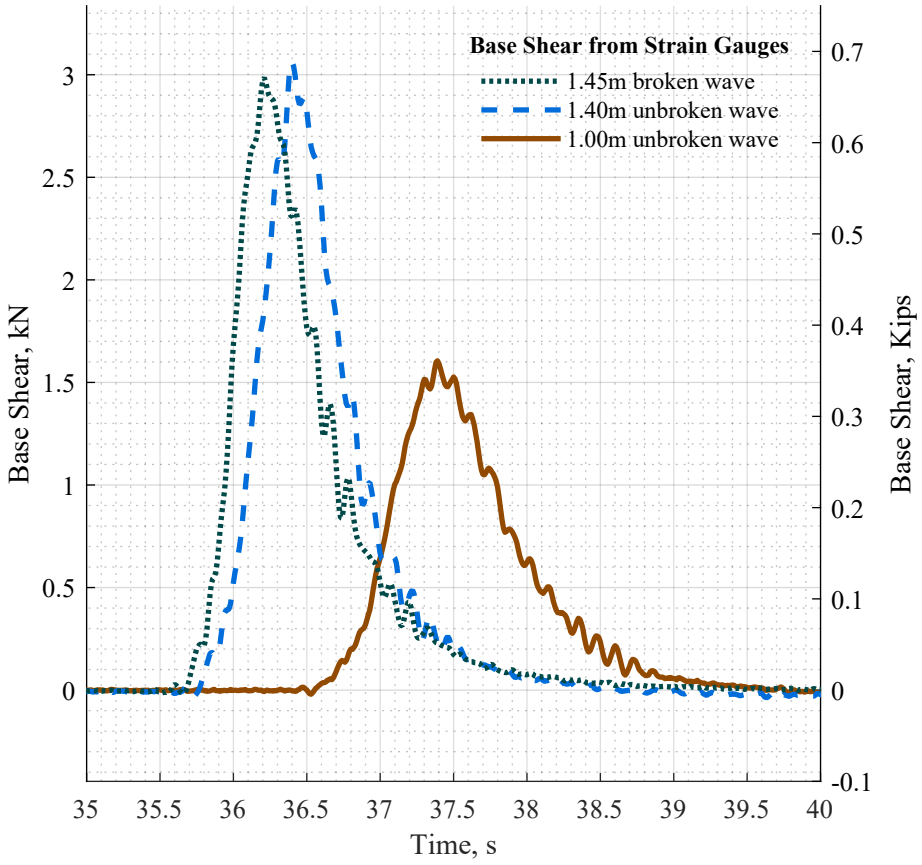

Figure 6.10: Comparison of Base shear between wave types for experiment conditions with the soil box half filled.

The base shear trend in the piles continue to change in the experiment condition with the full soil box, shown in Figure 6.13. The 1.45m wave has the largest base shear in the piles of 2.50 kN (0.56kips), the 1.40m wave is next highest with 2.38 kN (0.54kips). The 1.00m wave is the smallest

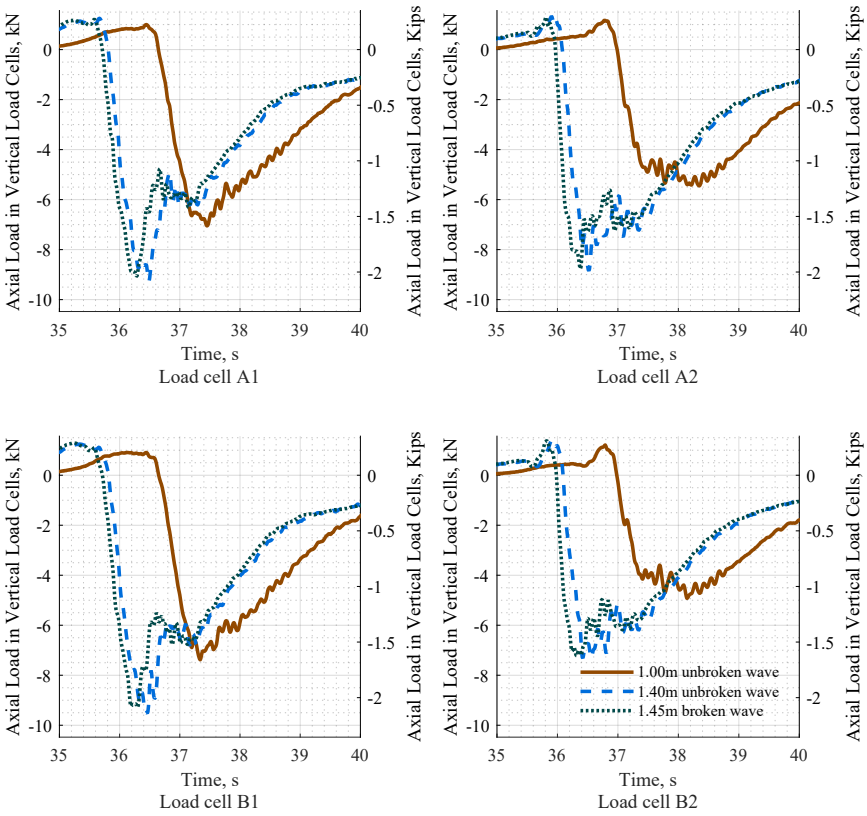

Figure 6.11: Axial load in the vertical load cells with the soil box half filled.

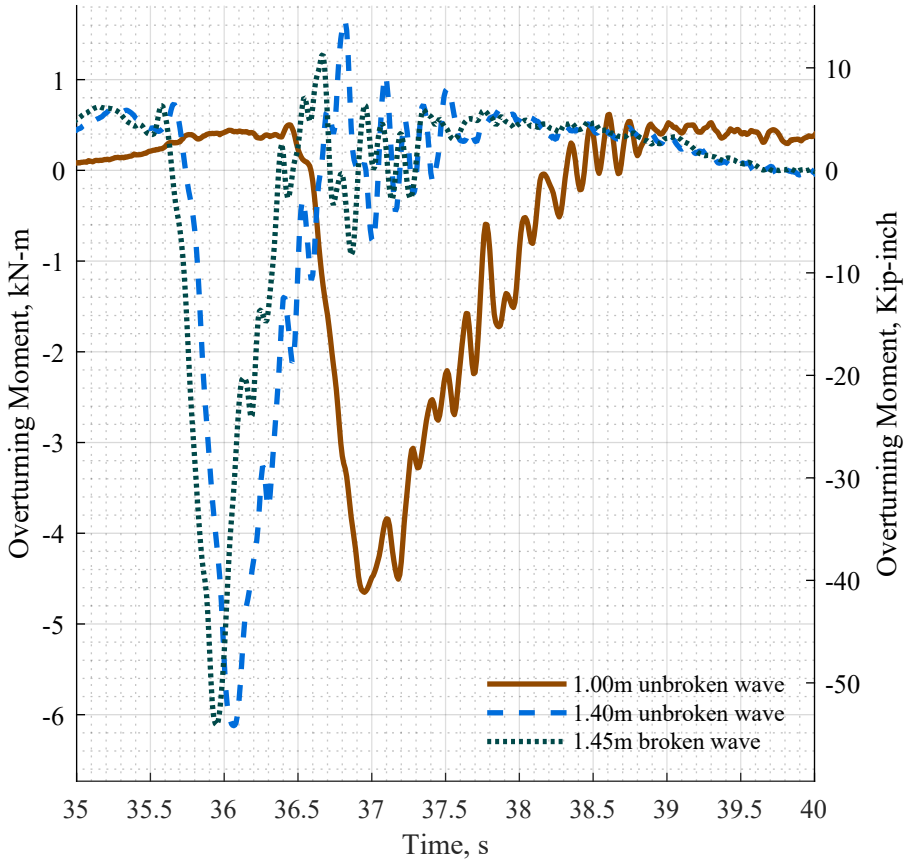

Figure 6.12: Moment in the specimen set up from the vertical load cells with the half filled soil box

with a base shear in the piles of 0.91 kN (0.2kips). The axial force in the vertical load cells and moment trends, shown in Figure 6.14, and Figure 6.15, are the similar for the full soil box and the empty soil box because these instruments are independent of the soil.

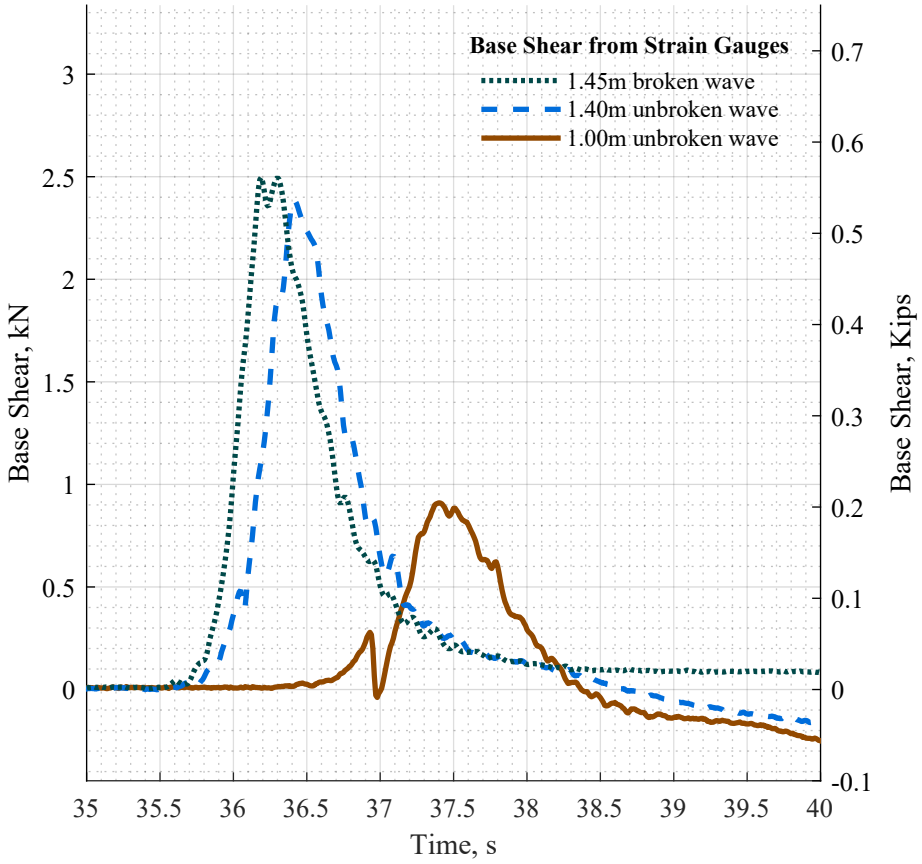

Figure 6.13: Comparison of Base shear between wave types for experiment conditions with the soil box full.

6.2.2 Soil Level in the Soil Box

The soil level in the box plays a role on results taken from instruments inside on the piles, in the soil box, but much less, if any, impact on measurements taken form the load cells surrounding the specimen. Figure 6.16 shows the base shear in the piles for the three soil box levels for the 1.00m wave. As the soil level is increased, less base shear is transferred all the way through the piles. From

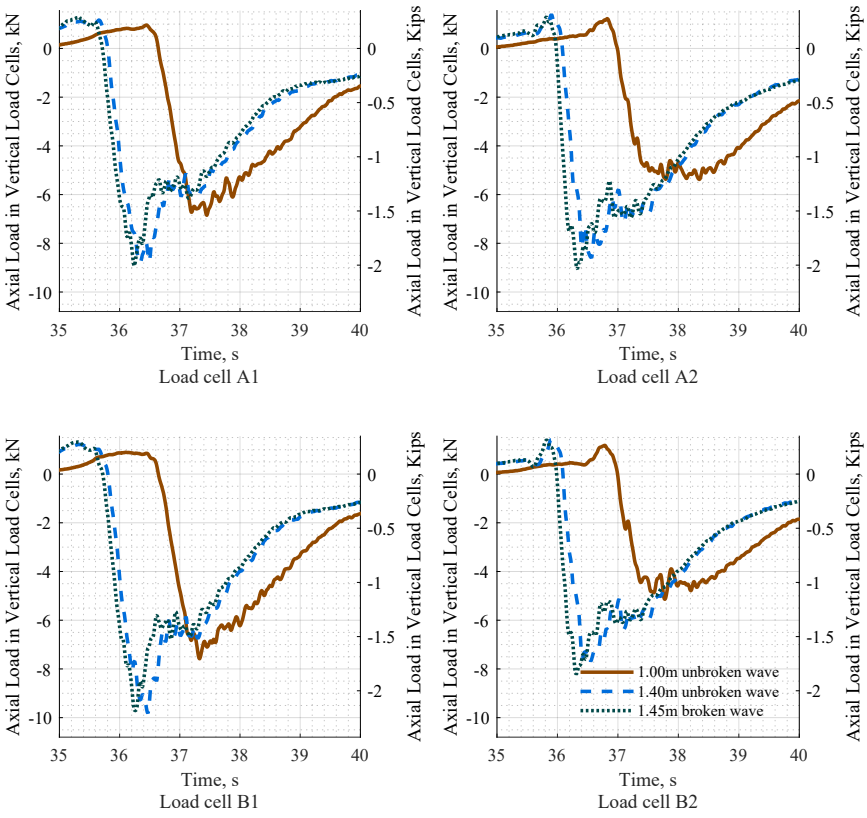

Figure 6.14: Axial load in the vertical load cells with the soil box full.

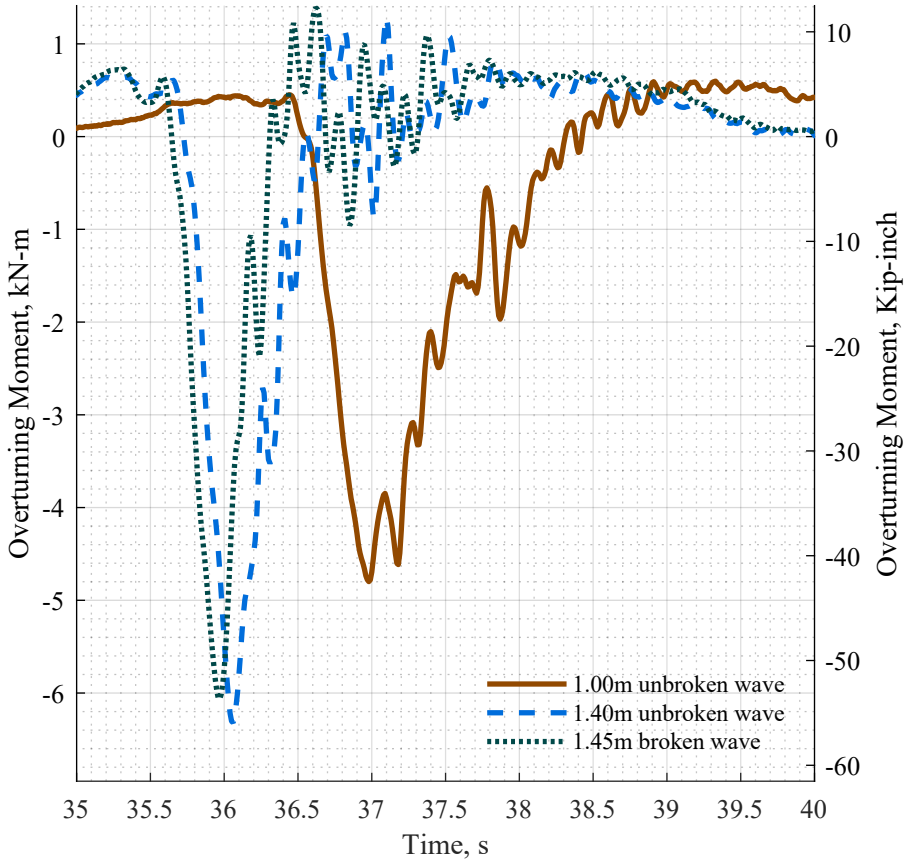

Figure 6.15: Moment in the specimen set up from the vertical load cells with the full soil box

the load cell plot, it appears there is slightly more base shear when the soil box is half filled and full than when the soil box is empty. This would correspond with the slightly stiffer specimen, when the soil is in position to constrain some of the flexibility from the fixed slab to the still water level. The base shear from load cells shown in Figure 6.16, has been filtered according to the procedure laid out in Section 5.2.2, but still shows noise in the form of large swings between values compared to the base shear calculated from strain in the piles. This makes it difficult to fully attribute the light increase in base shear to the soil in the soil box. The periodic appearance of the base shear load cell data, when compared to the strain gauge base shear, may be due to vibrations in the specimen, or more likely, vibrations in the experiment set up, of specimen, soil box, and load cells. The axial force in the vertical load cells and associated moment for the 1.00m wave are shown in Figure 6.17 and Figure 6.18, with instantaneous maximum in Table 6.2. Figure 6.19 and Figure 6.20 show the axial loads in the piles. Figure 6.21 and Figure 6.22 show the overturning moment calculated from the strain in the piles.

Figure 6.23 shows the base shear in the piles and measured by the load cells when the specimen is tested with the 1.40m wave. The base shear in the piles reduces by 27% when soil is added to the experimental conditions. Similar to the 1.00m wave, the base shear from the load cells is slightly larger for the full soil box, again giving credence to the notion that a slightly stiffer specimen will attract slightly larger load and transfer it into the load cells. Figure 6.24 and Figure 6.25 present the axial load in the vertical load cells and moment in the soil box system. There is minimal impact of soil box level on the axial load cells and moment in the system. The instantaneous maximums are presented in Table 6.3. Figure 6.26 and Figure 6.27 show the axial loads in the piles. Figure 6.28 and Figure Figure 6.29 show the moment in the piles calculated from the strain in the piles.

Figure 6.30 shows the base shear in the piles and measured by the load cells when the specimen is tested with the 1.45m wave. The base shear in the piles reduces by 12% when soil is added to the experimental conditions. Unlike the 1.00m wave, the base shear from the load cells is slightly smaller for the full soil box, suggesting that any trend in base shear from the load cells is purely coincidental. Figure 6.31 and Figure 6.32 present the axial load in the vertical load cells and moment in the soil box system. There is minimal impact of soil box level on the axial load cells and moment in the soil box system. The instantaneous maximums are presented in Table 6.4. Figure 6.33 and Figure 6.34 show the axial loads in the piles. Figure 6.35 and Figure 6.36 show the overturning

Table 6.2: Instantaneous Maximum values for 1.00m wave and multiple soil box levels. The impulse is the integration of force over time experienced by the specimen.

	In Piles			Vertical Load Cells	
Soil Box Level	instant max V	Impulse from V	Instant max axial Force	Instant max axial Force	Moment
Empty	1.51 kN (0.34kips)	1.33 kN-s (0.30 kips-s)	2.77 kN (0.62 kips)	-25.22 kN (-5.67 kips)	-4.87 kN-m (-43.12 kips-in)
Half Filled	1.61 kN (0.36 kips)	1.44 kN-s (0.32 kips-s)	2.93 kN (0.66 kips)	-22.68 kN (-5.10 kips)	-4.65 kN-m (-41.17 kips-in)
Full	0.91 kN (0.20 kips)	0.70 kN-s (0.16 kips-s)	15.07 kN (3.39 kips)	-23.00 kN (-5.17 kips)	-4.80 kN-m (-42.47 kips-in)

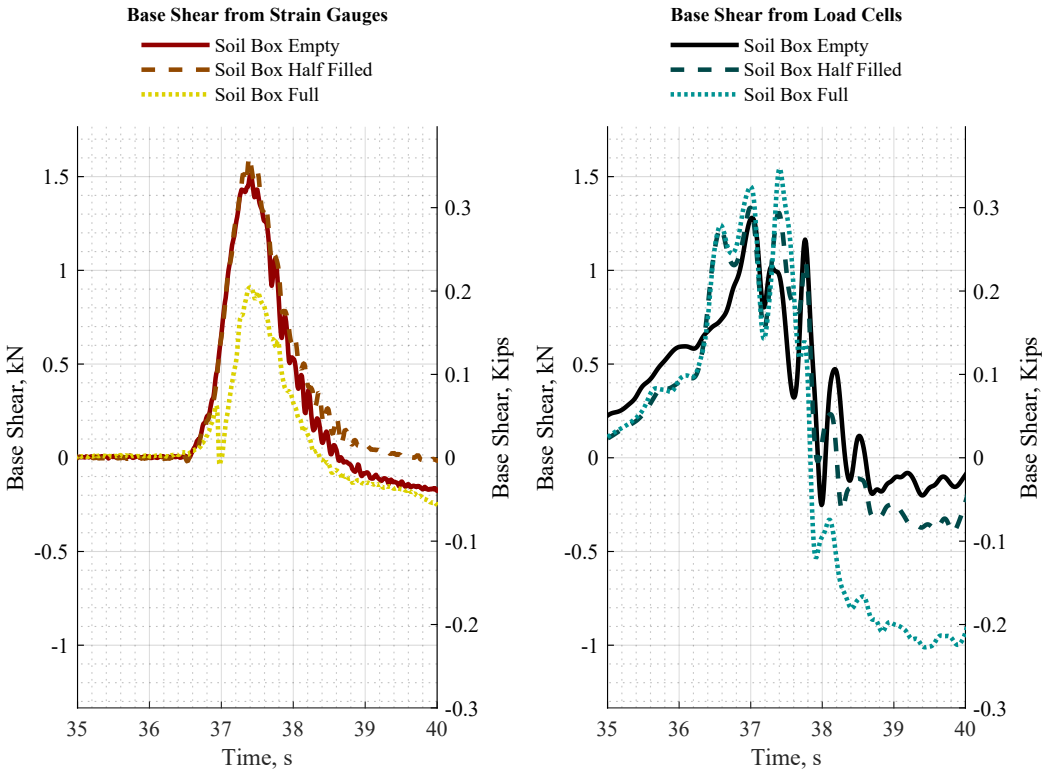

Figure 6.16: Comparison of Base Shear between soil box levels impacted by 1.00m wave and Base shear in the piles vs. base shear in the load cells.

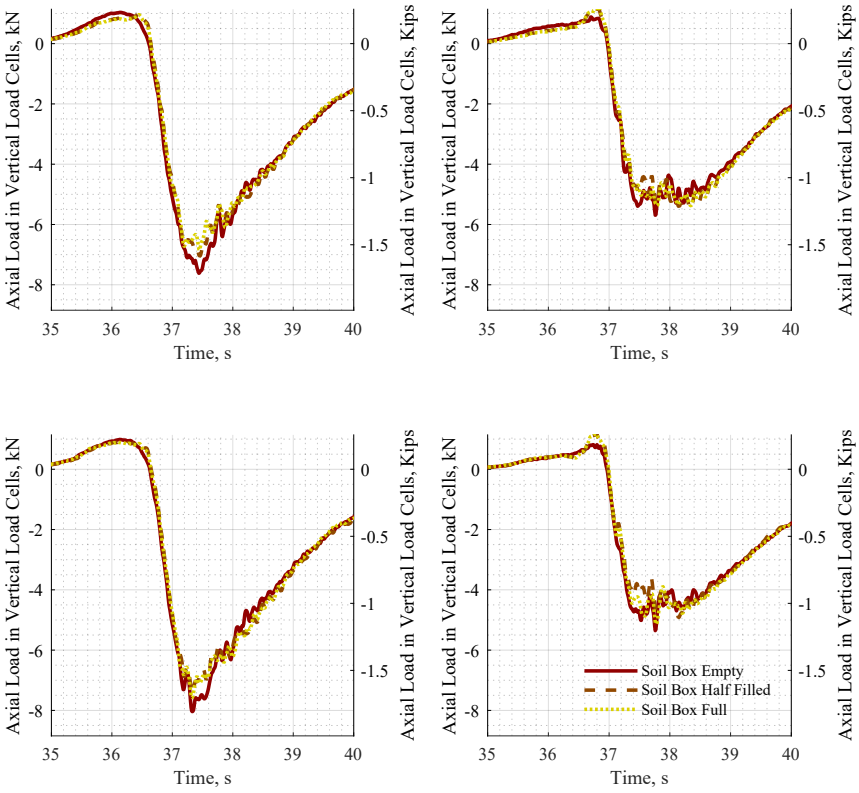

Figure 6.17: Axial force in vertical load cells from 1.00m wave.

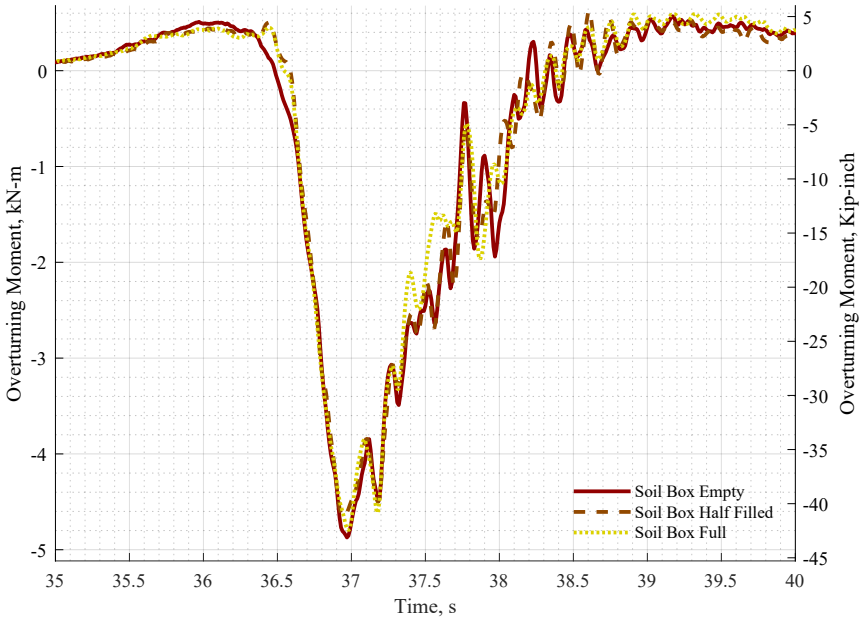

Figure 6.18: Moment in vertical load cells from 1.00m wave.

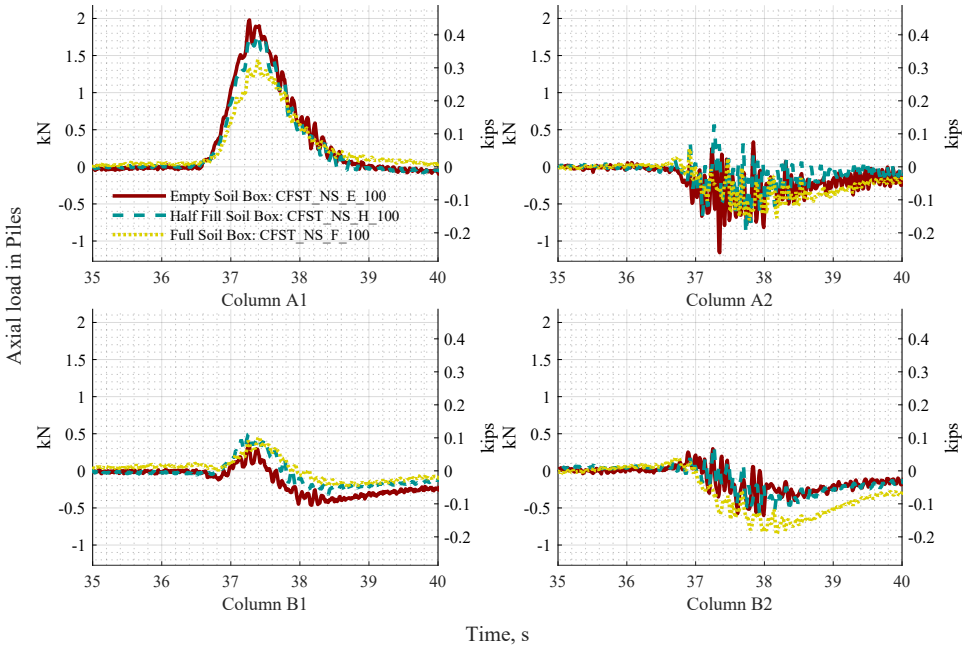

Figure 6.19: Axial force at base of piles from 1.00m wave.

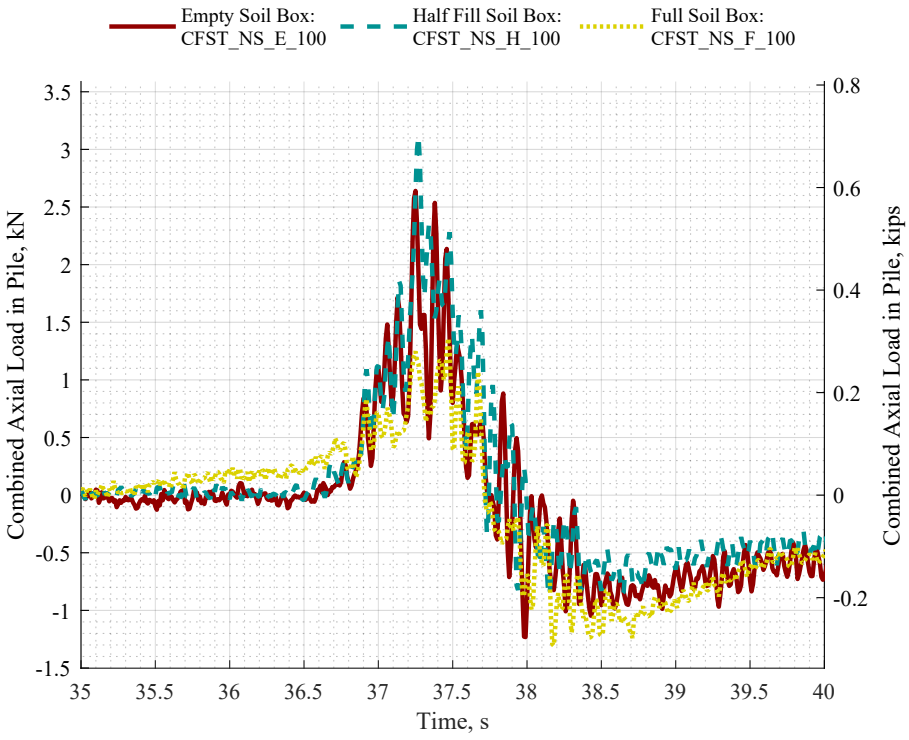

Figure 6.20: Combined axial force at base of piles from 1.00m wave.

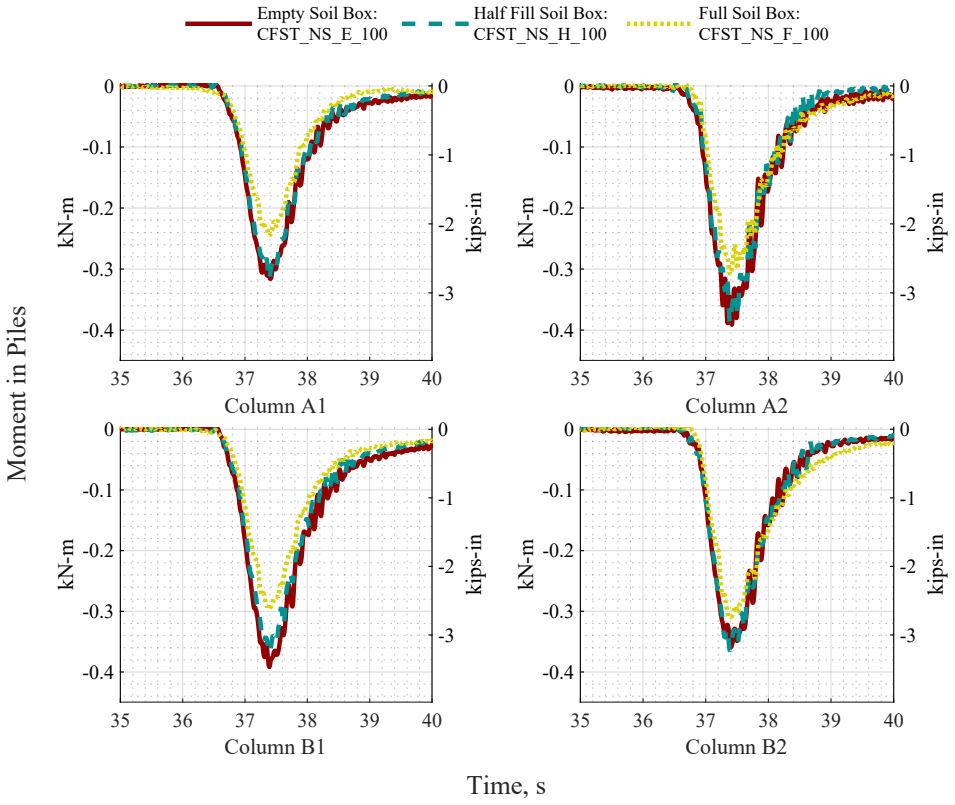

Figure 6.21: Moment at base of piles from 1.00m wave.

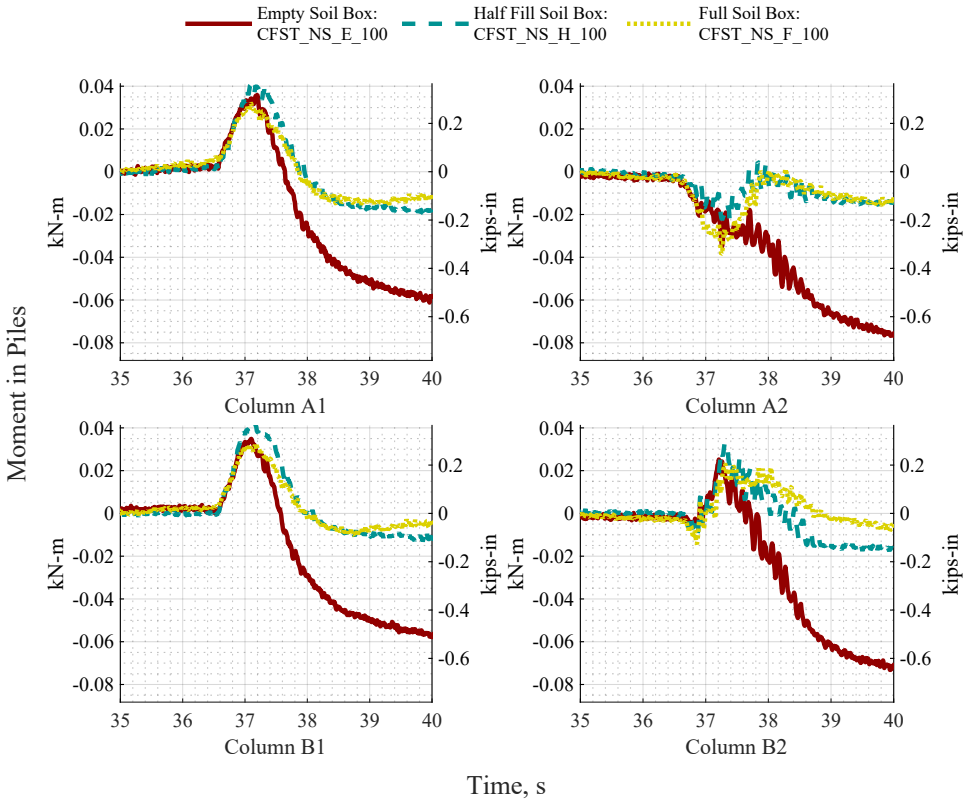

Figure 6.22: Moment at still water level of piles from 1.00m wave.

Table 6.3: Instantaneous Maximum values for 1.40m wave and multiple soil box levels. The impulse is equivalent to the integration of force over time experienced by the specimen.

	In Piles			Vertical Load Cells	
Soil Box Level	instant max V	Impulse from V	Instant max axial Force	Instanta max axial Force	Moment
Empty	1.51 kN (0.34kips)	1.33 kN-s (0.30 kips-s)	2.77 kN (0.62 kips)	-25.22 kN (-5.67 kips)	-4.87 kN-m (-43.12 kips-in)
Half Filled	1.61 kN (0.36 kips)	1.44 kN-s (0.32 kips-s)	2.93 kN (0.66 kips)	-22.68 kN (-5.10 kips)	-4.65 kN-m (-41.17 kips-in)
Full	0.91 kN (0.20 kips)	0.70 kN-s (0.16 kips-s)	15.07 kN (3.39 kips)	-23.00 kN (-5.17 kips)	-4.80 kN-m (-42.47 kips-in)

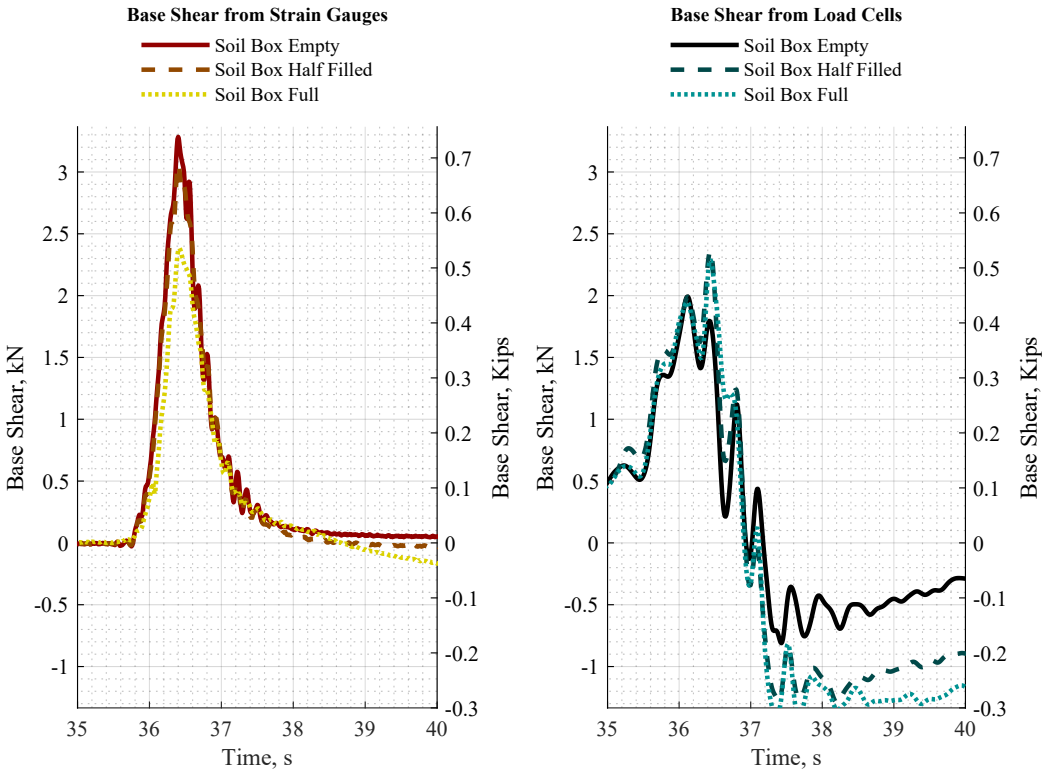

Figure 6.23: Comparison of Base Shear between soil box levels impacted by 1.40m wave and Base shear in the piles vs. base shear in the load cells.

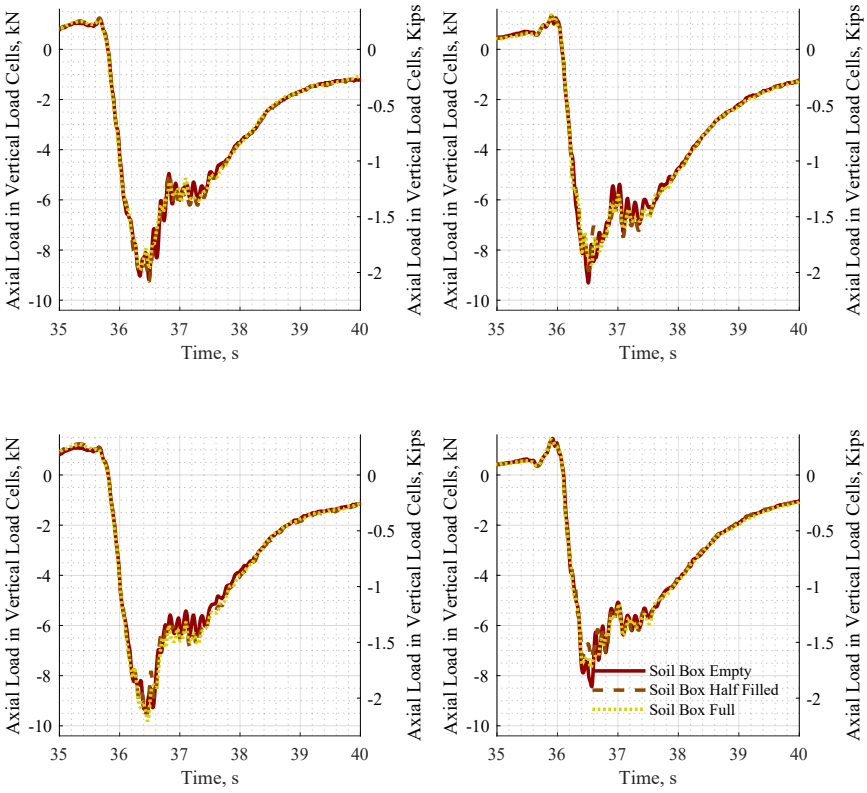

Figure 6.24: Axial force in vertical load cells from 1.40m wave.

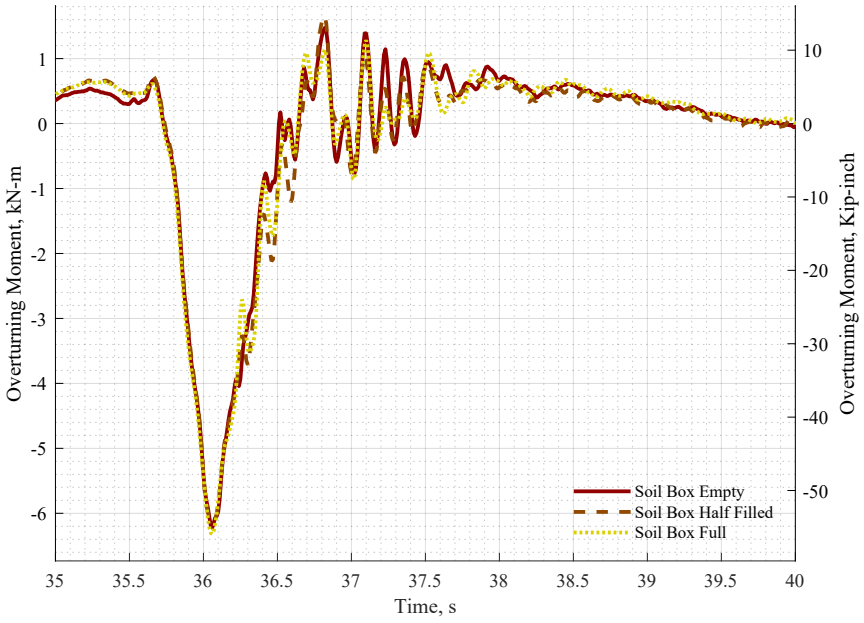

Figure 6.25: Moment in vertical load cells from 1.40m wave.

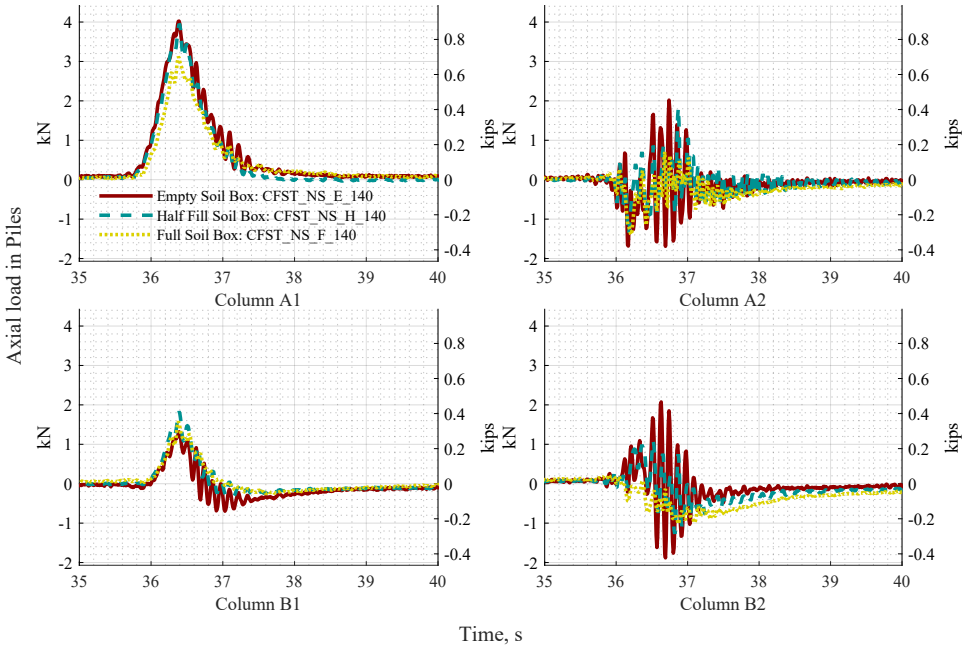

Figure 6.26: Axial force at base of piles from 1.40m wave.

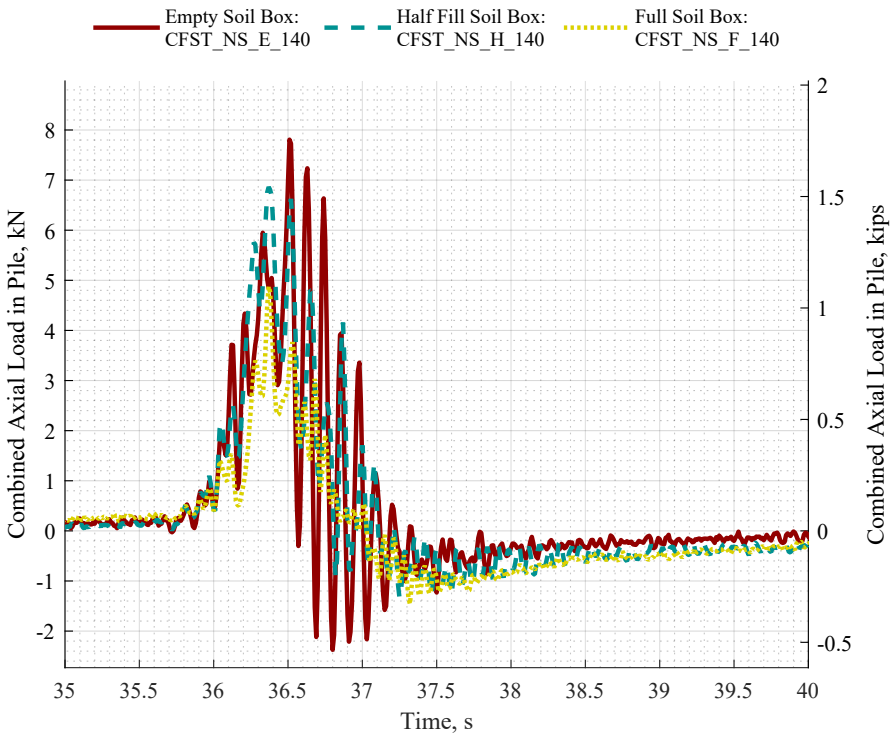

Figure 6.27: Combined axial force at base of piles from 1.40m wave.

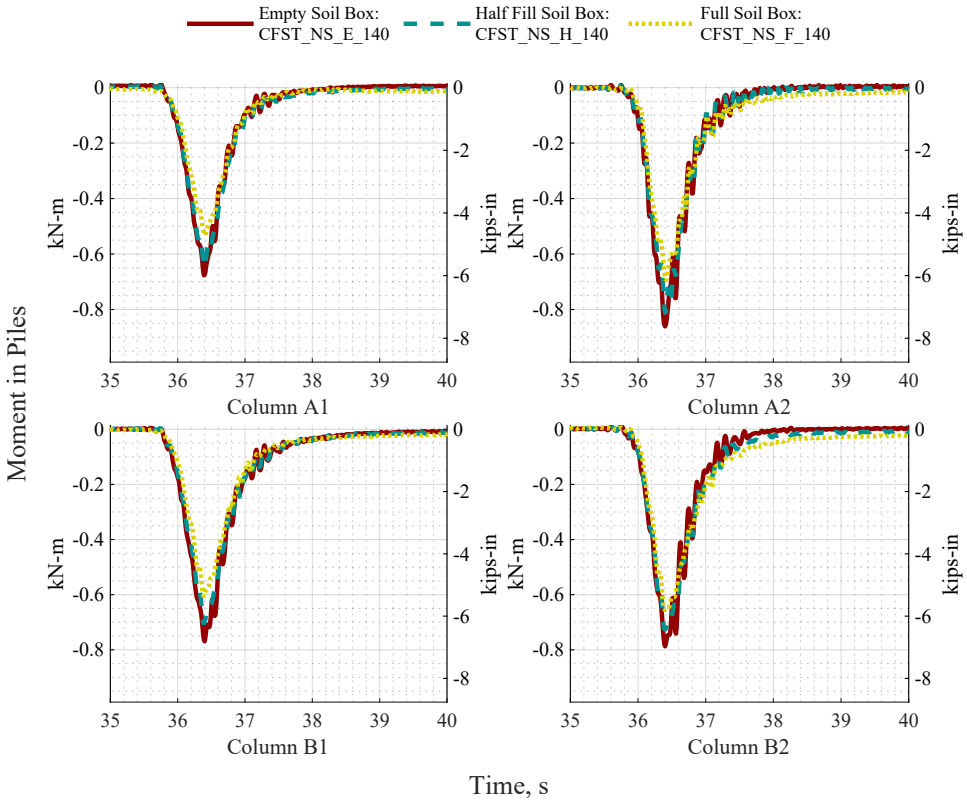

Figure 6.28: Moment at base of piles from 1.40m wave.

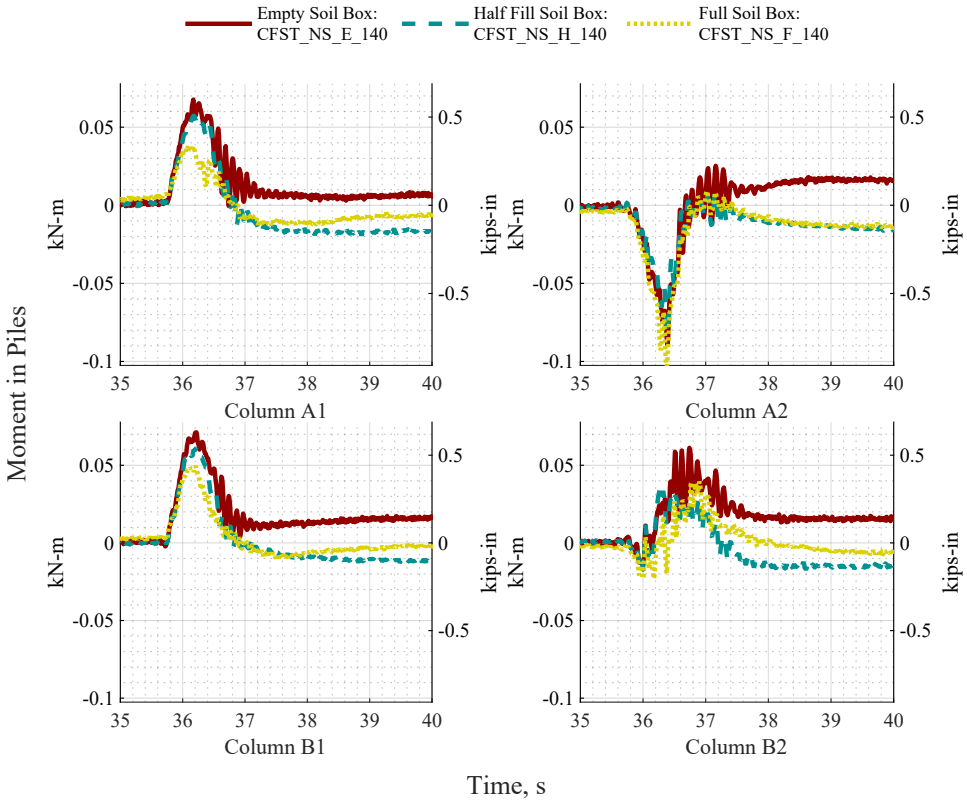

Figure 6.29: Moment at still water level of piles from 1.40m wave.

Table 6.4: Instantaneous Maximum values for 1.45m wave and multiple soil box levels. The impulse is equivalent to the integration of force over time experienced by the specimen.

	In Piles			Vertical Load Cells	
Soil Box Level	instant max V	Impulse from V	Instant max axial Force	Instanta max axial Force	Moment
Empty	2.85 kN (0.64 kips)	2.11 kN-s (0.48 kips-s)	6.59 kN (1.48 kips)	-9.26 kN (-2.08 kips)	-5.89 kN-m (-52.10 kips-in)
Half Filled	2.99 kN (0.67 kips)	2.20 kN-s (0.49 kips-s)	7.34 kN (1.65 kips)	-1.24 kN (-0.28 kips)	-6.11 kN-m (-54.11 kips-in)
Full	2.50 kN (0.56 kips)	1.94 kN-s (0.44 kips-s)	6.66 kN (1.50 kips)	2.84 kN (0.64 kips)	-6.06 kN-m (-53.66 kips-in)

moment calculated from the strain in the piles.

6.2.3 Evaluation of fixed and break away slab and back wall to specimen with open plan

The advantage of a purely CFST structure, without any walls or slabs below the inundation depth, is that it allows the wave to flow through the open area between the columns, with very little area subjected to the wave. In reality, this is not a very realistic structure due to the reduced usable square footage and dedicating two full floors for the wave to pass through. Figure 6.37 compares three CFST specimens with different intermediate floor types. The specimen with only CFST columns exposed to the oncoming wave producing the lowest base shear, with only 3.28 kN (0.74kips). The largest base shear of 20.37 kN (4.58kips), is recorded in the specimen with a fixed panel at the first floor height, and a fixed back wall positioned between the rear columns. The specimen with a break away first floor panel recorded a maximum base shear in the piles of 17.47

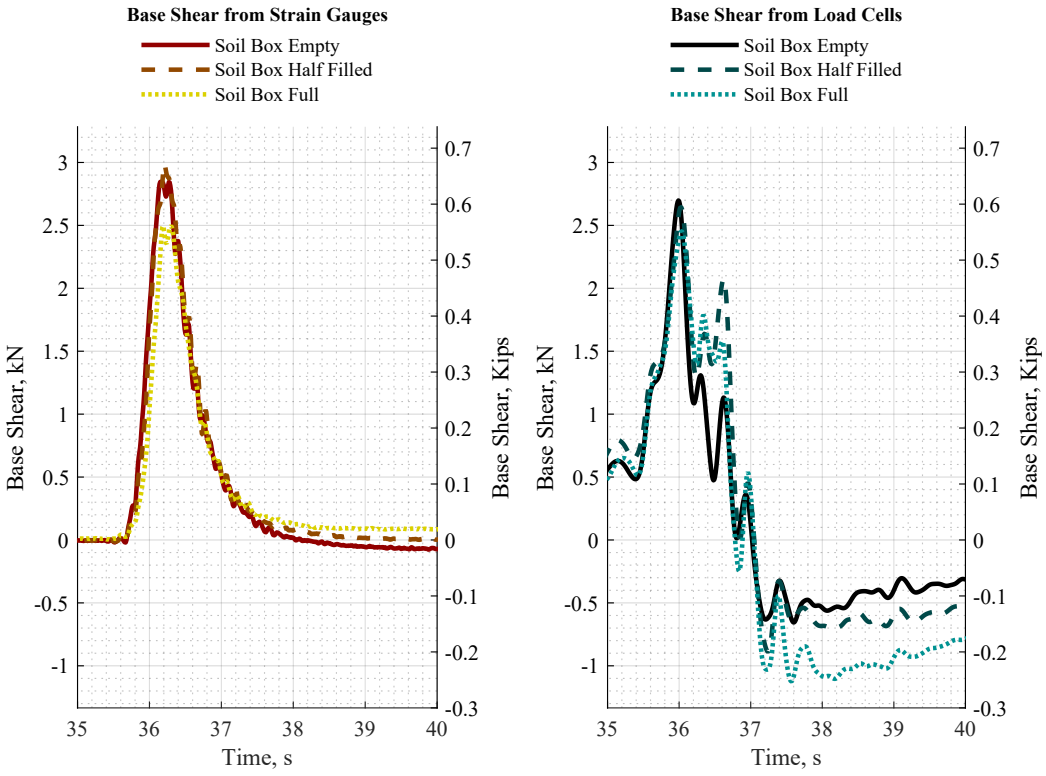

Figure 6.30: Comparison of Base Shear between soil box levels impacted by 1.45m wave and Base shear in the piles vs. base shear in the load cells.

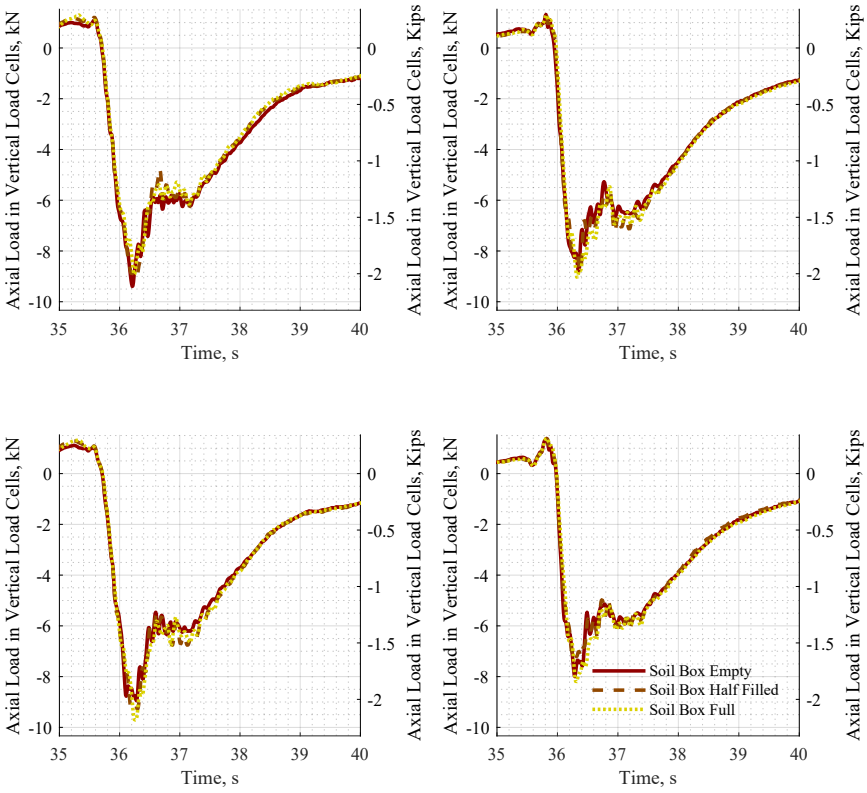

Figure 6.31: Axial force in vertical load cells from 1.45m wave.

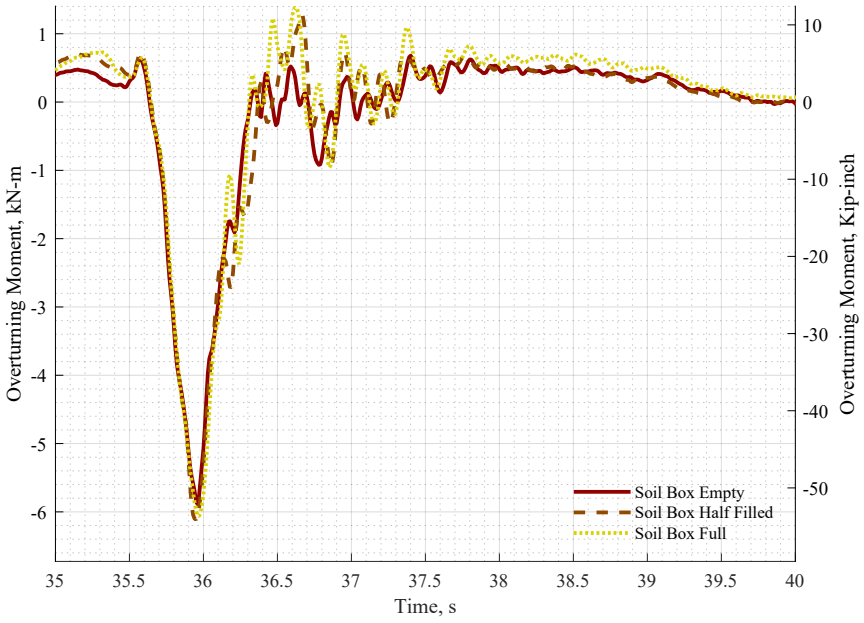

Figure 6.32: Moment in vertical load cells from 1.50m wave.

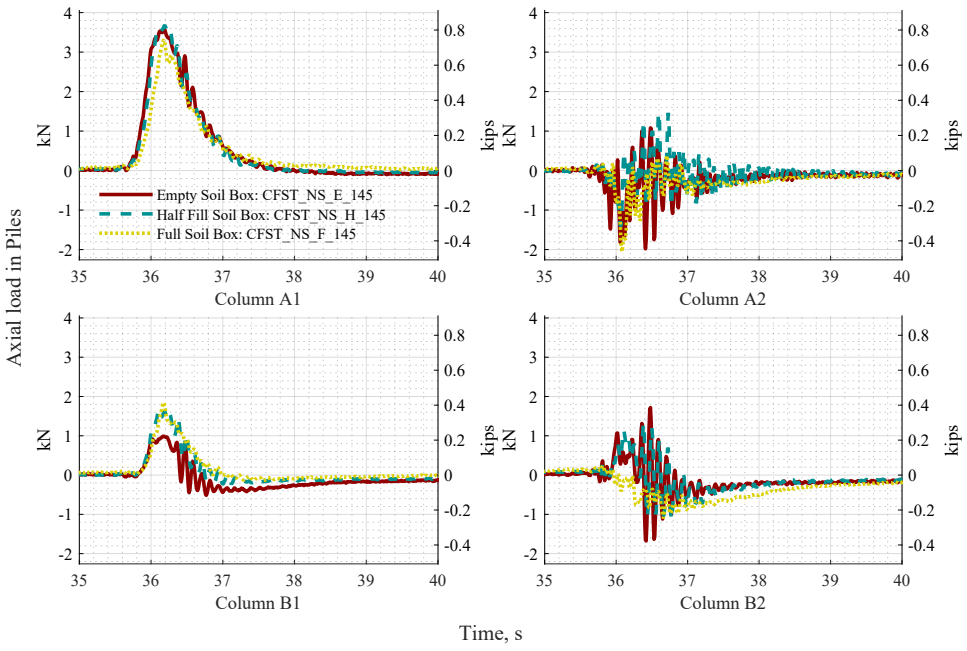

Figure 6.33: Axial force at base of piles from 1.45m wave.

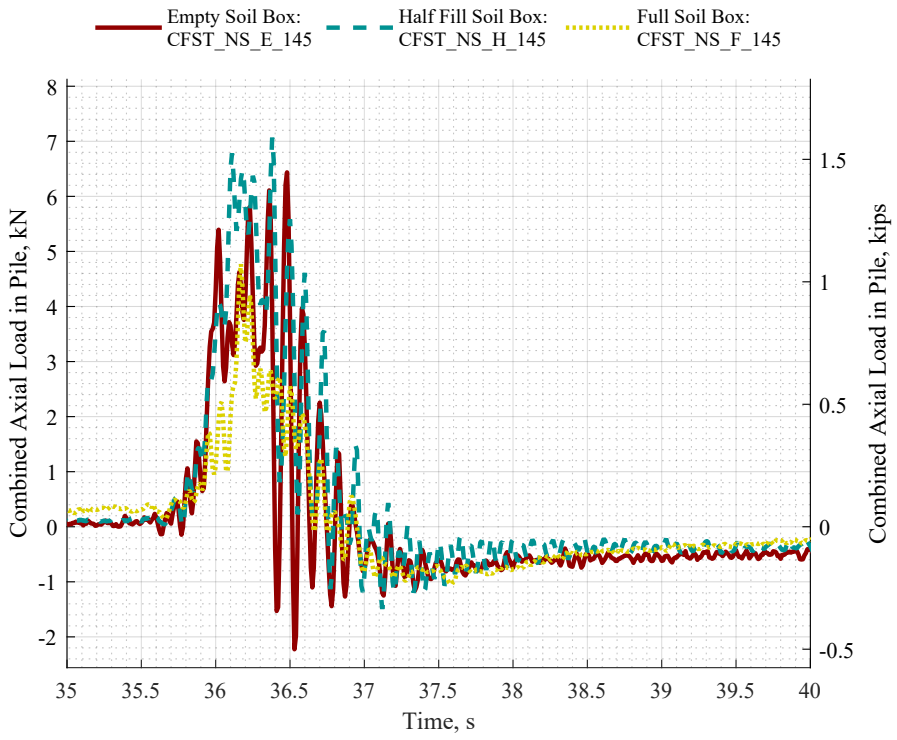

Figure 6.34: Combined axial force at base of piles from 1.45m wave.

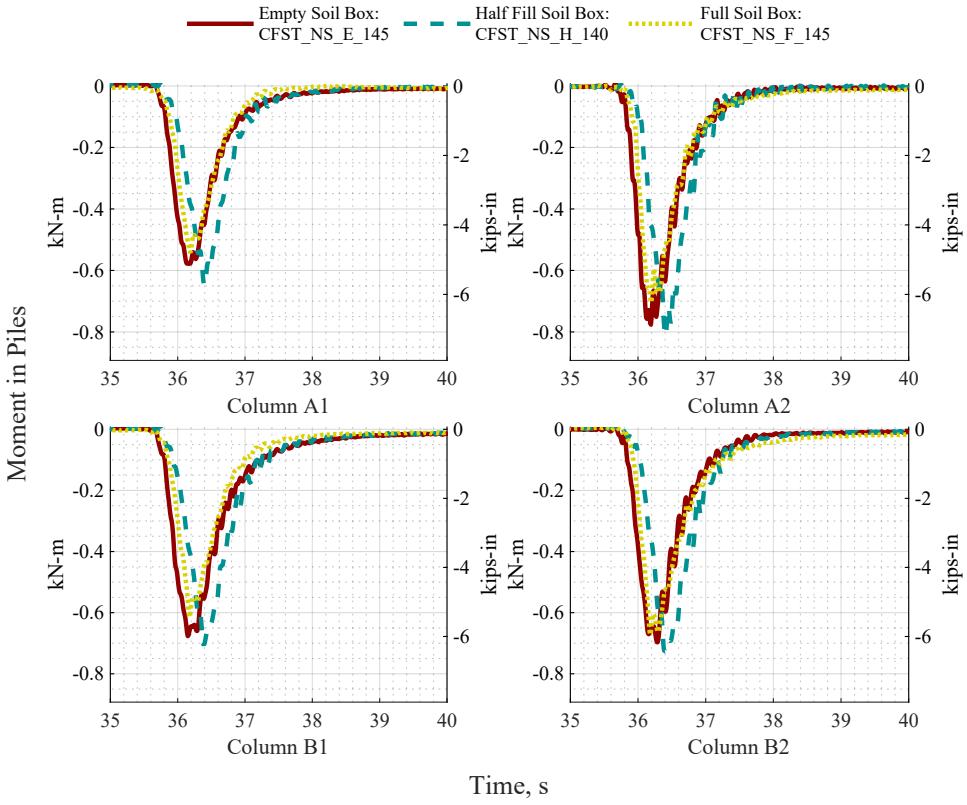

Figure 6.35: Moment at base of piles from 1.45m wave.

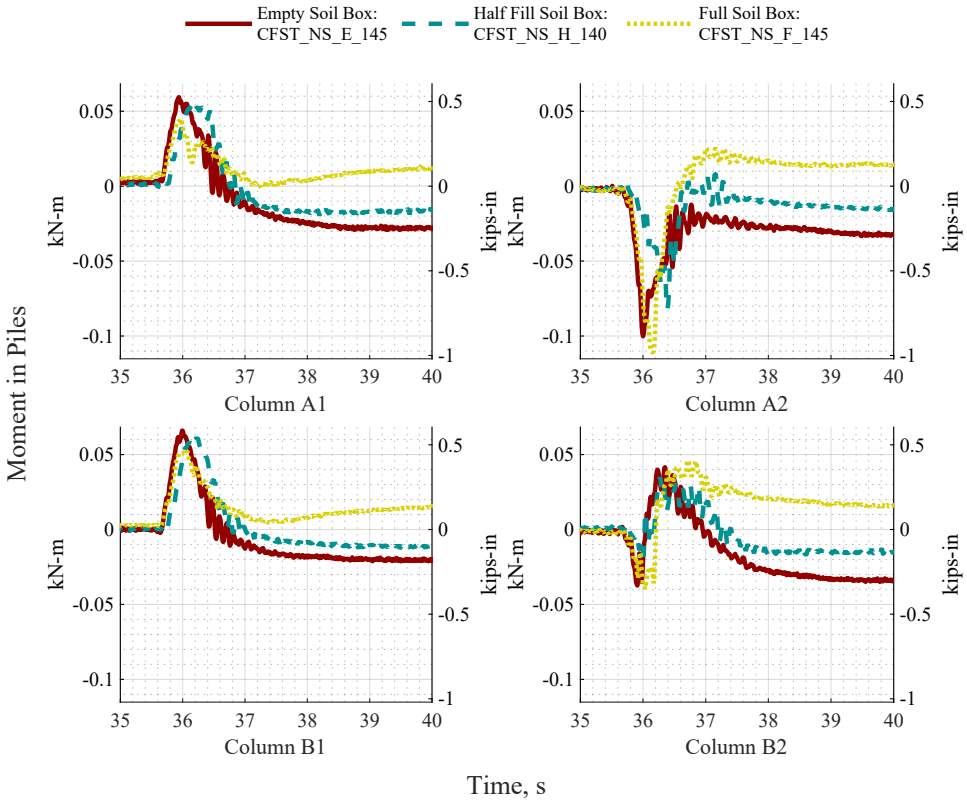

Figure 6.36: Moment at still water level of piles from 1.45m wave.

kN (3.93kips). For this experiment condition, the back wall remained fixed in place, and only the first story floor broke away. The base shear that is avoided from the specimen with the breakaway first floor is 3kN (0.67kips), but could be much greater depending on the turning of the breakaway connections. Furthermore, the base shear can be reduced by allowing the back wall to break away, as is the case for some facades in flood plane areas, or by not including a back wall at all, to form a more open structure, such as a parking garage, but still install a slab at the first story level.

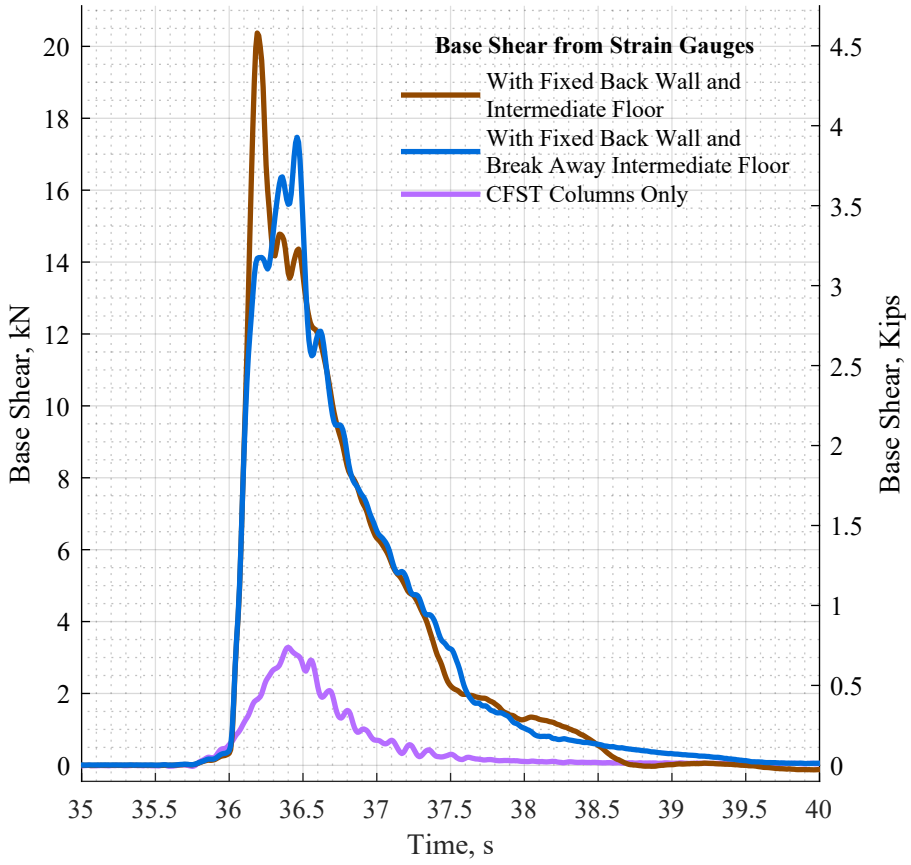

Figure 6.37: Comparison of measured base shear for specimens with an open first floor, a fixed back wall and break away first floor, and fixed back wall and fixed first floor

Figure 6.38 and Figure 6.40 show the axial load in the vertical load cells and moment in the specimen set up for the same three specimens. Not surprisingly, the vertical load cells experience slightly less downward force, due to the wave being directed upward into the first floor by the back

wall. Intuitively, the specimen with the breakaway panel, experiences vertical force and moment similar to the specimen with the fully attached first floor until the panel reaches the maximum load capacity, at which point, the load is released and the load returns to neutral. The axial force in the piles, shown in Figure 6.39, creates a more distinct picture of this uplift in the piles because there is less unrealistic tributary area where the wave weight around the structure impact the reading.

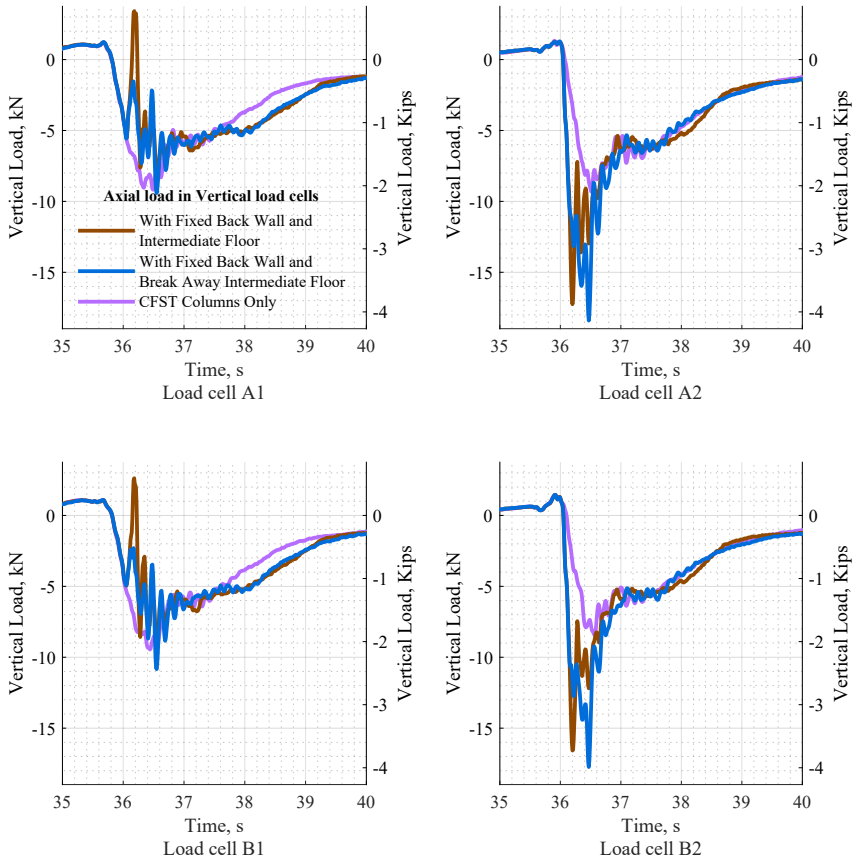

Figure 6.38: Axial Load in the vertical Load cells, with the 1.40m wave, soil box empty, and varying experiment conditions with the first floor.

6.3 Preliminary Comparison of Specimen Types

Tests conducted in October 2019 by Pyke (2020) were designed to be a close comparison to the CFST structure presented in this thesis. First the pressures on the front column and front wall

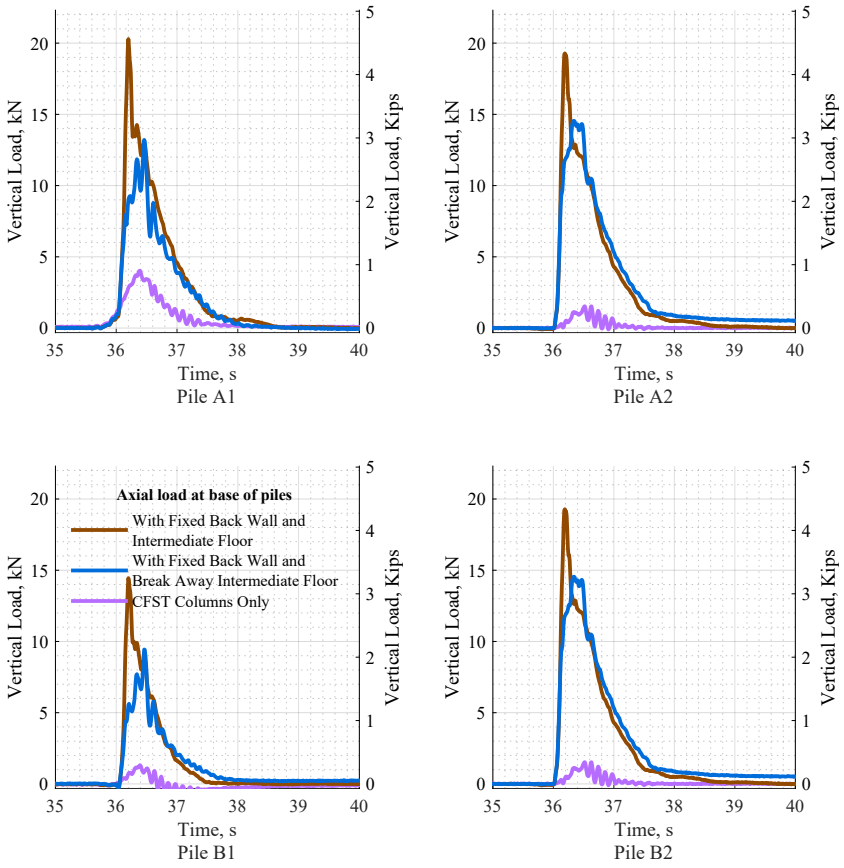

Figure 6.39: Axial Load at the base of the Piles, with the 1.40m wave, soil box empty, and varying experiment conditions with the first floor.

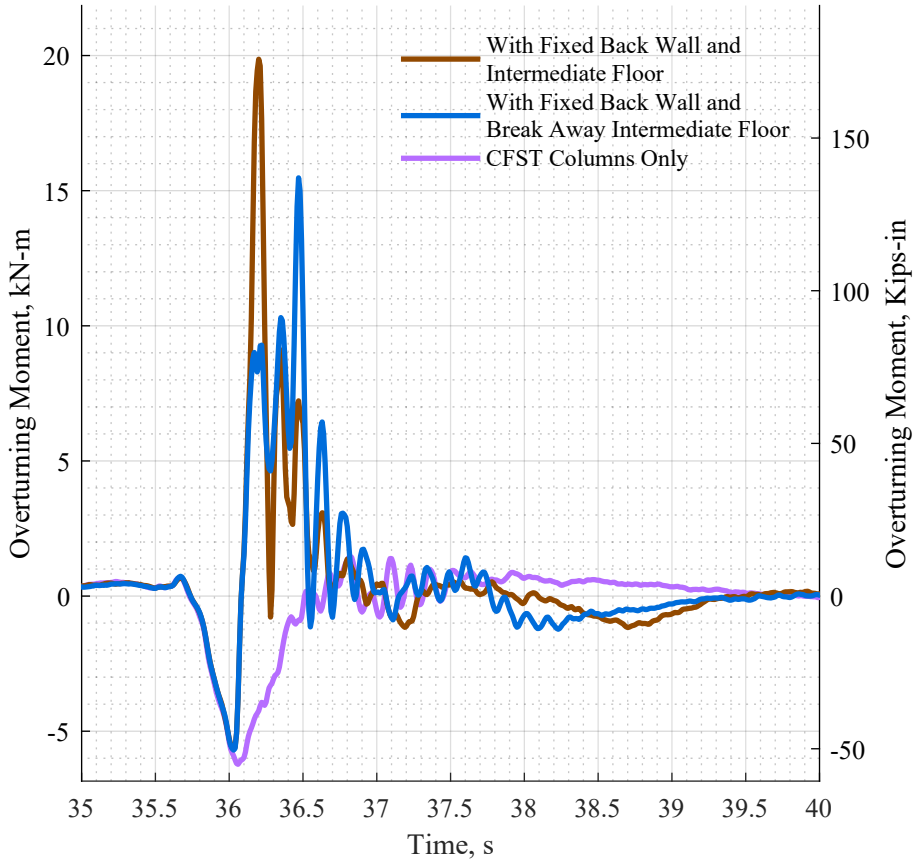

Figure 6.40: Moment measured by the vertical load cells, for the varying first floor experiment conditions.

are compared on the two specimens for the 1.40m wave and the 1.45m wave. Next, the base shear in the piles is compared between the specimen types for the 1.40m wave, because this is the wave tested with the CFST specimen with fixed and breakaway first floor panels. These experiments are not perfectly comparable due to the different placement of vertical walls and the presence or lack of a horizontal floor that is inundated by the wave.

6.3.1 Pressures

Pressure sensors are located on the front column of the CFST specimen, at the center of the column cross section facing into the oncoming wave. The elevations and locations of the pressure sensors are given in Figure 5.20 and Table 4.3. The locations of pressure sensors on the front face of the shear wall specimen are given by Figure 6.41. To achieve coverage of the entire set of 33 pressure sensor locations, four layouts were utilized to use the 12 working gauges. Two columns of sensors will be compared to the CFST specimen, column line B (which is the centerline of the front face of the shear wall), and column line D (which are the outermost pressure gauges, and closest to the physical location of the CFST instruments).

Figure 6.42 presents the pressures recorded along the height of the specimens for the 1.40m wave. The center line (column line B) of the shear wall specimen records slightly higher pressures than column line D, and the CFST. The instantaneous peak pressures on the shear wall specimen are very close to the mean of the maximum two tenths of a second, meaning, the peak pressure is present for at least two tenths of a second, as the wave inundates the specimen. The CFST, on the other hand, shows some more variation in the instantaneous max pressure and the sustained max pressure at the higher elevations along the columns. Additionally the pressure gauges from column line D on the shear wall are closer to the CFST pressures, meaning the water flowing around the corner of the shear wall is more similar to the water flowing around the columns, than the water damming and redirection that occurs at the center of the wide shear wall.

Figure 6.43 shows the pressure sensor results along the height of the specimens for the 1.45m wave. This wave has broken by the time it reaches the specimens, and is more turbulent on first inundation. This results in more variation in the instantaneous maximum pressure and the sustained maximum pressure than the 1.40m wave for both column lines of the shear wall specimen

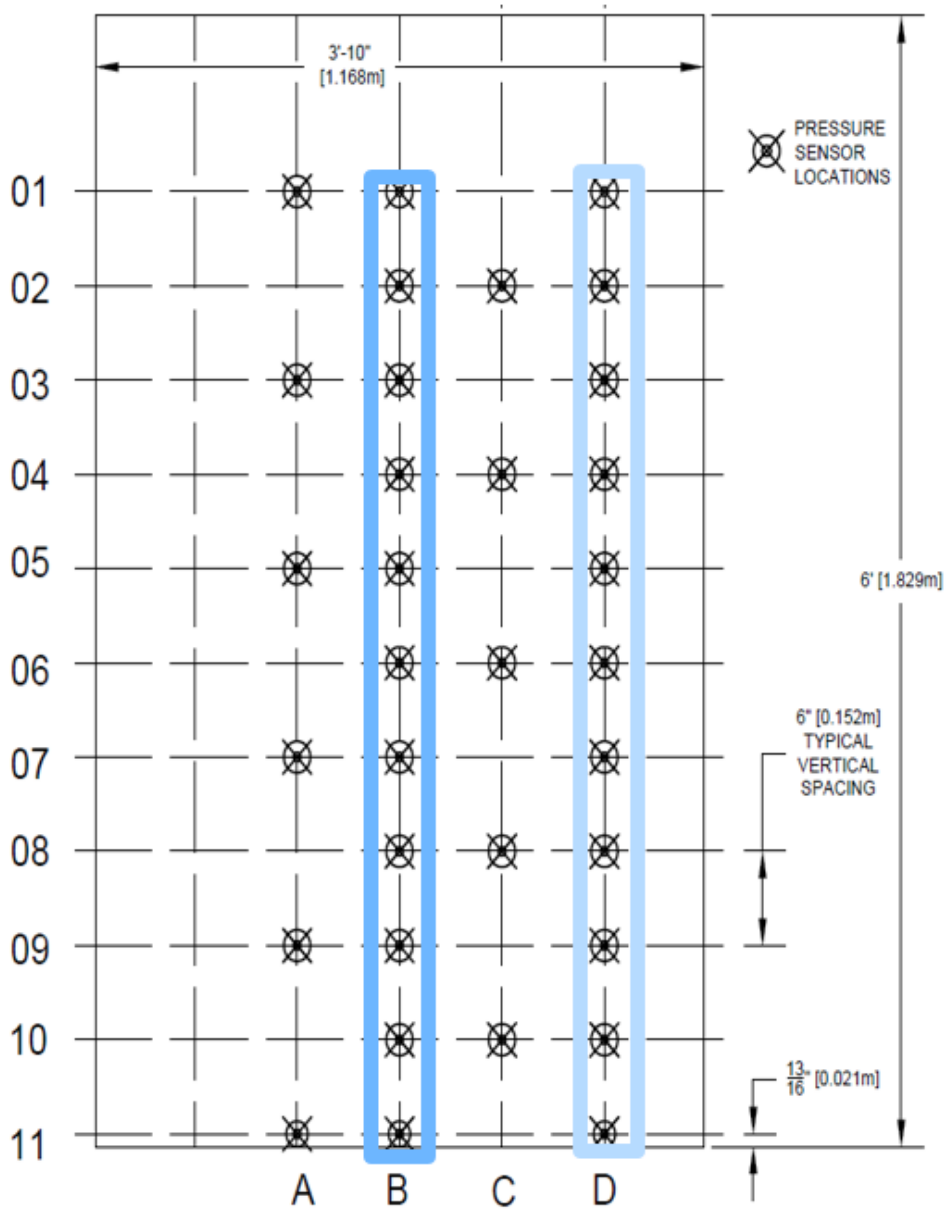

Figure 6.41: Pressure Sensor Locations on Concrete Shear Wall specimen.

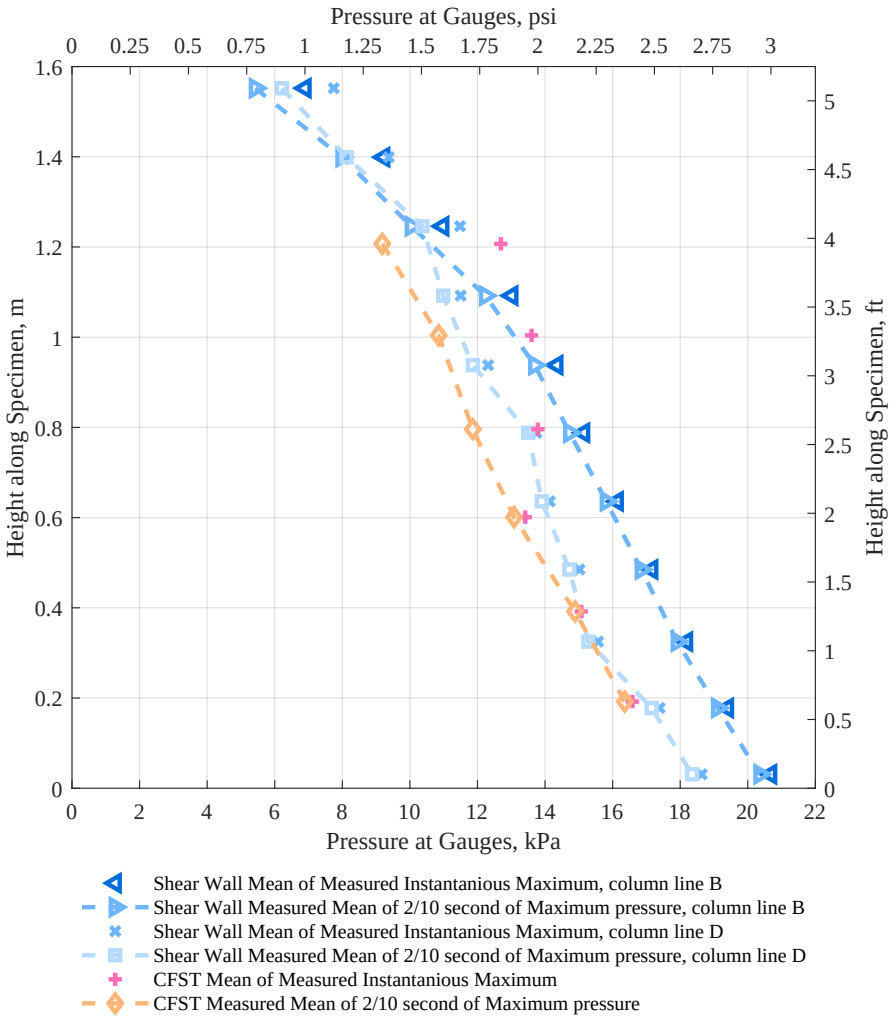

Figure 6.42: Comparison of Pressures along the height of the specimen for the 1.40m wave. The triangles represent pressures taken from column line B, the center of the specimen, while the x and o are pressures taken from the outside column of pressure sensors, closest to the CFST gauges.

and the CFST specimen.

6.3.2 Base Shear

The base shear in the specimens is a direct reference to the amount of load the lateral force resisting system and foundations need to be able to carry. Figure 6.44 presents the base shear in the piles for the shear wall specimen, CFST with fixed back wall and first floor, and the CFST specimen with open bays and only columns impacted by the wave. The specimens are not a pure one to one comparison, because the CFST specimens do not have a vertical wall in the same position in the flume bathymetry as the shear wall specimen. However, Figure 6.44 shows the potential to reduce the lateral load demand on the system by using a CFST frame with tuned break away slabs at the floors that are inundated by the wave. The instantaneous maximum base shears in the piles and impulse for each specimen type are presented in Table 6.5.

Table 6.5: Base shear and integration of force over time in Shear wall, CFST with back wall, and slab, and CFST with only columns specimens.

Specimen	Instant. maximum Base shear in piles	Integration of force over time from base shear in piles (Impulse)	Impulse ratio: CFST/Shear wall
Shear Wall	21.21 kN (4.77kips)	20.83 kN-s (4.68kips-s)	N/A
CFST w/ fixed wall & slab	20.37 kN (4.58kips)	14.92 kN-s (3.35kips-s)	0.72
CFST with columns only	3.28 kN (0.74kips)	2.30 kN-s (0.52kips-s)	0.11

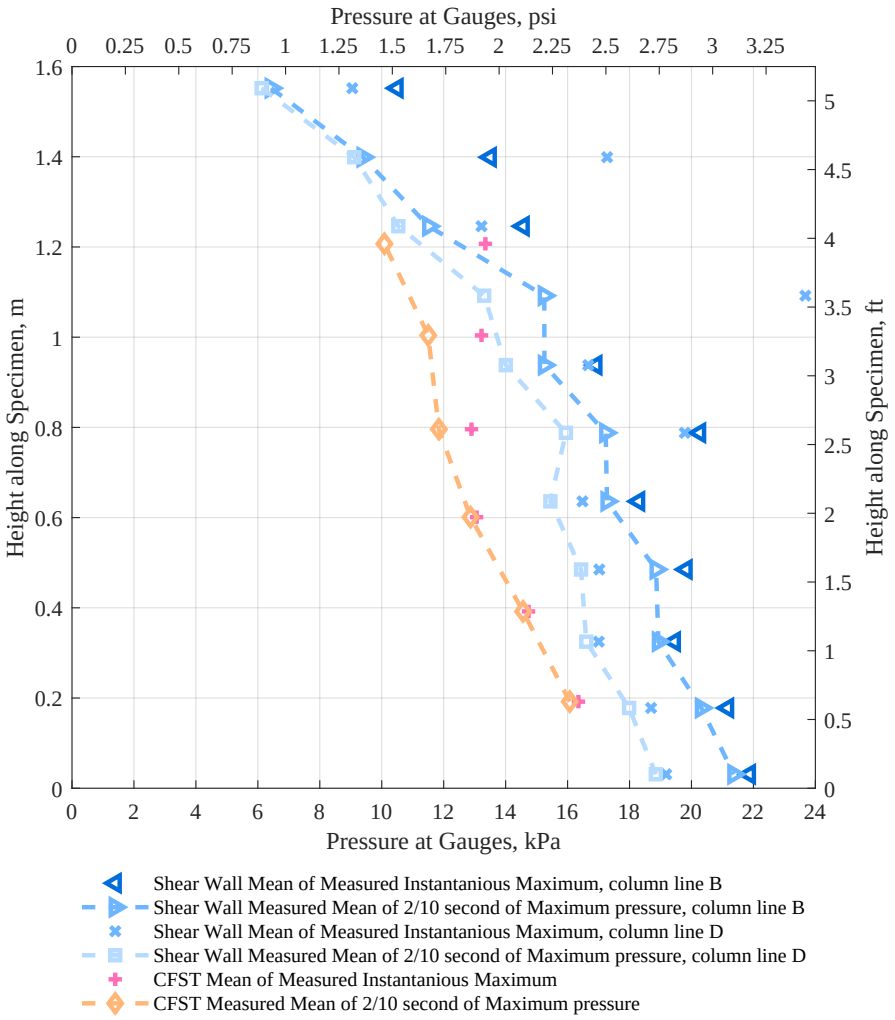

Figure 6.43: Comparison of Pressures along the height of the specimen for the 1.45m wave. The triangles represent pressures taken from column line B, the center of the specimen, while the x and o are pressures taken from the outside column of pressure sensors, closest to the CFST gauges.

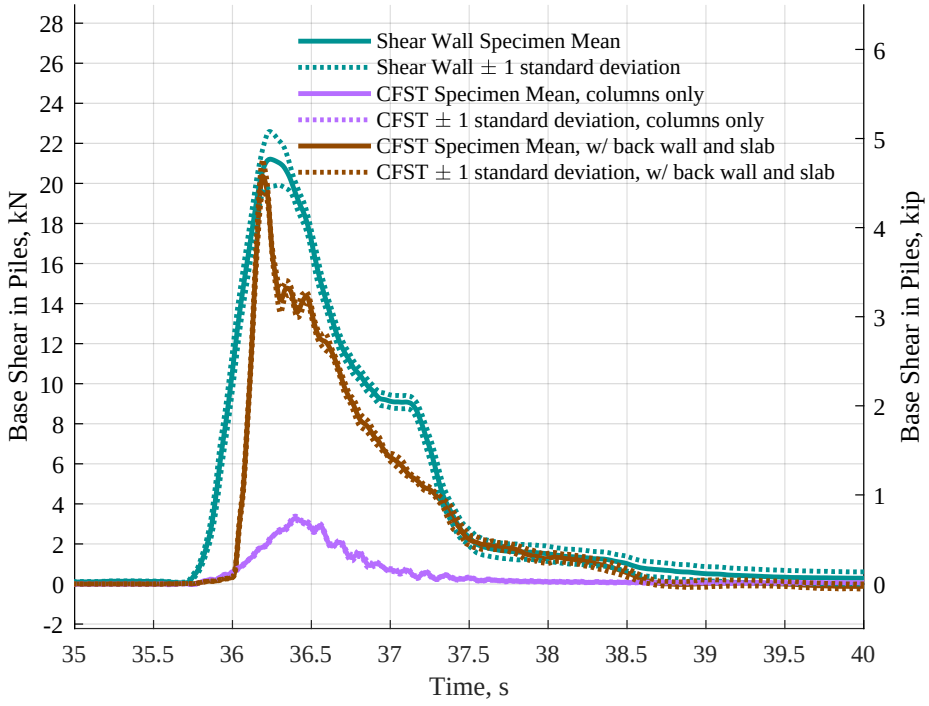

Figure 6.44: Comparison between base shear from the 1.40m wave as it impacts the Shear wall specimen, CFST specimen with back wall and fixed slab, and CFST specimen with open columns.

6.3.3 Alternative Specimen Types

The specimens tested in this experiment represent idealized representations of what could possibly be designed and build in reality. To get more use from a CFST vertical evacuation structure, and make it practical from an economic and government perspective, useable space must be built into the first two stories, even though these areas will be damaged or destroyed in the event of a tsunami. One potential is to design the lower floors as a parking garage with sides that are mostly open to allow water and debris flow through the building.

While the OpenFOAM results presented in Section 6.1.3 are not perfect simulations of the specimens in the flume, they are relatively close in terms of the energy input into the specimen. Referencing back to Table 6.1, the ratio of the integration of force over time for the experiment and simulation for the 1.40m wave, without back wall is 1.04. The ratio when a back wall is added to both the specimen and the simulation is slightly worse, but still quite good with 0.85. With this in mind it is reasonable to assume that Figure 6.45 shows a fairly realistic time history for CFST specimen in the wave flume with a fixed first floor panel, but no back wall. Compared to the specimen with a fixed back wall and slab, this is a major reduction in base shear. The base shear is also reduced when compared to the specimen with breakaway first floor, but fixed back wall. Unsurprisingly, the vertical wall catches a large portion of the force form the wave, and transfers it into the structure. The simulation of a specimen with only a fixed first floor shows a good compromise between useable square footage and lateral load being transferred into the specimen.

The OpenFOAM simulation shows the benefit of allowing vertical walls in the structure to break away, and still be able to use first floor for the structure when not experiencing a tsunami event. The simulation does not fully characterize the loads on this slab element and the surrounding system because OpenFOAM treats this portion of the model as a rigid boundary condition connected to the ridged columns extending from the flume floor. This means that while OpenFOAM results may suggest the ideal usable structure will have a fixed slab, and break away walls (or no walls), it may not be possible to design such a system within normal design constraints. A better solution is to design a connection for the first-floor slab that has a tuned yielding or breaking load. This would allow the system to withstand normal load patterns, but allow the specific pressure and load from a tsunami to release the fuse element and preserve the main gravity and lateral force resisting

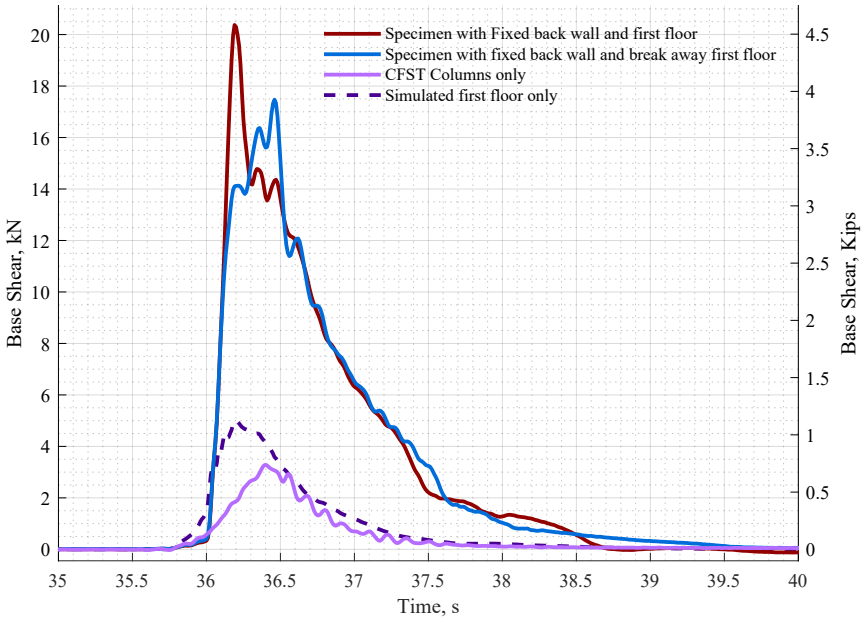

Figure 6.45: Comparison of Base Shear for experimental and simulated first floor conditions

system. One significant design challenge will be creating a connection that preforms as designed to release load from a tsunami, while still being strong enough to stay in place during the severe earthquake that will precede a subduction zone tsunami.

Chapter 7

SUMMARY AND CONCLUSIONS

This chapter includes three sub-sections. First, Section 7.1 provides a summary of the work presented in this thesis. Section 7.2 draws conclusions from the results and comparisons made in Chapter 5 and Chapter 6. Finally, Section 7.3 presents suggestions for future research and ways to improve this experiment.

7.1 Summary

Coastal communities in earthquake prone regions have the potential to experience subsequent disaster events from a large scale earthquake followed by a tsunami. This is especially likely in low lying areas, or communities without easy access to high ground, such as many areas in the Pacific Northwest of North America. A structure that provides artificial high ground closer to resident's homes and businesses could be the lifesaving infrastructure these communities need. This thesis builds on the research on shear wall systems in potential vertical evacuation structures, conducted by Pyke (2020), by examining the fluid structure response of a scaled concrete filled steel tube frame specimen in the large wave flume at the Hinsdale wave Laboratory at Oregon State University.

The specimen tested is a single bay by single bay frame with columns above the water level and a chevron braced frame hat truss in the equivalent of the third story. Piles extended 39 inches below the still water level with varying depths of soil before being fixed in a concrete slab at the base of the specimen. The concrete filled steel tubes are 4 inch outer diameter, with a wall thickness of 0.23 inches. The columns were placed 40 inches on center, for a total outside plan dimensions of 44 inches b 44 inches.

Testing involved three main variables. First the wave height of the wave generated by the wave maker in the flume was adjusted between 1.00m, 1.40m, and 1.45m. Next the depth of soil below the specimen was varied between empty, with no soil, 20 inches of soil, and full, with 39 inches of soil. Finally, the effect of a fixed first story slab and back wall was investigated by installing a plywood

and dimension lumber panel 25 inches above the still water level. The effect of a break away slab, and the influence of axial load in the piles was also investigated by replacing the plywood first story slab with scored hardyboard that broke and floated away when force from the wave reached the required level.

Significant results from this investigation include that a tuned breakaway first floor slab and back wall have a large impact on the overall forces experienced by the specimen. Furthermore, if a viable break away connection can be designed to withstand an earthquake before releasing load during a tsunami, the entire structure design will benefit from the reducing the large fluid pressures. Additionally, the effect of soil level on the specimen played a minimal role in the load applied by the wave, because the soil applied only a marginal increase in stiffness. However, in a real structure, the stiffness changes from tsunami's scouring away the soil around the foundations can play a much larger role.

7.2 Conclusions

Key conclusions from the results presented in Chapter 5 and Chapter 6 include:

- The CFST specimen without a first story slab or back wall experienced an impulse, calculated form the integration of force over time, 11% of the impulse experienced by the shear wall specimen. When a back wall and first story slab are added, the reduction in impulse, from the integration of force over time is 28%.

- The inclusion of a break away first floor slab can have a large impact on the axial load in the piles. The break away hardyboard slab tested in this experiment reduced the axial load in the piles by 35%. By tuning this slab to break away at a different axial load, the axial load in the piles could be further reduced.

- The pressure distribution given by OpenFoam matched the pressure distribution measured in the wave flume, despite the base shears being different. This suggests OpenFOAM is providing an accurate simulation of the fluid dynamics in the wave flume, but it lacks the capabilities to translate that into force for a complex structure in the flume.

- When soil is added to the soil box, there is a slight reduction in the load in the piles below the specimen. This change varies depending on the wave height, but in general is a reduction of 36%. This 36% of force when the soil box is full is transferred into the soil and into the soil box walls and slab before being transferred into the horizontal load cells.

- When soil is added to the soil box, the axial load in the piles varies slightly, but not by enough to become significant with relation to the noise and variation in the instruments.

- The 1.00m wave consistently produced the smallest structural response. The base shear in the piles when the soil box was empty was 1.5 kN, and when the wave height was increased to 1.40m, the base shear in the piles increased to 3.4 kN. The structural response for the 1.45m wave was consistently smaller than the 1.40m wave despite being created with a larger displacement of water in the flume. This is likely due to the wave starting to "slip" and become unstable between bays 3 and 4.

7.3 Recommendations for Further Research

Further research on utilizing CFST frame systems in vertical evacuation structures is encouraged. Improvements to this experiment include:

- Further investigation on the boundary conditions of the specimen, such as:
  - Pin the bottoms of the piles in the soil box rather than leaving them fixed.
  - Leave the piles free from direct restraint, but embed them in a compacted soil in the flume. This would allow for a more realistic boundary condition.
  - Create an indeterminate system with more load cells on each side of the soil box
  - Isolate the load cells so no load from the soil box or other tributary areas skews the measurements.

- Determine the displacement of the specimen with each inundation of the wave. Determine the stiffness of the specimen when a known load is applied.

- Determine the natural frequency of the specimen, and the specimen in the set up, so these vibrations can be removed from the measurements.

New experiments and research can also be designed to enhance the knowledge around using CFST lateral force resisting systems in vertical evacuation structures. Suggestions include:

- Testing a specimen composed of multiple bays of CFST frames in both plan dimensions. This could be conducted in a smaller scale or in a large wave basin or similar.

- Development and testing of a full scale break away connection.

- Integration of the structural response into OpenFOAM, such as by linking OpenFOAM to OpenSees.

BIBLIOGRAPHY

T. Lykke Andersen, P. Frigaard, M. L. Damsgaard, and L. De Vos. Wave run-up on slender piles in deign conditions – model tests and design rules for offshore wind. *Coastal Engineering*, 2010.

ASCE 7-16. *7-16 Minimum Design Loads and Associated Criteria for Buildings and Other Structures*. American Society of Civil Engineers, Reston, VA, 2017.

Gary Y. K. Chock. Design for tsunami loads and effects in the asce 7-16 standard. *J. Struct. Eng.*, 2016.

Cascadia Region Earthquake Workgroup CREW. Cascadia subduction zone earthquakes: A magnitude 9.0 earthquake scenario. *Washington State Department of Natural Resources*, 2013.

Stuart A. Fraser, Graham S. Leonard, Hitomi Murakami, and Ichiro Matsuo. Tsunami vertical evacuation buildings – lessons for international preparedness following the 2011 great east japan tsunami. *J. Disaster Research*, 2012a.

Stuart A. Fraser, Graham S. Leonard, Hitomi Murakami, and Ichiro Matsuo. Tsunami evacuation: Lessons from the 2011 great east japan earthquake and tsunami of march 11th 2011. *GNS Science Report 2012*, 2012b.

Maha M. Hassan, Hazem M. Ramadan, Mohammed N. Abdel-Mooty, and Sherif A. Mourad. Behavior of concentrically loadced cft braces connections. *Journal of Advanced Research*, 2013.

J. A. Heintz and M. Mahoney. Guidelines for design of structures for vertical evacuation from tsunamis. 2008.

Hinsdale Wave Lab. Large wave flume. *O.H. Hinsdale Wave Research Laboratory*, Oregon State University. `wave.oregonstate.edu/large-wave-flume`.

P. Lukkunaprasit, A. Ruangrassamee, and N. Thanasisathit. Tsunami loading on buildings with openings. *Science of Tsunami Hazards*, 2009.

Tim Maddux. *README: Guide to the Project Folder*. Oregon State University, September 2018.

Christopher Pyke. *Testing of a Reinforced Concrete Core Wall for Tsunami Vertical Evacuation Shelter Structures in a Wave Flume*. Department of Civil and Environmental Engineering, University of Washington, June 2020.

Charles W. Roeder, Brad Cameron, and Colin B. Brown. Composite action in concrete filled tubes. *Journal of Structural Engineering*, 1999.

Charles W. Roeder, Gregory MacRae, Chad Gunderson, and Dawn E. Lehman. Seismic design criteria for cft braced frame connections. In *Proceedings of the International Workshop on Steel and Concrete Composite Construction*, pages 97–106, 2003.

Stephen P. Schneider, Donald R. Kramer, and Douglas L. Sarkkinen. The design and construction of concrete-filled steel tube column frames. In *13th World Conference on Earchquake Engineering*, Vancouver B.C., Canada, August 2004.

Ikhlas S. Sheet, Umarani Gunasekaran, and Gregory A. MacRae. Experimental investigation of cft column to steel beam connections under cyclic loading. *Journal of Constructional Steel Research*, 2013.

J. Wienke and H. Oumeraci. Breaking wave impact force on a vertical and inclined slender pile – theoretical and large-scale model investigations. *Coastal Engineering*, 2005.

Andrew O. Winter. *Effects of Flow Shielding and Channeling on Tsunami-Induced Loading of Coastal Structures*. University of Washington, Department of Civil and Environmental Engineering, August 2019.

Nathan J. Wood, Jeanne Jones, Seth Spielman, and Mathew C. Schmidtleind. Community clusters of tsunami vulnerability in the us pacific northwest. *Proceedings of the National Academy of Sciences of the United States of America*, 2015.

Fei Xu, Ju, and Wei liang Jin. Experimental investigation and design of concrete-filled steel tubular chs connections. *Journal of Structural Engineering*, 2014.

You-Fu Yang, Min Liu, Chao Hou, and Xue-Meng Bie. Behaviour of four-legged square cfst latticed members under lateral cyclic loading. *Journal of Construction Steel Research*, 2019.

Harry Yeh, Ian Robertson, and Jane Preuss. Developmeent of design guidelines for structures that serve as tsunami vertical evacuation sites. 2005.

Appendix A

DESIGN OF FULL SCALE SPECIMEN

This appendix provides the excel sheets used to design the full scale vertical evacuation structure using ASCE 7-16 and the distributed plasticity method.

Site Coefficients

T_1	16	s	Long period transition period
S_s	1.3	g	0.2 s spectral response
S_1	0.7	g	1 s spectral respnse
F_a	1		Short Perio Table 11.4-1
F_v	1.7		Long Perioc Table 11.4-2

S_MS	1.3	g	Risk	(11.4-1)
S_M1	1.19	g	Targeted	(11.4-2)

Structure Coefficients

I_e	1.5		Importance Factor	
h_n	75	ft	structural height	
C_t	0.02		period parameters, Table 12.8-2	
x	0.75			
R	2		reduction factor	
C_u	1.4		Upper Limit on Calculated Period Coeffient	Table 12.8-1

T_a	0.509713	s	Approximate fundamental Period	(12.8-7)
T	0.713599	s	maximum fundamental period	Sec. 12.8.2

C_s

0.975	min
1.250703	
0.066	max
0.01	
0.2625	

Sec. 12.8.1.1

C_s 0.975

V 5484.375 kip

W_1floor	1125	kip
W	5625	kip
Num Frames	4	
Open Column Hei	30	ft

Lat load/frame 1371.094 kip

Equal stiffnesses

Vertical Distribution of Forces

w_x	h_x	w_x*h_x	C_vx	Fx	outside col	inside col
1125	75	84375	0.333333	457.0313	114.2578125	228.5156
1125	60	67500	0.266667	365.625	91.40625	182.8125
1125	45	50625	0.2	274.2188	68.5546875	137.1094
1125	30	33750	0.133333	182.8125	45.703125	91.40625
1125	15	16875	0.066667	91.40625	22.8515625	45.70313
1125	0	0	0	0	0	0
	sum	253125	1	1371.094		685.5469

Base shear Demand single collumn (k)

		Number of Frames		
		2	3	4
R	1	2742	1828	1371
	2	1371	914	686

Moment Demand single column (k-ft)

		Number of Frames		
		2	3	4
R	1	29000	19300	14500
	2	14500	9650	7250

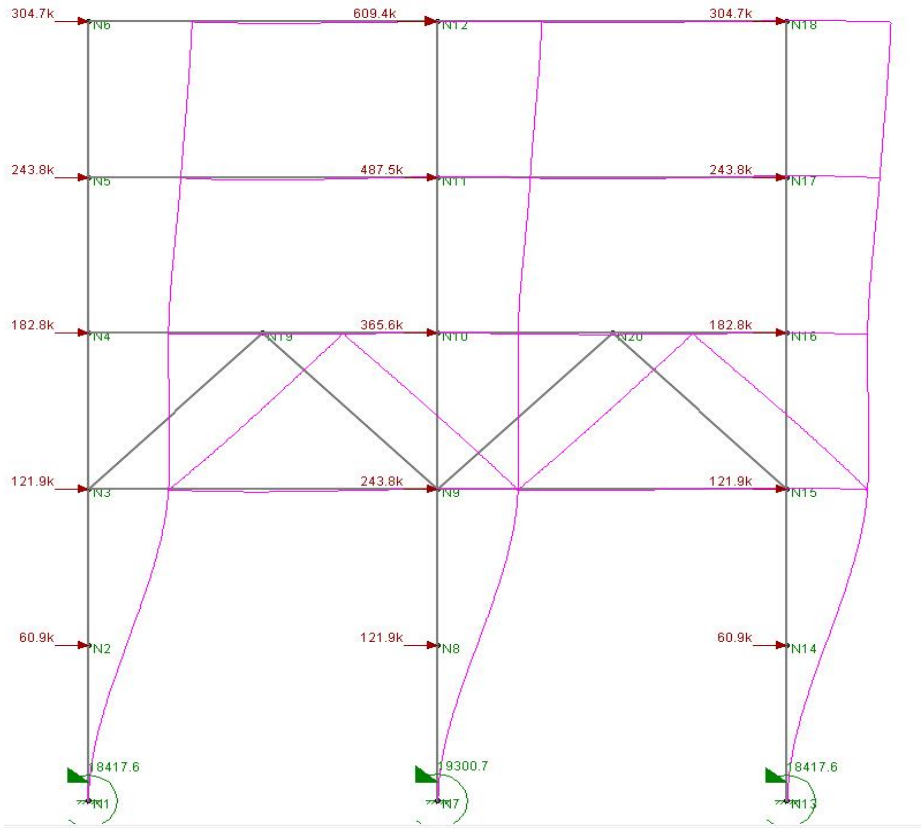

Site Coefficients

T_1	16	s	Long period transition period
S_s	1.30	g	0.2 s spectral response
S_1	0.70	g	1 s spectral respnse
F_a	1		Short Period site coeffi Table 11.4-1
F_v	1.70		Long Period Site Coeffi Table 11.4-2

S_MS	=B6*B4	g	Risk Targeted	(11.4-1)
S_M1	=B7*B5	g	Maximum Considered	(11.4-2)

C_s

=B9/(J7/J3)	min
=B10/(J13*J7/J3)	
=0.044*J3	max
0.01	
=0.5*B5/(J7/J3)	

Sec. 12.8.1.1

C_s =MAX(MIN(B16:B17),B18:B20)

V =B22*P4 kip

Structure Coefficients

I_e	1.50		Importance Factor	
h_n	75	ft	structural height	
C_t	0.02		period parameters, Table 12.8-2	
x	0.75			
R	2		reduction factor	
C_u	1.40		Upper Limit on Calculated Period Coeffient	Table 12.8-1
T_a	=J5*J4^J6	s	Approximate fundamental Period	(12.8-7)
T	=J12*J8	s	maximum fundamental period	Sec. 12.8.2

W_1floor	=60*150*10/12*150/1000	kip
W	=5*P3	kip
Num Frames	4	
Open Column Height	30	ft
Lat load/frame	=B25/P6	kip

Equal stiffnesses

Vertical Distribution of Forces

w_x	h_x	w_x*h_x	C_vx	Fx	outside col	inside col
=$P$3	75	=O17*P17	=Q17/$Q$23	=R17*$P$12	=$S17*0.25	=$S17*0.5
=$P$3	60	=O18*P18	=Q18/$Q$23	=R18*$P$12	=$S18*0.25	=$S18*0.5
=$P$3	45	=O19*P19	=Q19/$Q$23	=R19*$P$12	=$S19*0.25	=$S19*0.5
=$P$3	30	=O20*P20	=Q20/$Q$23	=R20*$P$12	=$S20*0.25	=$S20*0.5
=$P$3	15	=O21*P21	=Q21/$Q$23	=R21*$P$12	=$S21*0.25	=$S21*0.5
=$P$3	0	=O22*P22	=Q22/$Q$23	=R22*$P$12	=$S22*0.25	=$S22*0.5
	sum	=SUM(Q17:Q22)	=SUM(R17:R22)	=SUM(S17:S21)		=SUM(U17:U22)

				itterate to NA																	
Diam	R_O	t	Ri	c	c outer	b inner	b outer	alpha inner	alpha outer	Ac Inner	Ac Outer	Ac Steel comp	Ac steel tens	d_ci	d_co	d_steel comp	d_steel tens	Fy	0.95*f'c	axial	Moment
18.00	9.00	0.38	8.63	6.43	6.81	16.68	17.46	1.31	1.32	79.44	88.16	8.72	12.04	4.87	5.03	6.47	-4.68	52.00	5.70	-280.00	672.80
18.00	9.00	0.50	8.50	6.67	7.17	16.60	17.63	1.35	1.37	82.69	94.59	11.90	15.58	4.61	4.82	6.29	-4.81	52.00	5.70	-280.00	830.28
18.00	9.00	0.63	8.38	6.83	7.46	16.46	17.73	1.39	1.40	84.49	99.61	15.12	19.00	4.40	4.67	6.14	-4.89	52.00	5.70	-280.00	981.62
18.00	9.00	0.75	8.25	6.93	7.68	16.29	17.81	1.41	1.42	85.29	103.63	18.34	22.30	4.22	4.54	6.02	-4.95	52.00	5.70	-280.00	1127.43
18.00	9.00	0.88	8.13	6.99	7.87	16.09	17.86	1.43	1.44	85.37	106.92	21.55	25.52	4.07	4.44	5.91	-4.99	52.00	5.70	-280.00	1268.11
18.00	9.00	1.00	8.00	7.02	8.02	15.88	17.89	1.45	1.46	84.91	109.65	24.74	28.67	3.93	4.35	5.81	-5.01	52.00	5.70	-280.00	1403.96
18.00	9.00	1.13	7.88	7.03	8.15	15.66	17.92	1.46	1.48	84.06	111.97	27.91	31.74	3.81	4.28	5.72	-5.03	52.00	5.70	-280.00	1535.19
24.00	12.00	0.38	11.63	7.18	7.55	21.48	22.29	1.18	1.19	111.49	121.99	10.50	17.33	7.41	7.57	9.24	-5.59	52.00	5.70	-280.00	1232.82
24.00	12.00	0.50	11.50	7.65	8.15	21.67	22.73	1.23	1.24	120.78	135.31	14.53	22.38	7.02	7.23	8.98	-5.83	52.00	5.70	-280.00	1533.29
24.00	12.00	0.63	11.38	7.99	8.62	21.72	23.03	1.27	1.28	127.42	146.07	18.66	27.24	6.70	6.96	8.76	-6.00	52.00	5.70	-280.00	1822.39
24.00	12.00	0.75	11.25	8.25	9.00	21.69	23.24	1.30	1.32	132.14	154.98	22.84	31.94	6.43	6.75	8.58	-6.13	52.00	5.70	-280.00	2101.66
24.00	12.00	0.88	11.13	8.45	9.32	21.60	23.39	1.33	1.35	135.41	162.46	27.05	36.51	6.20	6.57	8.42	-6.24	52.00	5.70	-280.00	2372.17
24.00	12.00	1.00	11.00	8.59	9.59	21.47	23.51	1.35	1.37	137.57	168.85	31.28	40.98	5.99	6.42	8.27	-6.32	52.00	5.70	-280.00	2634.67
24.00	12.00	1.13	10.88	8.70	9.83	21.31	23.60	1.37	1.39	138.84	174.35	35.51	45.34	5.81	6.29	8.15	-6.38	52.00	5.70	-280.00	2889.70
30.00	15.00	0.50	14.50	8.51	9.01	26.41	27.50	1.15	1.16	161.65	178.65	17.00	29.34	9.50	9.71	11.70	-6.78	52.00	5.70	-280.00	2452.49
30.00	15.00	0.63	14.38	9.02	9.64	26.68	28.02	1.19	1.21	174.20	196.19	21.98	35.69	9.08	9.35	11.42	-7.04	52.00	5.70	-280.00	2927.94
30.00	15.00	0.75	14.25	9.42	10.17	26.81	28.40	1.22	1.24	183.92	210.99	27.07	41.85	8.73	9.05	11.19	-7.24	52.00	5.70	-280.00	3387.85
30.00	15.00	0.88	14.13	9.74	10.61	26.85	28.69	1.25	1.27	191.45	223.68	32.23	47.83	8.43	8.80	10.98	-7.40	52.00	5.70	-280.00	3834.18
30.00	15.00	1.00	14.00	9.99	10.99	26.83	28.91	1.28	1.30	197.25	234.68	37.43	53.67	8.16	8.58	10.80	-7.53	52.00	5.70	-280.00	4268.32
30.00	15.00	1.13	13.88	10.20	11.33	26.76	29.09	1.30	1.32	201.64	244.31	42.67	59.39	7.92	8.39	10.64	-7.64	52.00	5.70	-280.00	4691.29
36.00	18.00	0.63	17.38	9.94	10.57	31.41	32.79	1.13	1.15	224.06	249.20	25.14	44.32	11.53	11.79	14.12	-8.01	52.00	5.70	-280.00	4302.54
36.00	18.00	0.75	17.25	10.47	11.22	31.72	33.35	1.17	1.18	239.63	270.72	31.09	51.97	11.10	11.42	13.84	-8.28	52.00	5.70	-280.00	4991.66
36.00	18.00	0.88	17.13	10.90	11.78	31.91	33.78	1.20	1.22	252.28	289.42	37.14	59.41	10.73	11.10	13.59	-8.50	52.00	5.70	-280.00	5661.24
36.00	18.00	1.00	17.00	11.26	12.26	32.00	34.12	1.23	1.25	262.56	305.84	43.28	66.68	10.40	10.82	13.37	-8.68	52.00	5.70	-280.00	6313.46
36.00	18.00	1.13	16.88	11.56	12.68	32.03	34.39	1.25	1.27	270.90	320.38	49.47	73.78	10.11	10.58	13.17	-8.83	52.00	5.70	-280.00	6949.97
42.00	21.00	0.63	20.38	10.79	11.41	35.96	37.37	1.08	1.10	276.43	304.59	28.16	53.08	14.02	14.28	16.84	-8.93	52.00	5.70	-280.00	5949.51

42.00	21.00	0.75	20.25	11.43	12.18	36.46	38.12	1.12	1.14	298.55	333.48	34.93	62.27	13.52	13.84	16.52	-9.26	52.00	5.70	-280.00	6917.47
42.00	21.00	0.88	20.13	11.97	12.84	36.79	38.70	1.15	1.17	317.02	358.86	41.84	71.21	13.09	13.46	16.24	-9.54	52.00	5.70	-280.00	7858.87
42.00	21.00	1.00	20.00	12.42	13.42	37.01	39.17	1.18	1.20	332.50	381.37	48.87	79.93	12.71	13.13	15.98	-9.77	52.00	5.70	-280.00	8776.80
42.00	21.00	1.13	19.88	12.80	13.93	37.15	39.55	1.21	1.23	345.50	401.49	55.99	88.48	12.37	12.84	15.75	-9.97	52.00	5.70	-280.00	9673.63
48.00	24.00	0.75	23.25	12.32	13.07	41.04	42.73	1.08	1.10	360.18	398.80	38.62	72.71	15.99	16.30	19.22	-10.21	52.00	5.70	-280.00	9168.81
48.00	24.00	0.88	23.13	12.95	13.82	41.53	43.47	1.12	1.13	385.07	431.43	46.36	83.18	15.50	15.87	18.91	-10.54	52.00	5.70	-280.00	10431.52
48.00	24.00	1.00	23.00	13.49	14.49	41.88	44.07	1.14	1.16	406.35	460.60	54.25	93.41	15.07	15.49	18.62	-10.82	52.00	5.70	-280.00	11663.76
48.00	24.00	1.13	22.88	13.96	15.08	42.13	44.56	1.17	1.19	424.61	486.87	62.26	103.41	14.68	15.15	18.36	-11.06	52.00	5.70	-280.00	12868.68
54.00	27.00	0.88	26.13	13.87	14.74	46.14	48.11	1.08	1.10	455.95	506.67	50.72	95.31	17.95	18.32	21.60	-11.49	52.00	5.70	-280.00	13382.88
54.00	27.00	1.00	26.00	14.49	15.49	46.63	48.85	1.11	1.13	483.56	543.01	59.44	107.06	17.47	17.89	21.29	-11.82	52.00	5.70	-280.00	14978.82
54.00	27.00	1.13	25.88	15.04	16.16	46.99	49.46	1.14	1.16	507.62	575.93	68.31	118.57	17.03	17.50	21.00	-12.10	52.00	5.70	-280.00	16540.45
60.00	30.00	1.00	29.00	15.43	16.43	51.26	53.51	1.08	1.10	563.71	628.18	64.47	120.88	19.91	20.33	23.97	-12.79	52.00	5.70	-280.00	18725.79
60.00	30.00	1.13	28.88	16.05	17.17	51.74	54.24	1.11	1.13	594.02	668.20	74.18	133.91	19.43	19.90	23.66	-13.11	52.00	5.70	-280.00	20693.45
36.00	18.00	1.25	16.75	11.81	13.06	32.01	34.62	1.27	1.29	277.63	333.34	55.71	80.76	9.84	10.37	12.99	-8.96	52.00	5.70	-280.00	7572.03
36.00	18.00	1.50	16.50	20.80	22.30	31.86	34.96	1.31	1.33	287.24	355.48	68.24	94.34	9.38	10.01	12.68	-9.17	52.00	5.70	-280.00	8776.60

Moment Capacity of CFST Column (k-ft). Strain Compatibility Method

			Diameters (in)							
			18	24	30	36	42	48	54	60
Thickness (in)	1	0.125	280.5	519.2	801.2	1157.7	1583.6	2078.0	2641.2	3273.5
	2	0.25	520.2	967.4	1526.2	2244.0	3118.4	4153.8	5200.5	6410.0
	3	0.375	741.0	1376.0	2197.7	3265.0	4460.8	5900.2	7573.4	9481.2
	4	0.5	938.6	1756.5	2829.7	4161.2	5787.8	7739.4	9809.0	12209.5
	5	0.625	1128.7	2115.4	3430.6	5055.1	7058.0	9321.6	12015.3	15115.9
	6	0.75	1306.8	2456.9	4006.0	5928.1	8216.9	11007.9	14044.1	17581.8
	7	0.875	1475.0	2783.7	4524.6	6722.1	9413.6	12479.4	16133.8	20153.9
	8	1	1641.2	3097.7	5045.9	7508.9	10484.0	14051.8	18009.1	22637.4
	9	1.125	1793.9	3400.6	5554.5	8291.9	11586.5	15442.8	20007.4	24969.4

Moment Capacity of CFST Column (k-ft). Distributed Plasticity Method

			Diameters (in)							
			18	24	30	36	42	48	54	60
Thickness (in)	1	0.125								
	2	0.25								
	3	0.375	672.8	1232.8						
	4	0.5	830.3	1533.3	2452.5					
	5	0.625	981.6	1822.4	2927.9	4302.5	5949.5			
	6	0.75	1127.4	2101.7	3387.9	4991.7	6917.5	9168.8		
	7	0.875	1268.1	2372.2	3834.2	5661.2	**7858.9**	**10431.5**	13382.9	
	8	1	1404.0	2634.7	4268.3	6313.5	8776.8	11663.8	14978.8	18725.8
	9	1.125	1535.2	2889.7	4691.3	6950.0	9673.6	12868.7	16540.4	20693.5
	10	1.25				**7572.0**				
	12	1.5				8776.6				

Moment Capacity of CFST Column

			Diameters (in)							
			18	24	30	36	42	48	54	60
Thickness (in)	1	0.125								
	2	0.25								
	3	0.375	0.9079	0.8960						
	4	0.5	0.8846	0.8729	0.8667					
	5	0.625	0.8697	0.8615	0.8535	0.8511	0.8429			
	6	0.75	0.8627	0.8554	0.8457	0.8420	0.8419	0.8329		
	7	0.875	0.8597	0.8522	0.8474	0.8422	0.8348	0.8359	0.8295	0.0000
	8	1	0.8554	0.8505	0.8459	0.8408	0.8372	0.8301	0.8317	0.8272
	9	1.125	0.8558	0.8498	0.8446	0.8382	0.8349	0.8333	0.8267	0.8288

Moment Demand (k-ft)

		Number of Frames		
		2	3	4
R	1	29000	19300	14500
	2	14500	9650	**7250**

Appendix B

CONSTRUCTION DRAWINGS FOR CFST SPECIMEN

This appendix provides the construction drawings used in the construction of the CFST specimen in the UW lab in Seattle, Washington.

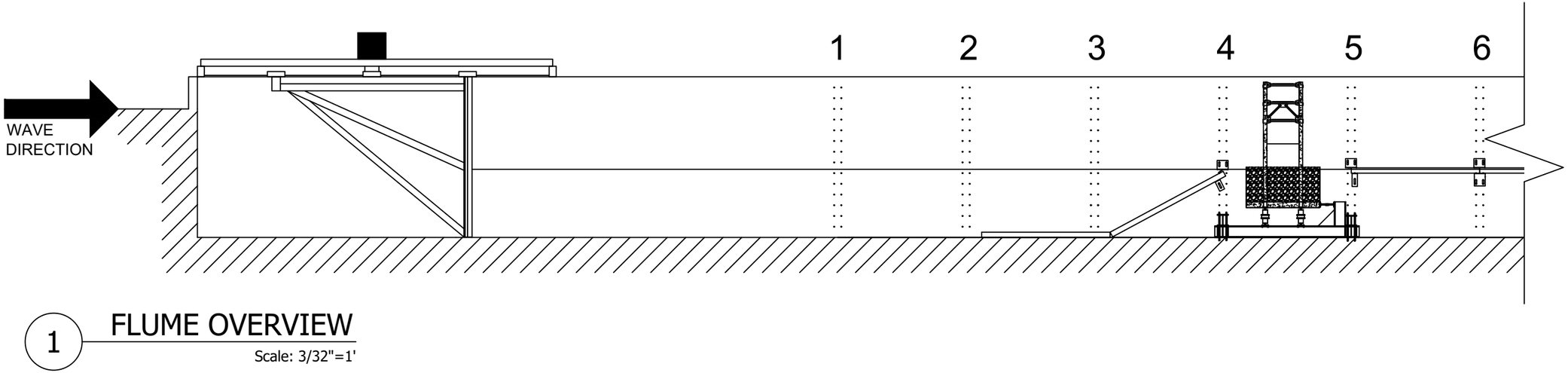

1 FLUME OVERVIEW

Scale: 3/32"=1'

2 TUBE STRUCTURE PLAN

Scale: 1/2" = 1'

CONTENTS	
S100	OVERVIEW
S101	TRUSS ELEVATIONS
S102	STREAMWISE TRUSS
S103	TRANSVERSE TRUSS
S200	BEAM & BRACE DIMENSIONS
S210	COLUMN DIMENSIONS
S211	COLUMN DIMENSIONS
S300	PLATE DIMENSIONS
S301	PLATE DIMENSIONS
S302	PLATE DIMENSIONS
S400	INSTRUMENTATION
S401	SENSOR DETAILS
S402	NOMENCLATURE
S500	LOAD CELL VALIDATION AT UW

CIVIL & ENVIRONMENTAL ENGINEERING

General Notes

DEFINITIONS:
CFT: CONCRETE FILLED STEEL TUBE
STREAMWISE (STRMS): DIRECTION OF WAVE FLOW
TRANSVERSE (TRVS): PERPENDICULAR TO DIRECTION OF WAVE FLOW; OUT OF PLANE OF FLUME

No.	Revision/Issue	Date

VERTICAL EVACUATION STRUCTURES

OVERVIEW

Project

Date 06/25/19

Scale AS NOTED

Sheet S100

PRODUCED BY AN AUTODESK STUDENT VERSION

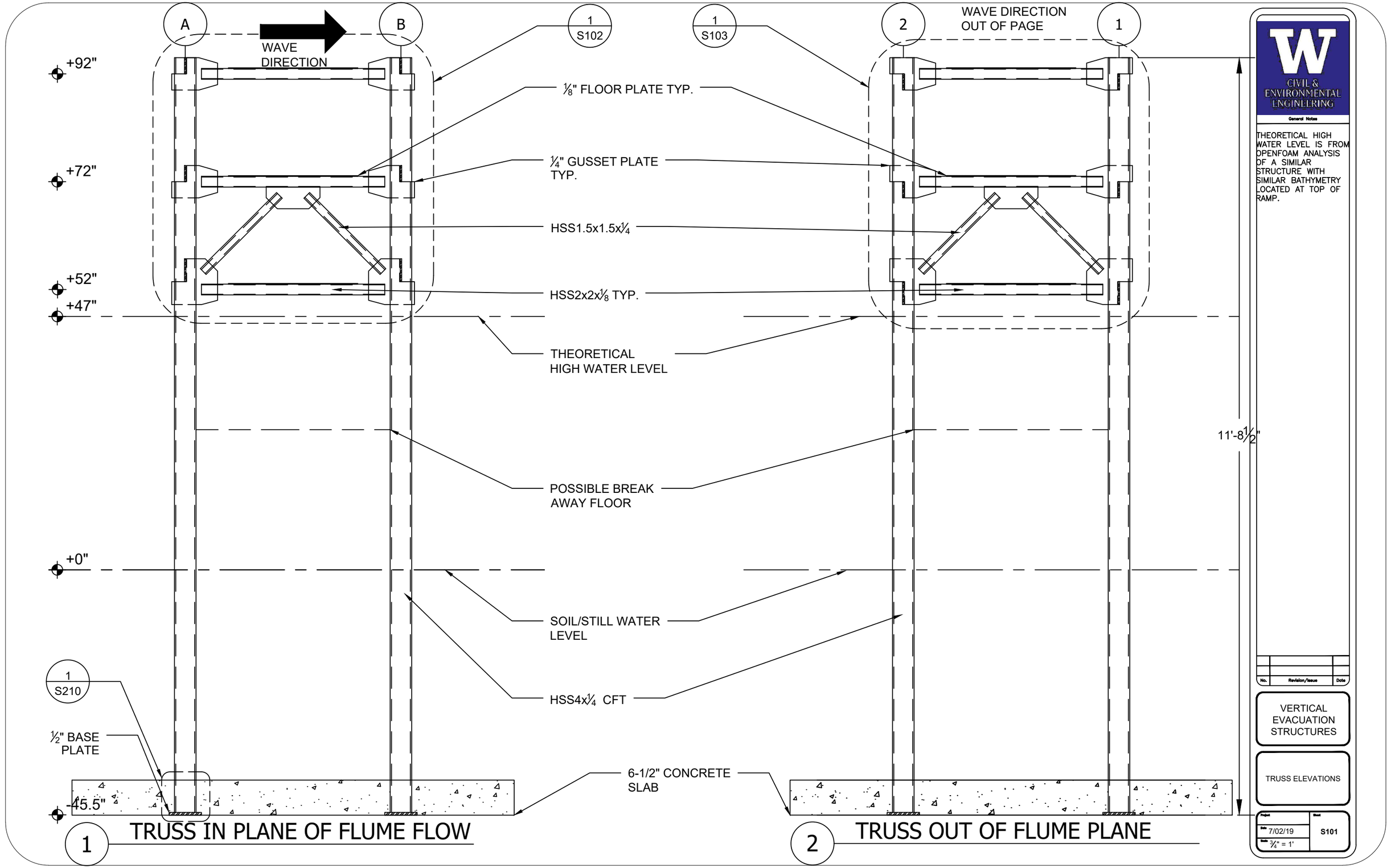

CIVIL & ENVIRONMENTAL ENGINEERING

General Notes

THEORETICAL HIGH WATER LEVEL IS FROM OPENFOAM ANALYSIS OF A SIMILAR STRUCTURE WITH SIMILAR BATHYMETRY LOCATED AT TOP OF RAMP.

No.	Revision/Issue	Date

VERTICAL EVACUATION STRUCTURES

TRUSS ELEVATIONS

Project

Date 7/02/19

Sheet S101

Scale ¾" = 1'

PRODUCED BY AN AUTODESK STUDENT VERSION

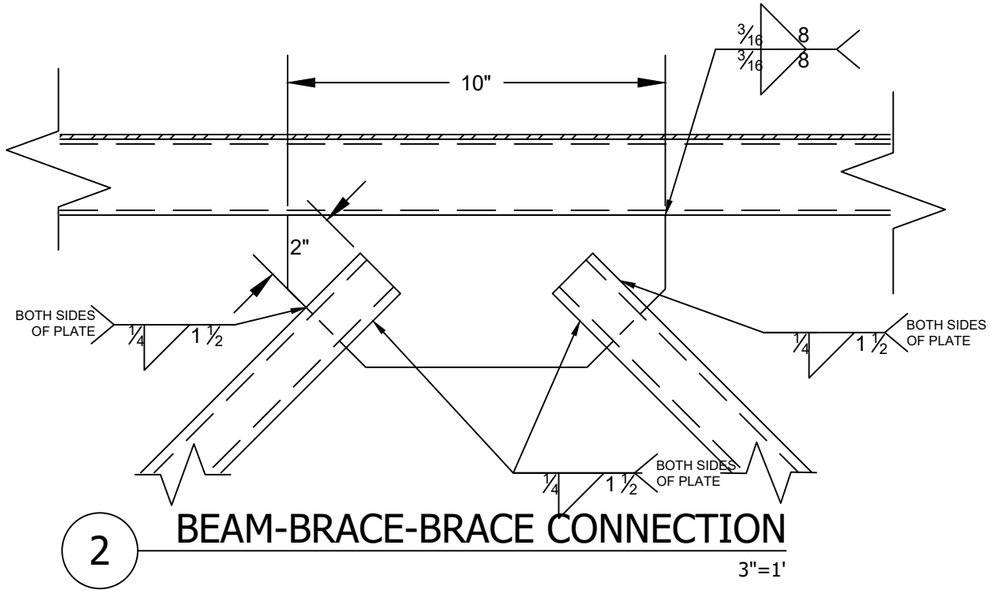

2 BEAM-BRACE-BRACE CONNECTION

3"=1'

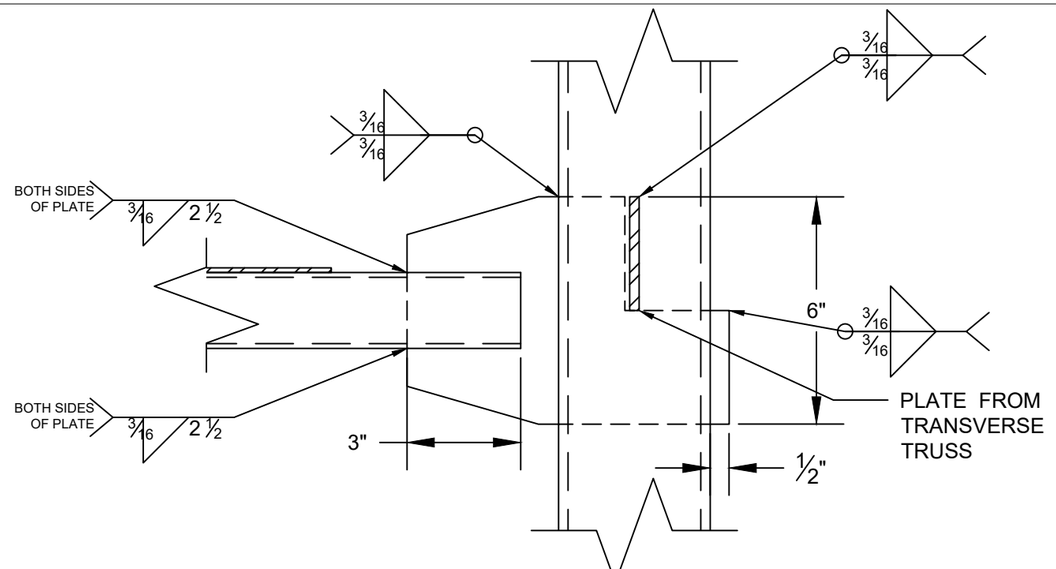

3 BEAM-COLUMN CONNECTION - STRWS

Scale: 3"=1'

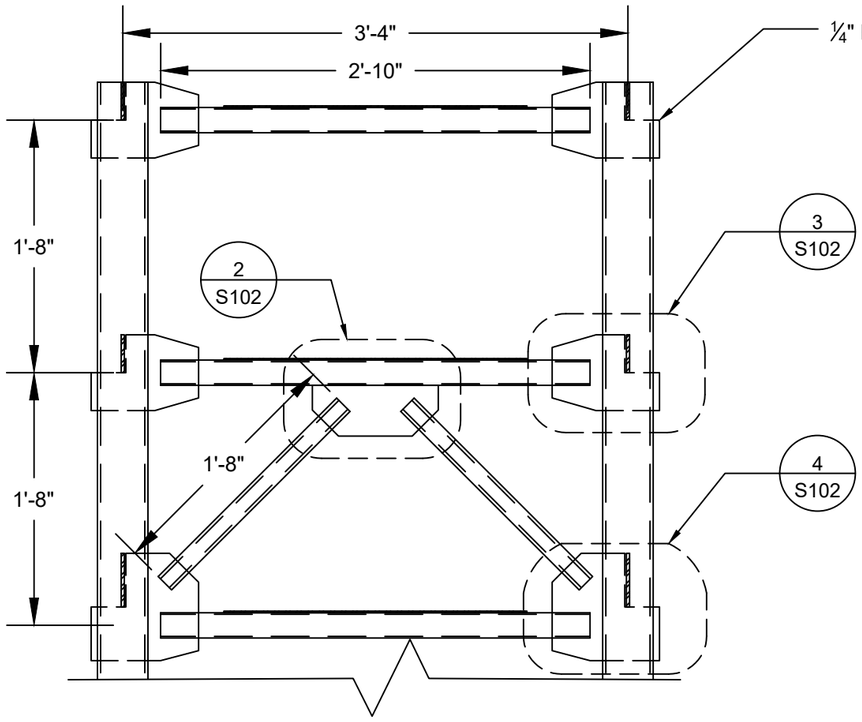

1 STREAMWISE TRUSS DETAIL

Scale: 1" = 1'

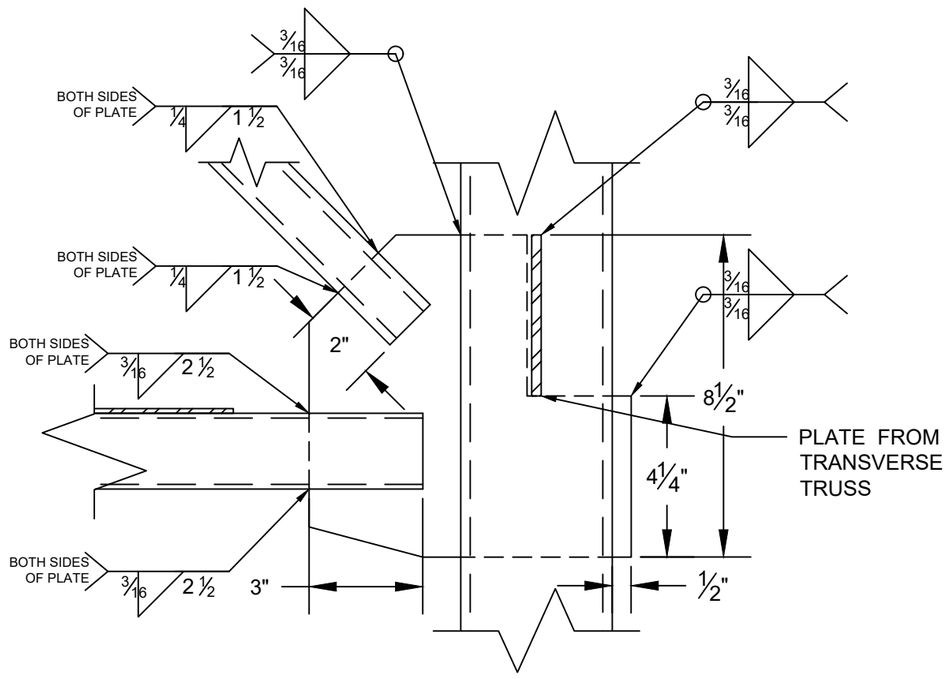

4 BEAM-BRACE-COLUMN CONNECTION - STRWS

Scale: 3"=1'

CIVIL & ENVIRONMENTAL ENGINEERING

General Notes

ALL WELDS ARE FILLET WELDS ON ALL REASONABLE JOINTS BETWEEN HSS MEMBERS AND GUSSET PLATES

No.	Revision/Issue	Date

VERTICAL EVACUATION STRUCTURES

STREAMWISE TRUSS

Project

Date 7/02/19

Scale AS NOTED

Sheet S102

PRODUCED BY AN AUTODESK STUDENT VERSION

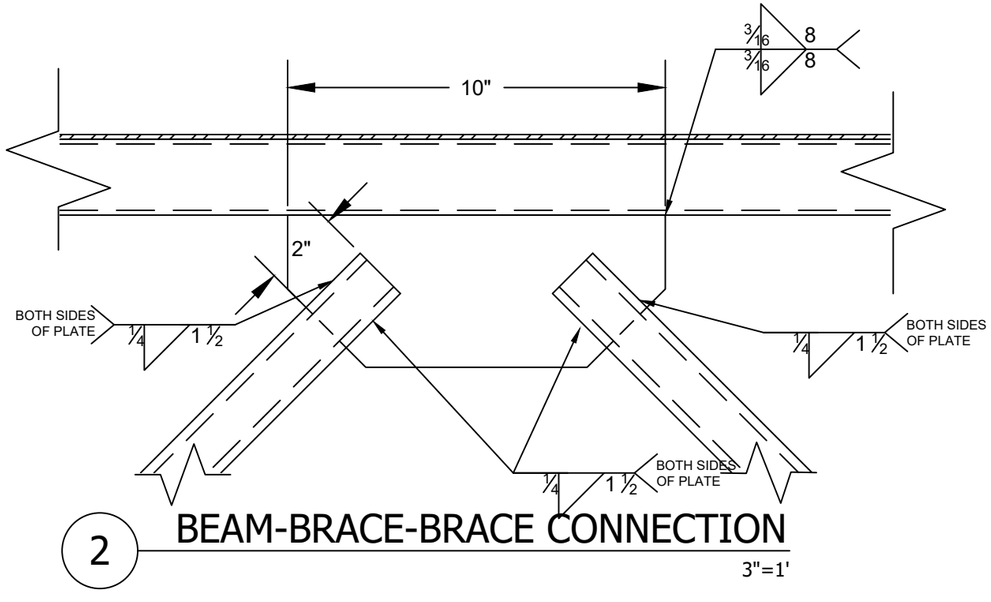

2 BEAM-BRACE-BRACE CONNECTION

3"=1'

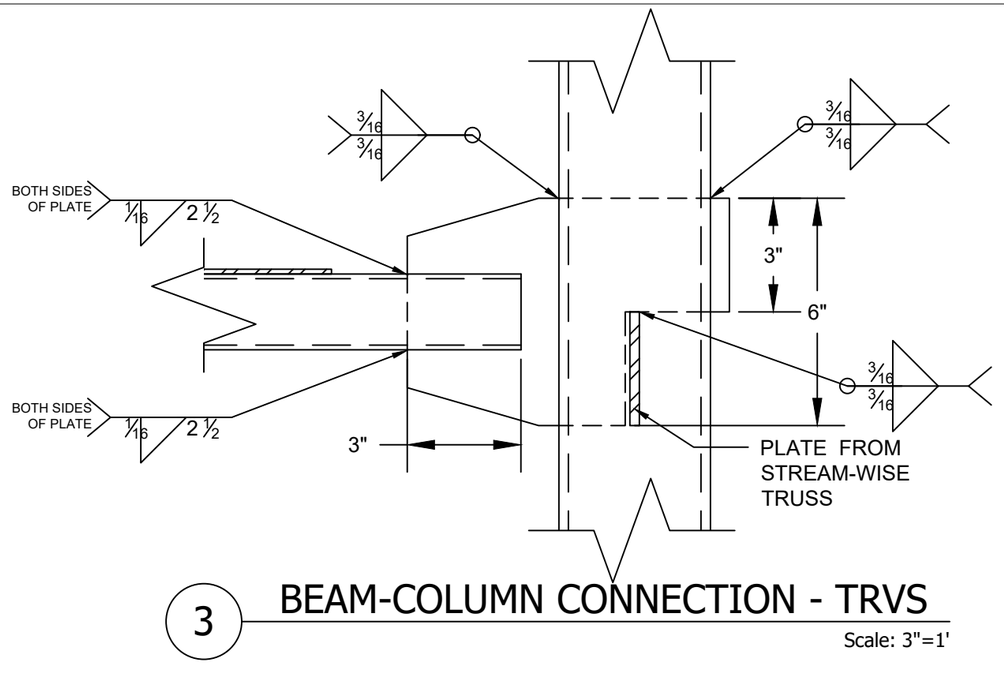

3 BEAM-COLUMN CONNECTION - TRVS

Scale: 3"=1'

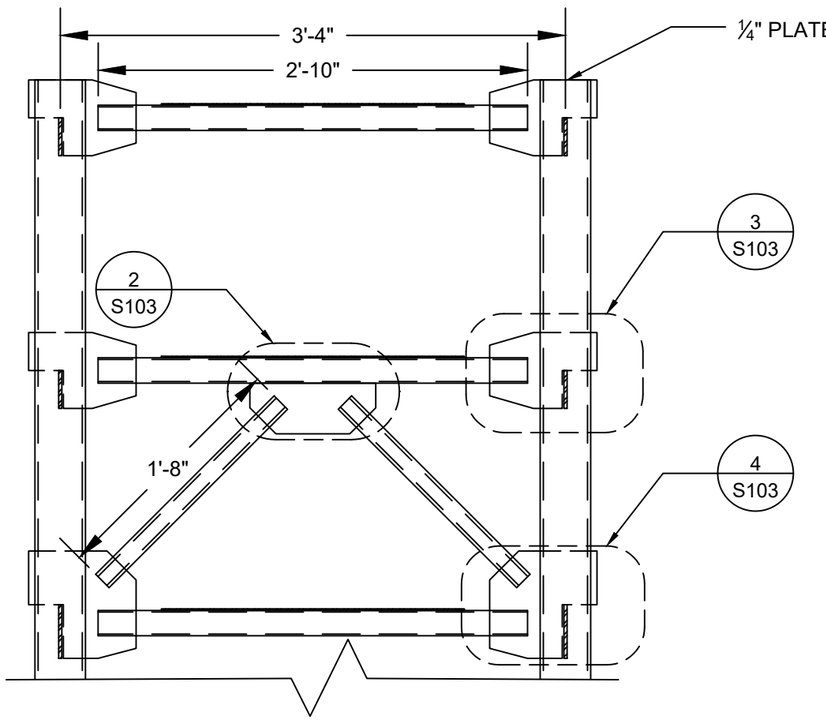

1 STREAMWISE TRUSS DETAIL

Scale: 1" = 1'

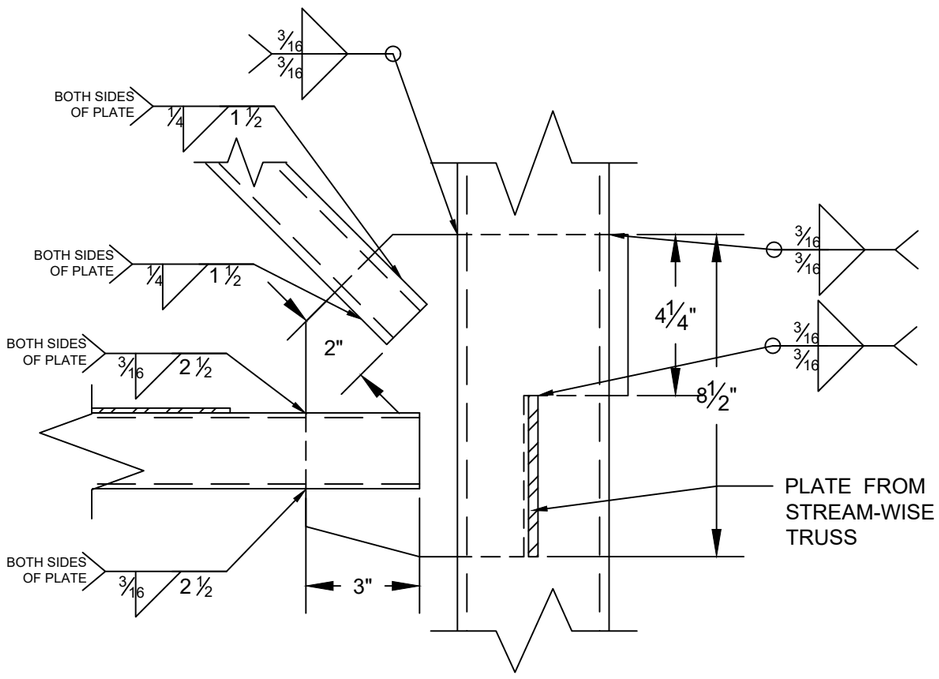

4 BEAM-BRACE-COLUMN CONNECTION - TRVS

Scale: 3"=1'

CIVIL & ENVIRONMENTAL ENGINEERING

General Notes

ALL WELDS ARE FILLET WELDS ON ALL REASONABLE JOINTS BETWEEN HSS MEMBERS AND GUSSET PLATES

No.	Revision/Issue	Date

VERTICAL EVACUATION STRUCTURES

TRANSVERSE TRUSS

Project

Date 7/02/19

Scale AS NOTED

Sheet S103

PRODUCED BY AN AUTODESK STUDENT VERSION

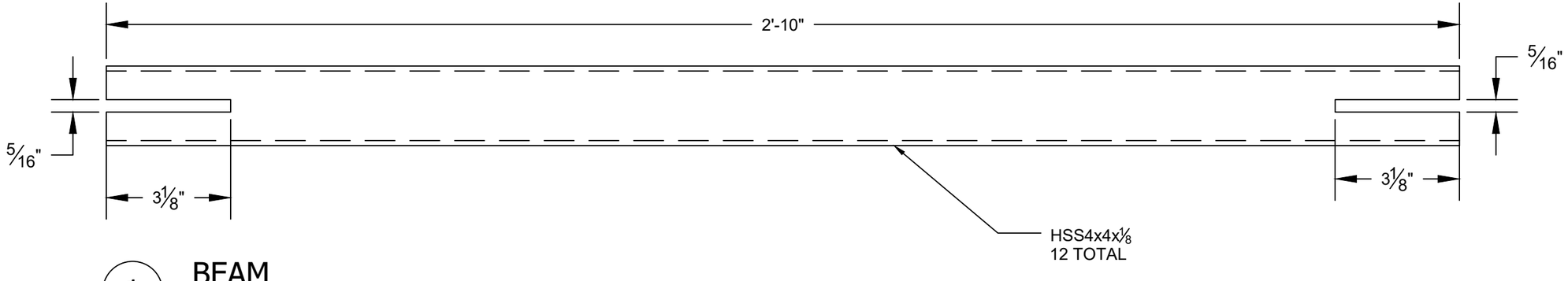

1 BEAM
Scale: 4"=1'

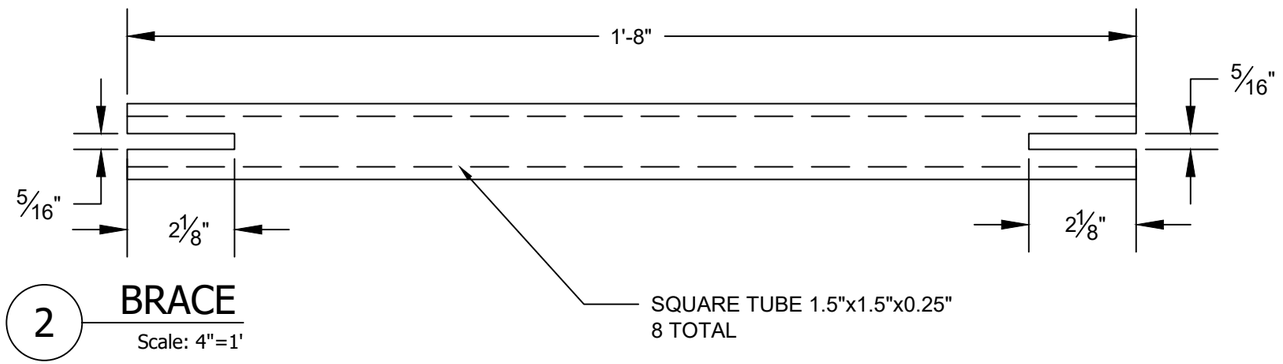

2 BRACE
Scale: 4"=1'

CIVIL & ENVIRONMENTAL ENGINEERING

General Notes

No.	Revision/Issue	Date

VERTICAL EVACUATION STRUCTURES

BEAM & BRACE DIMENSIONS

Project	Sheet
Date 6/24/19	S200
Scale AS NOTED	

PRODUCED BY AN AUTODESK STUDENT VERSION

PRODUCED BY AN AUTODESK STUDENT VERSION

PRODUCED BY AN AUTODESK STUDENT VERSION

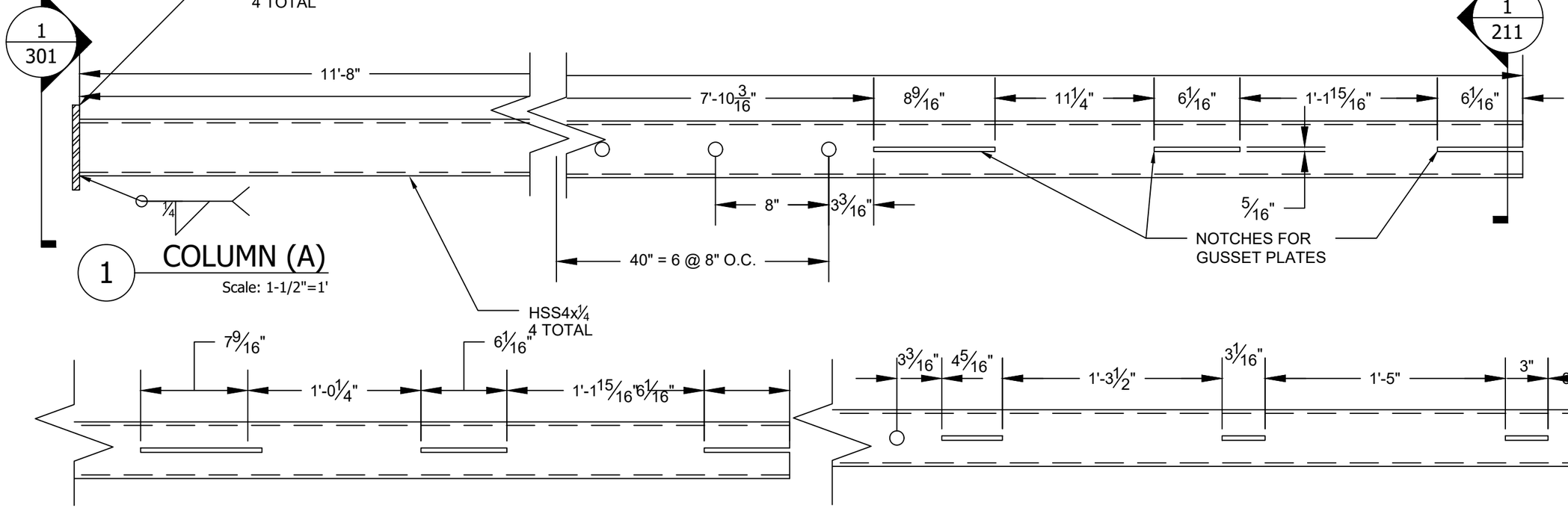

1 COLUMN (A)
Scale: 1-1/2"=1'

2 SIDE OF COLUMN (B)
Scale: 1-1/2"=1"

3 COLUMN BACK (C)
Scale: 1-1/2"=1"

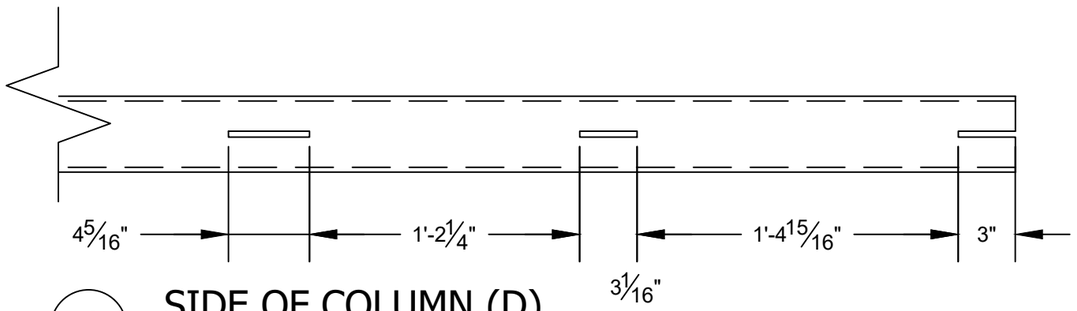

4 SIDE OF COLUMN (D)
Scale: 1-1/2"=1"

CIVIL & ENVIRONMENTAL ENGINEERING

General Notes

NOTE:
THE COLUMNS MUST BE LAID OUT CAREFULLY TO ACCOUNT FOR THE TRUSS ARRANGEMENT. TWO ADJACENT SIDES WILL HAVE LARGER SLOTS. THE OTHER TWO ADJACENT SIDES WILL HAVE THE SMALLER SLOTS, OFFSET TO CORRESPOND WITH THE CORRECT TRUSS. NOTCH LAYOUT DEFINED ON S211.

No.	Revision/Issue	Date

VERTICAL EVACUATION STRUCTURES

COLUMN DIMENSIONS

Project
Date 6/24/19
Scale AS NOTED
Sheet S210

PRODUCED BY AN AUTODESK STUDENT VERSION
PRODUCED BY AN AUTODESK STUDENT VERSION

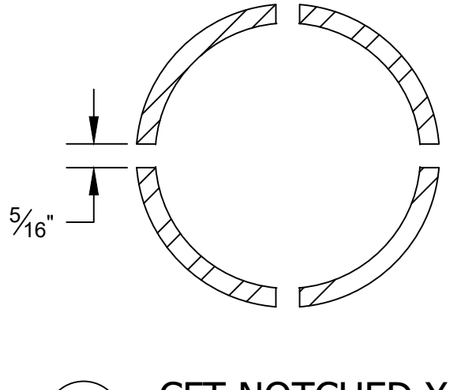

1 CFT NOTCHED X-SECTION, W/O GUSSET PLATES

Scale: 6"=1'

2 CFT NOTCHED X-SECTION, W/ GUSSET PLATES

Scale: 6"=1'

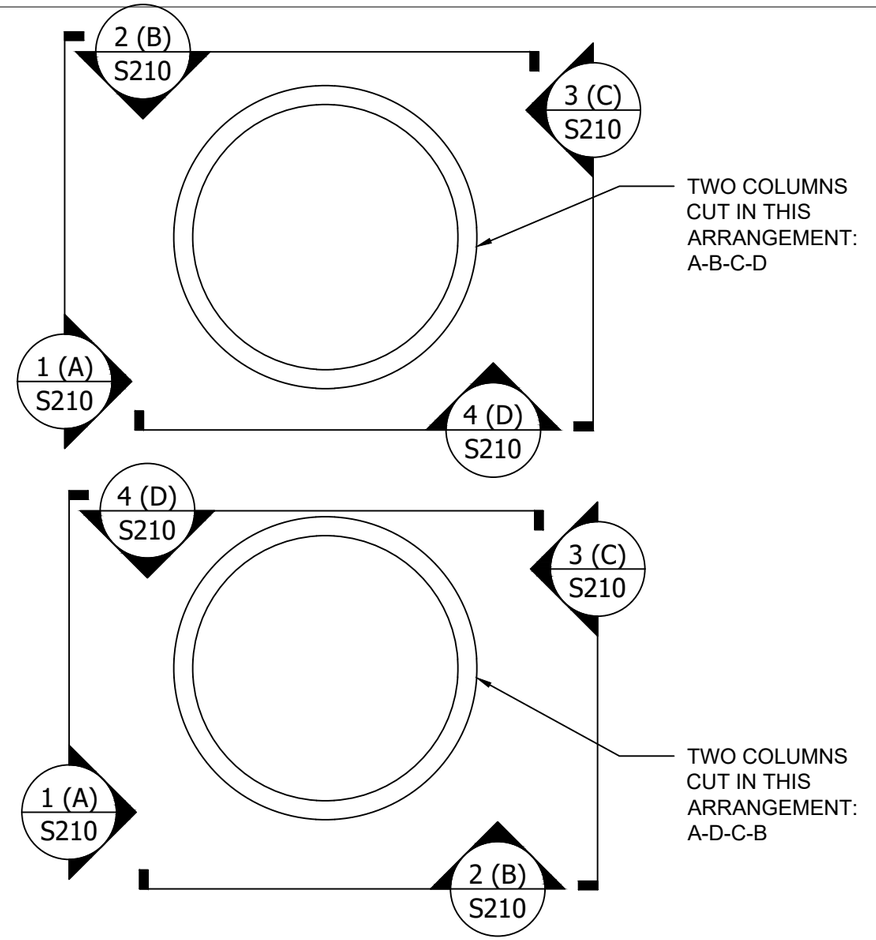

3 CFT NOTCH ARRANGEMENT

NOT TO SCALE

CIVIL & ENVIRONMENTAL ENGINEERING

General Notes

NOTE:
THE COLUMNS MUST BE NOTCHED TO CORRESPOND TO SYMMETRIC TRUSS LAYOUT.
2 COLUMNS: A-B-C-D.
2 COLUMNS: A-D-C-B.

No.	Revision/Issue	Date

VERTICAL EVACUATION STRUCTURES

COLUMN DIMENSIONS

Project	Sheet
Date 7/02/19	S211
Scale AS NOTED	

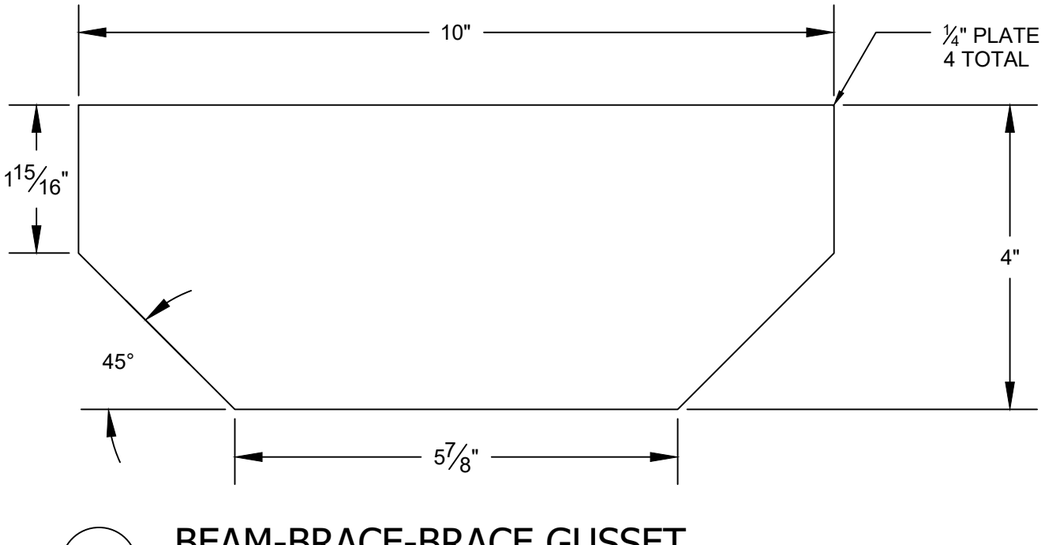

1 BEAM-BRACE-BRACE GUSSET

Scale: 6"=1'

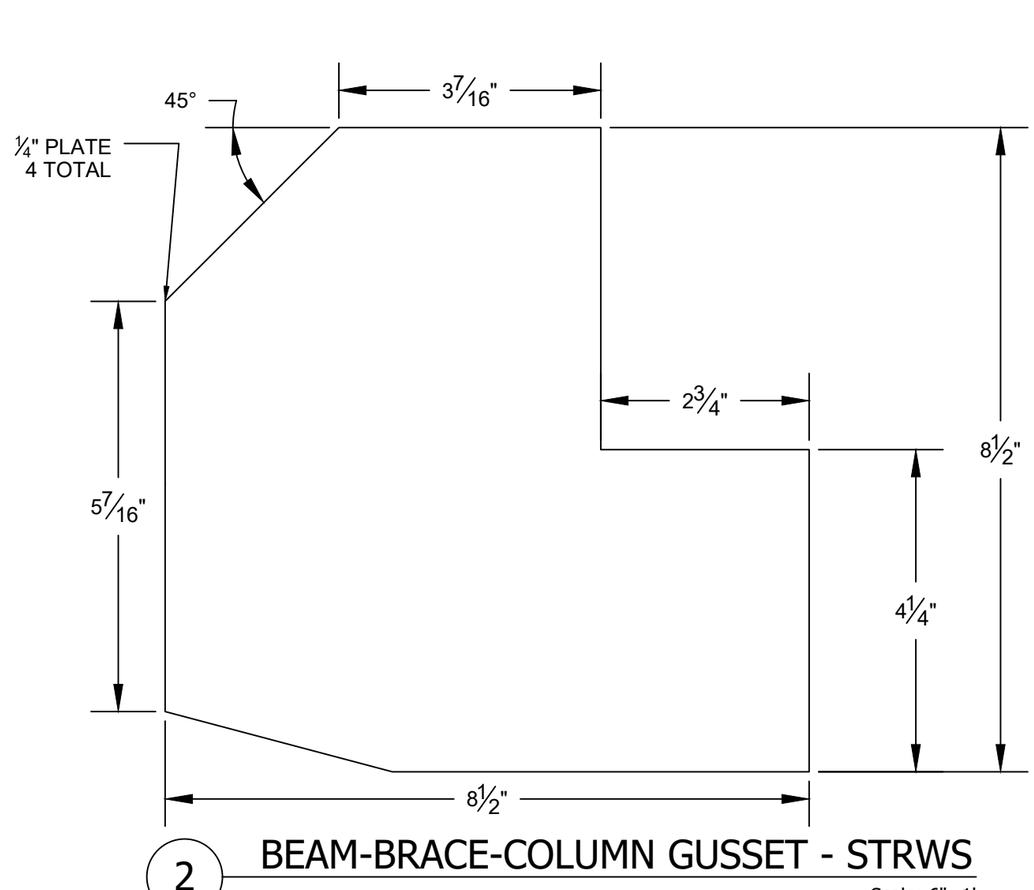

2 BEAM-BRACE-COLUMN GUSSET - STRWS

Scale: 6"=1'

CIVIL & ENVIRONMENTAL ENGINEERING

General Notes

No.	Revision/Issue	Date

VERTICAL EVACUATION STRUCTURES

PLATE DIMENSIONS

Project	Sheet
Date 7/03/19	S300
Scale 1:2	

PRODUCED BY AN AUTODESK STUDENT VERSION

PRODUCED BY AN AUTODESK STUDENT VERSION

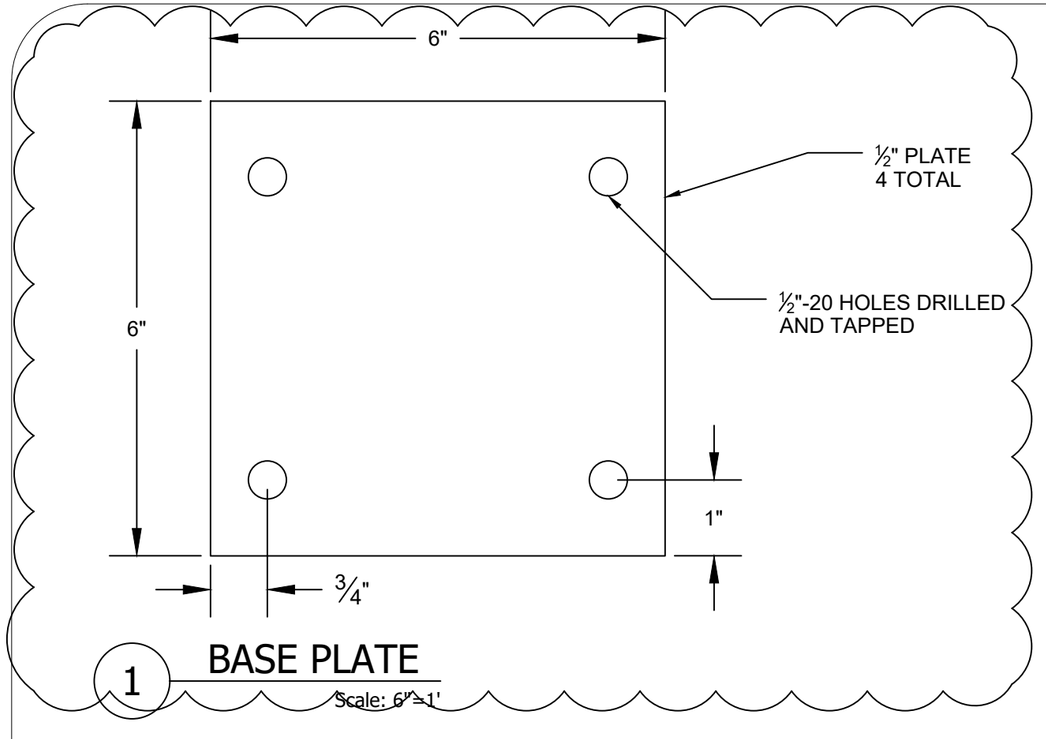

1 BASE PLATE
Scale: 6"=1'

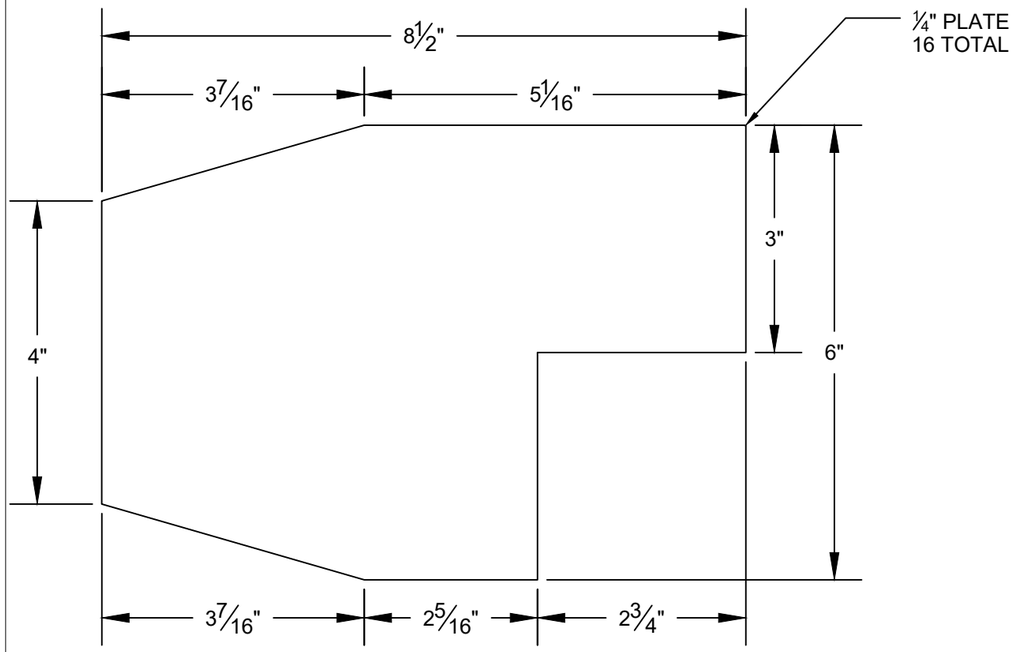

2 BEAM-COLUMN GUSSET
Scale: 6"=1'

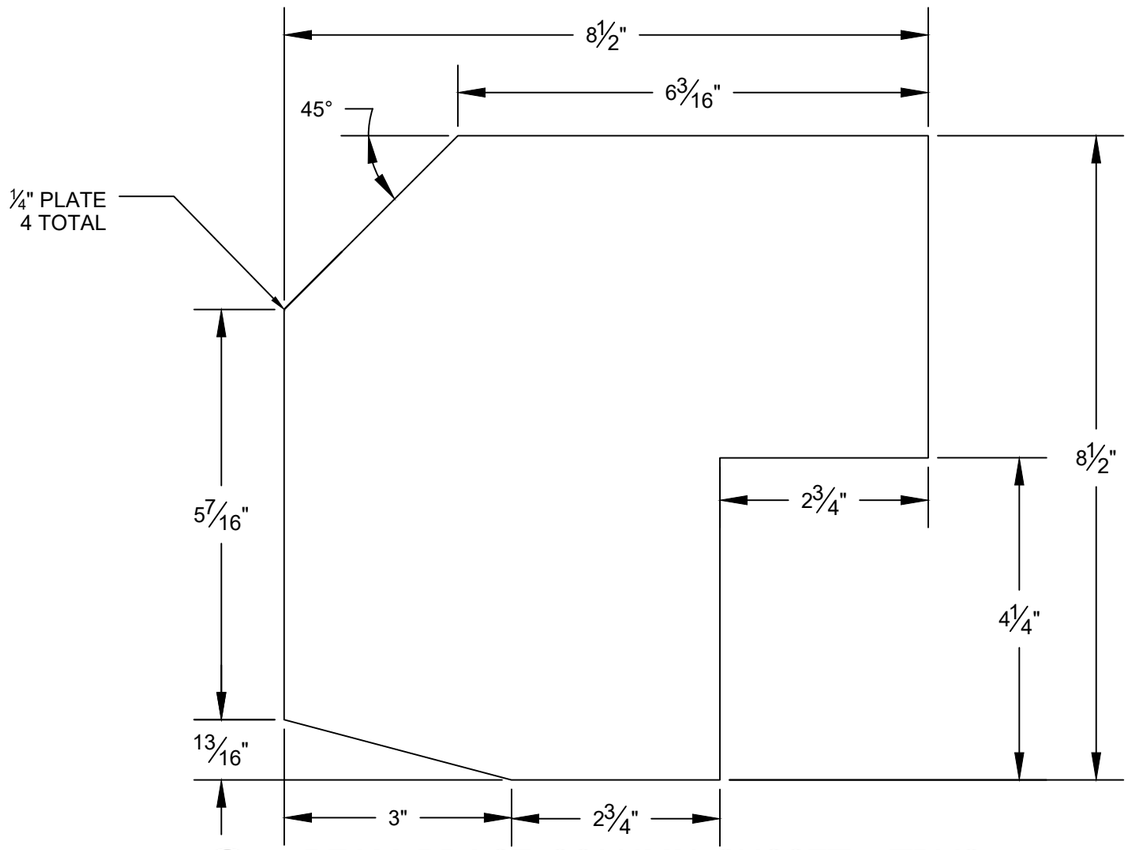

3 BEAM-BRACE-COLUMN GUSSET - TRVS
Scale: 6"=1'

CIVIL & ENVIRONMENTAL ENGINEERING

General Notes

No.	Revision/Issue	Date

VERTICAL EVACUATION STRUCTURES

PLATE DIMENSIONS

Project

Date 7/03/19

Scale 1:2

Sheet S301

PRODUCED BY AN AUTODESK STUDENT VERSION

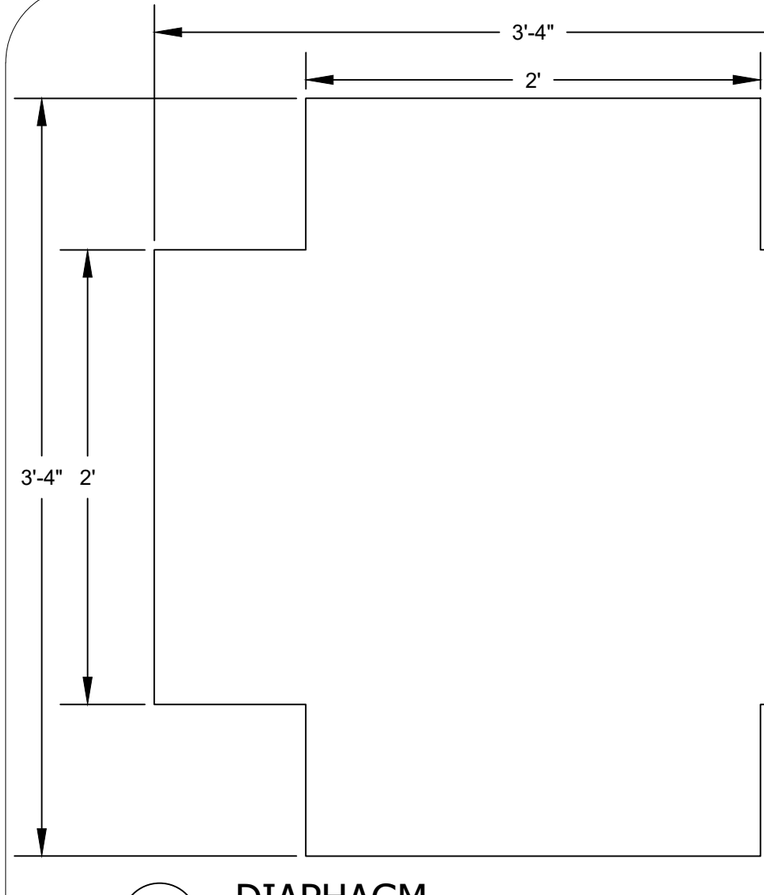

1 DIAPHAGM

Scale: 1-1/2"=1'

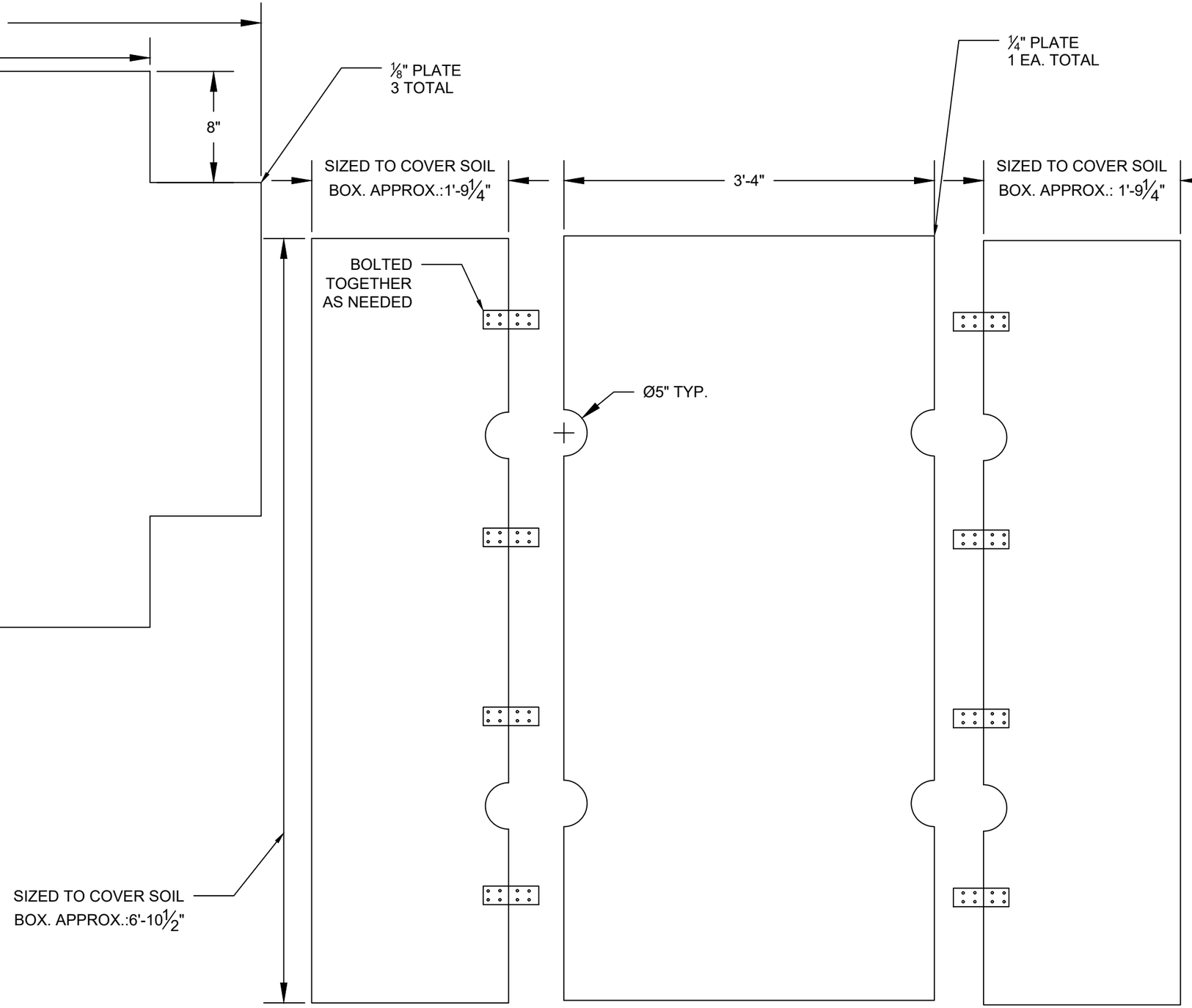

2 SOIL BOX COVER

Scale: 1"=1'

CIVIL & ENVIRONMENTAL ENGINEERING

General Notes

No.	Revision/Issue	Date

VERTICAL EVACUATION STRUCTURES

PLATE DIMENSIONS

Project	Sheet
Date 6/25/19	S302
Scale AS NOTED	

PRODUCED BY AN AUTODESK STUDENT VERSION

PRODUCED BY AN AUTODESK STUDENT VERSION

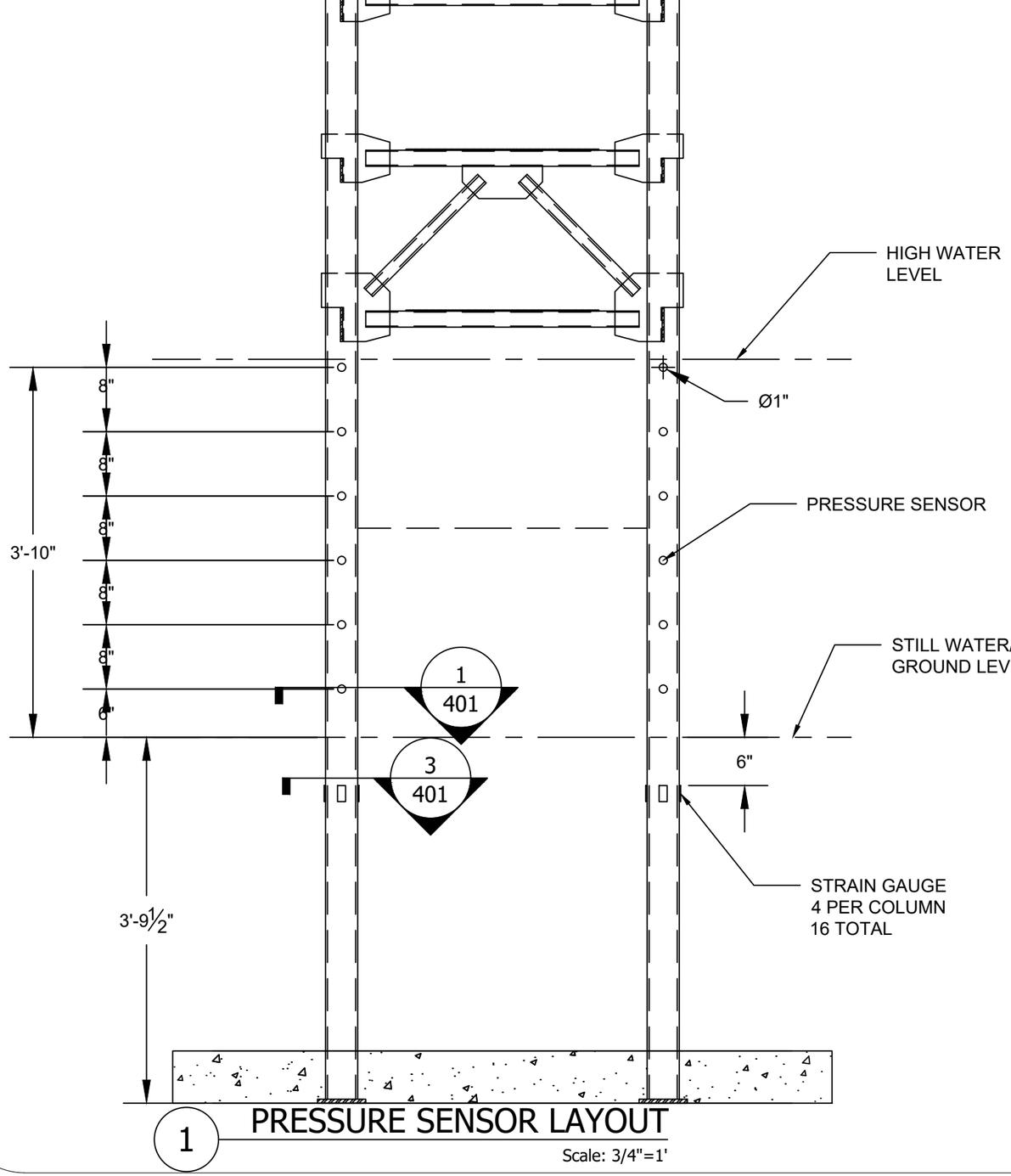

1 PRESSURE SENSOR LAYOUT

Scale: 3/4"=1'

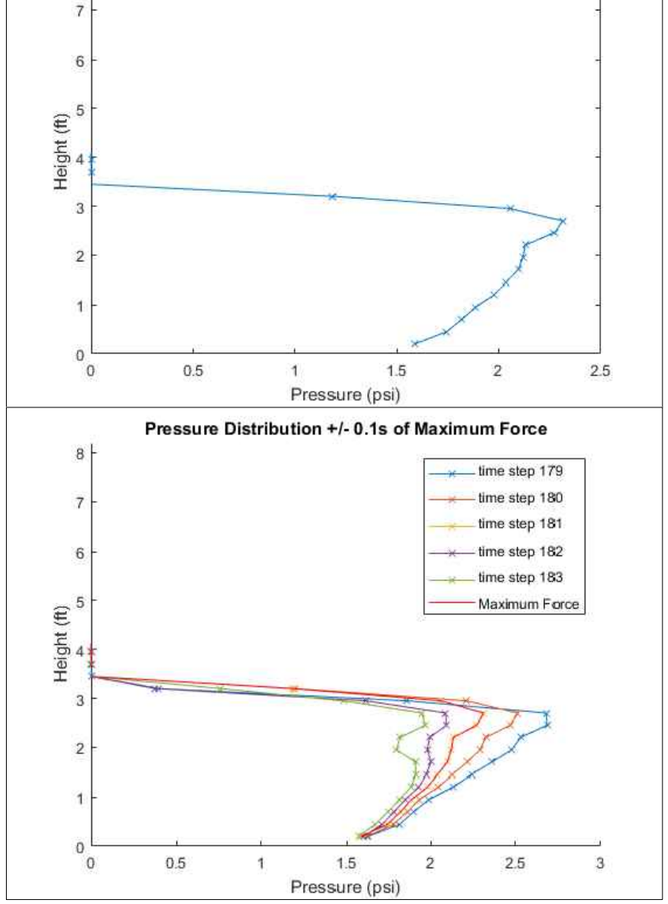

2 PRESSURE DISTRIBUTION OPENFOAM

CIVIL & ENVIRONMENTAL ENGINEERING

General Notes

SAME SENSOR LAYOUT FOR FRONT AND BACK TRUSS.
BACK TRUSS WILL SEE SUBSTANTIALLY LOWER PRESSURES AND INUNDATION DEPTHS.

No.	Revision/Issue	Date

VERTICAL EVACUATION STRUCTURES

INSTRUMENTATION LAYOUT

Project

Date 6/25/19

Scale AS NOTED

Sheet S400

PRODUCED BY AN AUTODESK STUDENT VERSION

PRODUCED BY AN AUTODESK STUDENT VERSION

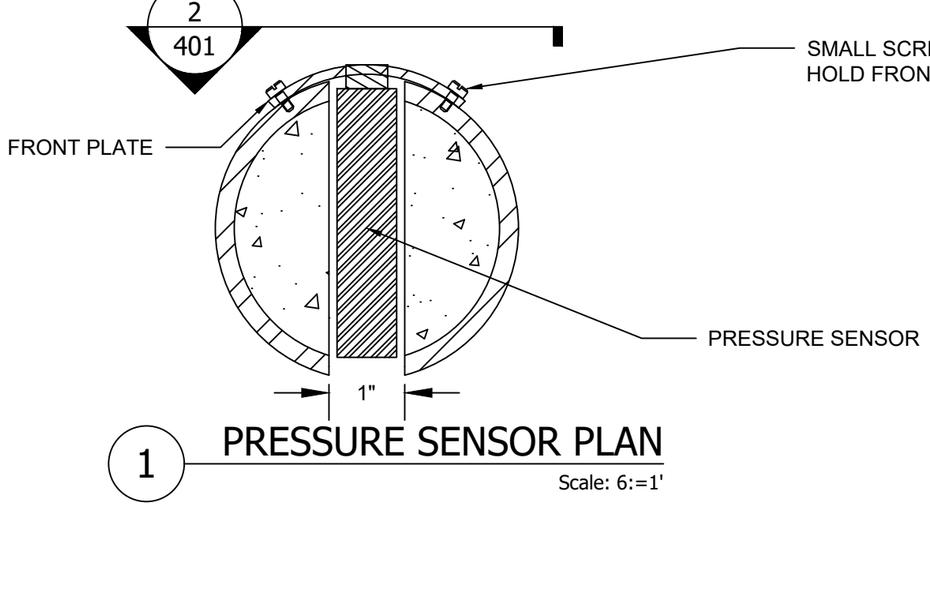

1 PRESSURE SENSOR PLAN

Scale: 6:=1'

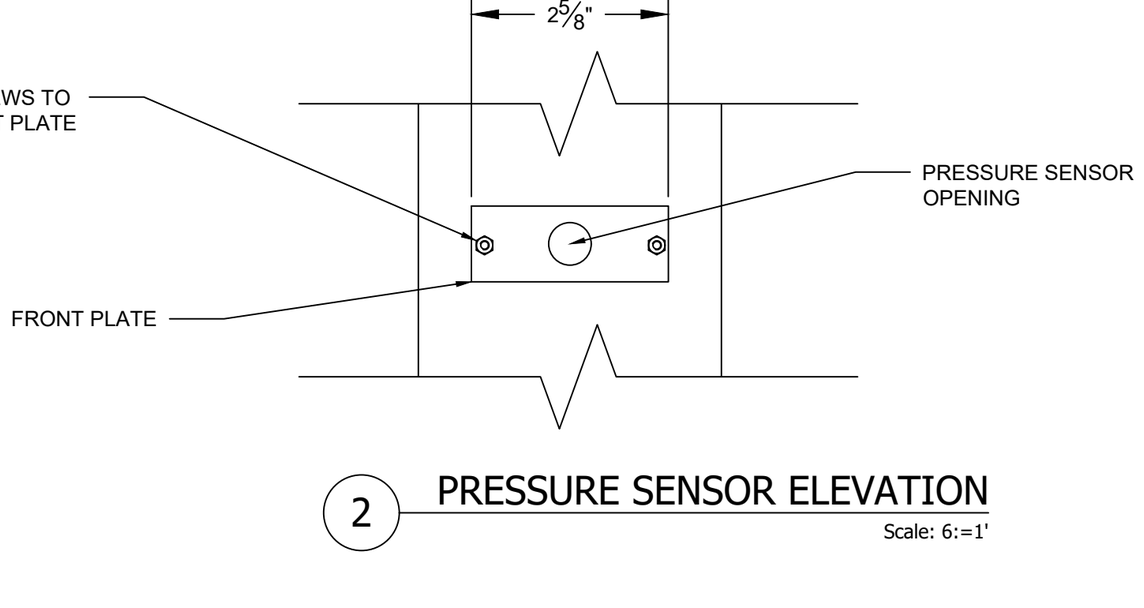

2 PRESSURE SENSOR ELEVATION

Scale: 6:=1'

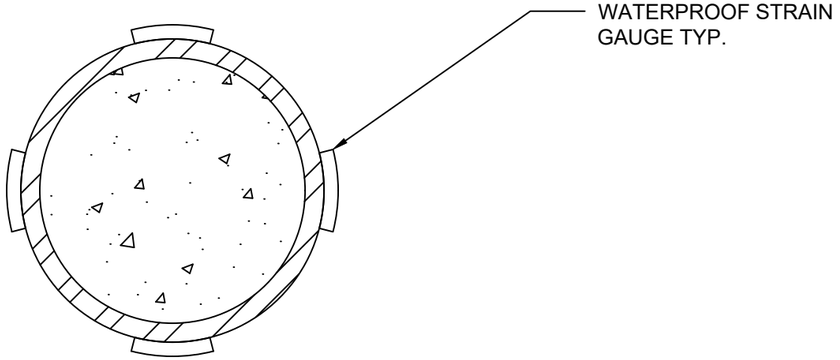

3 STRAIN GAUGE PLAN

Scale: 6"=1'

CIVIL & ENVIRONMENTAL ENGINEERING

General Notes

SAME SENSOR LAYOUT FOR FRONT AND BACK TRUSS.
BACK TRUSS WILL SEE SUBSTANTIALLY LOWER PRESSURES AND INUNDATION DEPTHS.

No.	Revision/Issue	Date

VERTICAL EVACUATION STRUCTURES

PRESSURE SENSOR/STRAIN GAUGE DETAIL

Project

Date 7/02/19

Scale AS NOTED

Sheet S400

PRODUCED BY AN AUTODESK STUDENT VERSION

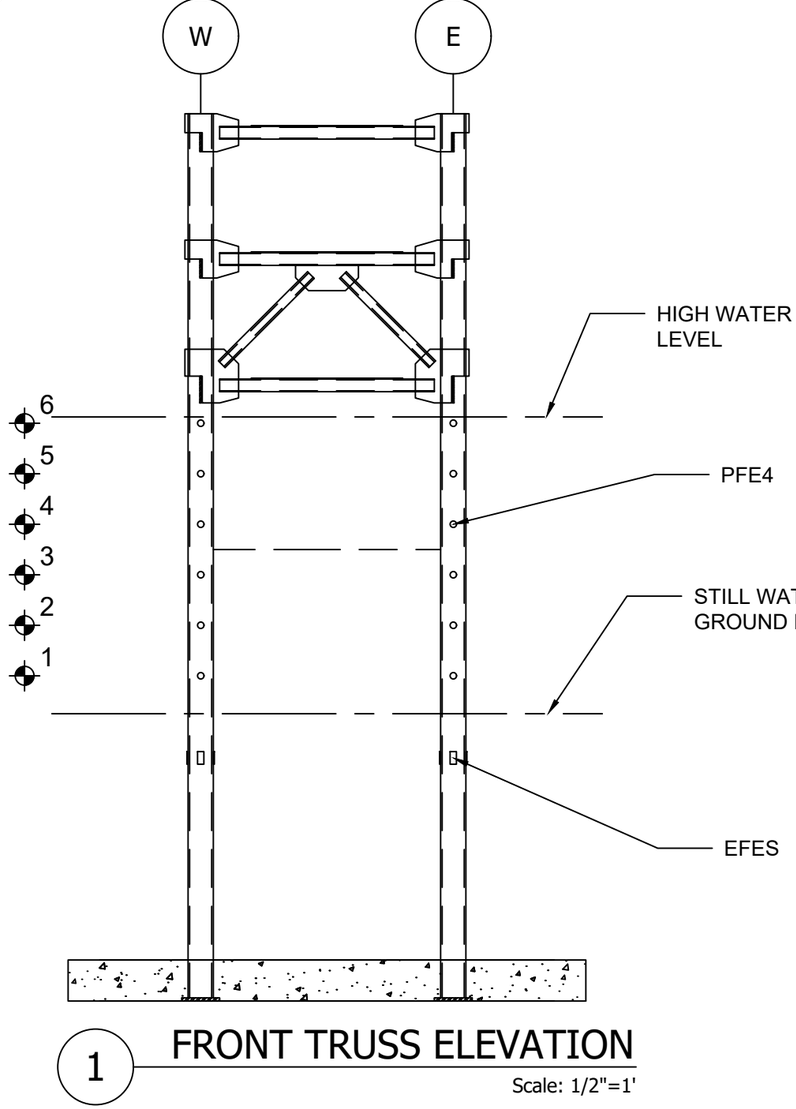

1 FRONT TRUSS ELEVATION
Scale: 1/2"=1'

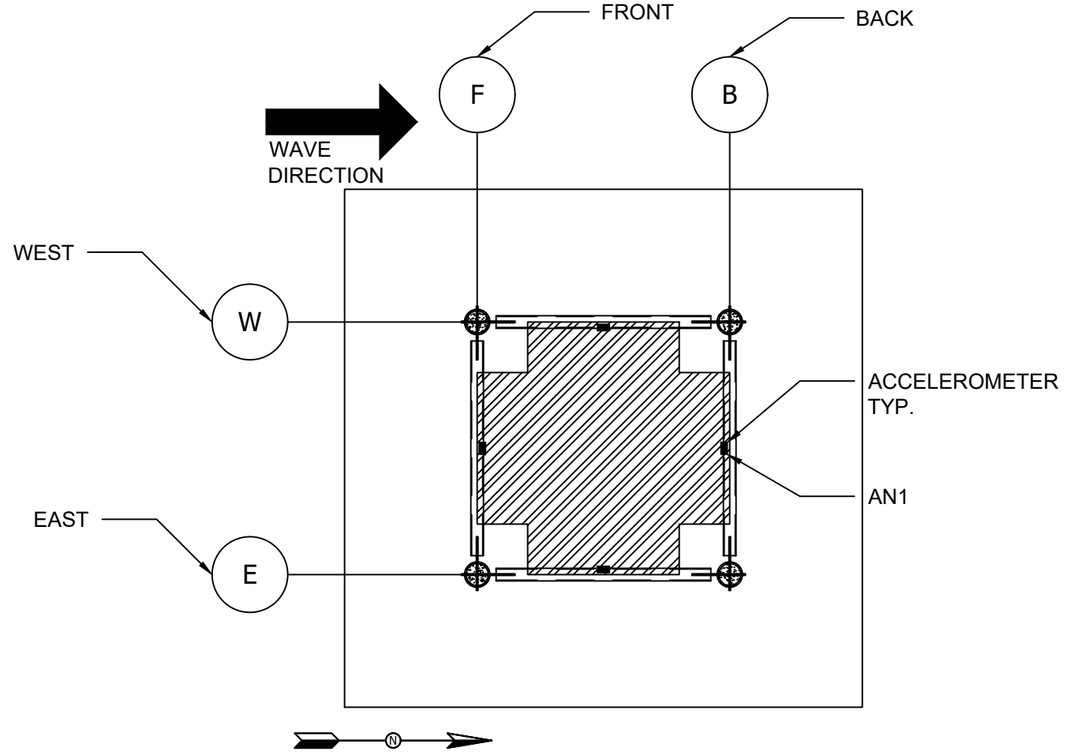

2 PLAN
Scale: 1/2" = 1'

NAMING CONVENTION PRESSURE SENSORS:
1. "P" FOR PRESSURE SENSOR
2. "F" FOR FRONT TRUSS, "B" FOR BACK TRUSS
3. "E" FRO EAST SIDE OF FLUME, "W" FOR WEST SIDE OF FLUME
4. LEVEL NUMBER

NAMING CONVENTION FOR STRAIN GAUGES:
1. "E" FOR STRAIN GAUGE
2. "F" FOR FRONT TRUSS, "B" FOR BACK TRUSS
3. "E" FRO EAST SIDE OF FLUME, "W" FOR WEST SIDE OF FLUME
4. "N" FOR NORTH, "S" FOR SOUTH, "E" FOR EAST, "W" FOR WEST SIDE OF COLUMN

NAMING CONVENTION FOR ACCELEROMETERS:
1. "A" FOR ACCELEROMETER
2. "N1" FOR NORTH, "S1" FOR SOUTH, "E1" FOR EAST, "W1" FOR WEST SIDE OF FLUME

EXAMPLE: PFE4 IS THE PRESSURE SENSOR ON THE FRONT TRUSS, EAST COLUMN, LEVEL FOUR. EFES IS THE STRAIN GAUGE ON THE FRONT TRUSS, EAST COLUMN, SOUTH SIDE (FACING THE WAVE MAKER).
AN1 IS THE ACCELEROMETER ON THE NORTH (BACK, AWAY FROM WAVE), SIDE OF STRUCTURE

CIVIL & ENVIRONMENTAL ENGINEERING
General Notes

No.	Revision/Issue	Date

VERTICAL EVACUATION STRUCTURES

NOMENCLATURE

Project
Date 7/05/19
Scale AS NOTED
Sheet S402

PRODUCED BY AN AUTODESK STUDENT VERSION

Appendix C

INSTALLATION, REMOVAL, AND DRY RUN OF CFST SPECIMEN IN LARGE WAVE FLUME

Prepared: 11 December 2019

Edited: 9 January 2020

Reviewed: 17 January 2020

Transcribed to LaTeX: 7 February 2020

Invalidated: 11 February 2020

DO NOT USE THIS PROCEDURE

C.1 Installation

1. ~~Install flume wall cross-shore spreader beam in appropriate bay (beam and hardware provided by OSU)~~

2. ~~Attach all soil box walls to specimen, while specimen is on stable blocking in the flume but not on the reaction frame~~

3. ~~Bolt soil box walls together, leave the soil box empty~~

4. ~~Install reaction frame to flume floor in appropriate bay with rods and bolts (OSU supplied). Refer to~~ Figure C.1

    - ~~Tighten all rods with large extender on wrench~~
    - ~~Tighten eight center rods in front and back first in alternating pattern (like putting wheel on car). Check that reaction frame is level as tightening~~
    - ~~Tighten eight outrigger rods second in alternating pattern so one side is not pulled lower than the other~~

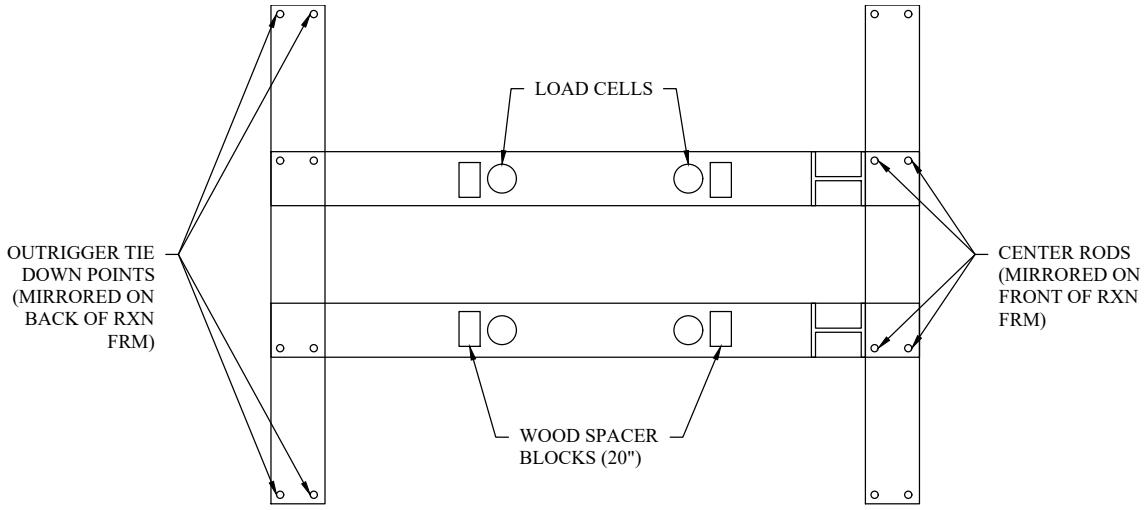

Figure C.1: Reaction Frame Plan View

5. ~~Attach bottom load cells (used to measure vertical loads), to reaction frame, leave bolts slightly loose. The load cell assembly is shown in Figure C.2~~

    - ~~Make sure load cell apparatuses are in compacted configuration with threaded rod screwed all the way into swivels and load cell attachments~~

6. ~~Place wood spacer blocks (20" tall) on reaction frame to support the specimen to support the specimen~~

7. ~~Lift and place specimen on spacer blocks with the crane~~

    - ~~Leave crane attached with tension in cable~~

8. ~~Attach bottom load cell assembly to bottom of specimen~~

    - ~~Unscrew rod from load cell attachment to extend the load cell assembly to 20" in length~~

9. ~~Attach cross-shore and alongshore load cells~~

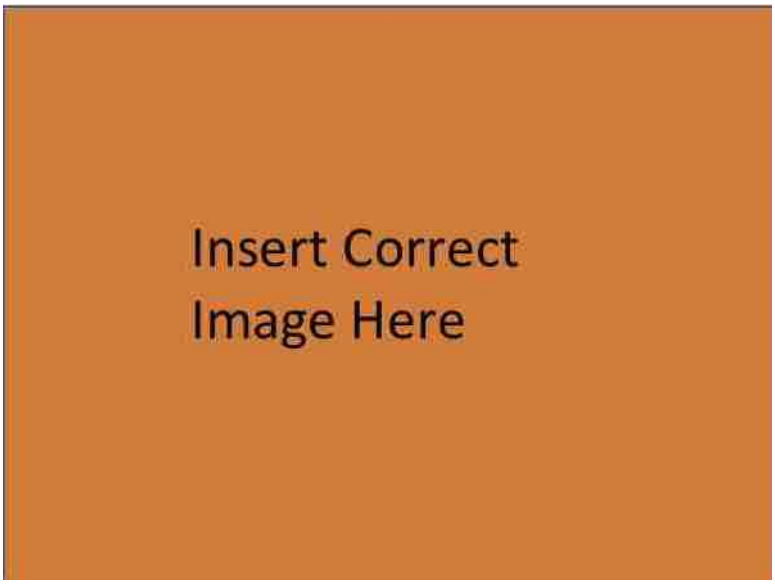

Figure C.2: Bottom Load Cell Assembly

- ~~Side load cells need to be installed simultaneously (with at least 2 people) to minimize shifting of the specimen when one gets tight~~
- ~~Do not fully tighten~~

10. ~~Unbolt bottom load cells from bottom of specimen~~]

11. ~~Lift specimen 1/4" to 1/2", just enough to remove spacer blocks~~

    - ~~Make sure side and back load cells remain loose and are not blown~~

12. ~~Extend and tighten bottom load cells~~

    - ~~Use this opportunity to level specimen~~
    - ~~Place plate spacers around threaded rod in bottom load cell assembly~~

13. ~~Tighten side Load cells~~

14. ~~Slowly remove tension in crane *BUT leave crane attached to top of specimen*~~

- ~~Specimen should be sitting on load cells but crane should not be loose~~

15. ~~Attach chain to back of specimen in cross shore direction, as shown in Figure C.3~~

Figure C.3: Load Cell Pretensioning Chain and Turnbuckle

16. ~~Place spreader bar strut between upright portions of reaction frame to prevent reaction frame tipping inward when the chain is tightened~~

17. ~~Tighten back load cells and chain to target load~~

    - ~~Need to calculate target preload based on any changes in load cell capacity, and angles of load cell and chain~~
    - ~~For concrete wall specimen targeted 1900 lb preload in tension member, 1475 lb preload in load cells ———— Need to calculate desired preload for CFT specimen~~
    - ~~Let rest for a couple minutes and record actual preloads~~

18. ~~Remove crane~~

19. ~~Measure load in all load cells~~

- ~~Make sure loads are close to same for each side/back load cell pair~~

C.2 Removal

1. ~~Remove soil/aggregate~~
2. ~~Attach crane to top of specimen in four connection spots~~
    - ~~Place in slight tension, just enough to remove slack and stretch in straps~~
3. ~~Check if any load cells are tight/loose~~
4. ~~Unbolt load cells from bottom of specimen~~
    - ~~Just unscrew bolts in all four plates~~
5. ~~Increase tension in crane slightly, but do not lift up yet~~
6. ~~Loosen load cells that are not already loose, but leave attached~~
    - ~~Care must be taken to loosen the rods in the load cells and not tighten them~~
7. ~~Lift Specimen slightly~~
    - ~~Less than 1/4"~~
8. ~~Place wood spacer blocks under specimen~~
9. ~~Remove bottom load cells completely~~
10. ~~Remove side and back load cells~~
11. ~~Lift and move specimen to stable location~~
12. ~~Remove soil box walls with crane~~
    (a) ~~Unbolt angles on inside of soil box walls (requires two people)~~

(b) ~~Attach crane to lifting hooks on wall to be removed~~

(c) ~~Remove slack from crane but do not lift up~~

(d) ~~Loosen nuts on threaded rod on bottom of steel plate~~

(e) ~~At least two people must help hold the wall in place and guide the crane and steel plate away from the specimen to a stable location~~

(f) ~~Repeat (b-f) for remaining steel plates~~

C.3 Dry Run Testing Procedure

After specimen is stable in flume and instrumentation set up is complete a dry run test can be done to ensure load cells are working properly before filling the flume

1. Attach along shore beam and brackets to flume walls
    - May have to remove top slope/beach clips on wall
2. Remove any pressure sensors and caps at elevation load will be placed
3. Attach load spreader beam to specimen
    - For concrete wall specimen a couple 2x6s work, just to minimize a point load on the concrete
    - For CFT specimen, probably need steel spreader bar with minimal deflection for the anticipated loads
    - Two kip max in each load cell, so should load specimen to 1.5 kips
    - Span is 40" – should determine acceptable deflection and pick beam accordingly
4. Cut 4x4 or larger to correct length between along shore beam, and specimen
    - Take into account load cell, spreader bar, and jack
    - Leave an inch or so of the jack extended
5. Hold components into place and apply very slight pressure to the specimen

6. Start daq

7. Use splitter to monitor the current load in the jack load cell on voltmeter

8. Load jack slowly and methodically to specified points

    - Probably best not to exceed 75% capacity of one back load cell
    - With the small bottle jack we used, we could only load up to approximately 2500 lb
    - Hold at maximum for a while to allow the specimen to shift into final stable location

9. Unload while daq still running

10. Repeat at least once to verify structure not shifting anymore

11. Do preliminary data analysis to check load cells are behaving symmetrically and all instruments are recording properly

This appendix provides the methods used to place and dry run test the CFST specimen in the OSU large wave flume.

Plan for the installation of the UW 2nd specimen in the Large Wave Flume

Current Status:

- Currently, between bays 9 and 10, a reaction frame is fixed to the floor consisting on two longitudinal beams and 2 cross-beams. 16 1” threaded bars have been used to bolt the beams to the flume floor.
- Four steel panels are laid on top of the slabs between bays 12 and 14.
- To the South, there is a concrete slab forming a ~45deg with the flume floor. The slab goes from bay 8 to 9 and reaches an elevation of 2 m.
- To the North, bay 10 to 11 is clean and empty. After bay 11, there is a series of concrete slabs forming a horizontal surface at an elevation of 2 m from the flume floor.
- Access to the specimen can be performed from the North via the flat slabs and at bay 11 with a secured ladder.
- The flume is equipped with a 6 ton carriage crane.
- Currently, the flume floor, made of concrete, is dry.
- The second specimen is currently outside of the flume, and it consists of a 82” by 82” by 7” concrete slab and a rectangular steel structure formed by 138” long steel tubes, 4” in diameter.
- The specimen weight is 2.2 tons.

Specimen geometry, current status and parts (side view)

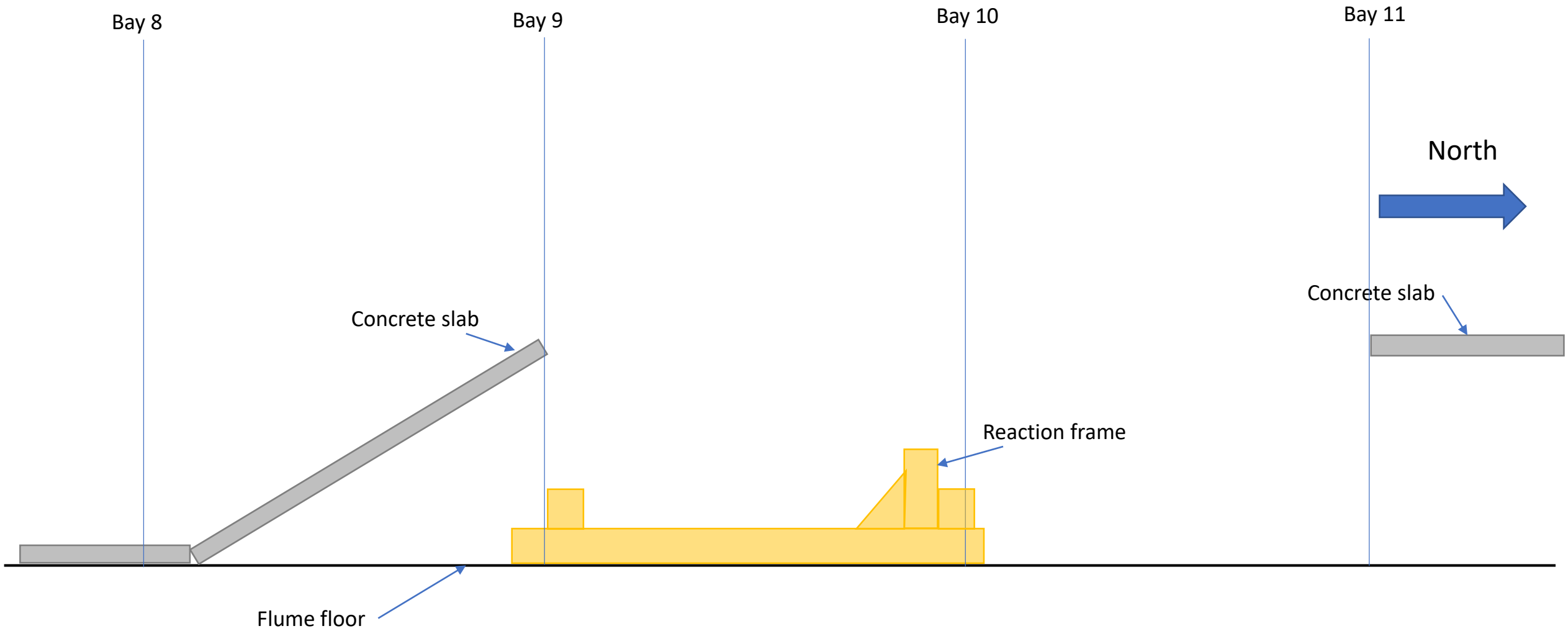

Specimen geometry, current status and parts (top view)

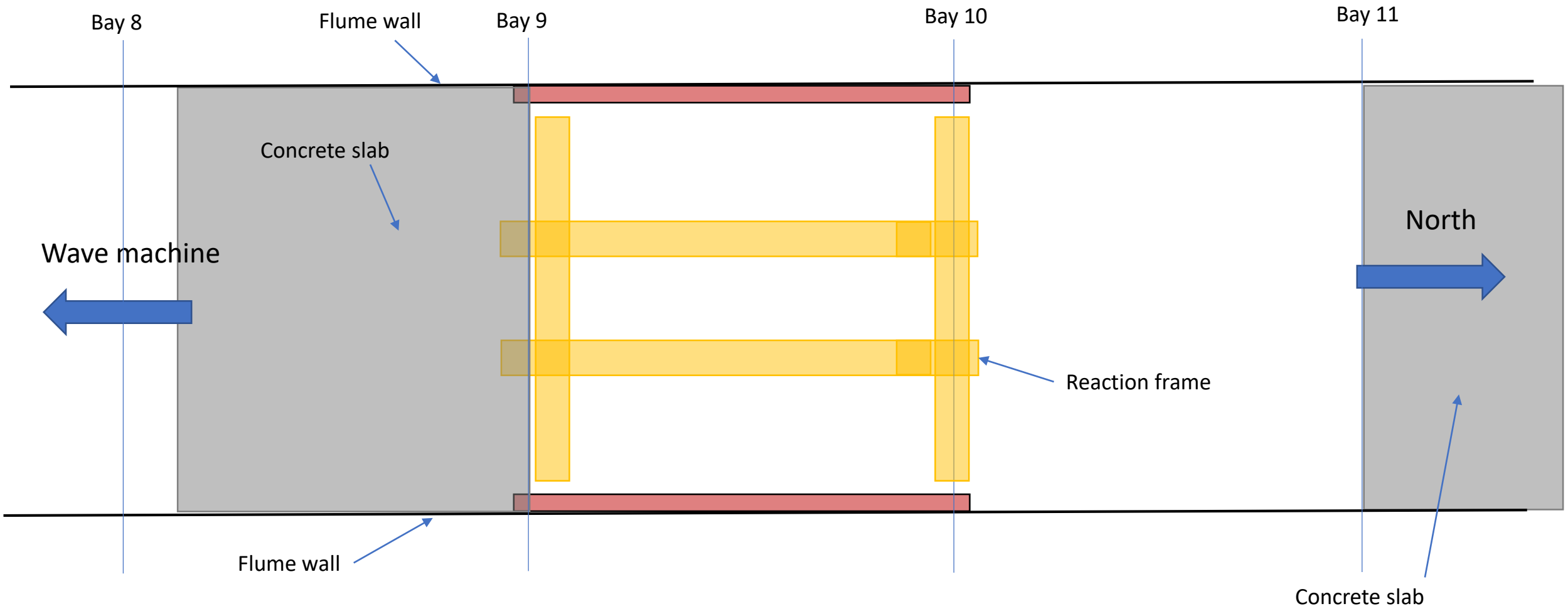

Specimen geometry, current status and parts (NW view)

Current Status:

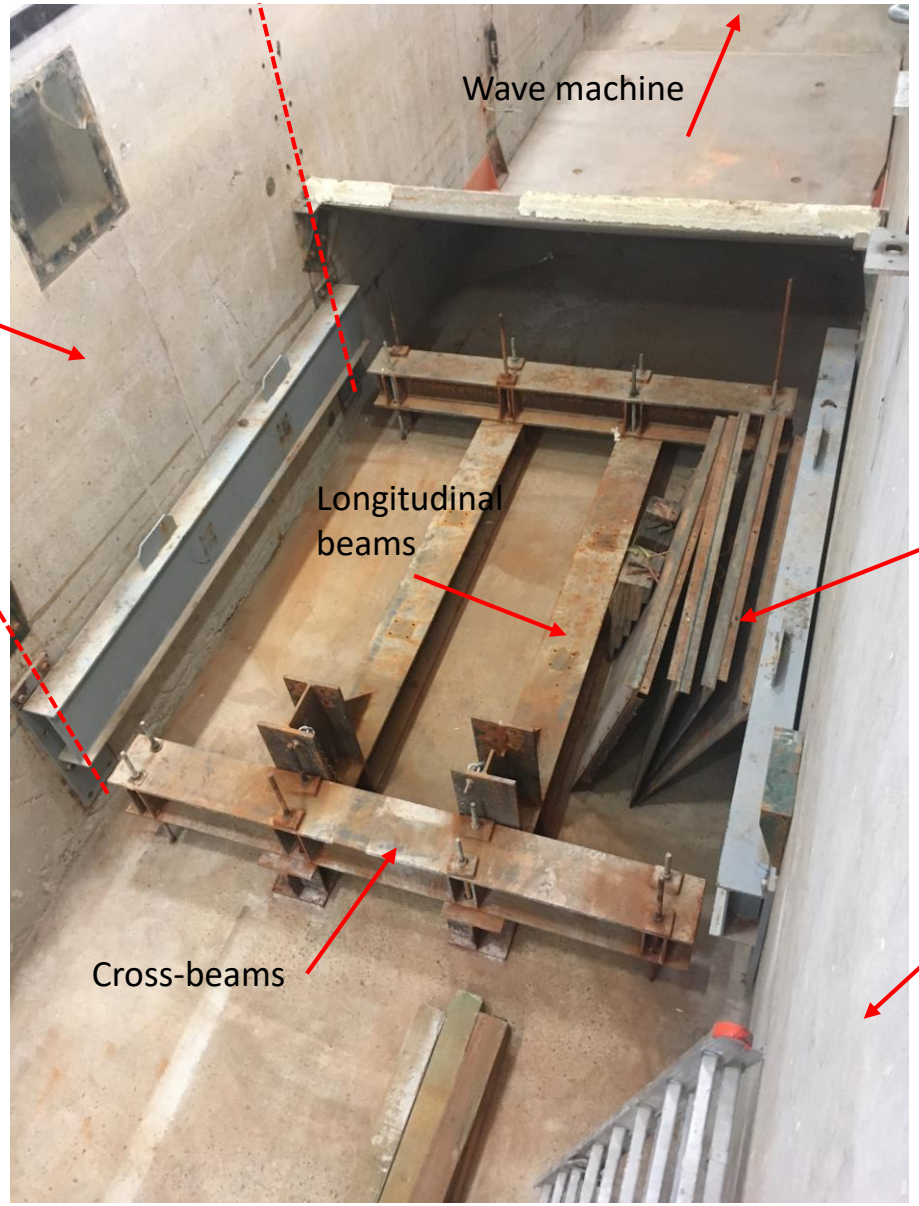

Specimen geometry, current status render (NW view)

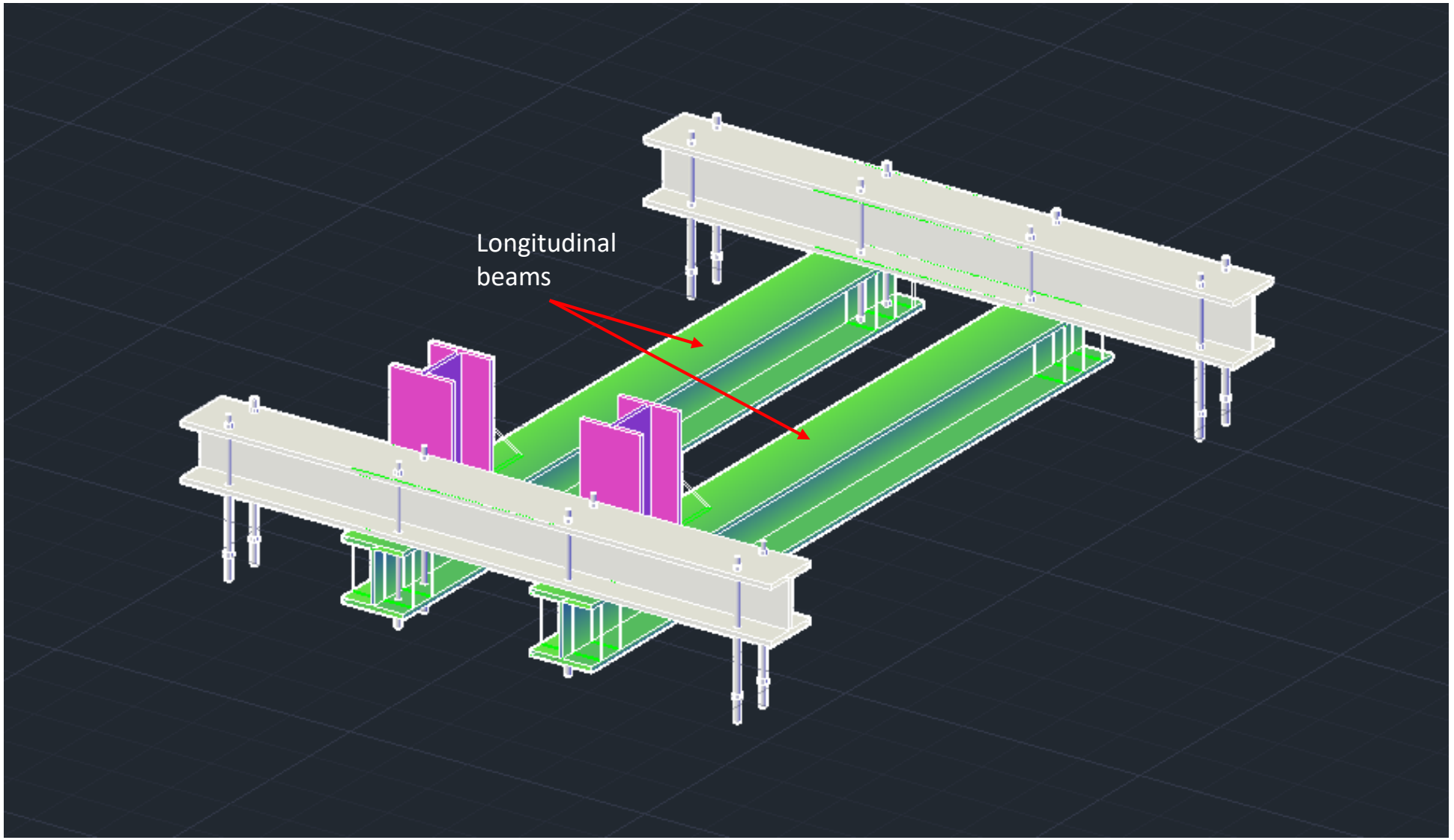

Specimen geometry, current status render (SE view)

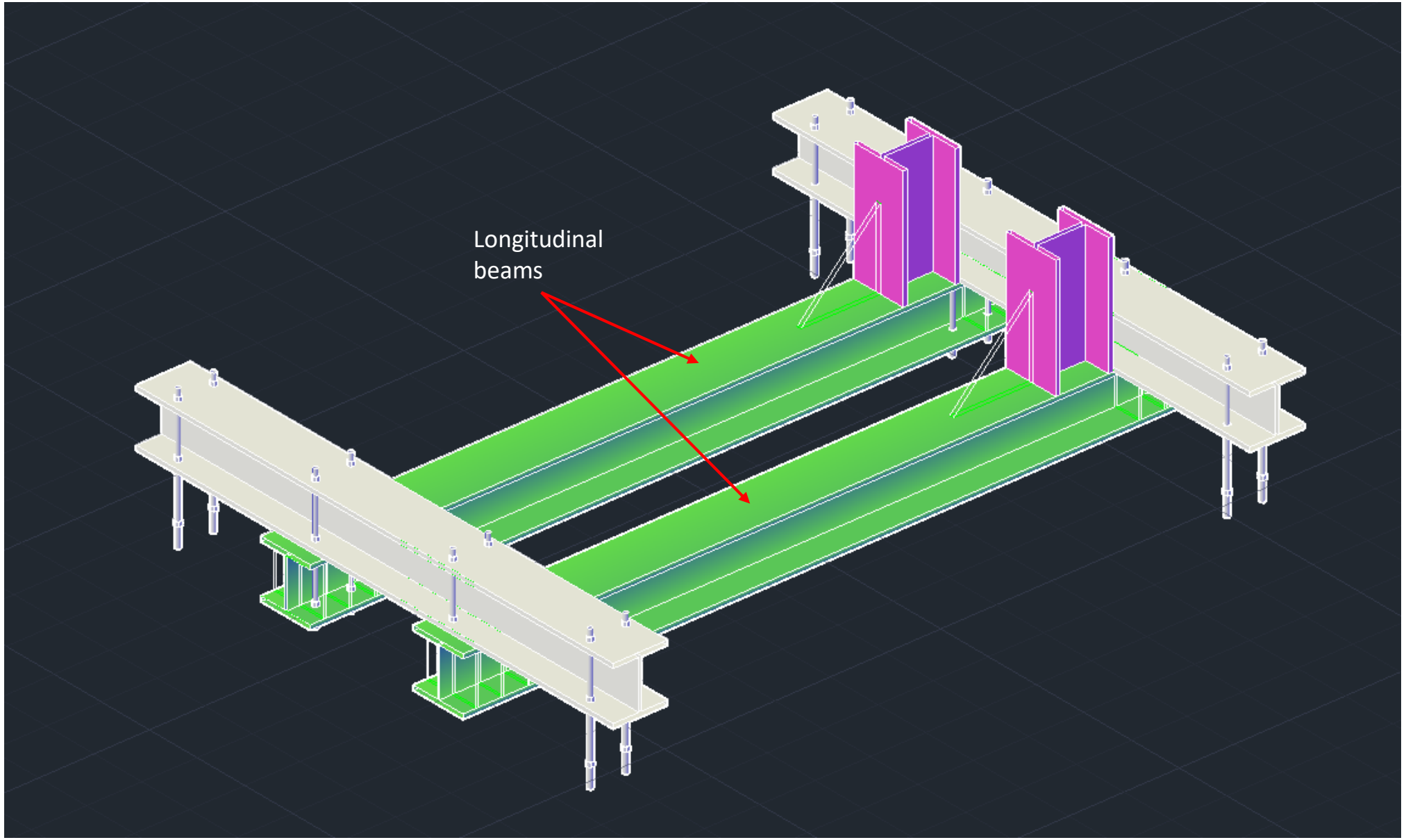

Step 1: Installation of plates and support beams

Use of steel plates and support beams to create a secure crib for the specimen. The plates are 12” by 12” by 2”, and the beams are 15” by 15” by 122” and are located at Hinsdale (belong to the Structures Lab)

Procedure:

1. Perform 8 x 1.25” boreholes on the longitudinal beams
2. Install steel plates (the steel plates already have the 8” by 8” borehole pattern)
3. Install the support beams using the crane
4. Fix the beams and the plates using 8 x 1” threaded bars/bolts

Tools and equipment:

1. Cart
2. Magnetic drill
3. 1” threaded bars/bolts
4. 1” nuts and washers

PPE:

- Gloves
- Safety shoes
- Hard-hat

Personnel:

1 crane operator
1 tech to attach beams

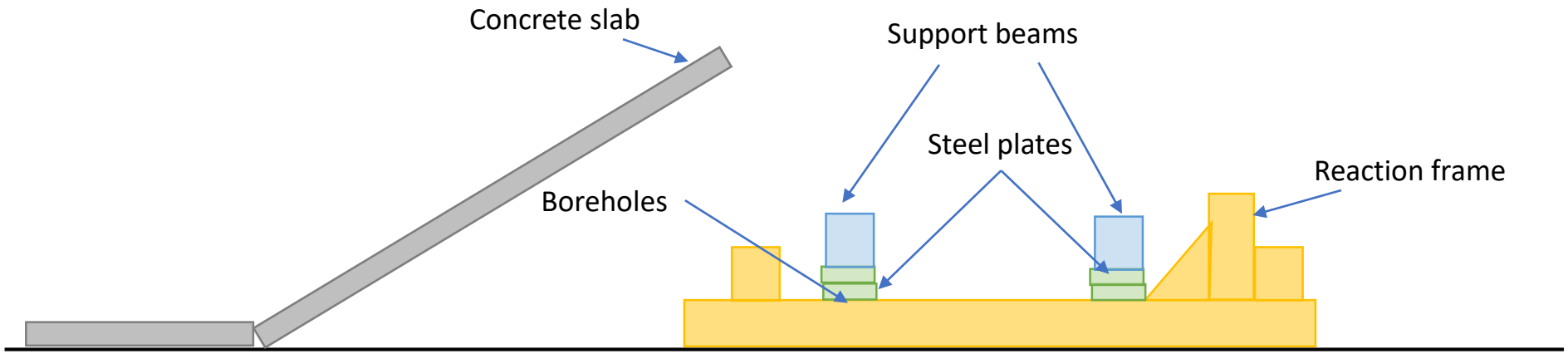

Step 1: Installation of plates and support beams (render)

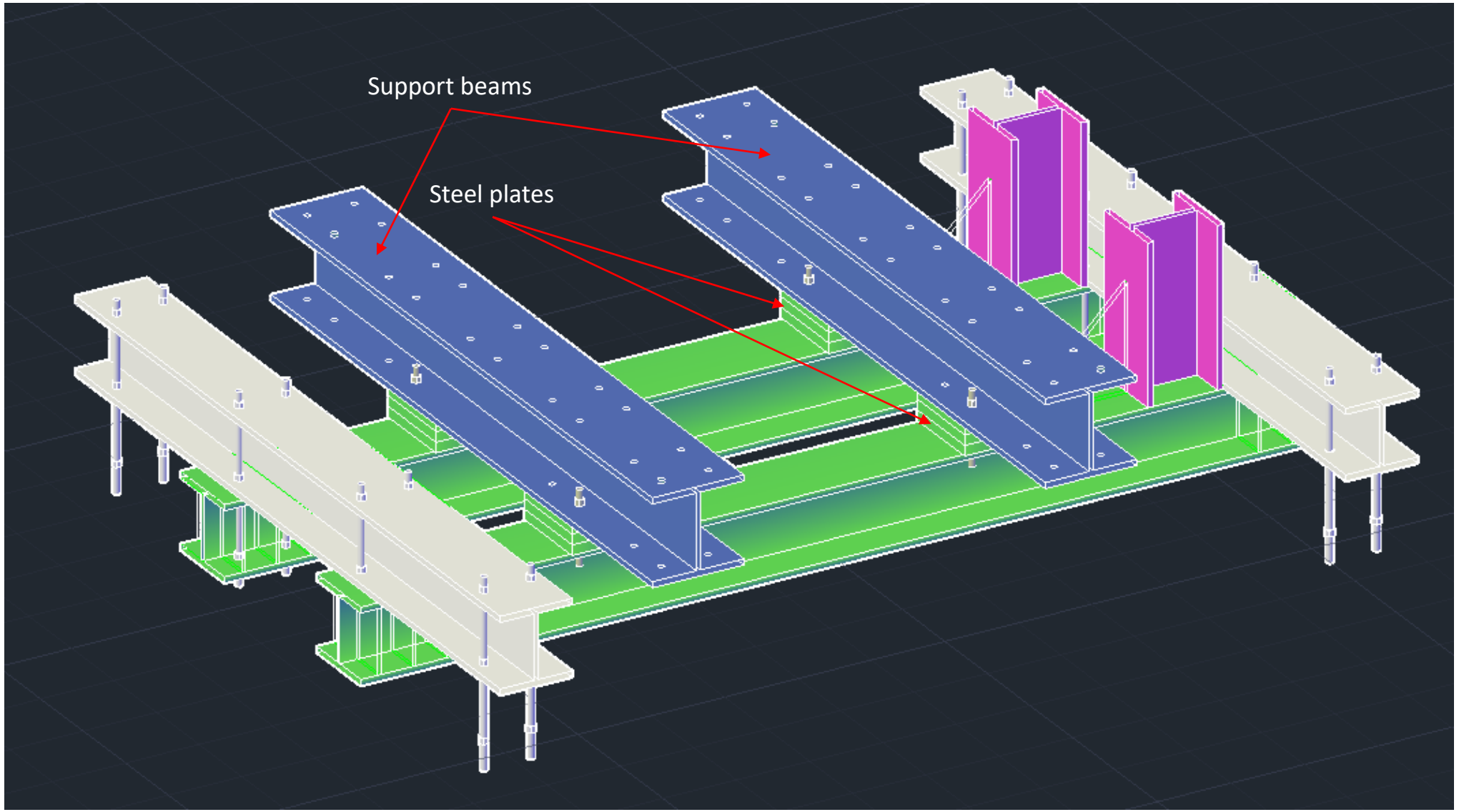

Step 2: Installation of shims and brackets

4 brackets will be installed on each corner of the supporting beams to guide and prevent lateral displacements of the specimen.
Additional shims/plates will be placed so the specimen will be resting at its final elevation.

Procedure:

1. Fasten each bracket embracing the width of the specimen
2. Add plates and shims on the projected corner of the specimen (shims are not fastened so they can be removed on a later stage)

Tools and equipment:

1. Brackets and bolts
2. Shims and plates

PPE:

- Gloves
- Safety shoes
- Hard-hat

Personnel:

1 tech to install brackets and shims

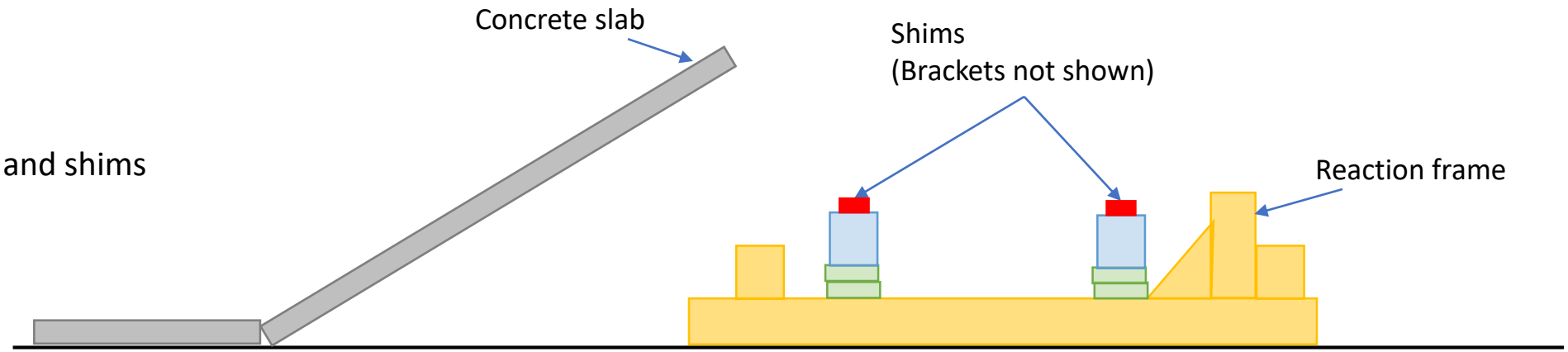

Step 2: Installation of shims and brackets (render)

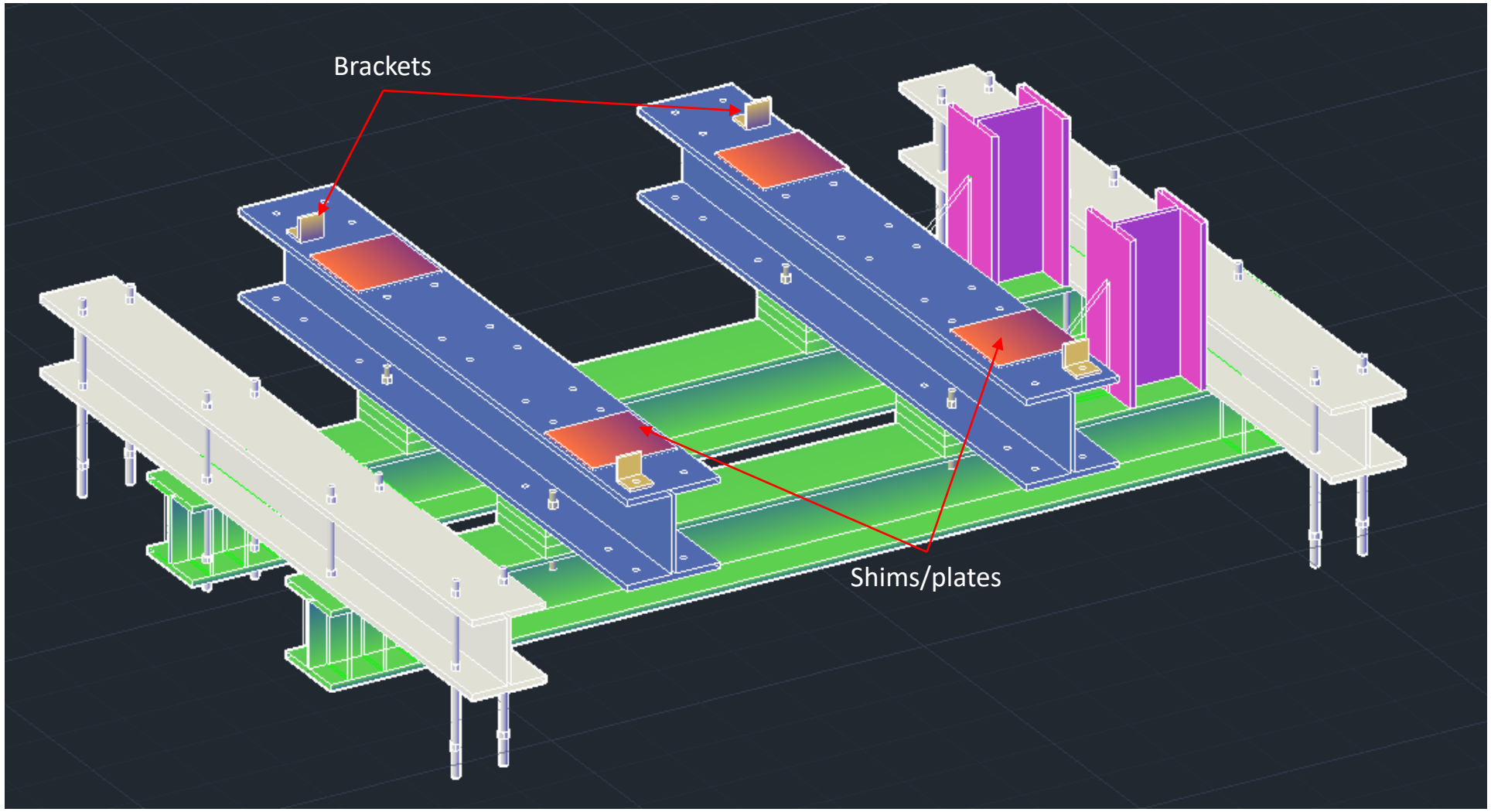

Step 3: Placement of the specimen

The specimen will be first brought to the flume using a crane (rental), and then positioned by the crane hoist of the flume. The specimen will rest on top of the shims.

Procedure:

1. Locate the specimen on the west side of the flume
2. Use a crane to bring it inside the flume and place it between Bays 10 and 11 on the flume floor (use wood to support it and allow the use of slings)
3. Use the flume cart/hoist to accurately place the specimen over the test rig, aligning the shims and let is rest. Keep the crane attached.

Tools and equipment:

1. Slings
2. Ropes to control the specimen at a distance

PPE:

- Gloves
- Safety shoes
- Hard-hat

Personnel:

1 crane operator
1 tech to control the specimen and attach the slings

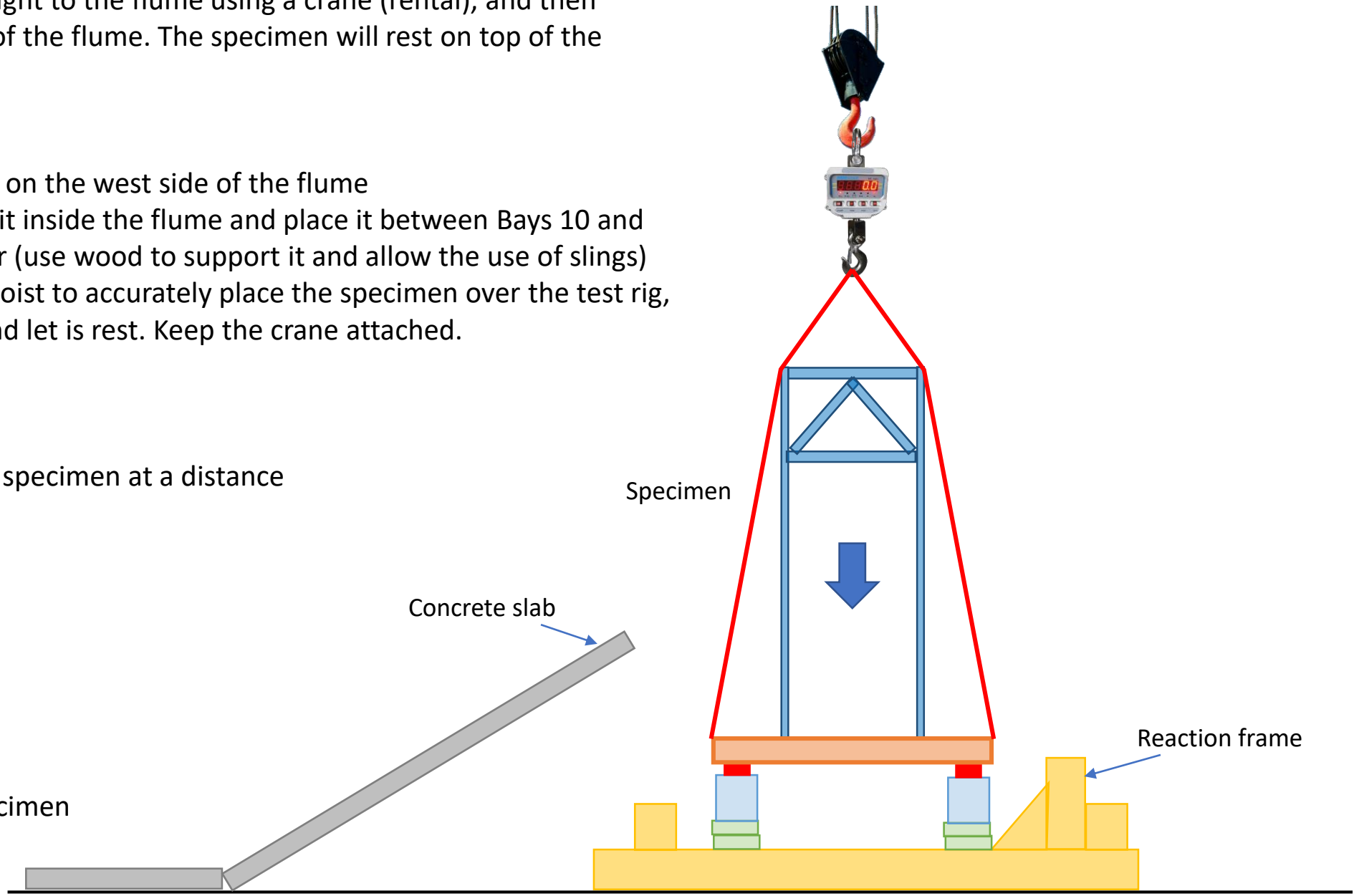

Step 3: Placement of the specimen (render)

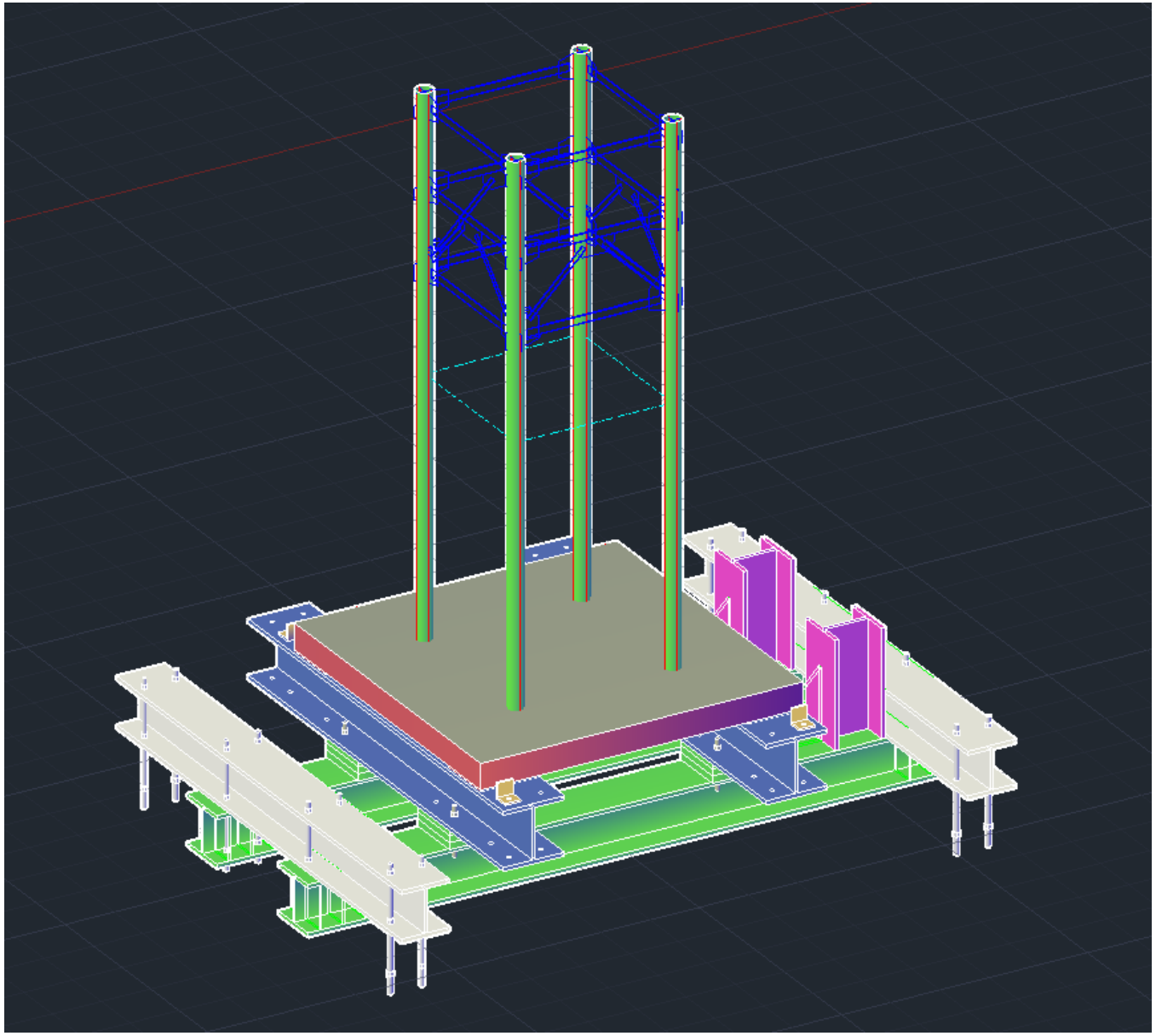

Step 3: Placement of the specimen (concrete slab transparent for visualization purposes)

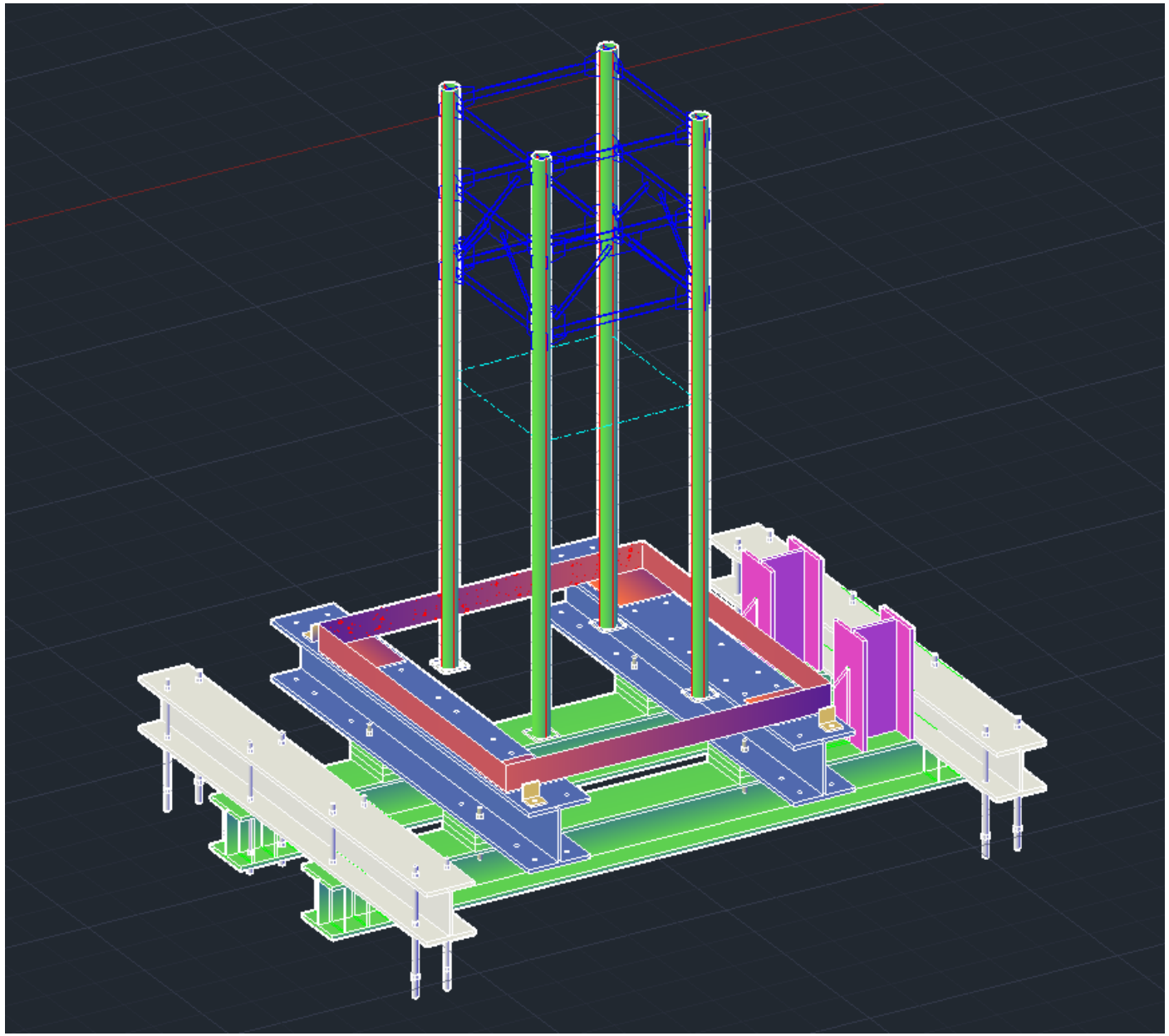

Step 4: Installation of pancake load cells

The pancake load cells (orange part in the figure) have attached two cylinders as a transition to the swivel (blue part of the figure). Threaded bolts are used from the cylinders to the swivel (red dots in the figure). The specimen is resting on the shims and is attached to the hoist.

Procedure:

1. Retract the bolts of the pancake load cells (red dot in the figure)
2. Attach the swivel to the specimen with bolts. Tighten the bolts (the specimen has threaded plates embedded).
3. Extend the bolts of the pancake load cells to reach the longitudinal beams. The pancake load cells have now the exact length of the final elevation of the specimen.
4. Attach the swivel to the longitudinal beams with bolts and nuts. Leave the nuts 10 mm from the tighten position. The load cells can support the specimen, and cannot move laterally due to the bolts.

Tools and equipment:

1. 8 bolts per load cell (total of 32)
2. Ratchet

PPE:

- Gloves
- Safety shoes
- Hard-hat

Personnel:
1 tech to install load cells

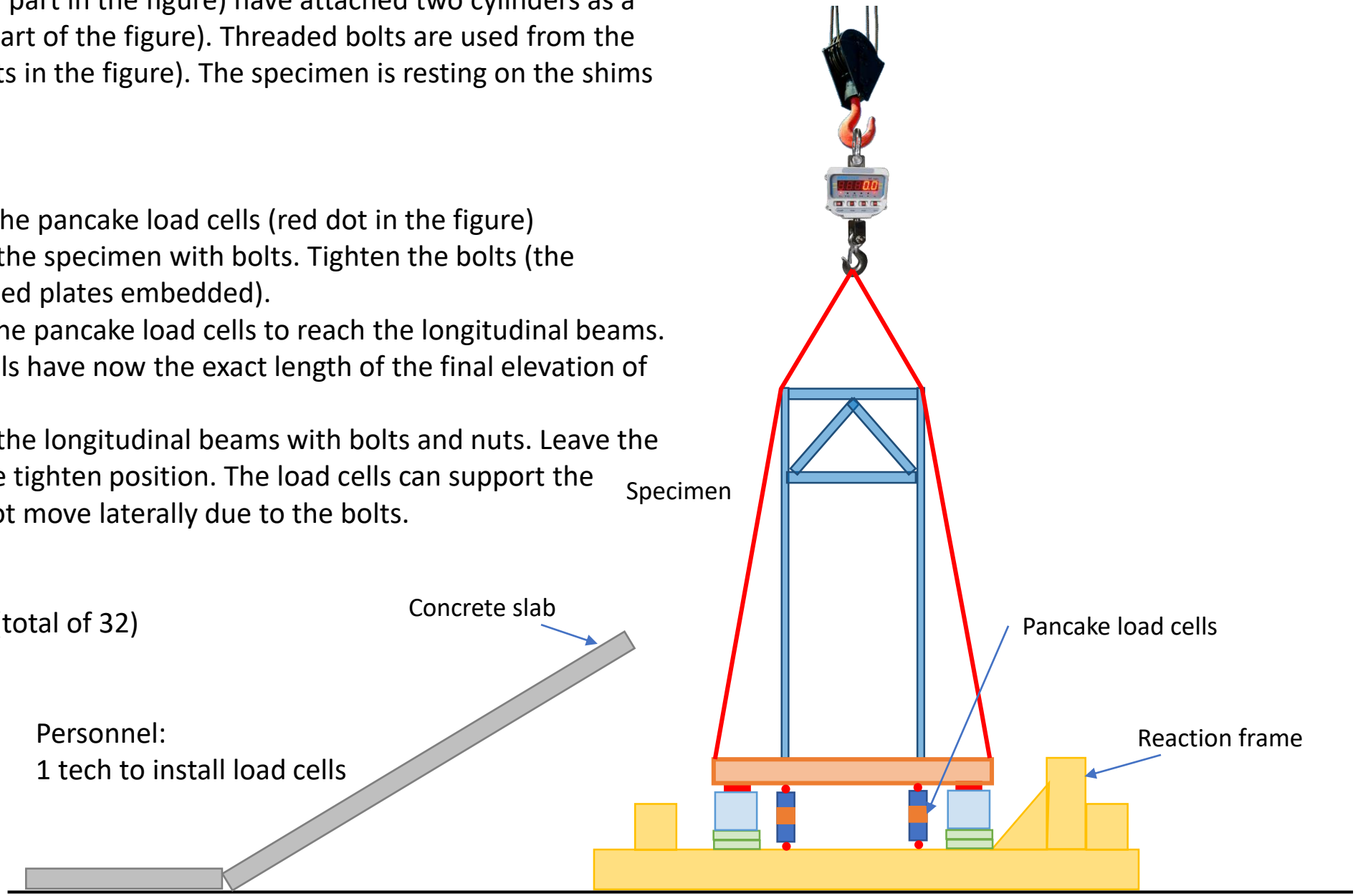

Step 4: Installation of pancake load cells

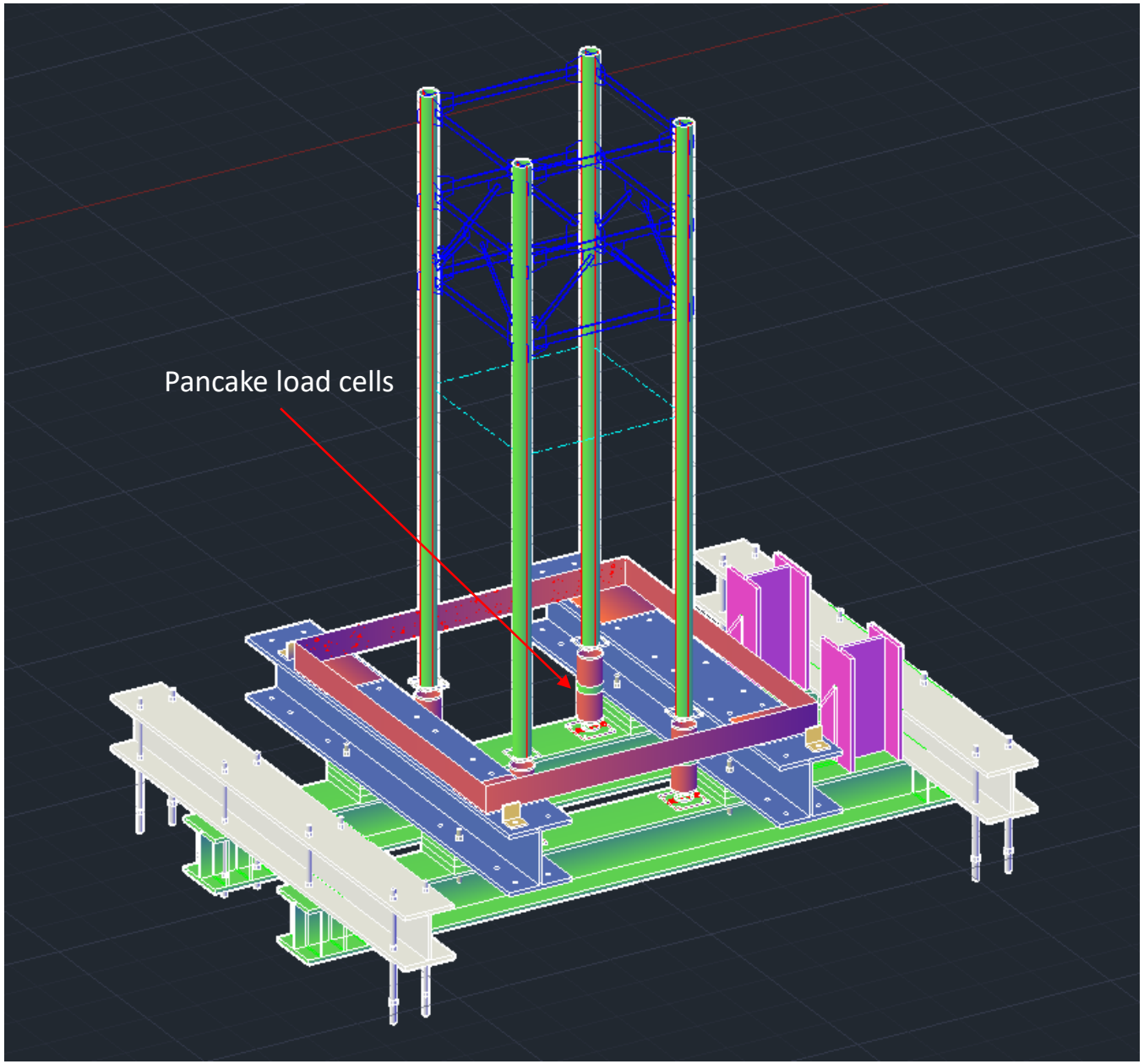

Step 5: Installation of the steel panels

The four steel panels should be bolted to the concrete slab and along the rivets between them. The specimen is resting on the shims and the cart hoist is used to bring the panels one by one, paying attention on the order. Once each panel that is bolted to the concrete slab, is secured. Bolts and nuts are necessary to connect the panels along the rivets between each other.

Procedure:

1. Detach the crane from the specimen and use it to bring a panel
2. Start with the panel closer to the wave machine (South)
3. Align the panel to the threaded rods and introduce the panel. This procedure can be done at a distance from the panel, since the hoist can align the panel to the rods. Guiding of the panel can be done from the outside plane of the panel ⑤, so the panel cannot move towards the person guiding.
4. Tighten the nuts to fix the panel ④. The panel is fixed at 5 locations along the specimen slab, the rods are located at different elevations, which fixes the panel.
5. Crane is detached from the slab of the specimen ⑤.
   (opposite of the threaded rods).

Tools and equipment:

1. Ratchet, bolts, nuts and washers
2. WS-40
3. Cart

PPE:

- Gloves
- Safety shoes
- Hard-hat

Personnel:
1 crane operator
1 tech to align and bolt

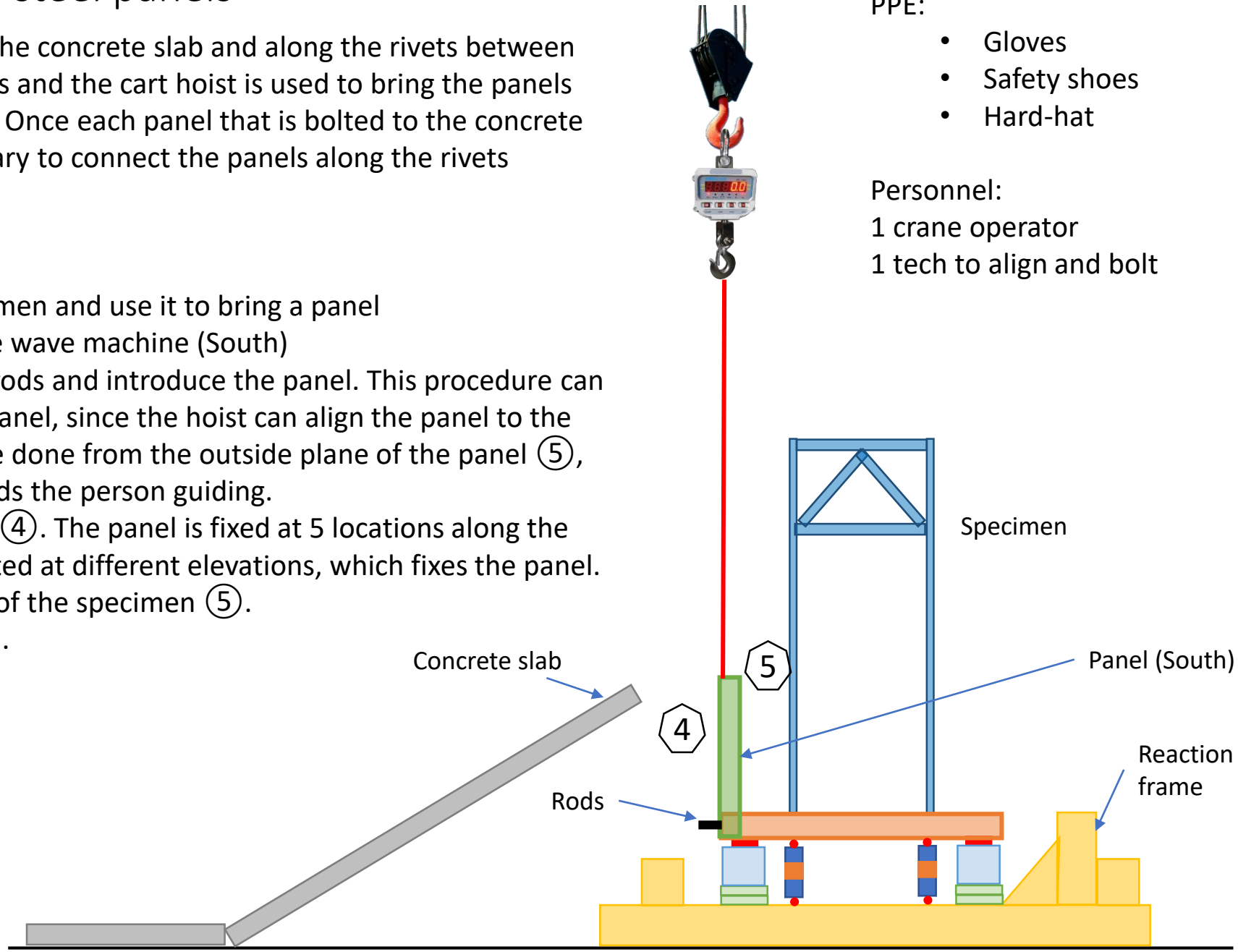

Step 5: Installation of the steel panels (cont.)

The four steel panels should be bolted to the concrete slab and along the rivets between them. The specimen is resting on the shims and the cart hoist is used to bring the panels one by one, paying attention on the order. Once each panel that is bolted to the concrete slab, is secured. Bolts and nuts are necessary to connect the panels along the rivets between each other.

Procedure:

1. Continue with the panel along the flume (West).
2. Align the panel to the threaded rods and introduce the panel. This procedure can be done at a distance from the panel, since the hoist can align the panel to the rods. Guiding of the panel can be done from the outside plane of the panel, so the panel cannot move towards the person guiding.
3. Tighten the nuts to fix the panel. The panel is fixed at 5 locations along the specimen slab, the rods are located at different elevations, which fixes the panel.
4. Tighten the bolts and nuts along the rivet, which connects the South panel and the West panel.
5. Crane is detached from the slab of the specimen (opposite of the threaded rods).
6. Repeat procedure for the other panel along the flume (East).

Tools and equipment:

1. Ratchet, bolts, nuts and washers
2. W-40
3. Cart

PPE:

- Gloves
- Safety shoes
- Hard-hat

Personnel:
1 crane operator
1 tech to align and bolt

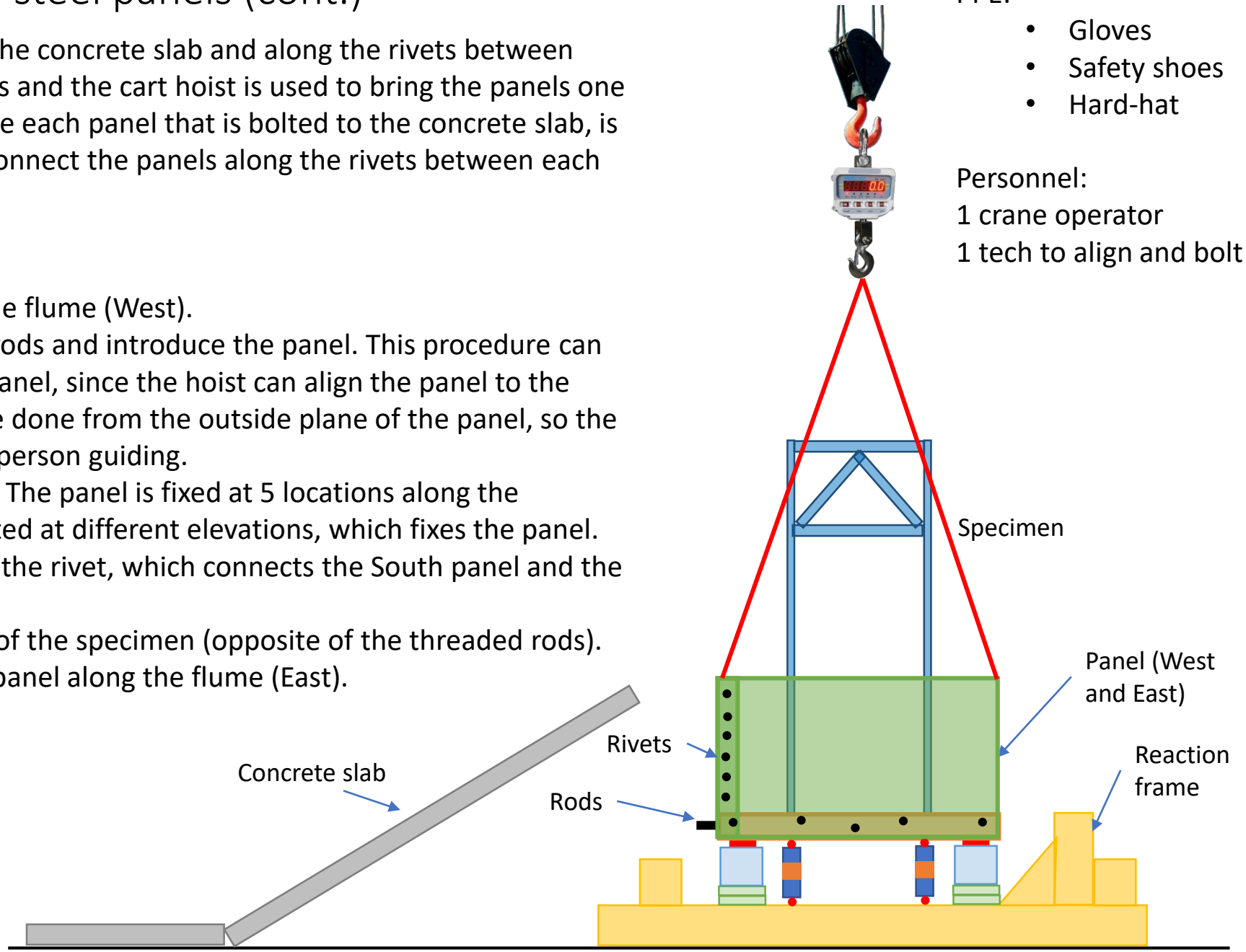

Step 5: Installation of the steel panels (cont.)

The four steel panels should be bolted to the concrete slab and along the rivets between them. The specimen is resting on the shims and the cart hoist is used to bring the panels one by one, paying attention on the order. Once each panel that is bolted to the concrete slab, is secured. Bolts and nuts are necessary to connect the panels along the rivets between each other.

Procedure:

1. Continue with the panel onshore (North).
2. Align the panel to the threaded rods and introduce the panel. This procedure can be done at a distance from the panel, since the hoist can align the panel to the rods. Guiding of the panel can be done from the outside plane of the panel, so the panel cannot move towards the person guiding.
3. Tighten the nuts to fix the panel. The panel is fixed at 5 locations along the specimen slab, the rods are located at different elevations, which fixes the panel.
4. Tighten the bolts and nuts along the rivets, which connects the East and West panels to the North panel.
5. Crane can be detached since all panels are interconnected.

Tools and equipment:

1. Ratchet, bolts, nuts and washers
2. W-40
3. Cart

PPE:

- Gloves
- Safety shoes
- Hard-hat

Personnel:
1 crane operator
1 tech to align and bolt

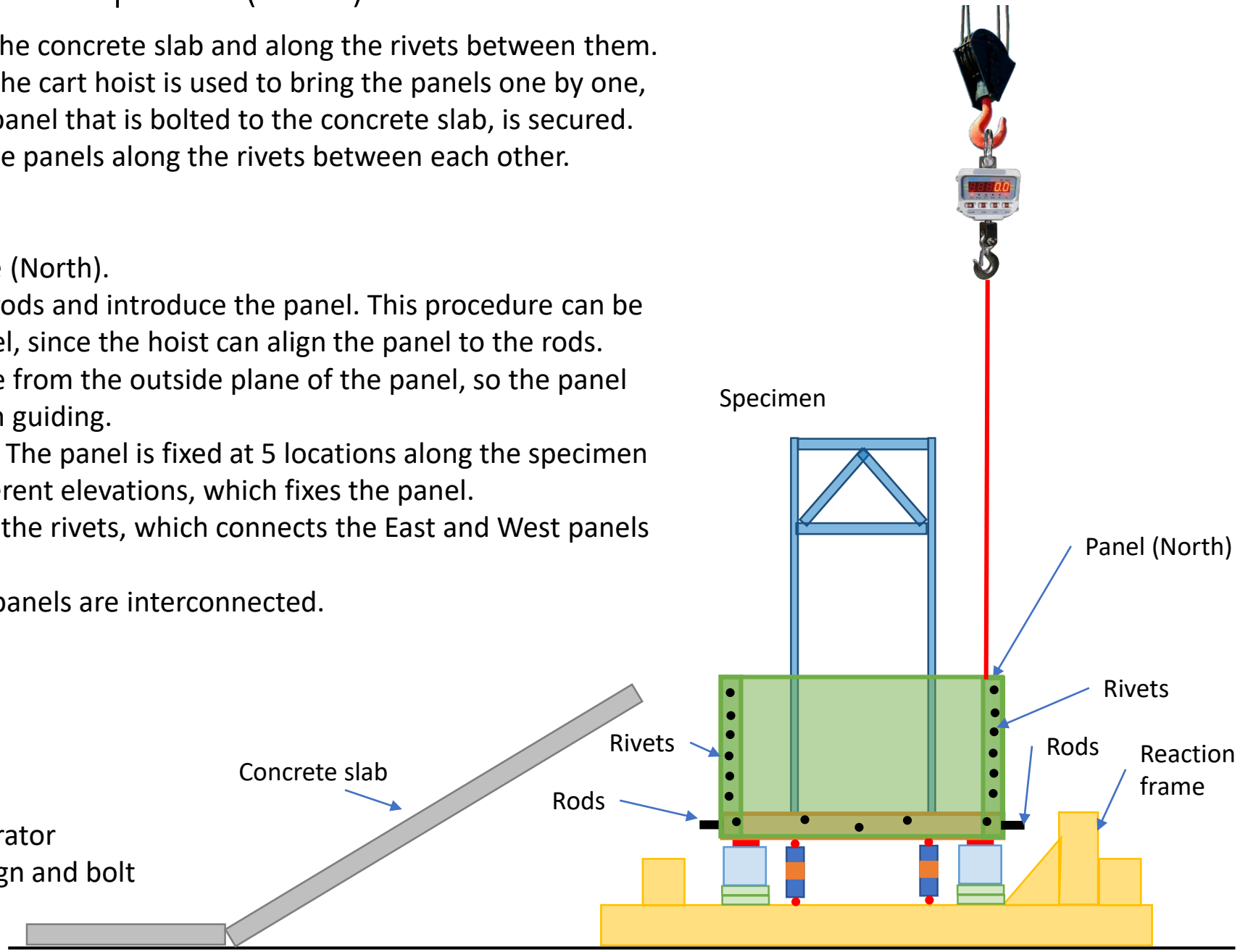

Step 5: Installation of the steel panels

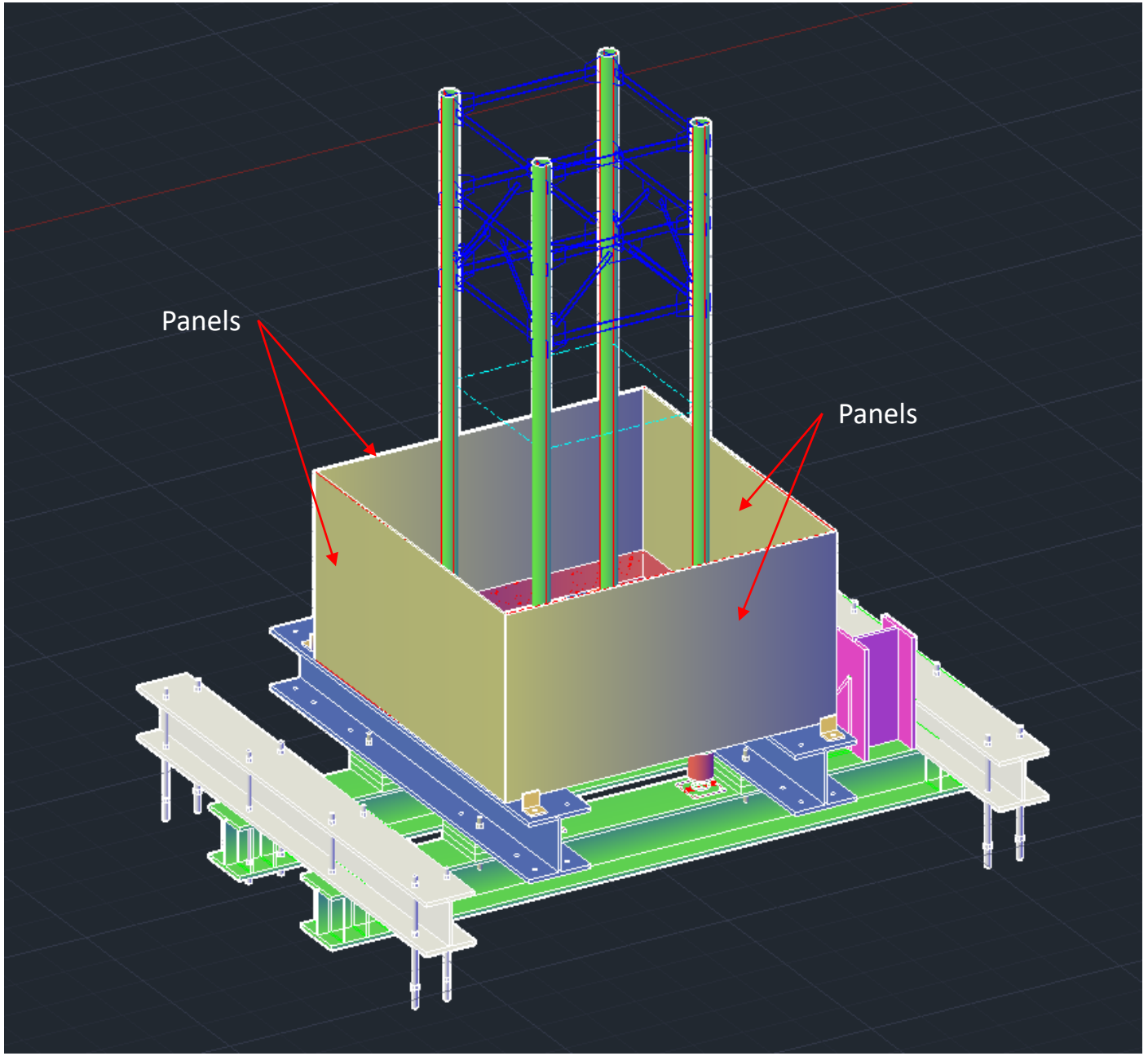

Step 5: Installation of the steel panels (shown transparent for visualization purposes)

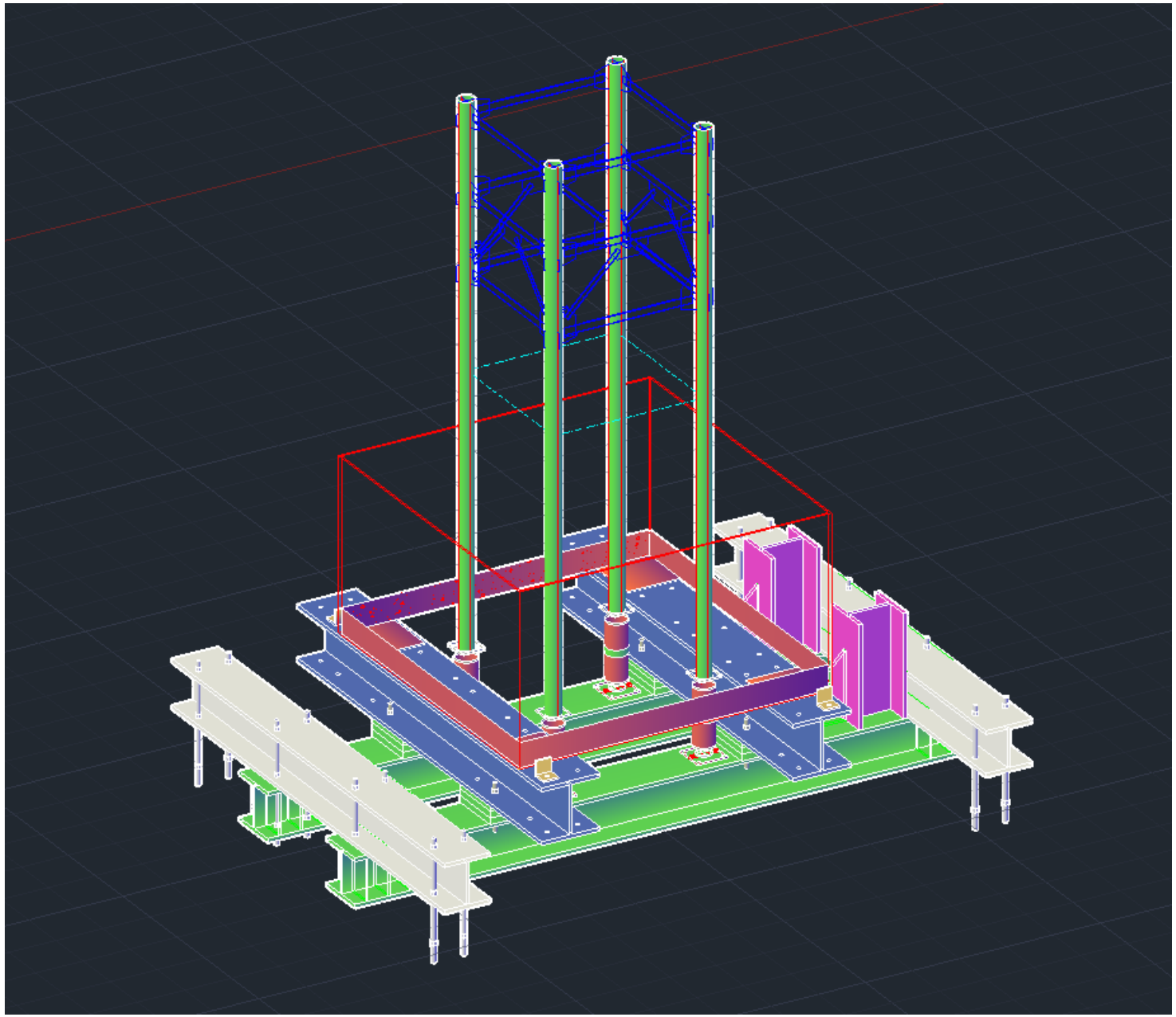

Step 6: Removal of the shims

The shims can be removed by lifting the specimen a couple of millimeters. The play is given by the bolts on the lower part of the pancake load cells. The shims can be removed by simply pushing them with a screwdriver from outside.

Procedure:

1. Connect the crane to the specimen
2. Lift the specimen 5 mm
3. Remove the shims
4. Lower the specimen so it rest over the load cells
5. Tighten the bolts on the lower part of the pancake load cells

Tools and equipment:

1. Long screwdriver or thin plate

PPE:

- Gloves
- Safety shoes
- Hard-hat

Personnel:

1 crane operator
1 tech

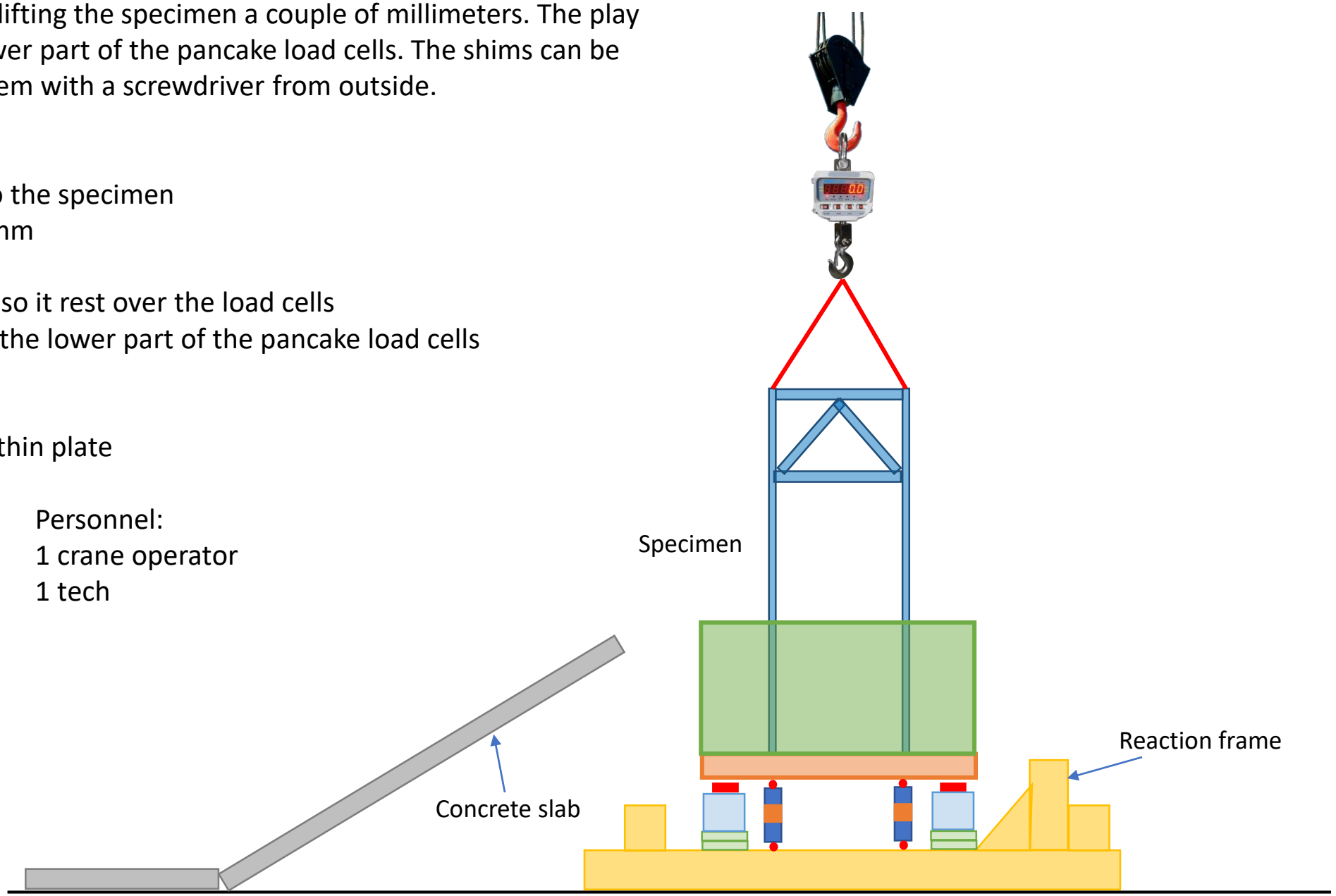

Step 7: Installation of in-line load cells

The in-line load cells are attached to swivels that are bolted to the reaction frame on one side, and to the specimen on the other, at the elevation of the concrete slab. The specimen is resting on the pancake load cells and supported by the crane. The in-line load cells closest to shore are attached first and then the chain is also used to fix the specimen to the vertical beams of the reaction frame. Then lateral in-line load cells are also attached.

Procedure:

1. Maintain the crane connected to the specimen
2. Connect the in-line load cells closest to shore
3. Fix the chain and apply tension on the turnbuckle to ensure pre-compressing the load cells (while measuring voltage output)
4. Connect the lateral in-line load cells and use the rods to create pre-compression on the load cells (while measuring voltage output)

Tools and equipment:

1. Bolts and ratchet

PPE:

- Gloves
- Safety shoes
- Hard-hat

Personnel:

1 crane operator

1 tech

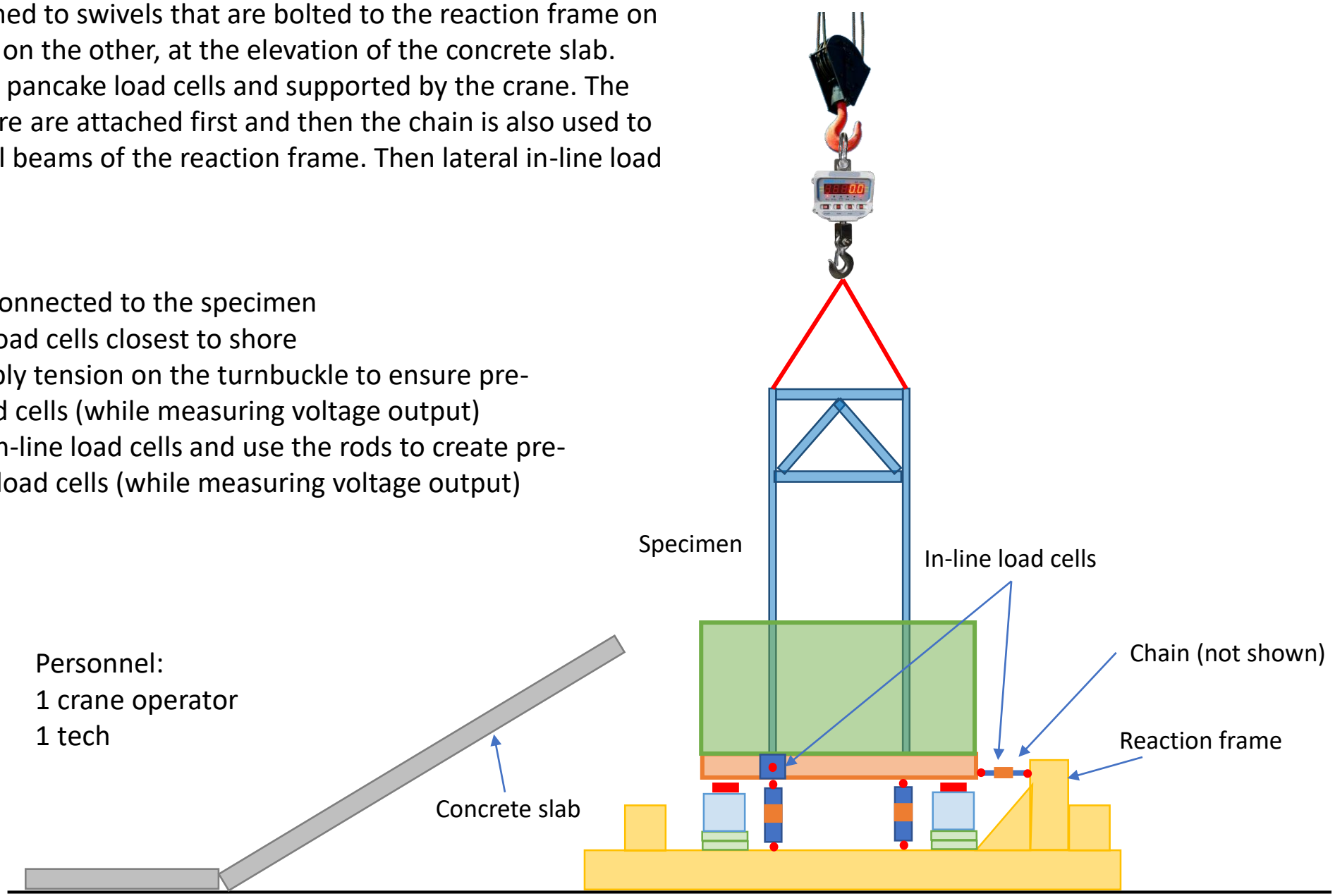

Step 7: Installation of in-line load cells

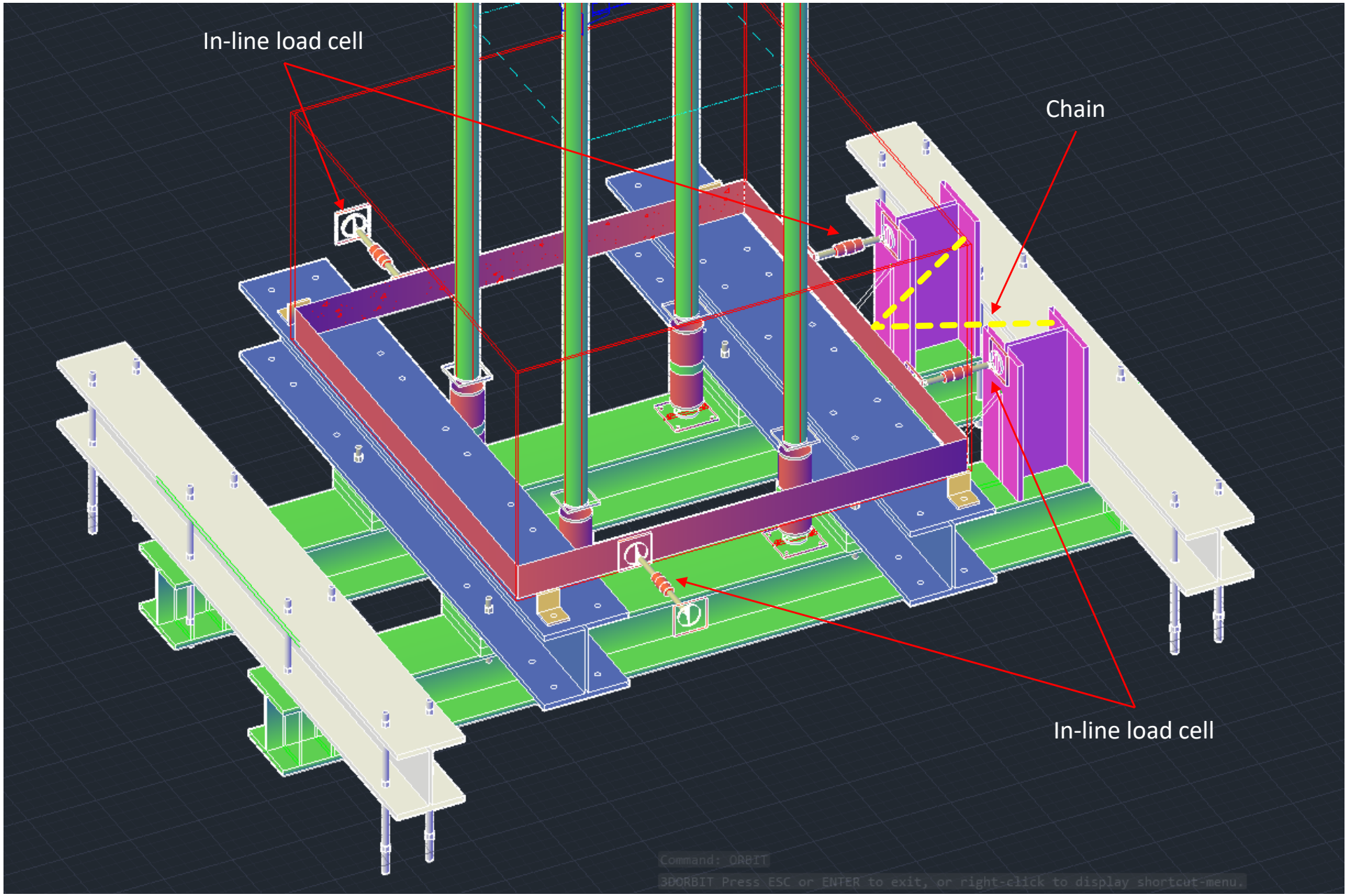

Step 7: Installation of in-line load cells (concrete slab shown)

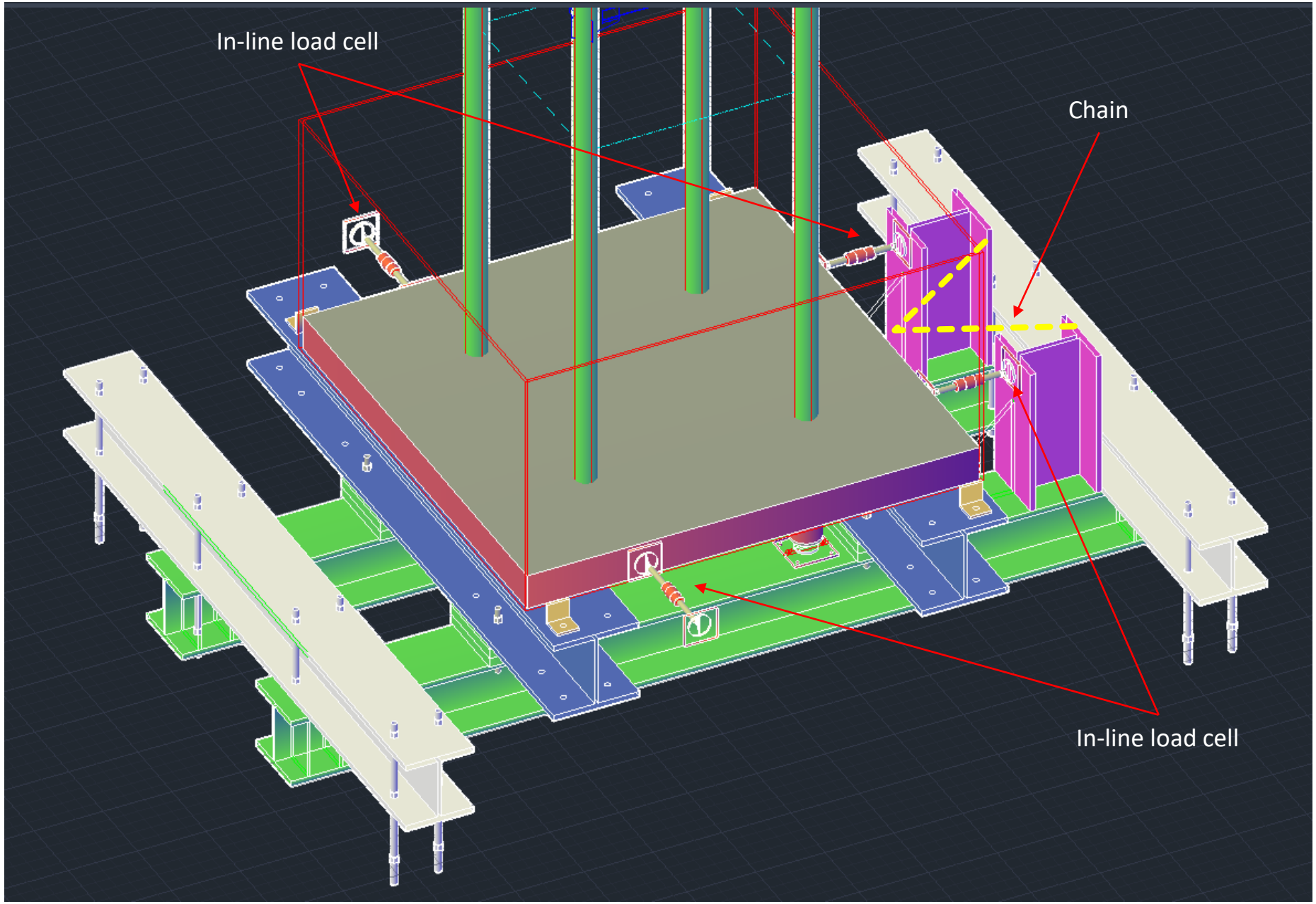

Step 7: Installation of in-line load cells (top view, concrete slab shown)

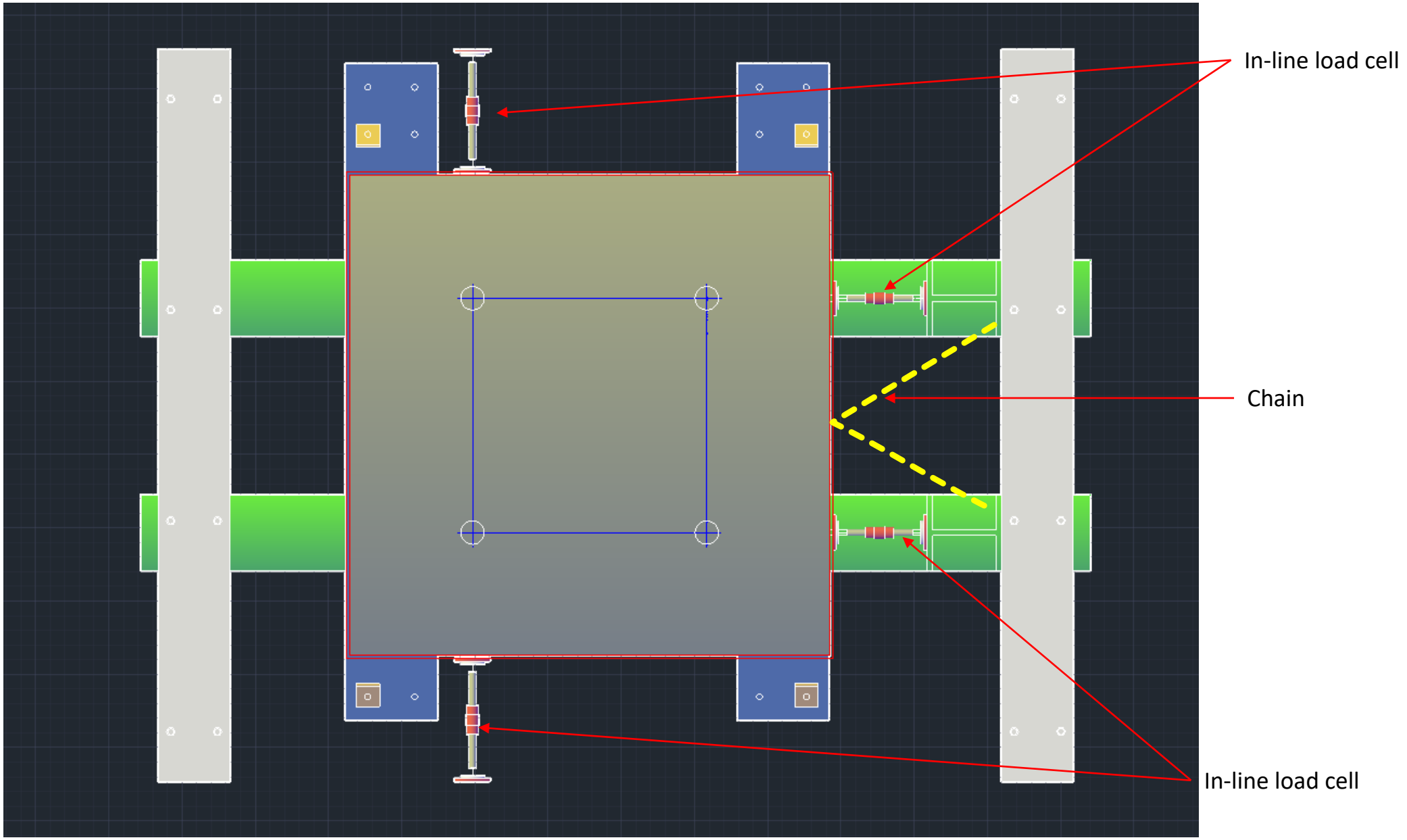

Step 7: Installation of in-line load cells (side view, concrete slab shown)

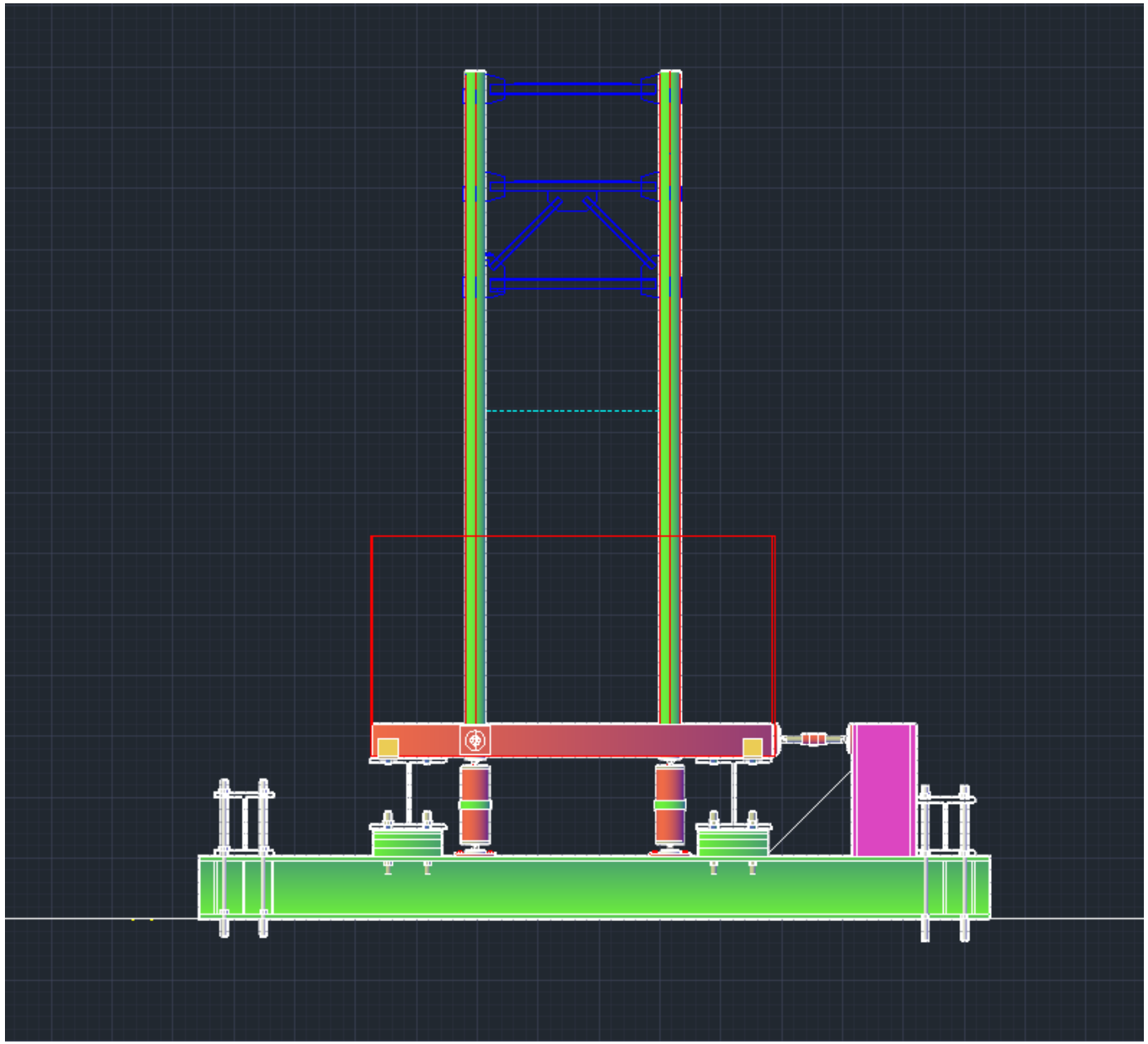

Step 7: Installation of in-line load cells (side view, concrete slab and panels shown)

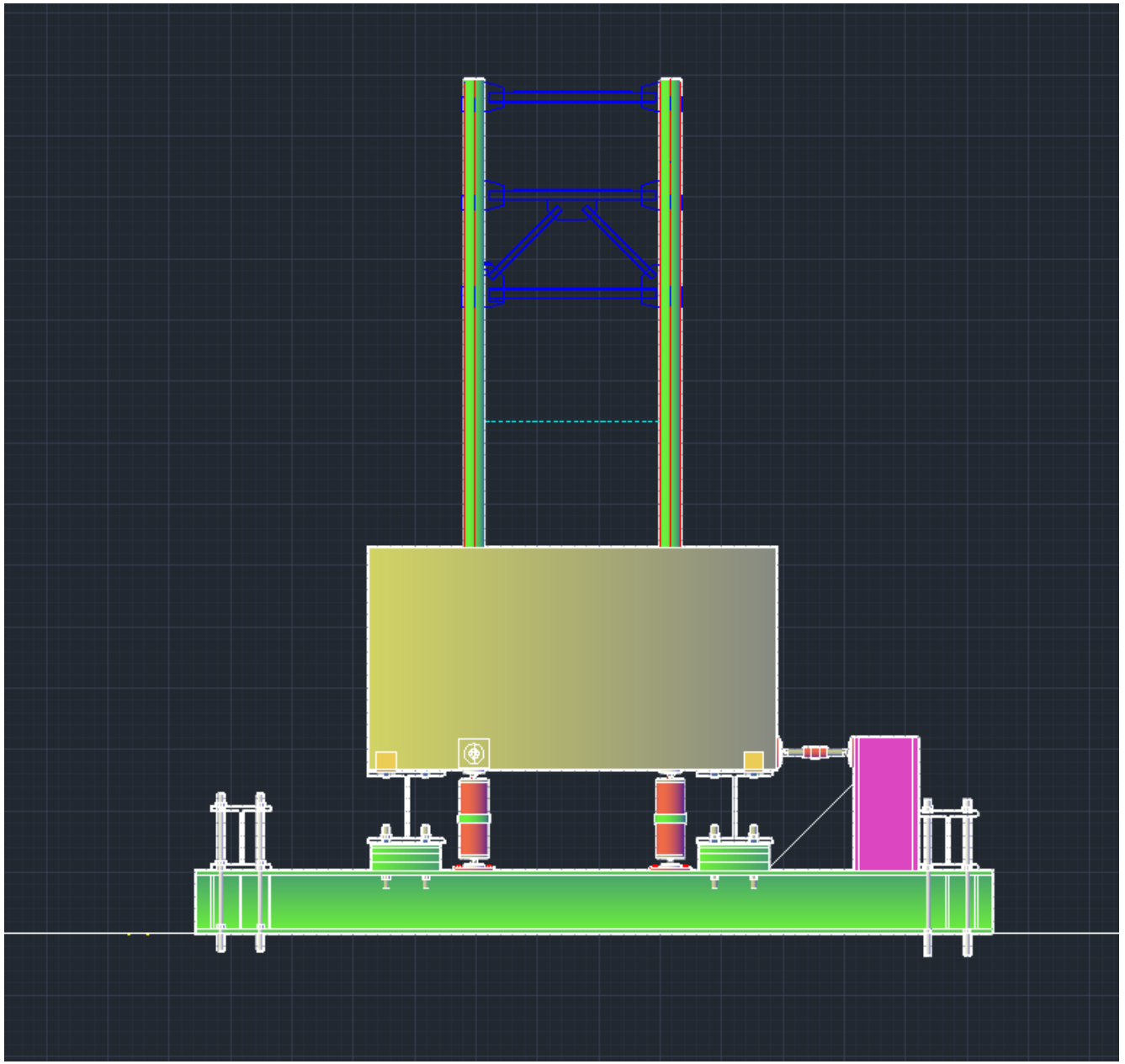

Step 8: Installation of concrete slab

Installation of specimen is complete. The specimen will be resting on the pancake load cells, restrained by the in-line load cells and chain, and supported by the crane. Then personnel can leave the area and the crane can be detached to install the flume's concrete slab.

Procedure:

1. Detach crane from specimen
2. Personnel leave the area
3. Attach the crane to the concrete slab and bring it to Bays 10-11
4. Fix the slab with the standard clips and bolts

Tools and equipment:

1. Concrete slab slings
2. Clips and bolts
3. Ratchet

PPE:

- Gloves
- Safety shoes
- Hard-hat

Personnel:
1 crane operator
1 tech

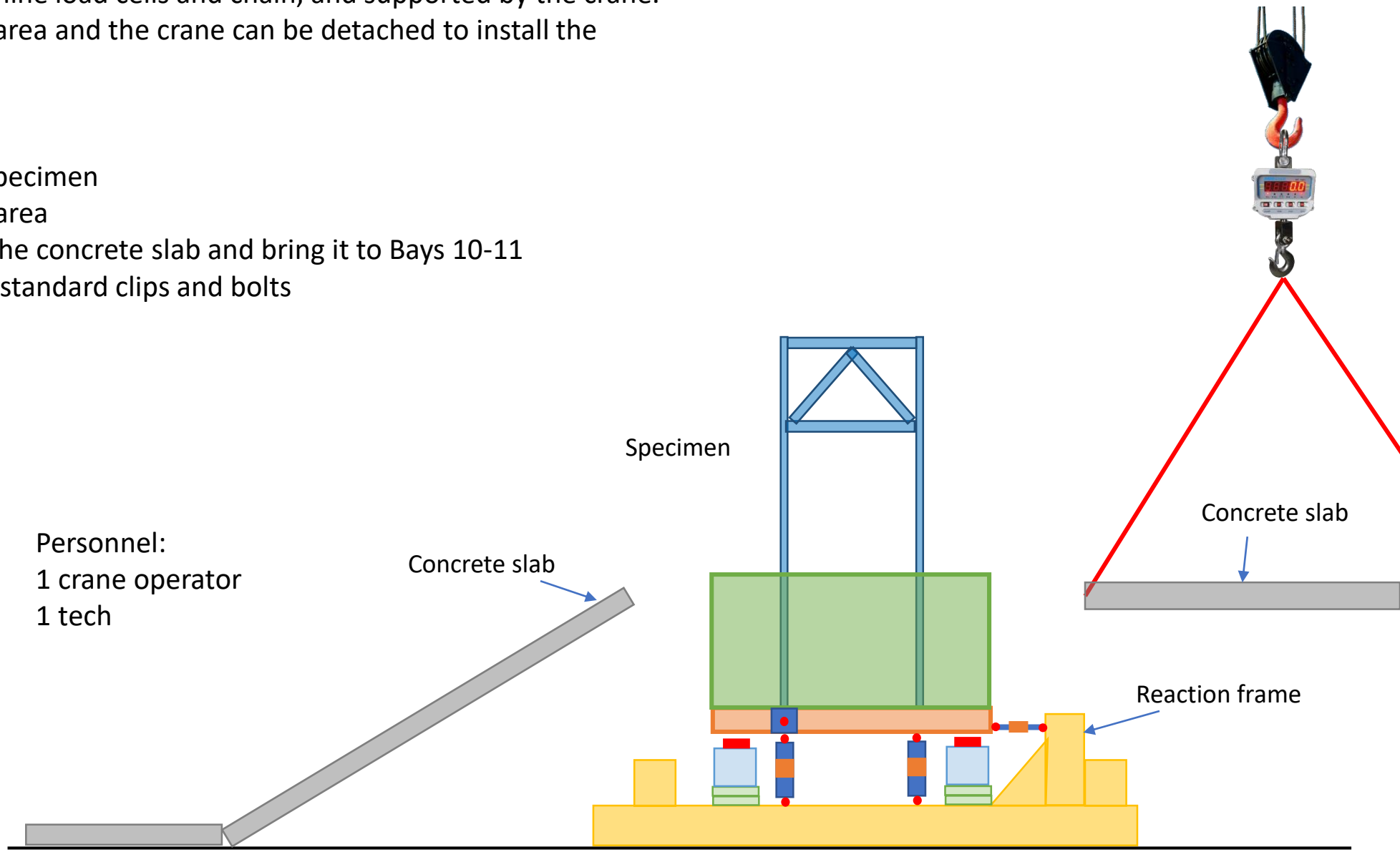

Step 9: Installation of wooden false floor

The wooden false floor is brought to Bays 9-10 to cover the gap between the specimen and the flume.

Procedure:

1. Use the crane to bring the false wooden floor
2. Place is over the existing clips and fix it
3. Disconnect the crane
4. Install the plywood panels covering the false wooden floor

Tools and equipment:

1. Cart
2. Clips, bolts and ratchet

PPE:

- Gloves
- Safety shoes
- Hard-hat

Personnel:

1 crane operator
1 tech

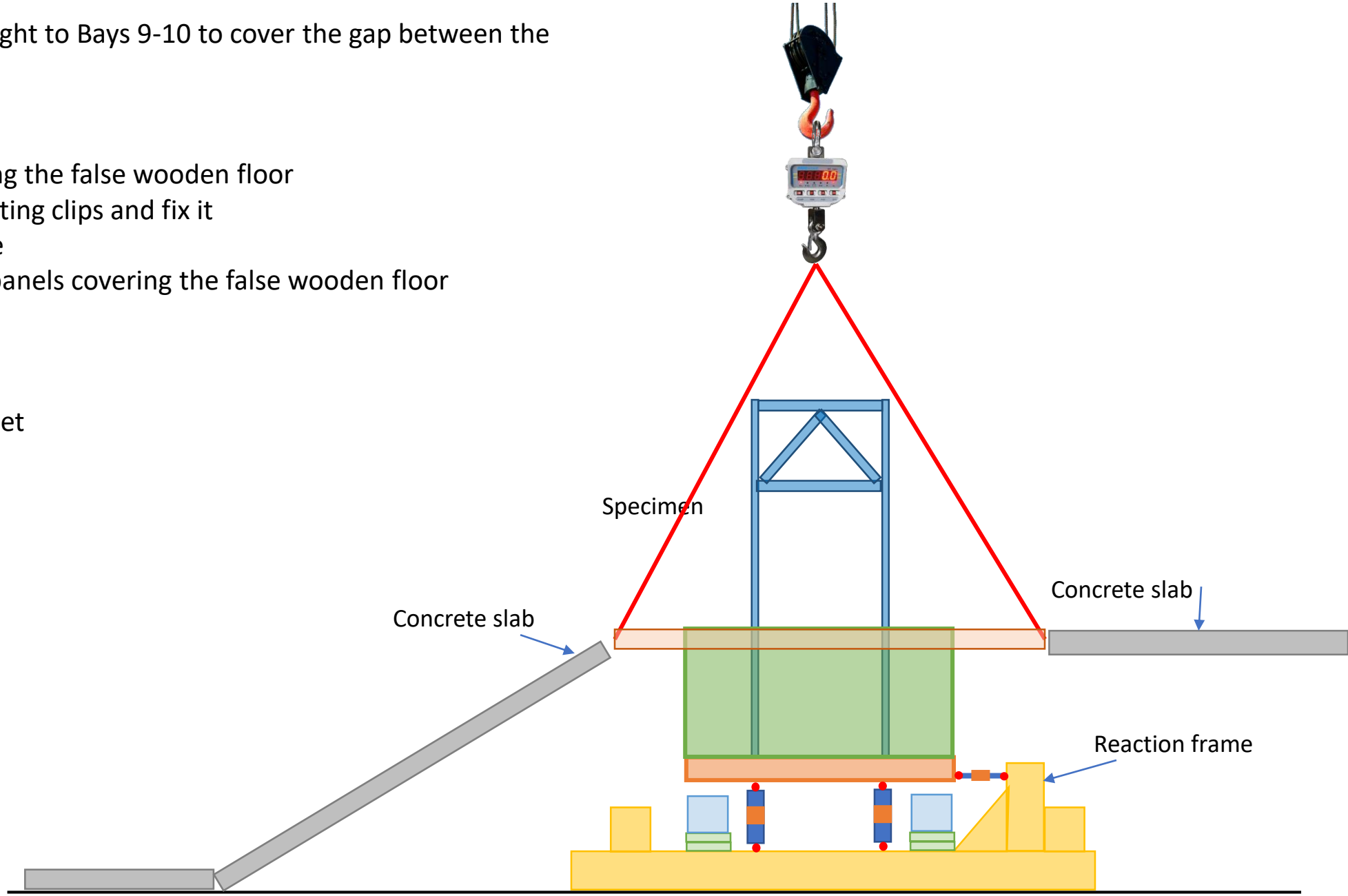

Step 10: Installation of steel cover plates

The steel cover plates closes the top of the box of the specimen. The plates need to be lifted by the crane and bolted to the box ribs.

Procedure:

1. Use the crane to bring the steel plates to Bays 9-10
2. Place the plates covering the box created by the panels
3. Attach the crane to the specimen for safety
4. Bolt the plates to the panel ribs

Tools and equipment:

1. Cart
2. Bolts and ratchet

PPE:

- Gloves
- Safety shoes
- Hard-hat

Personnel:

1 crane operator
1 tech

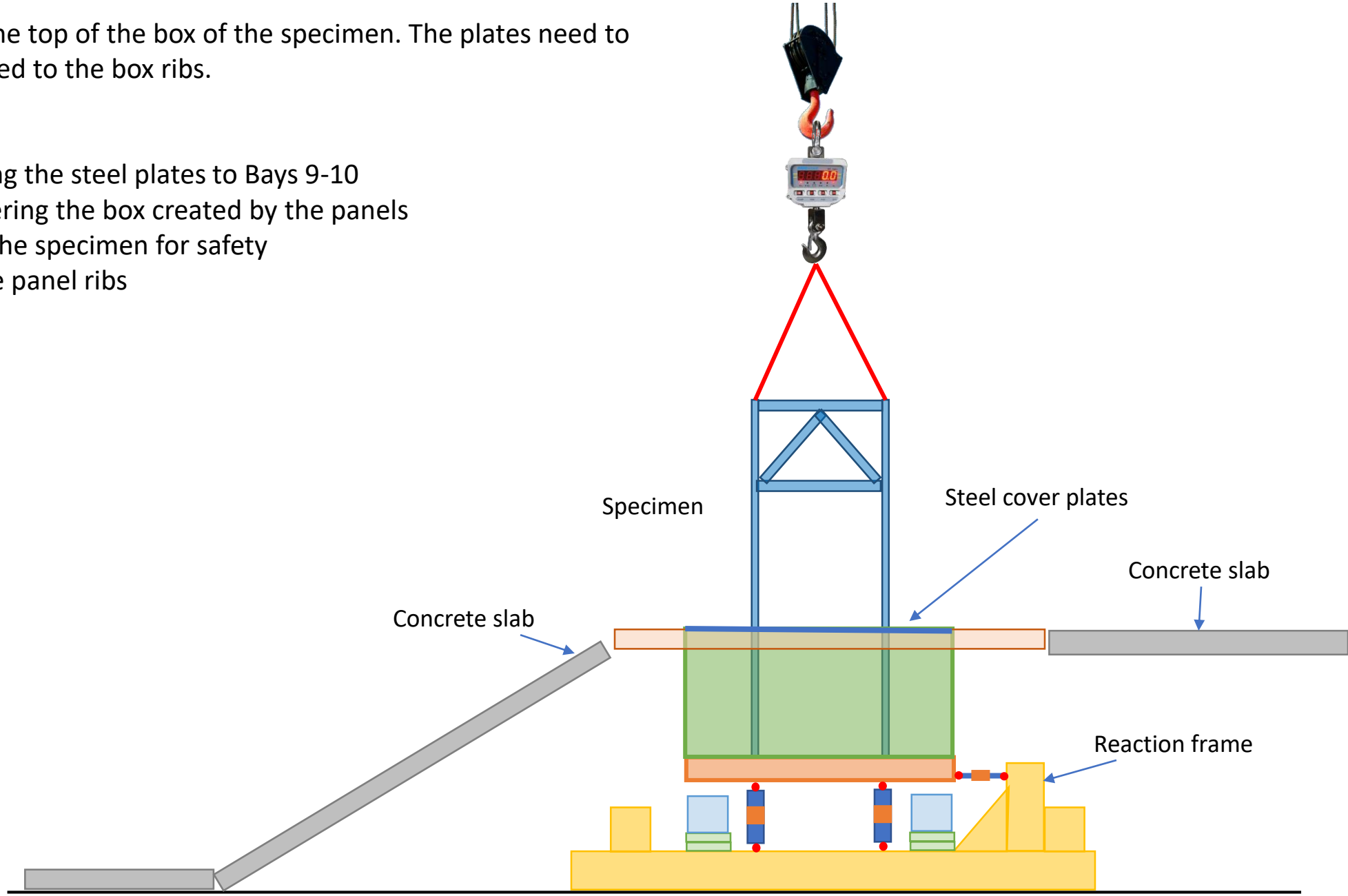

Step 11: Installation of pressure gauges (and connection of strain gauges)

12 pressure gauges will be installed on the columns of the specimen. Each column has 6 pre-existing rounded holes for the pressure gauges. 6 gauges will be installed on the SE column, 2 on the SW column, 1 on the NW column and 3 on the NE column. Strain gauges should also be routed and connected to the amplifiers

Procedure:

1. Bring the pressure gauge and introduce it in the tube
2. Attach a plate for fixing
3. Zip-tie the plate to the column
4. Repeat for all pressure gauges
5. Route the cables to the amplifiers outside

Tools and equipment:

1. 12 pressure gauges
2. Zip-ties
3. Clippers

PPE:

- Gloves
- Safety shoes
- Hard-hat

Personnel:

1 tech

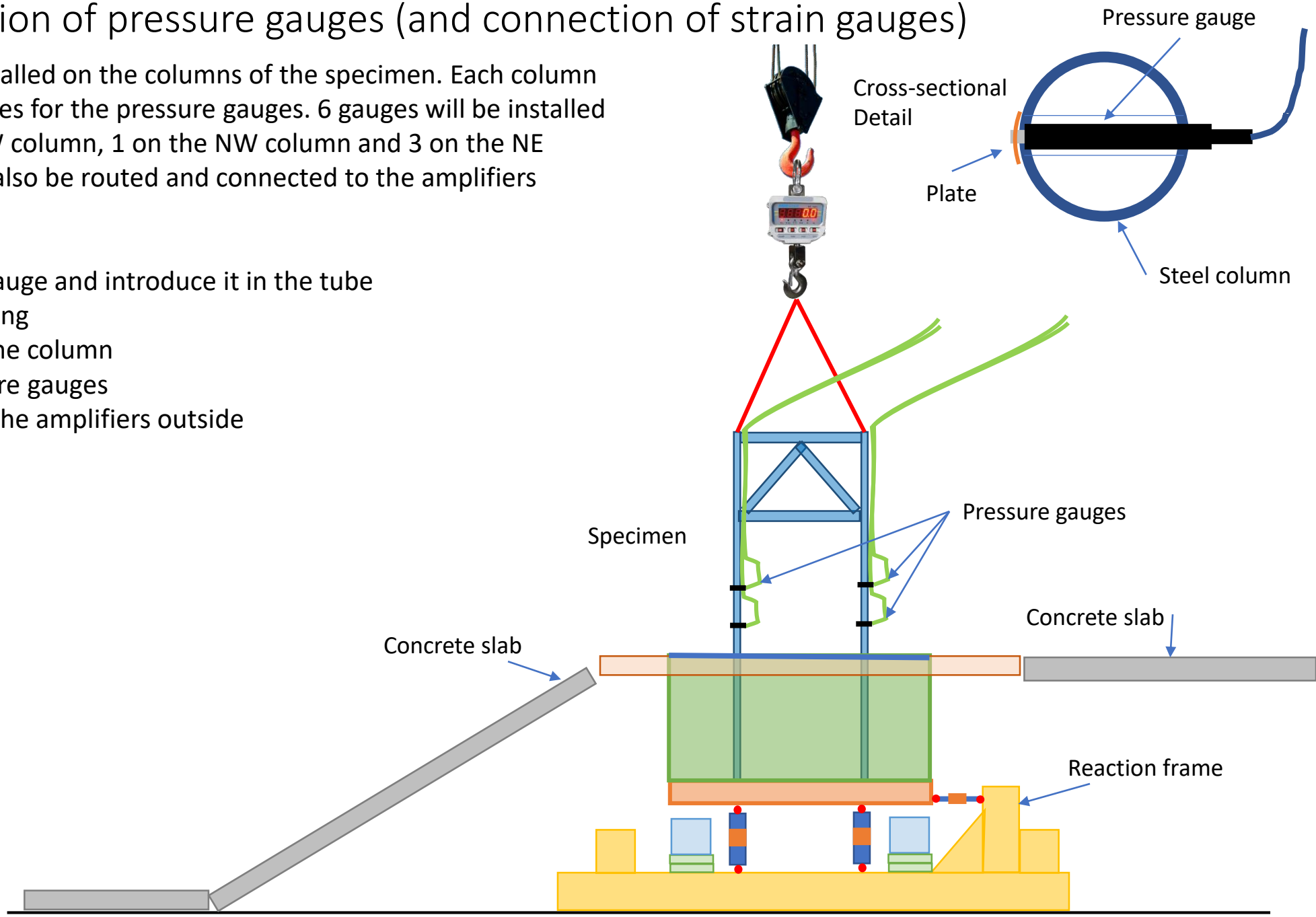

Step 12: Testing

The specimen is ready for testing.

Procedure:

1. Disconnect crane from specimen
2. Fill the flume
3. Perform experiments

PPE:

- Gloves
- Safety shoes
- Hard-hat

Personnel:

1 tech

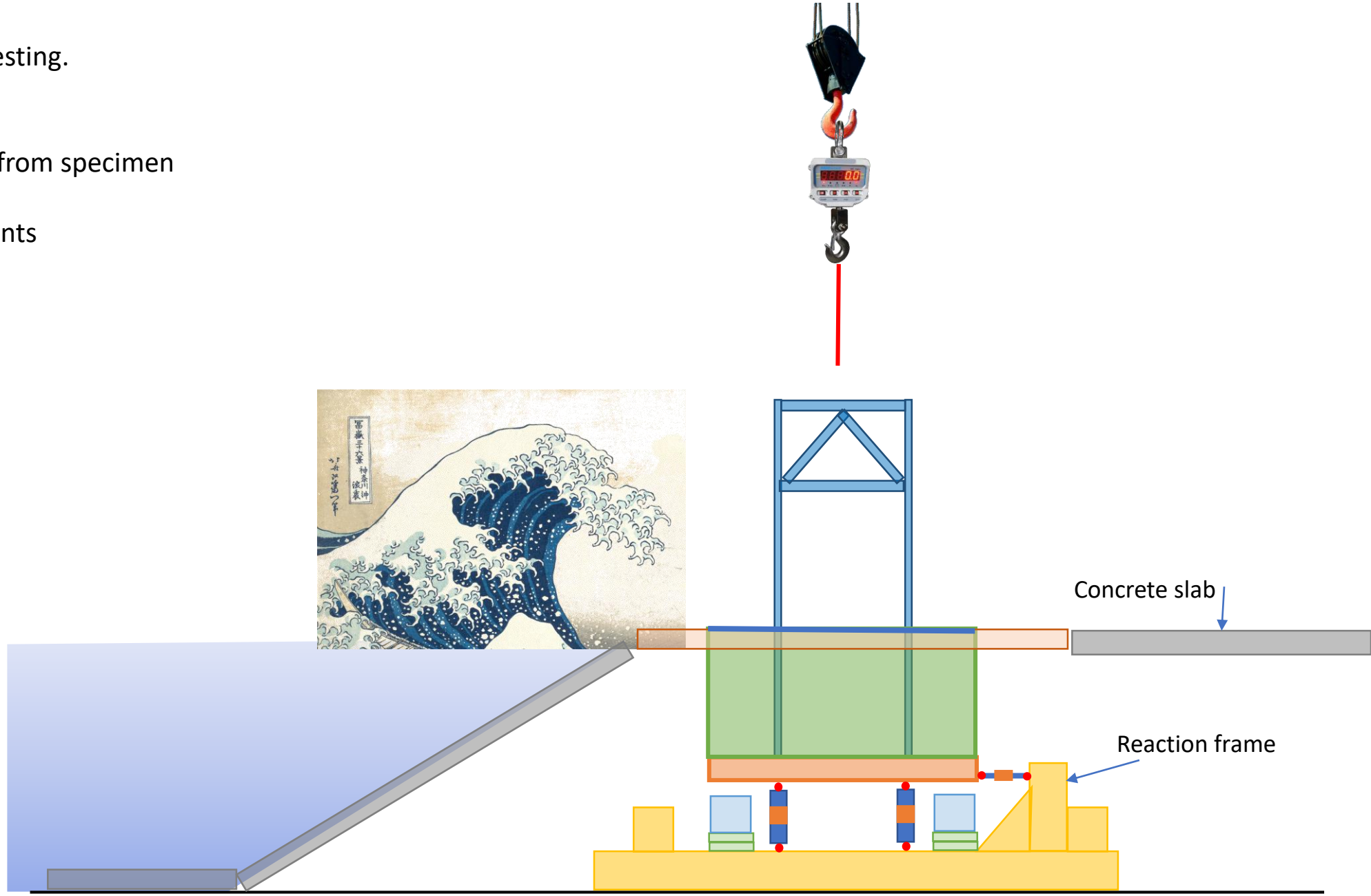

Appendix D

MATLAB FUNCTIONS FOR CALCULATING PILE LOADS FROM STRAIN

This appendix includes the MATLAB functions used for calculating pile loads from the strain gauges.

Table of Contents


```
function [axialForce,Moment] = axialMomentfromStrain(eps1,eps2)

%UNTITLED Summary of this function goes here
%   Detailed explanation goes here
```

Materials

assuming steel does not yield, concrete does not crack

```
Esteel = 29000000; % psi
fc = 3500; %psi
Ec = 57000*sqrt(fc); %psi
```

Geometry

```
Diam = 4; %in
thick = 0.226; %in

ro = Diam/2; %in
ri = ro - thick; %in

numLayers = 100;
layerthick = Diam/numLayers; %in
```

Calculations

```
c = Diam * eps1 / (eps1 - eps2);
phi = eps1/c;

strains = eps1 - phi*[1:1:numLayers]*layerthick;

areas = ones(numLayers,2);
stress = ones(numLayers,1);
for ii = 1:numLayers
    layerdepth = ii * layerthick;
    if layerdepth < thick || layerdepth > Diam - thick
        concwidth = 0;
        %stress(ii) = strains(ii)*Esteel;
    else
        concwidth = 2 * sqrt(ri^2 - abs(Diam/2 - layerdepth)^2);
        %stress(ii) = strains(ii) * Ec;
    end
```

```
    steelwidth = 2*sqrt(ro^2 - abs(Diam/2 - layerdepth)^2) -
 concwidth;
    areas(ii,1) = concwidth*layerthick;
    areas(ii,2) = steelwidth*layerthick;
end

layerforce = strains * Esteel .* areas(:,2)' + strains * Ec .*
 areas(:,1)';



%axialForce = length(layerforce);
axialForce = sum(layerforce); %pounds
%Moment = length([layerthick:layerthick:Diam]);
Moment = sum(layerforce .* [layerthick:layerthick:Diam]); % pound-inch

Not enough input arguments.

Error in axialMomentfromStrain (line 23)
c = Diam * eps1 / (eps1 - eps2);

end
```

Published with MATLAB® R2020b

```
function
 [Shearsoil,Shearwave,shearA1,shearA2,shearB1,shearB2,momentA1,momentA2,momentB1,m
 = strainShear(strainin)

eps = zeros(24,1);

h = figure('units','inch','position',[0,0,6,6]);
colororder({'k','k'})
t = tiledlayout(2,2);
ylabel(t, 'Vertical Force from Column Strain')
xlabel(t, 'Time, s', 'fontName','Times')
hold on
grid on
for trial = 1:length(strainin{1})
    time = [0:1/100:(length(strainin{1}{trial})-1)/100];
   for inst = 1:length(strainin{1}{trial})
       for gauge = 1:24
          eps(gauge) = strainin{gauge}{trial}(inst)*(10^-6);
       end
       [axialA1{1}{trial}(inst), momentA1{1}{trial}(inst)] =
 axialMomentfromStrain(eps(1),eps(2));
       [axialA1{2}{trial}(inst), momentA1{2}{trial}(inst)] =
 axialMomentfromStrain(eps(3),eps(4));
       [axialA1{3}{trial}(inst), momentA1{3}{trial}(inst)] =
 axialMomentfromStrain(eps(5),eps(6));

       [axialA2{1}{trial}(inst), momentA2{1}{trial}(inst)] =
 axialMomentfromStrain(eps(7),eps(8));
       [axialA2{2}{trial}(inst), momentA2{2}{trial}(inst)] =
 axialMomentfromStrain(eps(9),eps(10));
       [axialA2{3}{trial}(inst), momentA2{3}{trial}(inst)] =
 axialMomentfromStrain(eps(11),eps(12));

       [axialB1{1}{trial}(inst), momentB1{1}{trial}(inst)] =
 axialMomentfromStrain(eps(13),eps(14));
       [axialB1{2}{trial}(inst), momentB1{2}{trial}(inst)] =
 axialMomentfromStrain(eps(15),eps(16));
       [axialB1{3}{trial}(inst), momentB1{3}{trial}(inst)] =
 axialMomentfromStrain(eps(17),eps(18));

       [axialB2{1}{trial}(inst), momentB2{1}{trial}(inst)] =
 axialMomentfromStrain(eps(19),eps(20));
       [axialB2{2}{trial}(inst), momentB2{2}{trial}(inst)] =
 axialMomentfromStrain(eps(21),eps(22));
       [axialB2{3}{trial}(inst), momentB2{3}{trial}(inst)] =
 axialMomentfromStrain(eps(23),eps(24));

       [shearA1{1}{trial}(inst), shearA1{2}{trial}(inst)]
 = columnShear(momentA1{3}{trial}(inst),momentA1{2}{trial}
(inst),momentA1{1}{trial}(inst));
```

```
      [shearA2{1}{trial}(inst), shearA2{2}{trial}(inst)]
 = columnShear(momentA2{3}{trial}(inst),momentA2{2}{trial}
(inst),momentA2{1}{trial}(inst));
      [shearB1{1}{trial}(inst), shearB1{2}{trial}(inst)]
 = columnShear(momentB1{3}{trial}(inst),momentB1{2}{trial}
(inst),momentB1{1}{trial}(inst));
      [shearB2{1}{trial}(inst), shearB2{2}{trial}(inst)]
 = columnShear(momentB2{3}{trial}(inst),momentB2{2}{trial}
(inst),momentB2{1}{trial}(inst));


   end

   Shearsoil{trial} = shearA1{1}{trial} + shearA2{1}{trial} +
 shearB1{1}{trial} + shearB2{1}{trial};
   Shearwave{trial} = shearA1{2}{trial} + shearA2{2}{trial} +
 shearB1{2}{trial} + shearB2{2}{trial};

%    nexttile(1)
%    grid on
%    hold on
%    forcerange = [-500 500];
%    timerange = [35 40];
%    yyaxis right
%    %plot(time,(Shearsoil{trial}-Shearsoil{trial}(1)),'-+','Color',[1
 182/255 119/255])
%    p(1) = plot(time,axialA1{3}{trial}-axialA1{3}{trial}
(1),':','Color',[73/255 0 146/255]);
%    p(2) = plot(time,axialA1{2}{trial}-axialA1{2}{trial}
(1),'--','Color',[73/255 0 146/255]);
%    ylabel('lbf', 'fontName','Times')
%    ylim(forcerange)
%    xlim(timerange)
%    legend([p(1) p(2)],{'Bottom', 'Water Level'})
%    legend('boxoff')
%    yyaxis left
%    ylabel('kN','fontName','Times')
%    ylim(convforce(forcerange,'lbf','N')/1000)
%
%    nexttile(2)
%    grid on
%    hold on
%    yyaxis right
%    plot(time,axialA2{3}{trial}-axialA2{3}{trial}(1),':','Color',
[73/255 0 146/255])
%    plot(time,axialA2{2}{trial}-axialA2{2}{trial}(1),'--','Color',
[73/255 0 146/255])
%    ylabel('lbf', 'fontName','Times')
%    ylim(forcerange)
%    xlim(timerange)
%    yyaxis left
%    ylabel('kN','fontName','Times')
%    ylim(convforce(forcerange,'lbf','N')/1000)
%
```

```
%     nexttile(3)
%     grid on
%    hold on
%    yyaxis right
%    plot(time,axialB1{3}{trial}-axialB1{3}{trial}(1),':','Color',
[73/255 0 146/255])
%    plot(time,axialB1{2}{trial}-axialB1{2}{trial}(1),'--','Color',
[73/255 0 146/255])
%    ylabel('lbf', 'fontName','Times')
%    ylim(forcerange)
%    xlim(timerange)
%    yyaxis left
%    ylabel('kN','fontName','Times')
%    ylim(convforce(forcerange,'lbf','N')/1000)
%
%     nexttile(4)
%     grid on
%    hold on
%    yyaxis right
%    plot(time,axialB2{3}{trial}-axialB2{3}{trial}(1),':','Color',
[73/255 0 146/255])
%    plot(time,axialB2{2}{trial}-axialB2{2}{trial}(1),'--','Color',
[73/255 0 146/255])
%    ylabel('lbf', 'fontName','Times')
%    ylim(forcerange)
%    xlim(timerange)
%    yyaxis left
%    ylabel('kN','fontName','Times')
%    ylim(convforce(forcerange,'lbf','N')/1000)

end


% ylabel(t, 'Vertical Force from Column Strain')
% xlabel(t, 'Time, s', 'fontName','Times')

% ylabel('Vertical Force from column Strain, kN', 'fontName','Times')
% xlabel('Time, s', 'fontName','Times')
% xlim([35 40])


% set(h, 'PaperUnits','inches')
% set(h,'PaperSize',[6.1 6.1]);
% set(h, 'PaperPosition',[0 0 6 6]);
% set(findall(h,'type','text'),'fontSize',10)
% set(gca, 'fontName','Times')
%
% exportgraphics(h,[name
 'axialForceStrain.pdf'],'ContentType','vector','BackgroundColor','none')
% exportgraphics(h,[name
 'axialForceStrain.png'],'BackgroundColor','none')
```

```
end
```

```
Not enough input arguments.

Error in strainShear (line 12)
for trial = 1:length(strainin{1})
```

Published with MATLAB® R2020b

```
function [Vsoil,Vwave] = columnShear(Mbot,Mmid,Mtop)

dsoil = 37.5; % inch
dwave = 49.5; % inch

Vsoil = (Mbot - Mmid)/dsoil; %pound
Vwave = (Mmid - Mtop)/dwave; %pound

end
```

```
Not enough input arguments.

Error in columnShear (line 6)
Vsoil = (Mbot - Mmid)/dsoil; %pound
```

Published with MATLAB® R2020b

```
function compareforces(LCV, strainV, OFV,name)
% function compareforces(OFbaseshears)

LCV = -1*LCV;
strainV = -1*strainV;
time = 0:1/100:(length(LCV)-1)/100;
ofplot = zeros(1,length(time));
[strainmax, strainmaxidx] = max(strainV);
[OFmax, OFmaxidx] = max(OFV);
dif = strainmaxidx - OFmaxidx;
ofplot(dif+1:length(OFV)+dif) = OFV(1:end);

figure
colororder({'k','k'})
hold on

yyaxis left

p(3) = plot(time,ofplot/1000,'o-','Color',[36/255 1
 36/255],'Linewidth',1.5);



Vlimit = [-0.5 1.05*OFmax/1000];
ylim(Vlimit)
xlim([35 40])
grid on

ylabel('Base shear from Wave, kN')
xlabel('time, s')

yyaxis right
p(1) = plot(time,LCV,'-o','Color',[182/255 109/255
 1],'LineWidth',1.5);
p(2) = plot(time,strainV/1000-strainV(1)/1000,'--o','Color',[1 182/255
 119/255],'Linewidth',1.5);

ylim(convforce(Vlimit*1000,'N','lbf')/1000)
xlim([35 40])

ylabel('Base shear from Wave, Kip')

legend(p,{'Load Cells';'Strain in Piles';'OpenFOAM'})
legend boxoff

% figure
% colororder({'k','k'})
% hold on
%
% yyaxis left
%
```

```
% plot(0:1/100:(length(OFbaseshears(:,8))-1)/100,-
OFbaseshears(:,8)/1000,'-d','Color',[36/255 1 36/255],'Linewidth',1.5)
% ylabel('Force, kN','fontName','Times')
% xlabel('Simulation time, s','fontName','Times')
% xlim([0 5])
% ylim(convforce([-8500 100],'lbf','N')/1000)
% grid on
%
% yyaxis right
% ylabel('Force, kip','fontName','Times')
% ylim([-8.5 0.1])
% set(gca, 'fontName','Times')


end
```

```
Not enough input arguments.

Error in compareforces (line 4)
LCV = -1*LCV;
```

Published with MATLAB® R2020b

```
%clear all

name{1} = 'CFST_NS_E_100.mat';
name{2} = 'CFST_NS_H_100.mat';
name{3} = 'CFST_NS_E_140.mat';
name{4} = 'CFST_NS_H_140.mat';
name{5} = 'CFST_FS_E_100.mat';
name{6} = 'CFST_FS_E_140.mat';

for ii = 1:1
cd E:\kpsulliv\Research\Matlab\002_RawData\002_Experiment_CFT
load(name{ii})
cd E:\kpsulliv\Research\Matlab\003_Processed\002_Experiment_CFT
[Shearsoil,Shearwave,shearA1,shearA2,shearB1,shearB2,momentA1,momentA2,momentB1,mo
 = strainShear(strain);

lcbase = loadCells{7}{1}+loadCells{8}{1}-loadCells{7}{1}(1)-
loadCells{8}{1}(1);
compareforces(lcbase,Shearsoil{1},OF_NS_100,name{ii})

% h = figure;
% colororder({'k','k'})
% hold on
% grid on
%
% for trial = 1:length(loadCells{1})
%     time = [0:1/100:(length(loadCells{1}{trial})-1)/100];
%     yyaxis right
%     plot(time,(loadCells{7}{trial}-loadCells{7}{trial}
(1))+(loadCells{8}{trial}-loadCells{8}{trial}(1)),'-x','Color',
[182/255 109/255 255/255]);
% end
%
% timelim = [35 40];
% xlim(timelim)
% xlabel('Time, s','fontName','Times')
% yyaxis right
% ylabel('Force, kip','fontName','Times')
% forclim = [-5 0.1];
% ylim(forclim)
% yyaxis left
% ylabel('Force, kN','fontName','Times')
% ylim(convforce(forclim*1000,'lbf','N')/1000)
% set(gca, 'fontName','Times')
% set(findall(h,'type','text'),'fontSize',10)
%
% exportgraphics(h,[name{ii}
 'baseshearLC.pdf'],'ContentType','vector','BackgroundColor','none')
% exportgraphics(h,[name{ii}
 'baseshearLC.png'],'BackgroundColor','none')
```

```
end
```

```
Brace indexing is not supported for variables of this type.

Error in plotstrains (line 17)
lcbase = loadCells{7}{1}+loadCells{8}{1}-loadCells{7}{1}(1)-
loadCells{8}{1}(1);
```

Published with MATLAB® R2020b

Appendix E

PLOTS VERIFYING STRAIN GAUGE OUTPUTS

This appendix includes figures of all the strain data for the experiment conditions tested in this thesis. These figures are for completeness of the data and provided valuable validation checking for when strain gauges broke or became damaged.

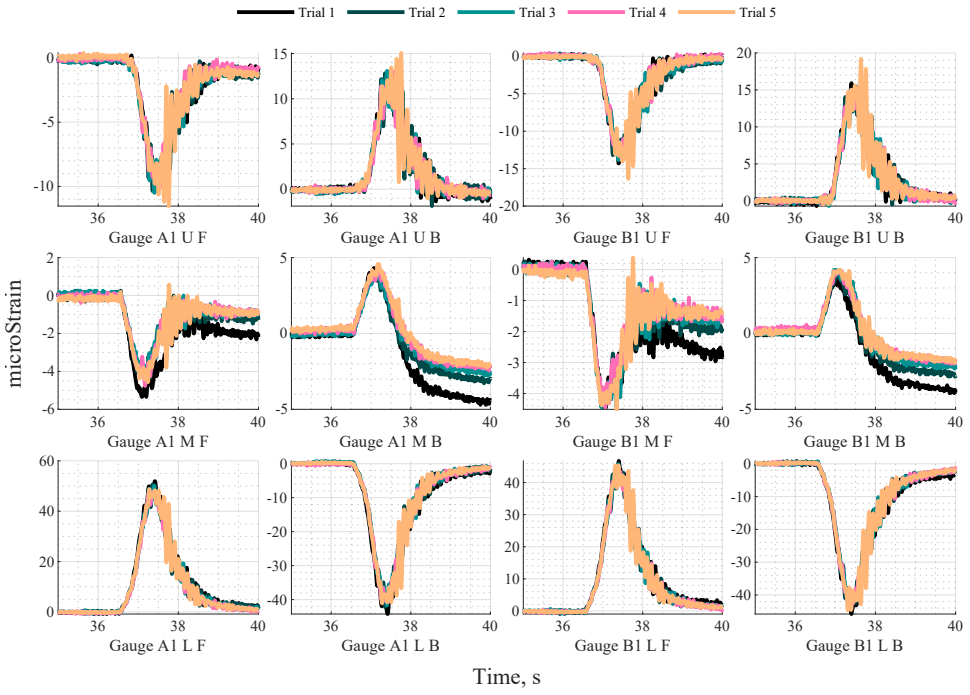

Figure E.1: Strain gauges on front columns CFST_NS_E_100

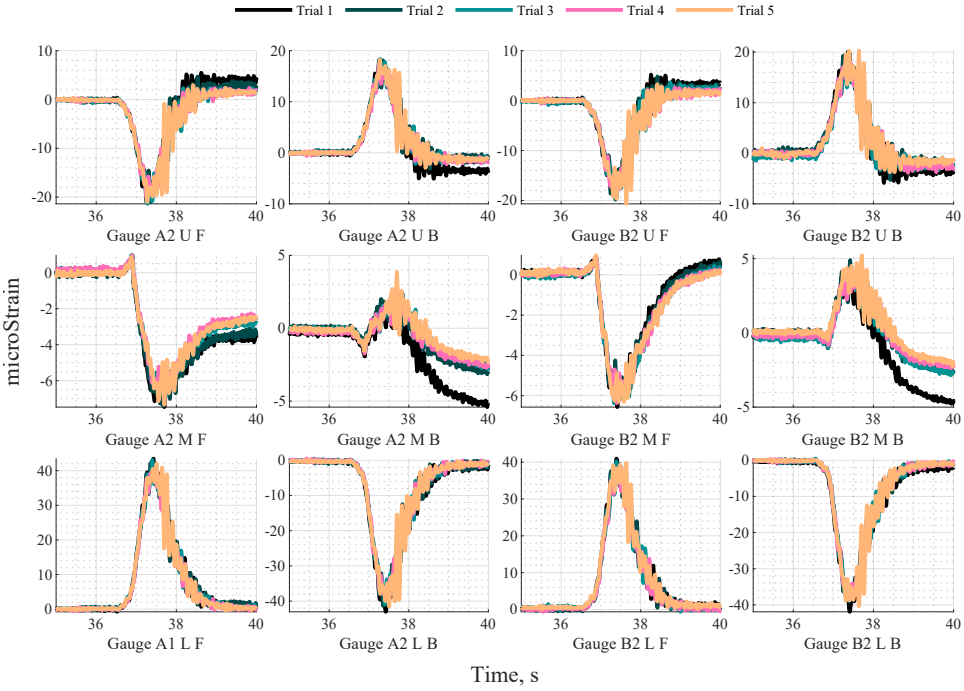

Figure E.2: Strain gauges on Back columns CFST_NS_E_100

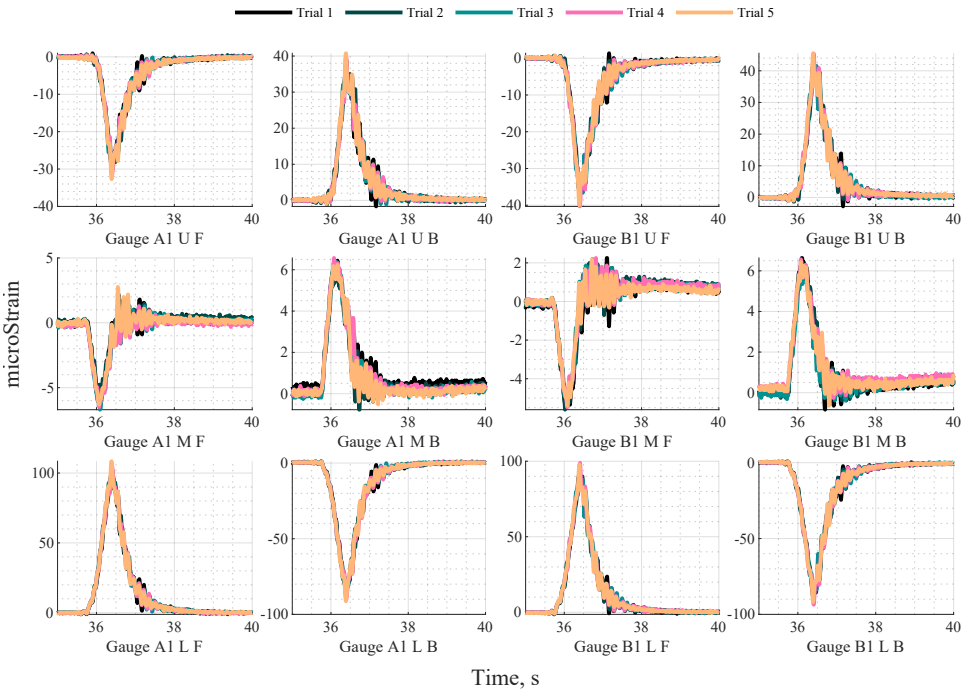

Figure E.3: Strain gauges on front columns CFST_NS_E_140

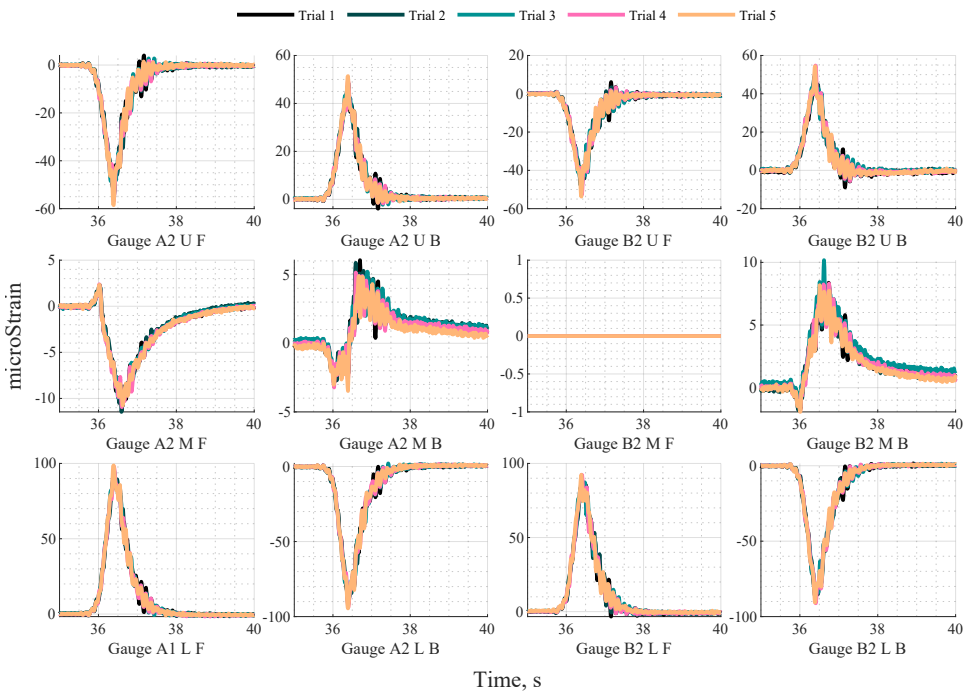

Figure E.4: Strain gauges on Back columns CFST_NS_E_140

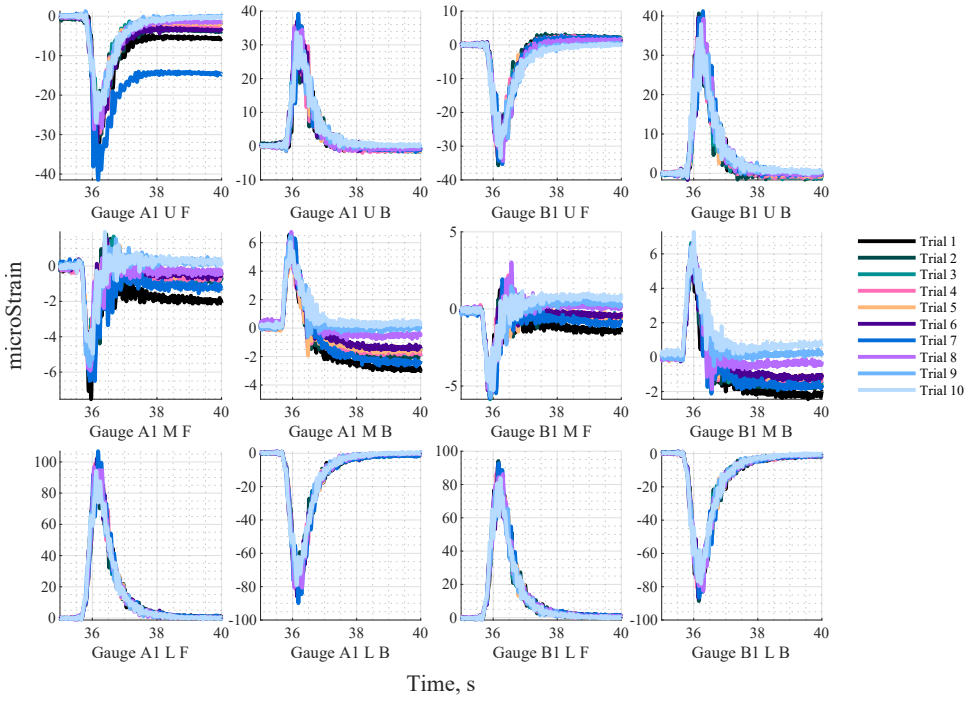

Figure E.5: Strain gauges on front columns CFST_NS_E_145

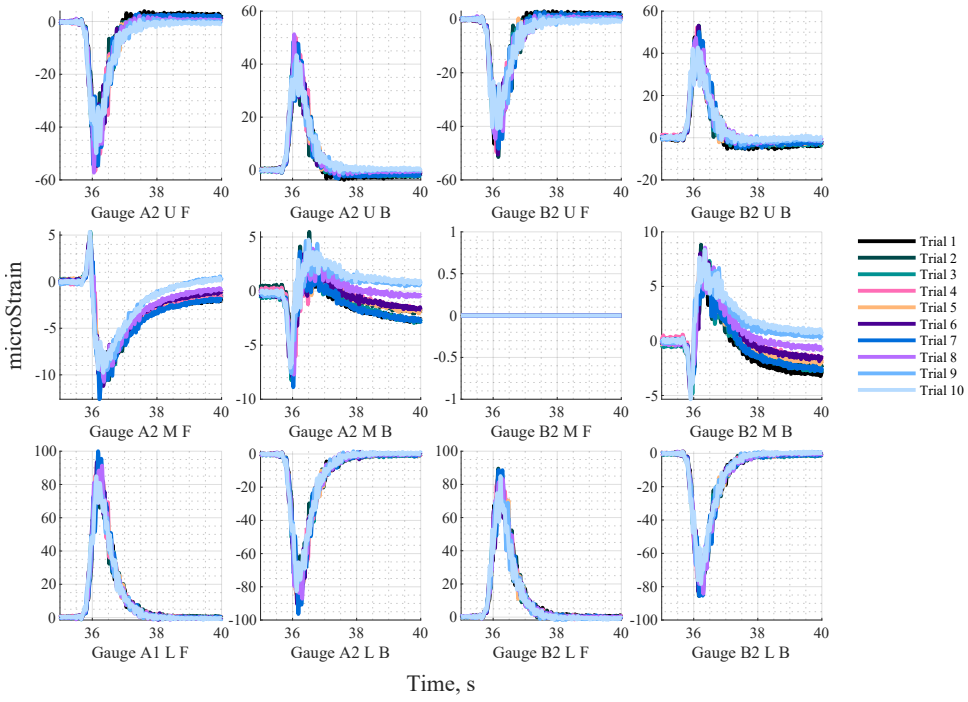

Figure E.6: Strain gauges on Back columns CFST_NS_E_145

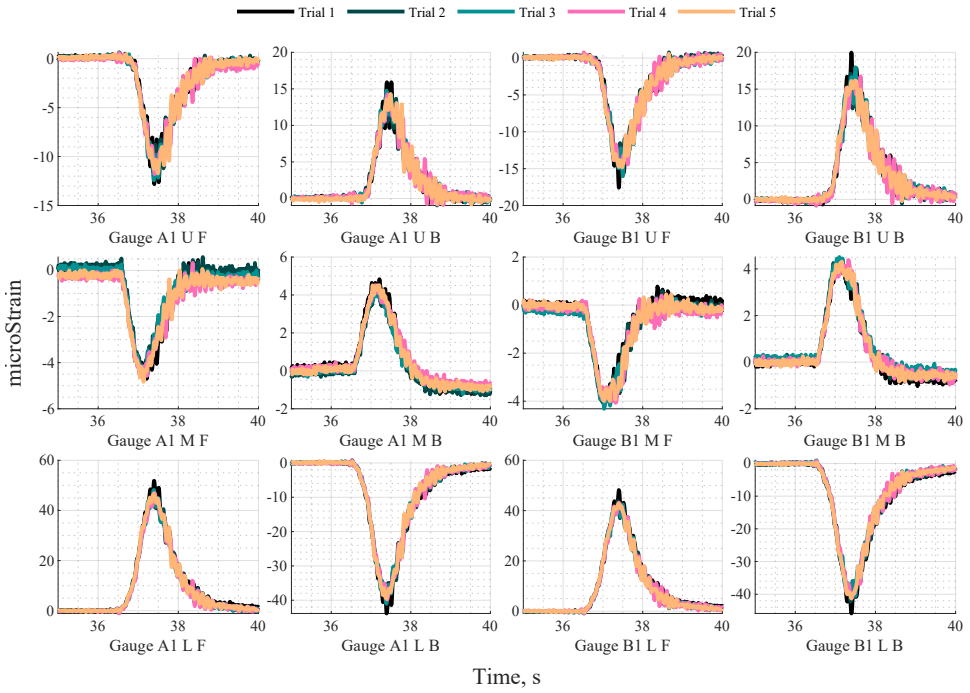

Figure E.7: Strain gauges on front columns CFST_NS_H_100

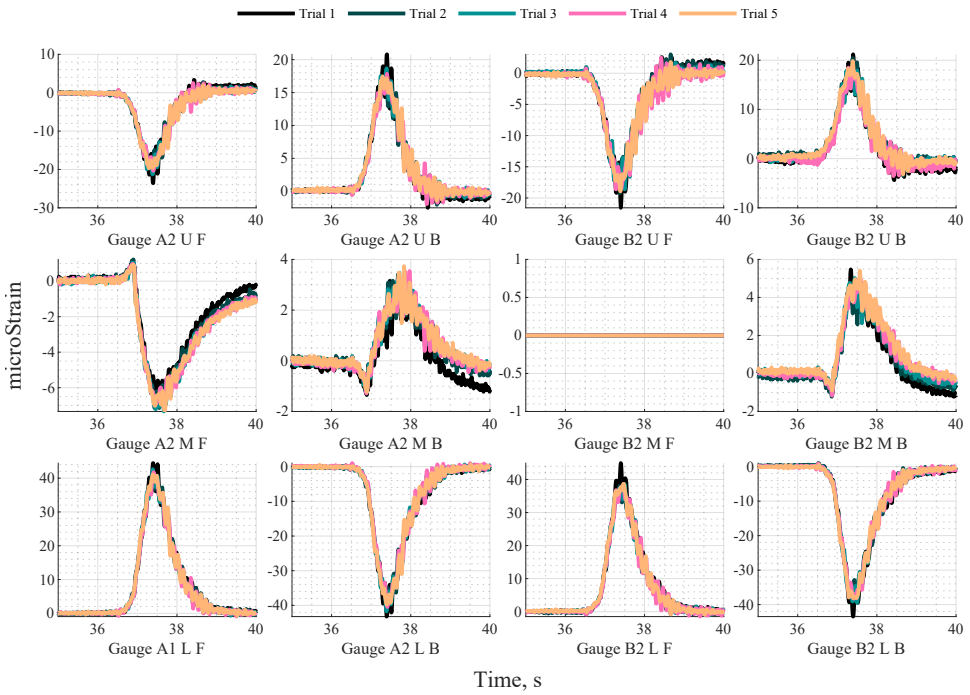

Figure E.8: Strain gauges on Back columns CFST_NS_H_100

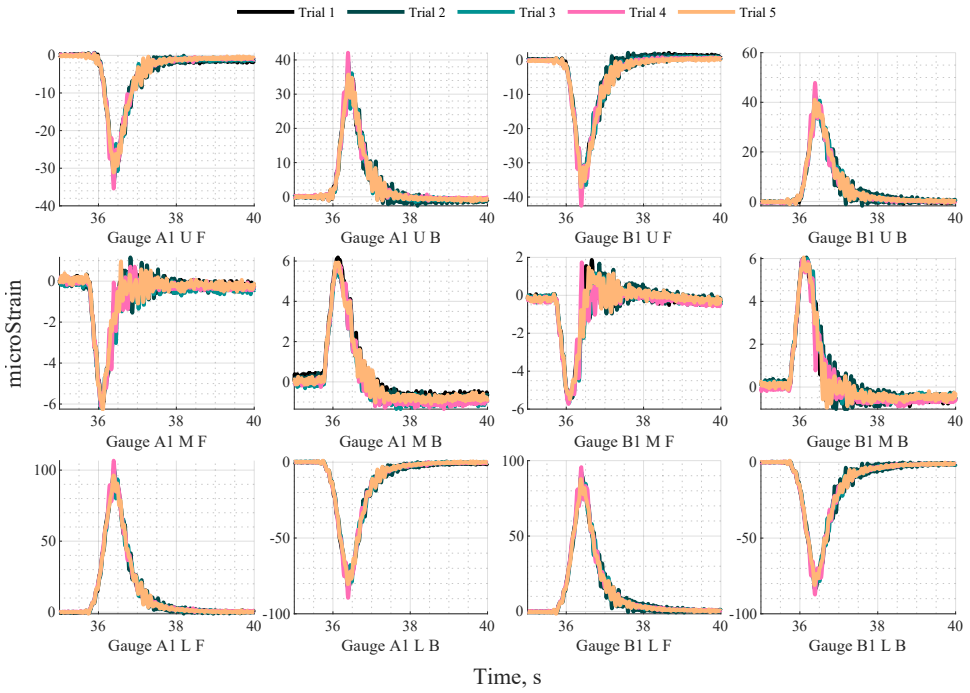

Figure E.9: Strain gauges on front columns CFST_NS_H_140

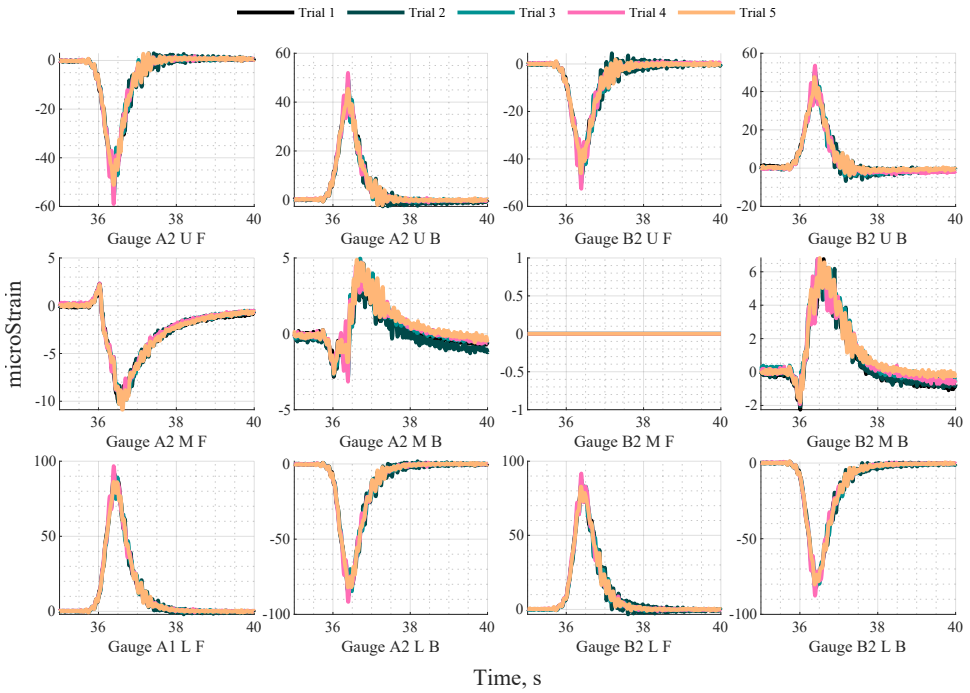

Figure E.10: Strain gauges on Back columns CFST_NS_H_140

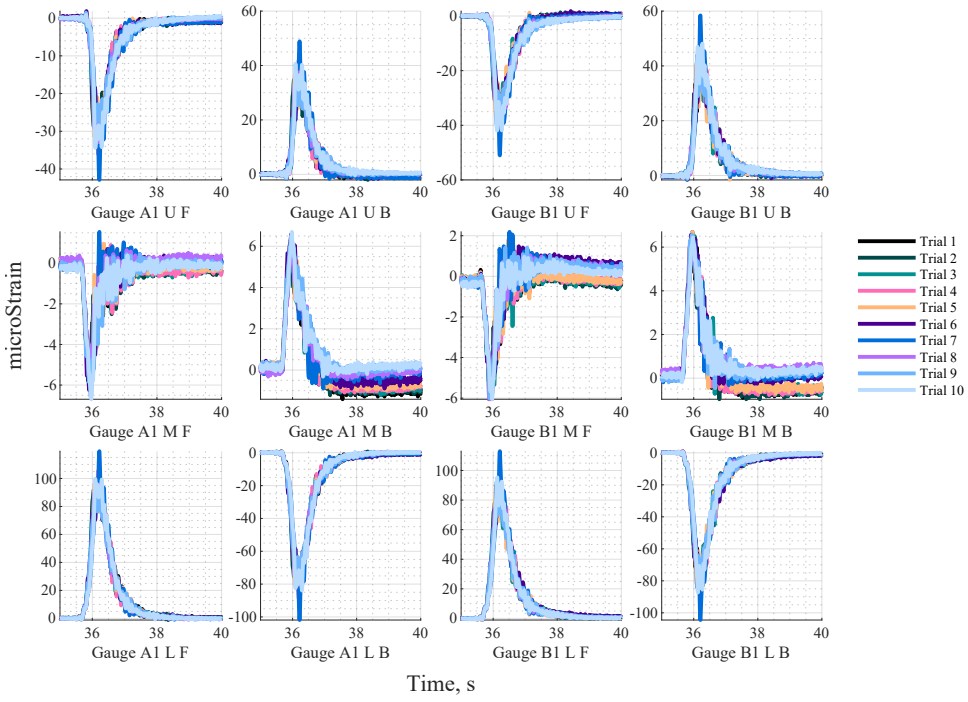

Figure E.11: Strain gauges on front columns CFST_NS_H_145

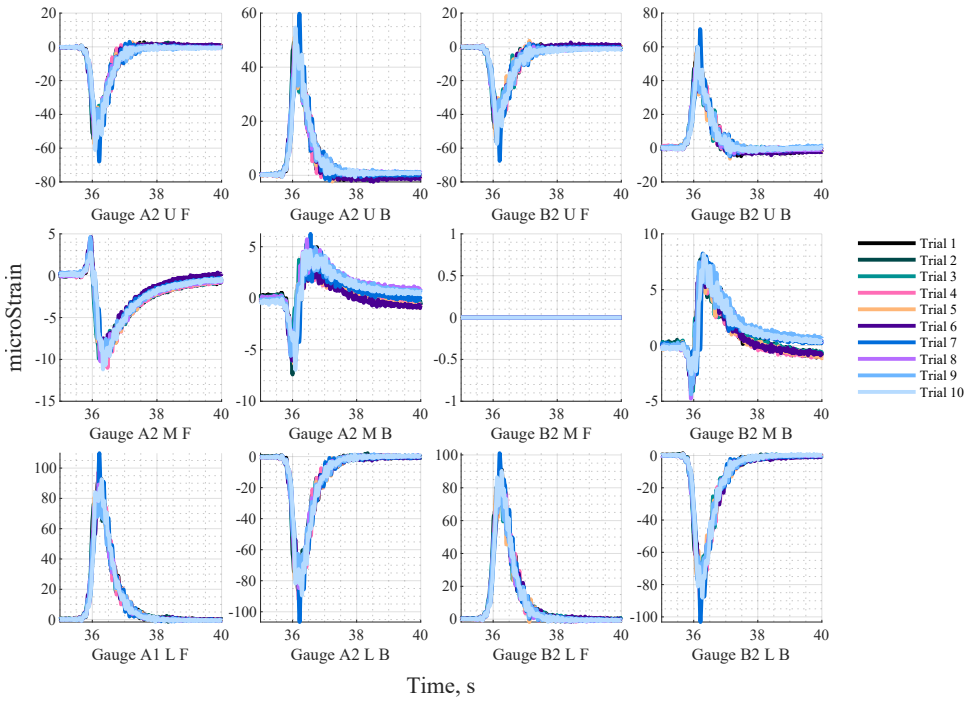

Figure E.12: Strain gauges on Back columns CFST_NS_H_145

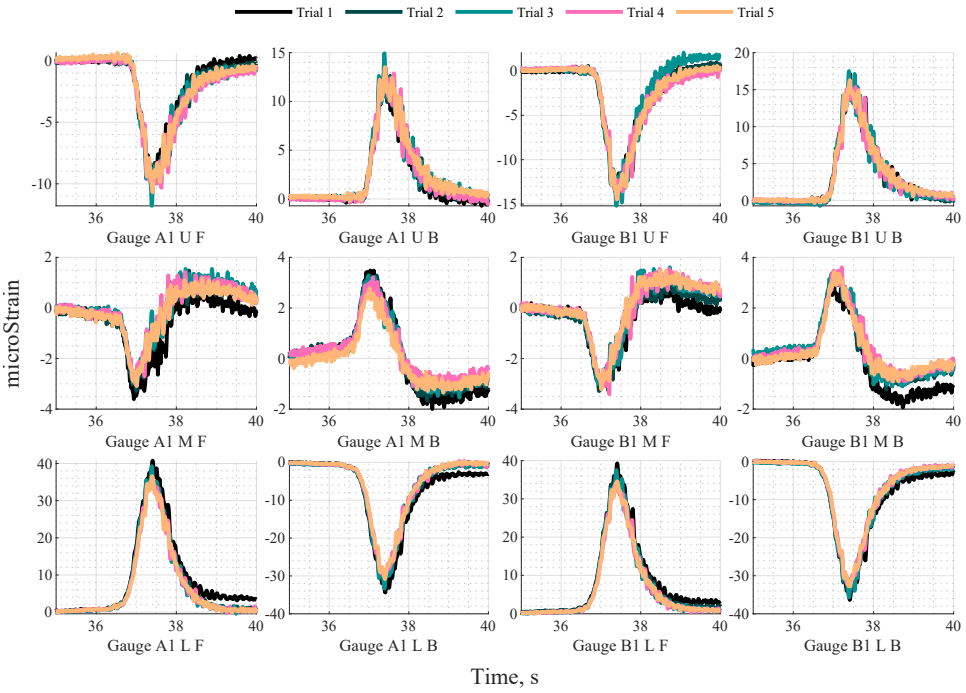

Figure E.13: Strain gauges on front columns CFST_NS_F_100

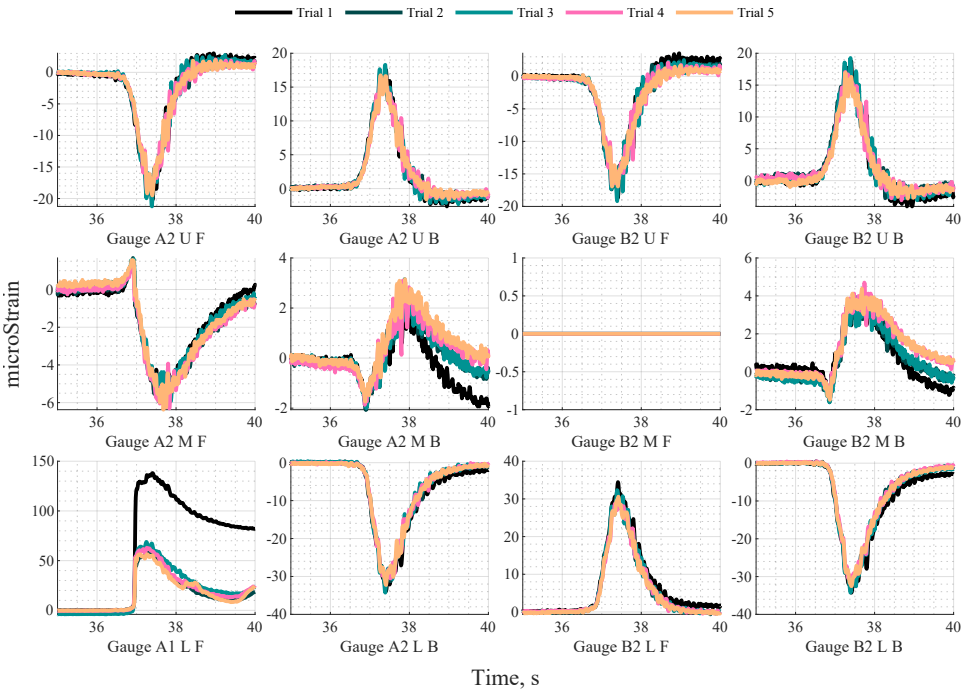

Figure E.14: Strain gauges on Back columns CFST_NS_F_100

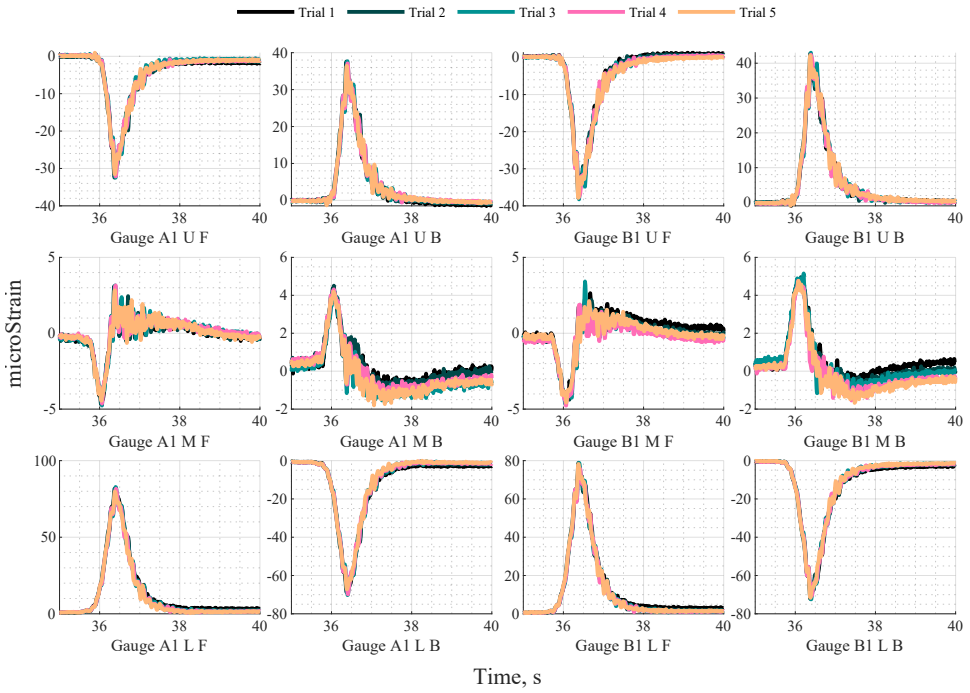

Figure E.15: Strain gauges on front columns CFST_NS_F_140

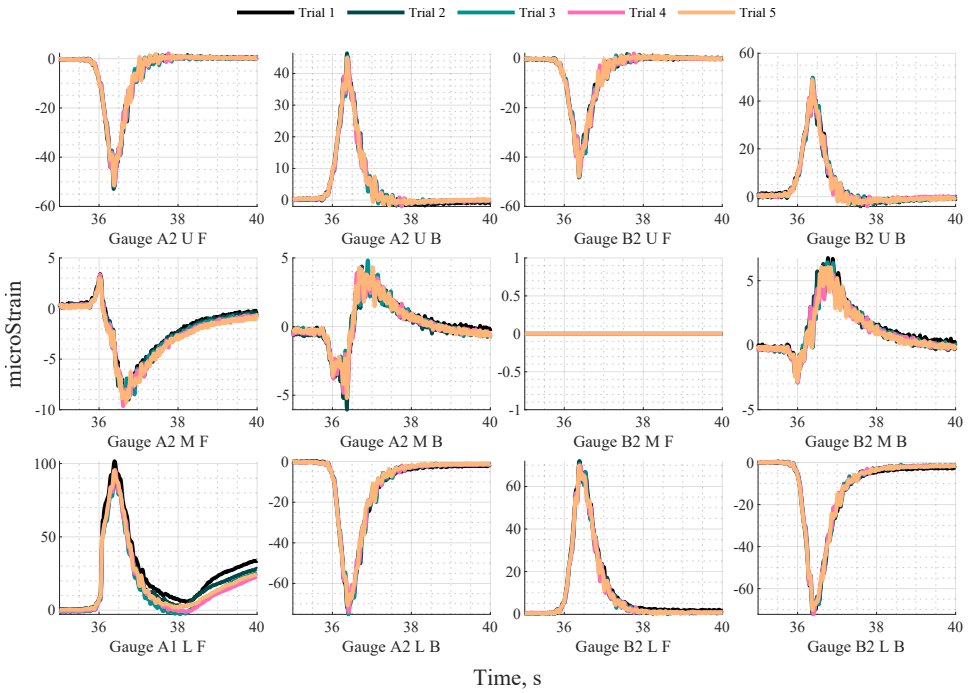

Figure E.16: Strain gauges on Back columns CFST_NS_F_140

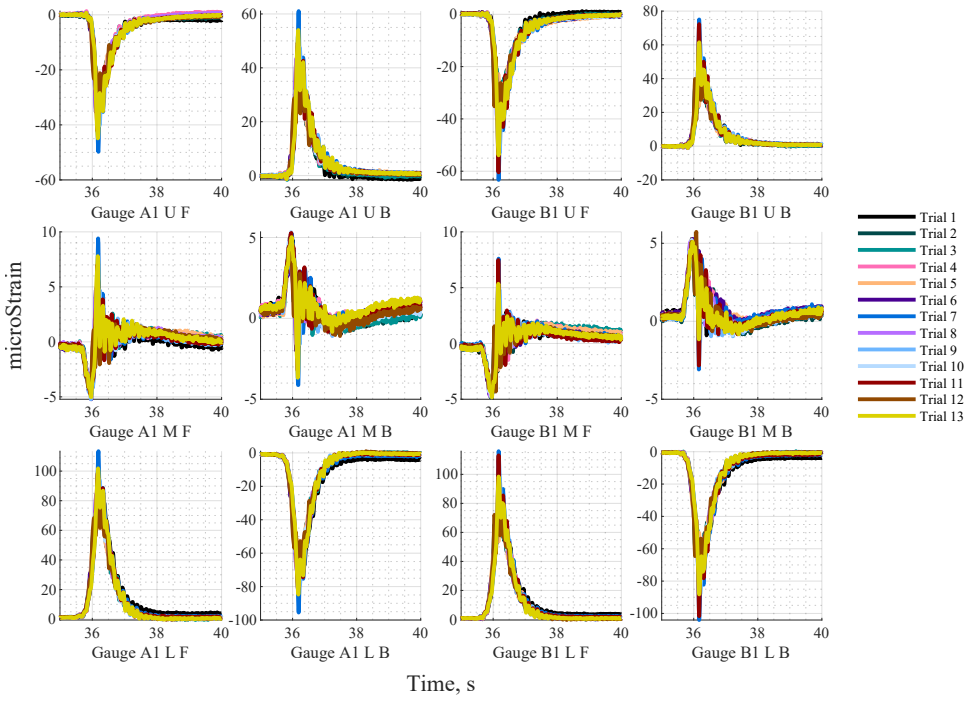

Figure E.17: Strain gauges on front columns CFST_NS_F_145

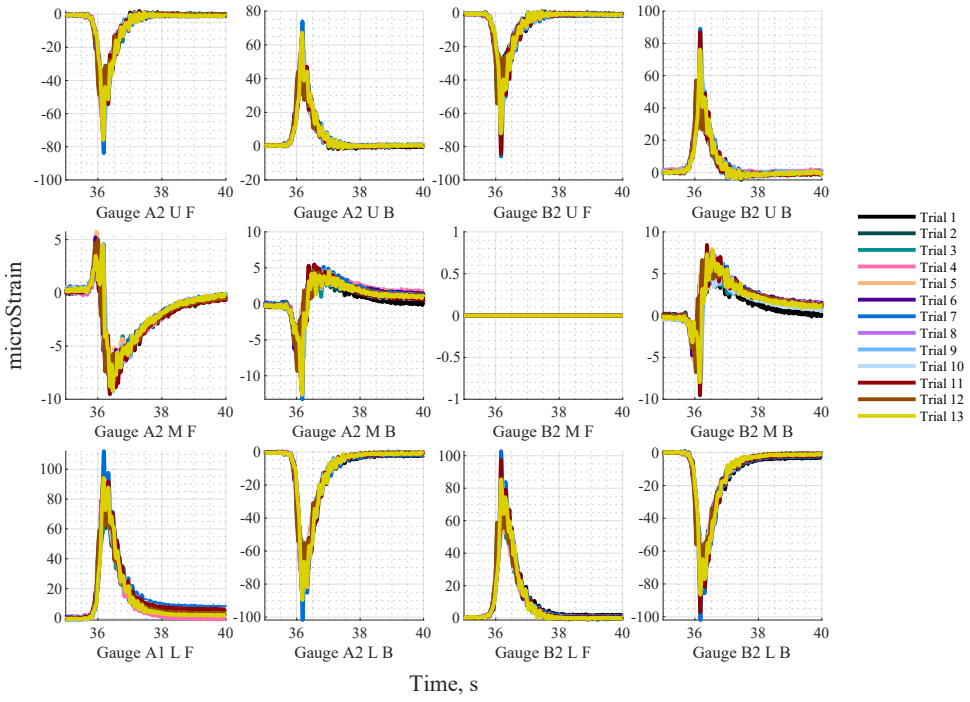

Figure E.18: Strain gauges on Back columns CFST_NS_F_145

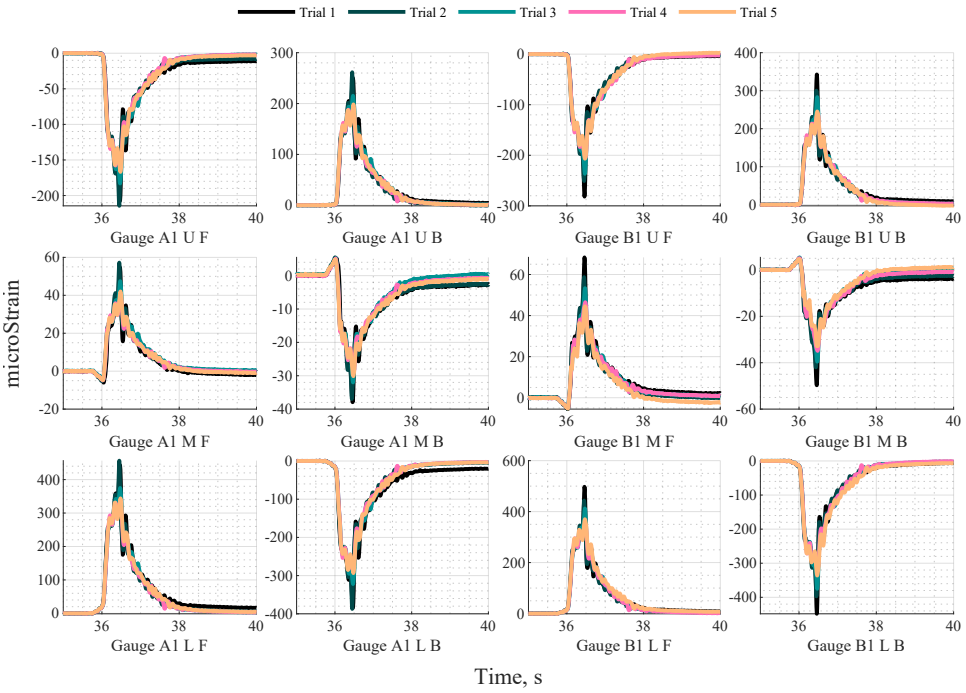

Figure E.19: Strain gauges on front columns CFST_BA_E_140

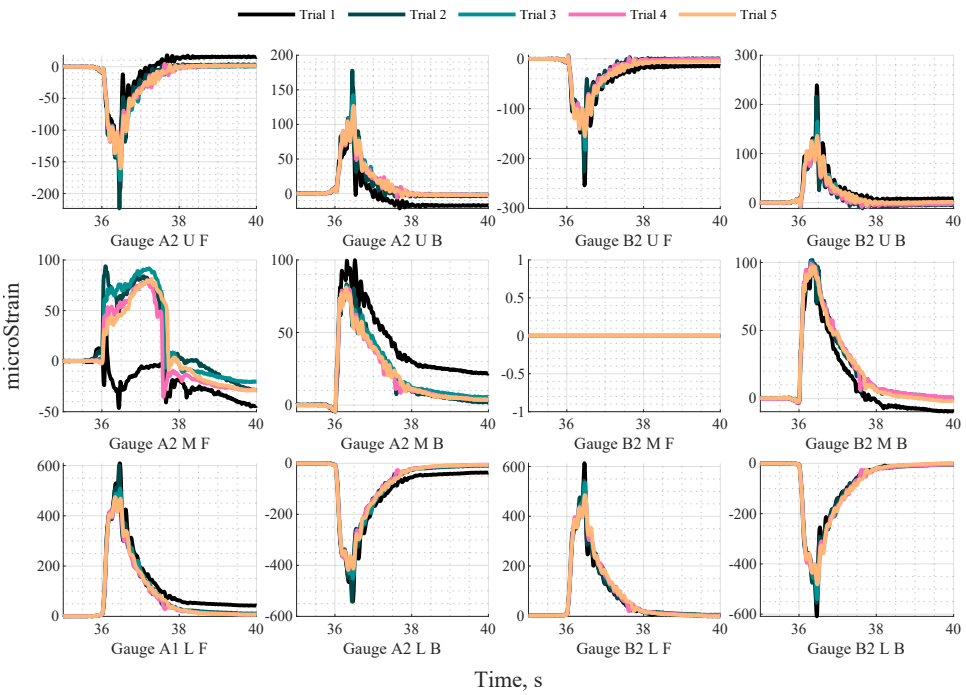

Figure E.20: Strain gauges on Back columns CFST_BA_E_140

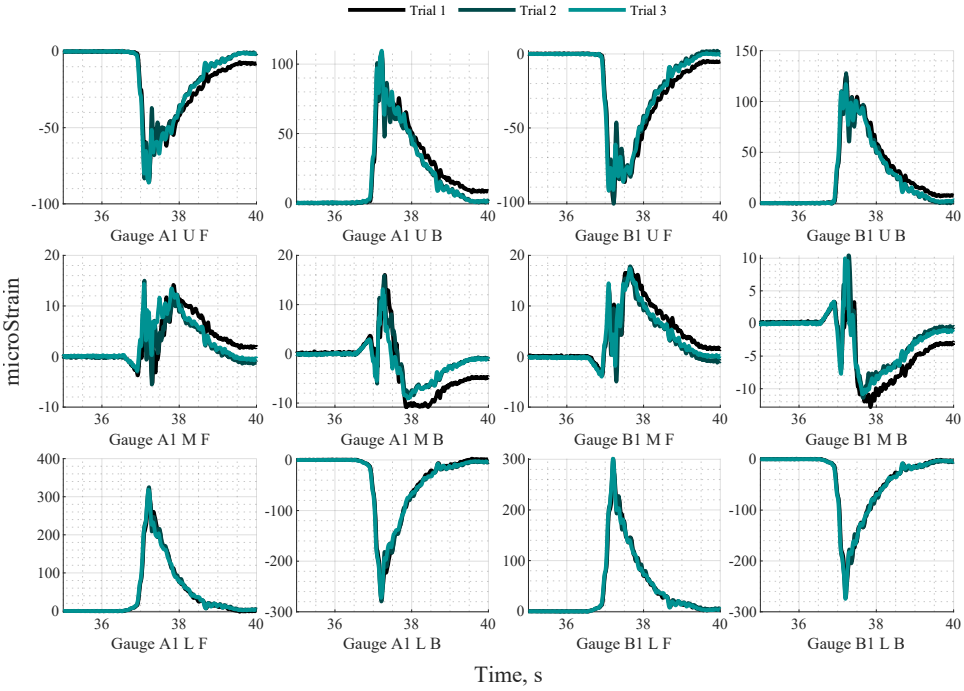

Figure E.21: Strain gauges on front columns CFST_FS_E_100

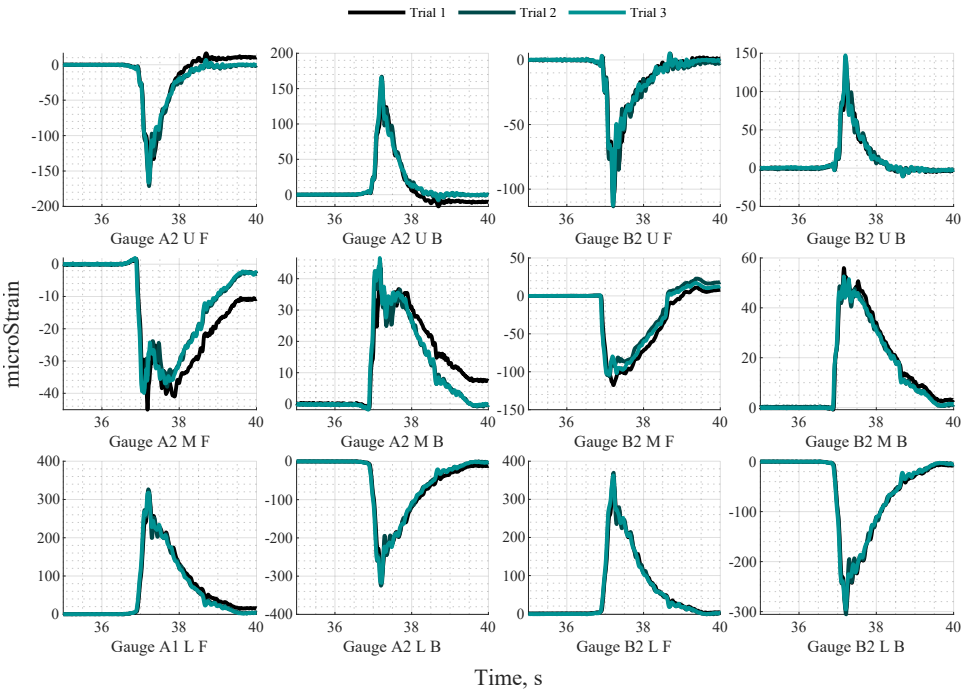

Figure E.22: Strain gauges on Back columns CFST_FS_E_100

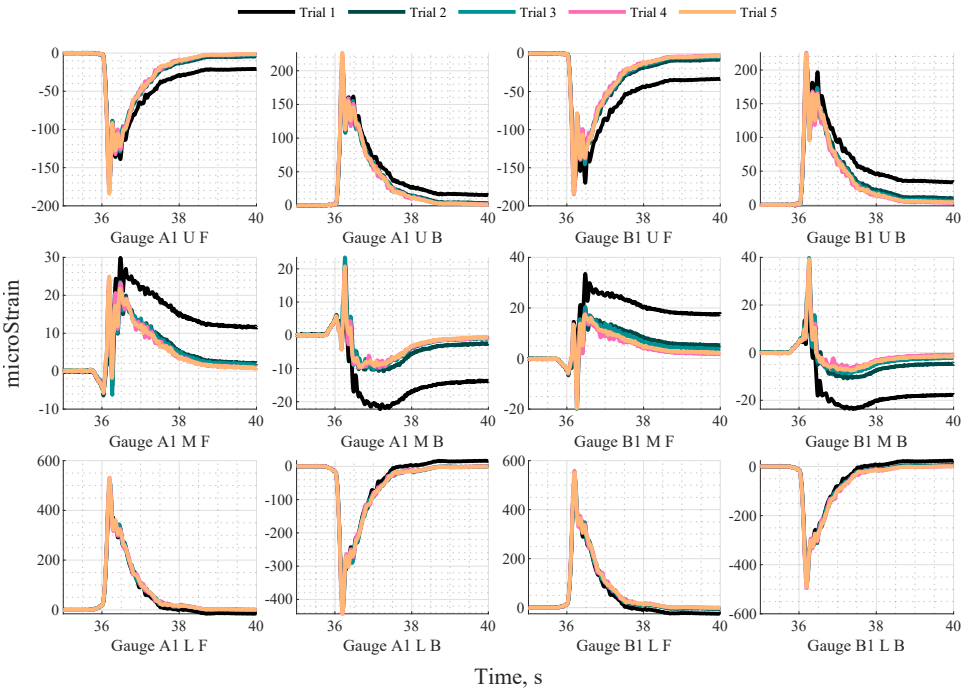

Figure E.23: Strain gauges on front columns CFST_FS_E_140

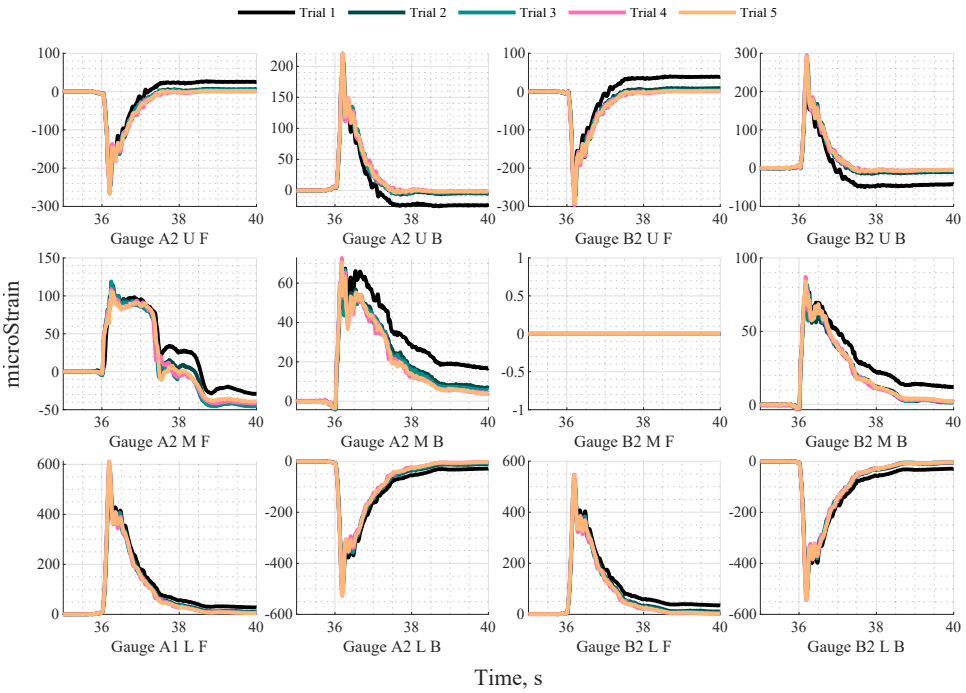

Figure E.24: Strain gauges on Back columns CFST_FS_E_140